İSTANBUL TECHNICAL UNIVERSITY ★ INSTITUTE OF SCIENCE AND TECHNOLOGY

GLASS, GLASS-CERAMIC AND SINTERED MATERIALS PRODUCED FROM INDUSTRIAL WASTES

Ph.D. Thesis by

M. Melek EROL, M.Sc.

Department : Chemical Engineering

Programme: Chemical Engineering

JUNE 2006

İSTANBUL TECHNICAL UNIVERSITY ★ INSTITUTE OF SCIENCE AND TECHNOLOGY

GLASS, GLASS-CERAMIC AND SINTERED MATERIALS PRODUCED FROM INDUSTRIAL WASTES

Ph.D. Thesis by

Melek Mümine EROL, M.Sc.

(506992108)

Date of submission : 4 March 2006

Date of defence examination: 23 June 2006

Supervisors (Chairman): **Prof. Dr. Sadriye KÜÇÜKBAYRAK**
Prof. Dr. Ayşegül ERSOY-MERİÇBOYU

Members of the Examining Committee **Prof.Dr. Hasancan OKUTAN (İ.T.Ü.)**

Prof.Dr. M. Lütfi ÖVEÇOĞLU (İ.T.Ü.)

Prof.Dr. Mehmet KOZ (M.Ü.)

Prof.Dr. Zeki ÇİZMECİOĞLU (Y.T.Ü.)

JUNE 2006

İSTANBUL TEKNİK ÜNİVERSİTESİ ★ FEN BİLİMLERİ ENSTİTÜSÜ

ENDÜSTRİYEL ATIKLARDAN CAM, CAM-SERAMİK VE SİNTERLENMİŞ MALZEMELERİN ÜRETİMİ

DOKTORA TEZİ

Y. Müh. Melek Mümine EROL

(506992108)

Tezin Enstitüye Verildiği Tarih : 4 Mart 2006
Tezin Savunulduğu Tarih : 23 Haziran 2006

Tez Danışmanları :	**Prof. Dr. Sadriye KÜÇÜKBAYRAK**
	Prof. Dr. Ayşegül ERSOY-MERİÇBOYU
Diğer Jüri Üyeleri	**Prof.Dr. Hasancan OKUTAN (İ.T.Ü.)**
	Prof.Dr. M. Lütfi ÖVEÇOĞLU (İ.T.Ü.)
	Prof.Dr. Mehmet KOZ (M.Ü.)
	Prof.Dr. Zeki ÇİZMECİOĞLU (Y.T.Ü.)

HAZİRAN 2006

Acknowledgements

To endure my difficulties of my thesis, it takes guidance and encouragement from the following people.

First of all I would like to thank Prof. Dr. Sadriye KÜÇÜKBAYRAK, who becomes more than my academic advisor, for teaching me how to work scientifically and independently. Ten years of working with her, from undergraduate to Ph.D. have given me valuable experiences for my future career. Her guidance, support, patience, care and understanding in so many ways helped me overcome difficulties during my years at here ITU.

I want to express my deepest gratitudes to my co-advisor Prof.Dr. Ayşegül ERSOY-MERİÇBOYU for her guidance, encouragement, support and trust throughout my master and Ph.D. studies.

I would like to thank my thesis committe, Prof. Dr. M. Lütfi ÖVEÇOĞLU and Prof. Dr. Cemalettin YAMAN for their helpful suggestions and constant concerns throughout this work.

I wish to extend my thanks to many friends and coaleagues who have been a meaningful part of my life professionally and personally at ITU: Assoc. Prof.Dr. Hanzade AÇMA, Assoc. Prof.Dr. Nilgün KARATEPE-YAVUZ, Dr. Ayşe ARİFOĞLU, Assoc. Prof.Dr. Reha YAVUZ, Assoc. Prof.Dr. Serdar YAMAN and Chem. Eng. (MSc.) A. Abdullah CEYHAN. I would like to thank Chem. Eng. (MSc.) Didem ÖZÇİMEN for her support and friendship.

Last but not the least, I would like to express my deepest gratitude to my family and relatives, their trust and love give warmth and strentgh to me. Especially, to my parents for their understanding, patience, support, encouragement and love. Special thanks should be expressed to my brother for his constant support, help and concern.

M.Melek EROL March, 2006

CONTENTS

ABBREVIATIONS

DTA	: Differential Thermal Analysis
JMA	: Johnson-Mehl-Avrami
DGMS	: Diethylene Glycol Monostearate
PVA	: Polyvinyl Alcohol
SEM	: Scanning Electron Microscopy
XRD	: X-Ray Diffraction
ICP	: Inductively Coupled Plasma Spectrometry
TCLP	: Toxicity Characteristic Leaching Procedure
MSW	: Municipal Solid Waste

TABLE LIST

FIGURE LIST

NOMENCLATURE

T_m	: Melting Temperature
T_g	: Glass Transition Temperature
U	: Crystal Growth Rate
E	: Activation Energy Of Crystal Growth
D''	: Diffusion Coefficient
ΔG	: Bulk Free Energy Of Crystallization
a_0	: Molecular Diameter
α	: Heating Rate
R	: Ideal Gas Constant
n, m and k	: Numerical Factors Which Depend On The Crystallization Mechanism
T_p	: Crystallization Peak Temperature
ν	: Frequency Factor
H_V	: Vickers Hardness
$\delta(T)_p$	: The height of the Crystallization Peak
N	: The Number of Nuclei
k	: The Reaction Rate Constant
C_p	: The Heat Capacity

ENDÜSTRİYEL ATIKLARDAN CAM, CAM-SERAMİK VE SİNTERLENMİŞ MALZEMELERİN ÜRETİMİ

ÖZET

Bu çalışmada, endüstriyel atıklardan cam, cam-seramik ve sinterlenmiş malzemeler üretilmiştir. Bu amaçla, Afşin-Elbistan, Çan, Çatalağzı, Çayırhan, Orhaneli, Seyitömer ve Tunçbilek termik santrallerinden uçucu küller temin edilmiştir. Silis dumanı ve Seydişehir alüminyum tesislerinden elde edilen kırmızı çamur ise katkı maddesi olarak kullanılmışlardır. Öncelikle, Afşin-Elbistan, Çayırhan, Orhaneli, Seyitömer ve Tunçbilek uçucu küllerinden cam üretimi gerçekleştirilmiştir. Üretilen cam numunelerine 1273 K'de ve 2 saat süreyle ısıl işlem uygulanmıştır. Cam numunelerine ısıl işlem uygulanması ile amorf faz kaybolmuş ve numunelerde diopsid, gelenit, wollastonit ve augit fazları oluşmuştur. Isıl işlem uygulanan cam numunelerinin, mekanik, fiziksel ve kimyasal özelliklerinin cam numunelerinkine oranla daha iyi olduğu görülmüştür. Cam numunelerine ısıl işlem uygulanması, numunelerin özelliklerini iyi yönde geliştirmiştir. Toksisite deneyi sonuçları, cam ve ısıl işlem uygulanmış cam numunelerinin çevreye zarar vermeyen malzemeler olduğunu göstermiştir.

Tunçbilek uçucu külünden ve Çayırhan ile Orhaneli uçucu küllerine kırmızı çamur ve silis dumanı ilavesi ile cam-seramik malzemeler üretilmiştir. Cam numunelerine, cam-seramik malzeme üretebilmek amacıyla hem klasik hem de sinterleme yöntemleri uygulanmıştır. Cam numunelerine; diferansiyel termal analiz sonucunda elde edilen bilgiler ışığında, çekirdeklenme ve kristalizasyon ısıl işlemleri uygulanarak cam-seramik malzemeler üretilmiştir. Kristalizasyon sıcaklığında bekleme süresinin üretilen cam-seramik numunelerinin mikroyapısal, kimyasal ve fiziksel özelliklerine olan etkisi incelenmiştir. Kristalizasyon sıcaklığında süresinin artması ile birlikte cam-seramik numunelerde oluşan kristal fazın oranı artmıştır. Ayrıca cam-seramik numunelerinin iyi yönde geliştiği gözlenmiştir. Klasik yöntem ile üretilen cam-seramik numunelerin özellikleri camın kimyasal yapısına ve uygulanan ısıl işlemlerin koşullarına bağlı olarak değişmektedir. Sinterleme yöntemi ile üretilen cam-seramik numunelerin özellikleri ise camın kimyasal yapısına, ortalama tane boyutuna, katkı maddelerine, ısıtma hızına, sinterleme basıncı ve sıcaklığına bağlıdır. Tunçbilek uçucu külünden üretilen cam-seramik numuneler hariç, sinterleme yöntemi ile elde edilen tüm cam-seramik malzemelerin özelliklerinin, PVA ilavesi ile iyi yönde geliştiği tespit edilmiştir. Toksisite sonuçları ağır metallerin, üretilen cam-seramik numunelerin yapıları içerisinde tutulduğunu göstermiştir.

Endüstriyel atıklardan üretilen cam numunelerinin kristalizasyon mekanizmaları izotermal ve izotermal olmayan yöntemler kullanılarak tespit edilmiştir. Ayrıca, cam numunelerinin tane boyutunun kristalizasyon mekanizmasına olan etkisi incelenmiştir. İzotermal olmayan yöntem kullanılarak tespit edilen aktivasyon enerjisi değerleri, tane boyutu büyük cam numuneleri için 233-578 kJ/mol, toz halindeki cam numuneleri için is 369-662 kJ/mol arasında değişmektedir. Cam numunelerinin aktivasyon enerjisi değerleri tane boyutunun düşmesi ile birlikte artmıştır. Tane boyutu büyük ve toz halindeki cam numunelerinin, izotermal ve izotermal olmayan yöntemler kullanılarak hesaplanan aktivasyon enerjisi değerleri birbirine

oldukça yakın çıkmıştır. Ancak, izotermal olmayan yöntemler kullanılarak hesaplanan aktivasyon enerjisi değerleri, izotermal yöntemler kullanılarak hesaplananlardan daha büyük çıkmıştır.

Yedi farklı termik santralden temin edilen uçucu küllerden herhangi bir katkı madde ilavesi olmadan sinterleme yöntemi kullanılarak seramik malzeme üretilmeye çalışılmıştır. Sinterleme sıcaklığının, üretilen malzemelerin yoğunluk, gözeneklilik, su emme, mekanik ve mikroyapısal özelliklerine olan etkisi incelenmiştir. Sinterleme yöntemiyle üretilen malzemelerin özelliklerinin, sinterleme sıcaklığı ve süresine, kullanılan uçucu külün kimyasal bileşimine ve tane boyutuna bağlı olduğu saptanmıştır. Sinterlenmiş malzemelerin özelliklerinin, sinterleme sıcaklığının artması ile birlikte iyi yönde geliştiği gözlenmiştir. Bu çalışma açıkça göstermektedir ki, endüstriyel atıklardan cam, cam-seramik ve sinterlenmiş malzemeler başarılı bir şekilde üretilebilmiştir.

GLASS, GLASS-CERAMIC AND SINTERED MATERIALS PRODUCED FROM INDUSTRIAL WASTES

SUMMARY

In this study, the production of glasses, glass-ceramics and sintered materials from industrial wastes has been investigated. For this purpose, coal fly ash samples were obtained from 7 different thermal power plants which are located in Afşin-Elbistan, Çan, Çatalağzı, Çayırhan, Orhaneli, Seyitömer and Tunçbilek. Beside coal fly ashes, red mud from Seydişehir alumina plant and silica fume from ferrosilicon alloy production were used as additives. To accomplish this study first of all, glass samples were produced from Çayırhan, Orhaneli, Seyitömer, Afşin-Elbistan and Tunçbilek fly ashes. The produced glass samples were heat treated for 2 h at 1273 K to observe the physical, microstructural and mechanical changes in the glass structure. When the heat-treatment process was applied to the glass samples, the amorphous phase had practically disappeared and diopside, augite, gehlenite and wollastonite phases occurred in the samples. Physical, mechanical and chemical properties of the heat-treated glass samples are better than those of the produced glass samples. The heat-treatment process improved the properties of the glass samples. TCLP results revealed that the both glass and the heat treated glass samples can be taken as non-hazardous materials.

Glass-ceramic materials were produced from Tunçbilek, Çayırhan and Orhaneli coal fly ashes without or with the addition of red mud and silica fume. Both classical and sintering methods were applied to the produced glass samples. The nucleation and crystallization experiments were carried out on the basis of differential thermal analysis results to produce glass-ceramic materials. The effect of different holding times at the crystallization temperature on the microstructure and the properties of the produced glass-ceramic samples was also investigated. It was observed that the volume of the crystalline phase increased with the increase in holding time at the crystallization temperature in all glass-ceramic samples and this result caused to improve the physical, mechanical and chemical properties of the glass-ceramic samples. The properties of the bulk glass-ceramic samples were influenced by the glass composition, glass production conditions and the heat treatment process while the properties of the sintered glass-ceramic samples are depending on the glass composition, particle size, the addition of the binder, heating rate, sintering pressure and the firing temperature. It was observed that, in all glass-ceramic samples, except glass-ceramic samples produced from Tunçbilek fly ash, addition of PVA improved the properties of the produced samples. TCLP results indicated that the heavy metals successfully solidified into the glass-ceramic samples' structures.

A comprehensive investigation of the kinetics of nucleation and crystal growth mechanisms of glasses obtained from waste materials was studied by both isothermal and non-isothermal methods. The influences of the particle size on the crystallization kinetics of glasses was investigated. The activation energies of crystal growth which were determined by using non-isothermal methods for the coarse and fine glasses are in the range of 233-578 kJ/mol and 369-662 kJ/mol, respectively. The activation energy values for crystallization increased with

the decrease in particle size of the waste glasses. The Avrami constants and crystallization activation energy values of all coarse and fine glasses for the non-isothermal and isothermal methods are roughly close.

Coal fly ash samples obtained from seven different thermal power plants were sintered to form ceramic materials using conventional powder processing based on milling, powder compaction and firing, without the addition of organic binders or other inorganic additives. The effect of firing temperature on the density, porosity, water adsorption, microstructure and mechanical properties of sintered fly ash samples was investigated. The sintering process results showed that the properties of the produced materials are depending the sintering temperature and time, the particle size and distribution of the powder, the composition of the system and packing pressure. The properties of the sintered materials improved with the increase in the sintering temperature since the crystallization degree also increased with the increase in sintering temperature. This study has clearly shown that industrial wastes can successfully recycled in the glass, glass-ceramic and sintered materials production.

1.INTRODUCTION

Industrial development over the last few decades has generated large amounts of toxic and hazardous inorganic wastes, for example fly ashes from thermal power plants, metallurgical slags and muds of different origins.

Disposal of fly ash as a by-product of incineration of coal, municipal solid wastes, metallurgical slags and red muds from aluminium and beryllium extraction is becoming an increasing economic and environmental burden. As a consequence, there is a growing interest in looking for avenues where the material can be used as a potential resource for preparation of value added products. The majority of fly ash is generated by coal fired power stations and a percentage (typically 10-20%) does find reuse, primarily in cementitious (concrete and cement) products [1-2], but also in construction areas, such as highway road bases [3], grout mixes [4] and stabilizing clay based building materials [5].

However, despite positive uses, the rate of production clearly far outweighs consumption. In Turkey, annually 13 million tons of fly ash are produced from 11 different power stations, but only a small amount is utilized mainly in the construction sector [6]. For the remaining material, disposal practices involve holding ponds, lagoons, landfills and slag heaps, all of which can be regarded as unsightly, unenvironmentally undesirable and a non-productive use of land resources, as well as posing an on-going financial burden through their long-term maintenance.

Furthermore, for those coal power plants located in urban areas, finding disposal sites is becoming increasingly more difficult. With competition for limited space and tightening of regulations on surface water and ground water discharge, any waste resulting from fly ash disposal sites must be well managed(causing the leaching of materials into water beds), so that local surface and ground water supplies are protected [7]. Contamination of soil by chemicals and heavy metals (as Pb, Cr, Zn,

Cu, Cd and Hg) is often another serious environmental problem. This can cause significant economic burden to achieve the necessary water and land management. These factors have prompted researchers to look for alternative usages for fly ash, other than the cement and construction industry. It is thus necessary, for the inertization of fly ashes, to look for new technologies in order to immobilize their dangerous components in glass, glass-ceramic or ceramic materials.
The production of vitreous materials can be an effective route for recycling of wastes because the high temperature involved in the process leads to the complete destruction of the organic pollutants. Furthermore, heavy metals can be either incorporated in the glassy product [8]. The inert glass product can also be used as a secondary raw material, especially in building and construction. Unfortunately vitrification is an energy intensive process, which involves high cost[9]. Therefore, more effective and economic solutions must be considered to improve the properties of the waste glass materials.

Since the major constituents of fly ashes are various oxides of silicon and aluminum, these can be good candidates for glass-ceramic production [10]. Therefore by proper heat treatment and controlled crystallization, it should be possible to produce a new marketable materials like glass-ceramics, which can be used in many industrial applications [11].

Glass-ceramics are commercially important ceramics with unique thermal shock resistance and mechanical properties. For example, properties such as strength, hardness and corrosion resistance are superior to the parent glass making them attractive materials for the construction, mechanical and chemical industries [12].

Glass-ceramics have now became technologically important materials since their discovery in the 1950s, and are used in microwave radomes, microelectric substrates and packaging, domestic cooker tops and cooking utilities, astronomical telescopes, high integrity vacuum envelopes and biomedical applications [13,14].

Coal fly ash has also been incorporated into conventionally sintered ceramics [15]. This industry uses large volumes of silicate-based raw materials and therefore has the potential to use significant amounts of fly ash [16,17].

The present study concentrate on the production of glass, glass-ceramic materials from waste materials such as, coal fly ash, red mud from aluminum production and silica fume in order to reduce their volume, make them more inert and to produce a new markatable product (eco-product) useful in the construction industry. To achieve this first of all, glass samples are produced from coal fly ash samples obtained from seven different thermal power plants with or without the addition of red mud and silica fume. They have been heat treated for 2 h at 1273 K to observe the physical, microstructural and mechanical changes in the glass structure. Classical and sintering methods have been applied to the obtained glass samples to produce glass-ceramic materials. The effect of different holding times at the crystallization temperature on the microstructure and properties of glass-ceramic samples has been investigated.

A comprehensive investigation of the kinetics of nucleation and crystal growth mechanisms of glasses obtained from waste materials has been studied by both isothermal and non-isothermal methods. Special attention is paid to the influences of the particle size of the glasses on crystallization kinetics to assess the feasibility of producing glass-ceramics.

In addition, in this research coal fly ash samples obtained from seven different thermal power plants have been sintered to form ceramic materials using conventional powder processing based on milling, powder compaction and firing, without the addition of organic binders or other inorganic additives. The effect of firing temperature on the density, porosity, water adsorption, microstructure and mechanical properties of sintered fly ash samples is reported.

2. Glass

2.1 Definition of Glass

Glass might be described as a transparent substance possessing the properties of hardness, rigidity and brittleness. Thus, with the possible exception of transparency, the properties usually thought of as characterising glass are those normally associated with solids. However, glass possesses a number of properties that are characteristic of the liquid state and the classification of glass as a liquid of very high viscosity rather than as a solid would be in accordance with modern views [18].

Various definitions of glass have been put forward but one of them is widely accepted is that proposed by the A.S.T.M.: Glass is an inorganic product of fusion that has cooled to a rigid condition without crystallizing. This definition has several drawbacks. First, it suggests that glasses have to be inorganic and so excludes the many organic glasses. It fails to point the way to useful common areas between polymers and glasses. Most of all, it focuses on one method of preparation, that used in the glass industry and this has probably deflected effort from seeking alternatives. For example, in 1978 it was shown that good silica glasses can be made from gels without melting [19,20].

A more acceptable definition of a glass is a non-crystalline elastic solid, i.e. 2 nm maximum order, with a viscosity of $>10^{13.5}$ poise.

Man-made glasses appeared around 4000 BC in Egypt and Mesopotamia as decorative glasses and glass working was known by around 1500 BC as an art and a technology. Glass science was not further developed until the work of Faraday and later Zeiss, Abbé and Schott, who in 1881 began to develop new optical glasses. By 1900 these workers had used some thirty-four elements in experimental glass formulations. Although seventy elements have now been tried, only three major

commercial glass systems constitute 99% by weight of all glass production. These systems are:

- Soda (Na_2O)-lime (CaO)-silica (SiO_2)
- Lead crystal glass, PbO- SiO_2
- Low expansion borosilicate glass B_2O_3-SiO_2-Na_2O-CaO

Continued competitiveness requires serious reappraisal of glass structure and glass science, together with a willingness to explore new raw materials such as La_2O_3, V_2O_5 and non-oxide materials.

There is also the possibility that restrictive definitions and dominant views on glass structure have further delayed modern exploitation of new areas. The developments in glass science have paralleled major advances in surface treatments to improve strength and durability. Whether the material will continue to be constantly competitive is open to question, in the face of demands from the electrical industry for better metal sealing glasses and for glass able to withstand attack at high temperature by metal vapors; the electronics industry for electron-conducting glasses; the optical industry for high refractive index glasses for fibre optics; and the ceramics industry in general for compositions suitable for the manufacture of glass-ceramics [19].

2.2 Glass Formation

Traditionally, glasses have been processed by cooling a liquid fast enough to prevent detectable crystallization. From this kinetic viewpoint, we can define glass formation as the avoidance of crystallization. In principle, any liquid can be rendered glassy given a sufficiently rapid cooling rate. It is the difference in respective rates of crystallization that allows us to form many commercial oxide glasses by cooling at a leisurely rate of a few degrees per minute (^{0}/min), while metallic glasses must be quenched at more than 10^6 degrees per second (^{0}/sec). Glass-ceramics are commercially important ceramics with unique thermal shock and mechanical properties, made by controllably nucleating a very high density of crystals in a parent glass body.

Glasses can also be made by a number of alternative processes, which have in common the aspect of consolidation at low temperatures to defeat crystallization. Condensation of a vapor onto a cold substrate is one method (physical or chemical vapor deposition), often used for the preparation of electronic thin-films (glassy and crystalline). Another is the precipitation of a disordered ceramic from liquid chemical solution (referred to as sol-gel processing), followed by densification into a glass. The structure and properties of glasses made by these techniques can differ substantially from those prepared from the melt. For applications that require a monolithic body, the vast majority of glasses continue to be processed from the melt. When the glasses are produced by cooling from the melt, the phase transformation from liquid to solid occurs at a glass transition temperature (T_g) that lies below the melting temperature T_m at which crystallization would otherwise take place. At T_g there is a transformation in physical properties from those of a liquid to those of a solid; one such property illustrated in Figure 2.1 is the specific volume. The slope of this curve is directly related to the volume expansion coefficient α ($=\partial V/V\partial T$ at constant composition and pressure). Above T_m one has a liquid; between T_m and T_g there exist a supercooled liquid. Figure 2.1 shows a transition to a glassy state where structural rearrangements are no longer to take place on a reasonable time scale and where the thermal expansivity and other properties become that of a solid.

Since glass is a supercooled liquid it does not have a sharp melting point but softens gradually and eventually becomes fluid due to the continuous fall of viscosity with increase of temperature.

The relationship between viscosity and temperature for glasses is important in a number of respects. For example, during the melting of glasses a low viscosity favors the rapid rise of gas bubbles through the melt thus permitting clear bubble free glass to be produced. Also the annealing of glass (to remove strains introduced as a result of uneven cooling during the shaping operations) depends upon heating the glass to a temperature where its viscosity is low enough to permit stress relief without resulting in distortion of the glass. In making glass-ceramics, which involves nucleation and crystallization of glasses under carefully controlled conditions, the selection of optimum heat-treatment temperatures is governed by the viscosity-temperature characteristics of the glasses [18].

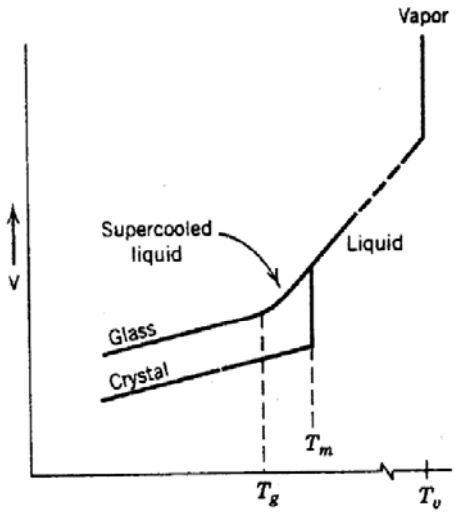

Figure 2.1: Volume-temperature relations for liquid, crystal and glass phases [21].

Smooth curves can be drawn relating the viscosities of glasses to temperature for a wide range but it is often more convenient to define the viscosity-temperature relationship in terms of certain characteristic temperatures which are given in Table 2.1 together with the corresponding values of viscosity [21].

Table 2.1: Characteristic temperatures with corresponding viscosities for glasses [21]

Characteristic Temperature (K)	Viscosity (poise)
Working point	10^4
Softening point	$10^{7.6}$
Annealing point	$10^{13.4}$
Glass transition point	$10^{13\text{-}14.5}$

2.3 Glass Structure

Glass possesses the mechanical properties of a solid. Unlike the structure of most other solids, glass, however, is a non-crystalline and has a structure similar to that of a liquid. Although there are other important glass types, most glasses used in waste immobilization is some type of silicate glass. Glasses are produced by melting crystalline materials and/or frit (previously formed glasses) at elevated temperatures to produce liquids. These liquids are then cooled to a rigid condition without

crystallization. The glass composition is predominatly inorganic with silica being the most common constituent.

There are two types of theories for glass formation: structural and kinetic. Within the structural type, there are many theories for glass formation of which Zachariasen and Sun are two that have contributed significantly. Zachariasen's theory is based on the argument that the atomic forces of a crystalline material and a glass material must be of the same order of magnitude because mechanical properties of glass are similar to those of the corresponding crystals [22-24]. Zachariasen noted that silicate glasses were not composed of discrete molecules in a close-packed structure, but were three dimensional networks. These networks consisted of the basic structure, a silicon oxygen tetrahedral, where the silicon atom is bonded to four oxygen atoms [22, 25]. The silica tetrahedra is linked at the corners where each of the oxygen's can be shared with another tetrahedron. All or some of the oxygen can be shared with other tetrahedra to form a three dimensional network. The irregularity of the structure and the random bonds are what prevent crystallization.

After determining that the formation of the network was necessary for glass formation to occur. Zachariasen formalized his considerations of the structural arrangements into four rules. They are:

1. The number of oxygen atom is linked to no more than two atoms,
2. The number of oxygen atoms surrounding network cation must be small, specially either three or four,
3. The cation polyhedra share corners, not edges nor faces,
4. At least three corners are shared.

These rules are known as "Zachariasen Random Network Theory".

Bond strength has also been used as a criterion for predicting glass formation. Sun argued that strong bonds did not allow for reorganization of the melt into a crystalline structure upon cooling and therefore caused glass formation. The higher the bond strength, the better the oxide was able to form glass. The bond strength defined as the dissociation energy divided by the number of cation-anion bonds in the unit cell. Sun's "Single Bond Strength Criterion", as his theory became known, contributed the classification of substances into three divisions based on their glass

forming ability (glass network formers, intermediates and glass network modifiers)[22-24].

More recent glass formation theories recognize that the defining factor is not whether a material will form a glass, but rather how fast the melt must be cooled to avoid crystallization. Crystallization requires first the presence of a nucleus (nucleation) and second, a rate at which the crystal will grow to a noticeable size (crystal growth). To avoid crystallization, nucleation and crystal growth must not exist.
Nucleation and crystal growth occur simultaneously during the cooling of a melt. The rates of each are continuously changing with the change in temperature throughout the process. Any realistic approach to glass formation must deal with the interactions between these two processes. To develop a quantitative model calculations for nucleation as a function of temperature and crystal growth as a function of temperature are needed. The results must be combined to determine an approximation for the amount of material crystallized as a function of time. When the assumption of dependence between nucleation/crystal growth and temperature is made, the result is the ability to construct a curve that yields the time necessary to cause a given volume fraction of crystallization. These curves are called TTT(time-temperature-transformation) diagrams. The general shape of the curve (as seen in Figure 2.2) is due to the competing nature of kinetic and thermodynamic factors for both nucleation and crystal growth rates. The least favorable condition for glass formation occurs at the temperature corresponding to the nose of the curve [23]. As long as the cooling rate is greater than the rate given by the tangent at the nose, glass formation is present [24].

2.4 Glass Chemistry

The oxides used in commercial glass production can be classifies into three general categories: Network forming oxides, modifying oxides and intermediate oxides.

2.4.1 Network forming oxides

Oxides, which form glassy structure when melted and cooled, and vitrify are called network-forming oxides because of their ability to buildup continuos three-dimensional random networks. Examples are SiO_2, B_2O_3 and P_2O_5.

Glasses made solely from network formers often have limited utility. Pure B_2O_3 glass is not water resistant and pure SiO_2 glass, while valued for its chemical durability, high application temperature and thermal shock resistance, must be processed above 2000 K. Therefore to alter processing and properties, oxide modifiers and intermediates are used [12,26].

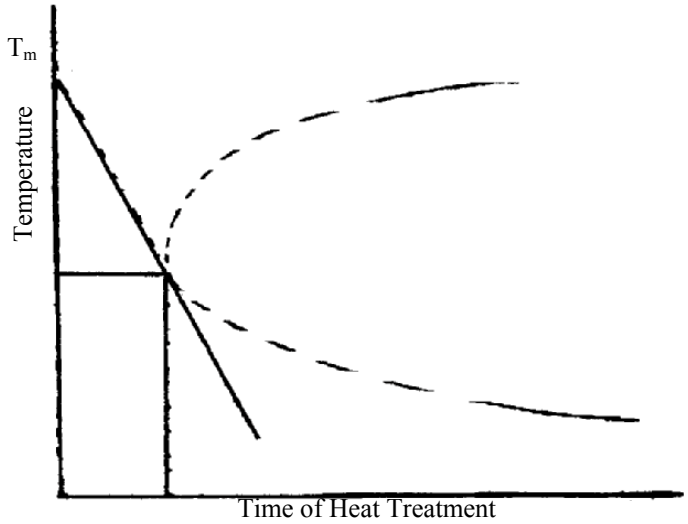

Figure 2.2: A time-temperature-transformation (TTT) curve for a glass forming melt [23].

2.4.2 Modifying oxides

Modifying oxides do not form glass by themselves but, when used in certain proportions, enable the modification of the manufacturing conditions or properties of the resulting glass. This may include reducing the viscosity of the glass, increasing the thermal expansion coefficient, or lowering the melting point. Examples of modifiers are Na_2O, K_2O and Li_2O [27].

While alkaline oxides are very effective modifiers, the result is that glasses are not chemically durable. The chemical durability is greatly improved with the additional modifier of CaO. The oxides such as PbO, MgO, ZnO and BaO may also act as modifying oxides and prevent deterioration of the finished product[12].

2.4.3 Intermediate oxides

Although not usually capable of forming a glass, these oxides can be incorporated into the glass network. Examples are Al_2O_3, BeO, TiO_2 and ZrO_2. The following Table 2.2 gives the percentages by weight of oxides in the common commercial types of glass and some special types. Secondary components are always used in small proportions and are used to change the color (transition metal oxides) or manufacturing conditions (arsenic and antimony oxides)[27].

Table 2.2: The percentage by weight of oxides in the common commercial types of glass and some special types [27].

	SiO_2	B_2O_3	Al_2O_3	Na_2O	K_2O	CaO	BaO	MgO	PbO	Fe_2O_3
Sheet Glass	72.5		1.5	13	0.3	9.3		3		0.1
Bottle Glass	73		1.0	15		10				0.05
Light Bulb	80.6		1.0	16	0.6	5.2		3.6		
Pyrex	54.6	12.6	2.2	4.2		0.1		0.05		0.05
Glass Fiber	55.5	8.0	14.8	0.3	0.3	17.4		4.5		
Crystal	28				11.0				33	
Optical Glass				1.0	1.0				70	
Na Lamp Glass		36	27				27	10		

In a typical commercial glass, the number of different oxide constituents within each classification is usually small. However, this is not true of glass made from hazardous wastes. The waste include a large number of components and any waste can contain up to 69 of the elements in the periodic table. The relationship between chemical durability and these large numbers of chemical constituents that are to be used in the formation of vitrified waste forms is quite complicated and not completely understood. Additives can affect the rate of corrosion in different ways depending on what solution comes in contact with the glass. The understanding of this relationship is critical in the control of the vitrification process for waste treatment [28].

3. Glass-ceramic

3.1 Definition and History of Glass-ceramic

A glass-ceramic is initially a glass in which, at some stage, the formation of nuclei is enhanced either by the addition of a nucleating agent or by using special compositions which are self nucleating. The resulting material contains very small crystals [19].

A more common definition of glass-ceramic is that glass-ceramics are polycrystalline solids prepared by the controlled crystallization of glasses. Crystallization is accomplished by subjecting suitable glasses to a carefully regulated heat treatment schedule that results in the nucleation and growth of crystal phases within the glass. In many cases, the crystallization process can be taken almost the completion but a small proportion of residual glass phase is often present [18]

These definitions point immediately to some advantageous general properties and directs the attention to important areas to consider in more detail.

Glass manufacturing techniques have the advantage that any shape is easily produced with close control of dimensions and high speed automation can be applied. The method of production leads to zero porosity and an outstanding uniformity of properties in the finished ceramic, because of the molten state first achieved and the nature of the nucleation process. Dimensional changes in manufacture are consequently small compared to any other ceramic process.

Experience show that many practical advantages arise. In principle, it is possible to engineer materials to order, with specific properties, from any composition that can be cooled to the glassy state. Properties that can be built into ceramics by design at the base composition stage include thermal expansions in the range -20×10^{-7} to 200×10^{-7} $^{o}C^{-1}$, strengths in the range 6×10^{7}-10^{8} N/m^2, any degree of transparency,

durabilities from soluble to inert and electrical properties from semi conducting to insulating [19]. New crystalline phases unobtainable by other routes are sometimes produced which adds to the excitement of this field [29].

The factors that influence the final properties of a glass-ceramic and therefore those that the technologist seeks to control can be listed as follows and Figure 3.1 summarizes this philosophy.

1. Properties of crystalline phases*:* In this case, as compared to traditional ceramics, the intrinsic properties of the crystals will have a major effect on the final properties of the material and the role of texture will be less dominant.
2. Grain size.
3. Intergranular bounding. This property, together with grain size, dominates in the final strength and appearance of the product.
4. Crystal orientation.
5. Percentage crystallinity and distribution of any remaining glassy phase. Although glass-ceramics should be 100% crystalline, this is not always possible to attain and indeed for some applications it is desirable to have a residual glass phase [19].

The development of practical glass-ceramics is comparatively recent although it has long been known that most glasses can be crystallized or devitrified if they are heated for a sufficient length of time at a suitable temperature. This knowledge led to the early attempts by Réaumur (1739), a French chemist, to produce polycrystalline materials from glass. He showed that if glass bottles were packed into a mixture of sand and gypsum and subjected to red heat for several days they were converted into opaque porcelain like objects. Although Réaumur was able to convert glass into a polycrystalline ceramic, he was unable to achieve the control of the crystallization process since the obtained materials had low mechanical strengths [18].

It became recognized that, in order to achieve the desired end product, it would be necessary to provide many sites within the glass body on which subsequent crystal growth take place. It was not, however, until the 1950s that research Corning Glassworks (USA) and subsequently at other establishments in the worldwide demonstrated that, under suitable conditions, a usable polycrystalline ceramic could be obtained by the controlled devitrification of a glass.

It has also been known for many years that a considerable number of glasses are, in fact, not single phase, but are to some extent (and possibly only a microscale) separated into two or more distinct phases. This phenomenon has been seen to be a necessary step in the preparation of a glass-ceramic but over the years it has posed a problem for the glass technologist in that a phase separated glass is likely to possess inferior properties, particularly in terms of corrosion resistance. In certain cases this has been turned to advantage, for example, in the Corning Vycor process [30] for making a high silica glass from a borosilicate glass and also for the preparation of microporous membranes for the desalination of water [31,32].

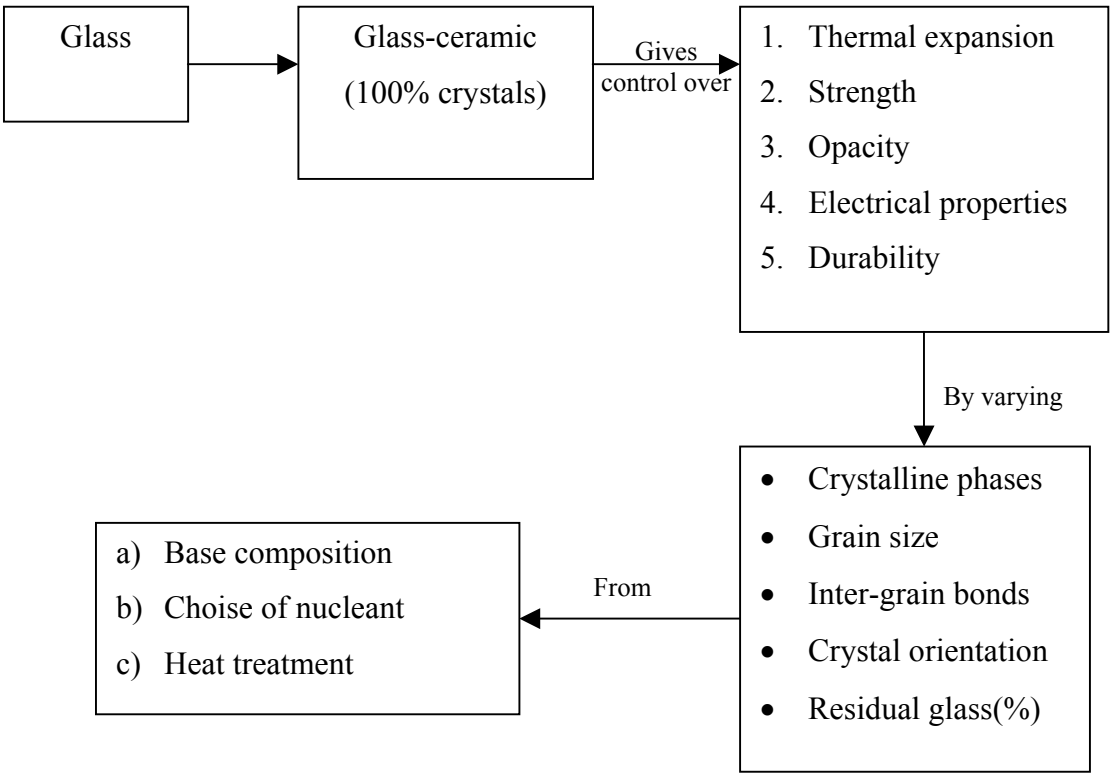

Figure 3.1: Controlling variables in glass-ceramic production [19]

Over the years, greater understanding of phase separation in glasses and of nucleation and crystallization phenomena has been achieved [33,34]. This has enabled the range of materials, because their mode of preparation are referred to as glass-ceramics [35,36]. A wide range of glass-ceramics is now possible and is continually being added to, so that materials possessing the properties to fulfil many

applications can be made or are becoming available. The advent of glass-ceramics has enabled the overall range of polycrystalline ceramic materials to be extended and amplified and has enabled applications to be addressed that would not readily be possible with other types of ceramics, e.g. sintered materials [14].

3.2 The Scientific and Technological Importance of Glass-ceramics

The investigation and development of glass-ceramics are closely related to studies of nucleation and crystallization of supercooled liquids and are therefore of general interest in this field. Crystal nucleation and growth studies are investigations of amorphous phase separation. This subject is of the basic phenomena involved and with regard to modifications of glass properties that accompany the structural change.

The wide range of compositions that can be produced in the vitreous state is particularly valuable since it allows phase transformations to be investigated in widely differing chemical environments. The development of many crystal types, including metastable and stable phases and the formation of solid solutions, can be investigated under controlled conditions. Because molten glass is a good solvent for metal oxides, for certain metals and some for halides and other compounds, the effects of these, present as minor constituent, upon crystal nucleation and growth processes can be investigated. Such studies, in addition to their basic importance, are of considerable interest in relation to the development of glass-ceramic microstructures.

In addition to their value for the study of physico-chemical effects, glass-ceramics are also valuable for fundamental investigations of certain physical properties. One important field is the investigation of mechanical strength and fracture process for brittle solids. Glass-ceramics are especially valuable in such studies because they can be produced to have a very fine microstructure and in addition can contain a wide variety of crystal types. A further valuable possibility is that for identical chemical compositions, the degree of crystallinity can be varied from the amorphous glass at one extreme to the almost completely crystalline glass-ceramic at the other. This

latter possibility is of interest not only in studies of mechanical failure but also in the investigation of properties that are dependent on diffusion process.

In materials science, glass-ceramics are of importance because they offer combinations of physical properties not available with other classes of materials. To the glass technologist, the development of glass-ceramics is of great interest not only because they extend the possible applications of glass making techniques but also because the search for new glass-ceramic stimulates research into glass compositions and the relative stabilities of various types of glass. Many of these data can be a value in the development and production of conventional glasses. In the field of conventional glasses it is interesting to study the relationship between crystallographic constitution and physical properties. Investigations of glass-ceramics may be particularly valuable because the crystal phases present can be varied in a controlled manner and materials having identical chemical compositions at different crystallographic compositions can be prepared. The possibility of investigating the effects of variations in the proportion and chemical composition of the vitreous phase in glass-ceramics is also a value since in some conventional ceramics the vitreous phase plays an important part in determining certain properties.

An important feature of the glass-ceramic process is that it is applicable to a wide range of compositions and this, together with the variations which can be applied in the heat treatment process, means that various crystal types can be developed in controlled proportions. As a result, the physical characteristics of glass-ceramics can be varied in a controlled manner and this fact has an important bearing upon the practical applications of glass-ceramics. For example, the thermal expansion coefficients of glass-ceramics can be varied over a very wide range so that at one extreme materials possessing low expansion coefficients and having very good resistance to thermal shock are possible while at the other extreme materials possessing very high thermal expansion coefficients closely matched to those of common metals can be obtained.

The use of glass working processes such as pressing, blowing or drawing offers certain advantages over the techniques available for shaping conventional ceramics since glass lends itself to the use of high speed automatic machinery. In general, the

techniques used for shaping conventional ceramics, such as extrusion, jolleying or slip casting are slower than glass shaping methods and a further point is that the ceramic ware usually requires extended drying and firing periods to avoid distortion and cracking. The advantages of the glass-ceramic process are particularly apparent in the production of thin-walled hollow-ware and other shapes where the section of the material is small since unfired conventional ceramic articles of this type are fragile, while the parent glass articles in the glass-ceramic process are relatively strong.

During conversion of the glass to the glass-ceramic form, a change in dimension occurs. However, this change is small and controllable so that control of the shape and dimensions of the glass-ceramic article can be achieved without too much difficulty. With conventional ceramics, relatively large shrinkages (40 to 50 % by volume) occur during the drying and firing operations and these dimensional changes may be accompanied by distortion. Consequently, control of the final dimensions is more difficult for conventional ceramics than for glass-ceramics.

The glass-ceramic process has certain special characteristics which allow new process to be applied. Since the materials originate as glasses they can be bonded to metals by relatively simple processes based on the fact that glass in its molten state will wet other materials. Thus it is possible to seal the parent glass to a suitable metal and to heat the composite article to convert to glass into a polycrystalline glass-ceramic. This method has many advantages over the processes available for conventional ceramics that involve complicated and expensive pre-treatment and furnacing procedures.

In recent years, important advances have taken place in the control of glass-ceramic microstructures resulting, for example, in the development of machinable glass-ceramics and in the production of bulk and fibreous glass-ceramics having orientated microstructures.

Glass-ceramics have become established as commercially important materials in the fields such as consumer products, vacuum tube envelopes, astronomical telescopes, radomes for the aerospace industry, protective coatings for metals, microwave

radomes, microelectronic substrates, packaging, domestic cooker tops, cooking utensils and biomedical applications [14,18].

Glass-ceramics can be regarded as a most valuable addition to the materials available to the design engineer. Being inorganic and non-metallic they combine useful high temperature capabilities with a high degree of chemical stability and corrosion resistance. Their unique combination of properties is likely to make them attractive for a number of specialised engineering applications [18].

3.3 The Crystallization Process

Crystallization is the process by which the regular lattice of the crystal is generated from the less well-ordered liquid structure. In its simplest form, crystallization is observed when a melt of a single pure element or compound is cooled; conversion from the liquid to the solid state occurs at a temperature that is fixed for a given pressure and is known as the freezing point.

A very important and fundamental observation which is valid for crystallization process and indeed for other phase transformation processes such as the formation of liquid drops in a vapor phase is that the transformation does not occur simultaneously throughout the mother phase. The transformation proceeds from distinct centers and crystal growth takes place by deposition of material upon the first tiny crystals or nuclei. Two stages of the crystallization processes are therefore distinguished: Nucleation and crystal growth. The first part involving the formation of a stable nucleus and the second, growth of a nucleus to form a crystal.

3.3.1 Nucleation

Nucleation involves the formation of regions of longer range atomic order than are normally present in the liquid phase. These unstable intermediate states are known as embryos and the embryos having a critical minimum size which are capable of developing spontaneously into gross particles of the stable phase are known as nuclei. Nucleation is classified as homogeneous if it occurs within a pure phase and as heterogeneous if the nucleus is formed at an interface, such as container walls, bubbles or particles of a second phase. Glass materials form because of the large

energy barrier to homogeneous nucleation then it is likely that heterogeneously nucleation is more important in the formation of glass-ceramics. Therefore nucleation catalysts are added to the base of glass composition. In order to consider the addition of such agents less empirically and to explain the features they should possess, it is useful to compare the two nucleation mechanisms on a quantitative basis [18,19].

3.3.1.1 Homogeneous nucleation

When a liquid is supercooled, formation of a crystal nucleus is possible. This involves two changes: First, a liquid to solid phase transformation; second, the formation of a solid-liquid interface. For homogeneous nucleation all foreign nuclei must have been excluded and this is always difficult to prove.

Tamman (1925) made classical studies of crystallization in supercooled liquids including inorganic glasses which contributed greatly to the knowledge of nucleation and crystallization processes [18]. He showed that below the equilibrium melting temperature there exists a temperature interval, referred to as the metastable zone, in which nuclei do not form at a detectable rate. In this zone, however, crystals can grow if nuclei are provided, i.e. if the melt is seeded or inoculated. At temperatures below this region the crystallization process is controlled by two factors: The rate of formation of nuclei and the crystal growth rate. Melts which increase rapidly in viscosity during cooling, such as those which can form glasses, show maxima in nucleation and crystal growth rates because at the lower temperatures the high viscosity hinders the atomic rearrangements and diffusion processes which are necessary for nucleation and crystal growth. Consequently, curves for nucleation and crystal growth rate for a viscous melt have the form shown in Figure 3.2.

It is evident from this figure that if the aim is to produce the largest possible number of small crystals, nucleation should occur at or near to the temperature at which the maximum nucleation rate occurs. It is clear that selection of the optimum nucleation temperature is important in the production of glass-ceramics.

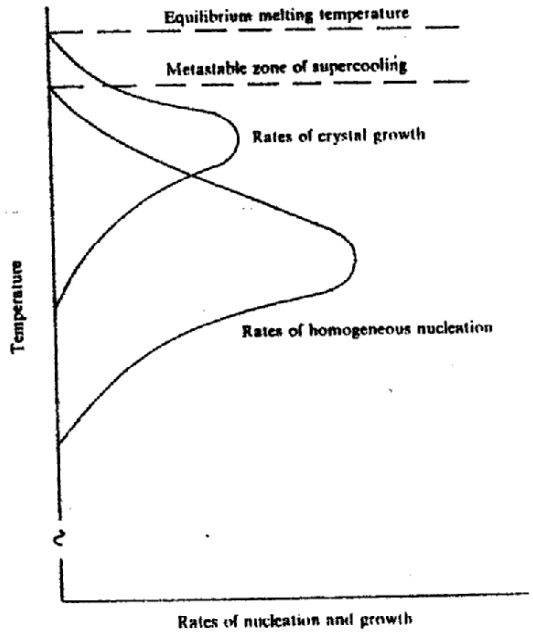

Figure 3.2: Rates of homogeneous nucleation and crystal growth in a viscous liquid [18]

The metastable zone of supercooling (T_1-T_2) below the equilibrium melting temperature occurs because the very tiny crystal nuclei have melting temperatures appreciably below that of the bulk material. Similarly, the metastable zone of supersaturation in solutions results from the higher solubility of small crystallites as compared with that of larger crystals. From Figure 3.2 it will be noted that there also exists a temperature, T_3, below which the homogeneous nucleation is zero due to the high viscosity of the melt [18].

3.3.1.2 Heterogeneous nucleation

In heterogeneous nucleation the nucleus develops on the surface of a foreign solid (substrate). The substrate may be container wall or it may be a solid dispersed throughout the liquid. If we introduce a suitable substrate into an undercooled liquid, we are able to reduce the energy barrier to nucleation. However, choosing a suitable substrate is an important point. The substrate needs to be thoroughly wetted by the liquid, but that is all we know. Crystal chemistry here comes to aid in the form of epitaxial growth, sometimes called oriented overgrowth. If we put into an undercooled liquid a seed crystal which has a low index plane in which the atomic

spacing and arrangement are similar to those of one of the low index planes in the crystal that wishes to form, then the liquid will start to crystallize on the foreign nucleus. If there is no near match, then the liquid will not crystallize. But, how much disregistry can be tolerated? It seems to at least 15% maximum for metal systems. In the case of glass-ceramics however, a digregistry of 8% would seem to be the maximum which can be tolerated. Even so, after only six lattice spacings there will be complete mismatch [22].

The effect of pre-existing surfaces (such as colloidal inclusions, container walls, etc.) in a supersaturated solution or a supercooled melt is to reduce the value of ΔG, the free energy for homogeneous nucleation, by decreasing the interface energy. The volume free energy change between the liquid phase and the crystal phase is not altered by heterogeneous nucleation and neither is the activation energy for diffusion, E. The important feature of heterogeneous nucleation is that the interfacial tension between the heterogenity and the nucleated phase must be low. Therefore, the influence of the catalysing surface is determined by the contact angle at the substrate-melt-precipitate junction.

To summarize the considerations of heterogeneous nucleation; there are two important criteria which determine the effectiveness of a nucleation catalyst. There are:

- The interfacial tension between the nucleation catalyst and the primary crystal phase must be low.
- The crystal structures must be closely similar so that the digregistry on low index planes is not more than about 15%[18].

It is generally agreed that crystallization in glass forming systems almost always occurs by heterogeneous nucleation, usually proceeding from an external surface or an interior bubble or other discontinuity [37].

3.3.2 Crystal Growth

The controlled crystallization of glasses involves crystal growth as well as nucleation. While the latter process is highly critical to the production of microcrystalline glass-ceramics, the growth process is also of considerable

importance in determining the morphology of the material produced. Crystal growth is dependent upon two factors:

- The rate at which the irregular glass structure can be rearranged into the periodic lattice of the growing crystal
- The rate at which energy released in the phase transformation process can be eliminated. This is the rate of heat flow away from the crystal glass interface.

Considering first the process of structural transformation; an atom in the crystal structure has a lower free energy than a corresponding atom in the glass phase by an amount ΔG, the bulk free energy of crystallization. Also, for an atom to cross the interface between the glass and crystal phases it must overcome an energy barrier corresponding to an activation energy of crystal growth, E. Thus an expression for crystal growth rate, U, can be derived:

$$U = \frac{f}{a_0} D''\left[1 - \exp(-\Delta G / RT)\right] \qquad \textbf{(3.1)}$$

where f is the fraction of site at the interface where molecules can preferentially be added, a_0 is the molecular diameter, D'' is the diffusion coefficient for transport across the crystal liquid interface.

The expression describes what is known as normal growth. It is based on the assumption that the probability of an atom being added to or removed from a given site is the same for all sites on the crystal liquid interface and this requires the interface to be rough on atomic scale [18,38].

Returning the equation (3.1), the diffusion coefficient is generally expressed as follows:

$$D'' = D_0 \exp\left[-\frac{E}{RT}\right] \qquad \textbf{(3.2)}$$

where E is the activation energy for diffusion, D_o is the pre-exponential constant. At relatively low temperatures, the temperature dependence term of the [1-exp(-$\Delta G/RT$)] is negligibly small compared with that of D''[39]; therefore, equation (3.1) can be rewritten as

$$U = U_0 \exp\left[-\frac{E}{RT}\right] \qquad \textbf{(3.3)}$$

where the energy E may be considered as the activation energy for crystal growth[38].

It is also important to emphasis the effect of change of viscosity in modifying crystal growth rates in glasses. Thus although the growth rate increases at first as the melt is cooled below the liquidus temperature, the rapid increase of viscosity soon exerts a dominating influence causing the growth rate to fall and giving rise to the typical growth rate curve (Figure 3.2)[18].

3.3.2.1 Determination of activation energy for crystal growth by differential thermal analysis

The controlled transformation of glass into a polycrystalline material occurs during a predetermined heat-treatment process. The heating rate, time and temperature influence average dimensions of crystals, volume fractions of crystalline and vitreous phases and types of crystal. As a result, properties and characteristics of the glass-ceramics can be varied in a controlled manner. Therefore, the determination of the heat treatment schedule is one of the most important steps in the production of glass-ceramic material [18,40,41].

Parameters required for the heat treatment process can be obtained from crystallization kinetic studies. Differential thermal analysis (DTA) has been extensively used in investigating the crystallization kinetics of glasses as a rapid and convenient means for detecting the reaction process. The rate of chemical reaction was analyzed quantitatively by DTA and the activation energies were obtained. Furthermore this method was used to obtain the activation energy for the crystallization of glass, assuming that the process of crystallization is a first order reaction. The physical meaning of the activation energy thus obtained is obscure, however, considering that the crystallization of glass is advanced by nucleation and growth mechanism [38].

Theoretical analysis

As the crystallization proceeds in glass, the heat of crystallization is evolved and the exothermic peak appears on the DTA curve. The heat balance during a time period, dt, in the DTA process can be approximately expressed by the equation [42,43].

$$d(\Delta H) = C_p\, d(\Delta T) + K\Delta T\, dt \qquad \textbf{(3.4)}$$

Where C_p is the heat capacity, ΔT is the temperature difference between the sample and reference material, ΔH is the amount of heat associated with crystallization and K is the heat transfer coefficient. Assuming C_p and K to be independent of temperature and accordingly, of time over the reaction period, the following expression can be derived,

$$\Delta H = C_p \int_{t_1}^{t_2} d(\Delta T) + K \int_{t_1}^{t_2} \Delta T dt \qquad \textbf{(3.5)}$$

Since ΔT is zero at both $t=t_1$ and $t=t_2$, the first term of the right hand side of the equation is zero. The integral in the second term means the total area under the curve, A. Therefore,

$$\Delta H = KA \qquad \textbf{(3.6)}$$

Substituting the relation $dx = d(\Delta H)/\Delta H$ (where ,x is the volume fraction of crystal) and equation (3.6) into equation (3.4), we obtain,

$$\frac{dx}{dt} = \frac{1}{KA}\left[C_p \frac{d(\Delta T)}{dt} + k\Delta T \right] \qquad \textbf{(3.7)}$$

It is known that, usually, the rate of crystal nucleation in glasses reaches its maximum at a temperature somewhat higher than the glass transition temperature and then decreases rapidly with increasing temperature while the rate of crystal growth reaches its maximum at a temperature much higher than the temperature at which the nucleation rate is highest [44-49]. In other words, for the heating of glass at a constant heating rate, crystal nuclei formed at lower temperatures grow in size at higher temperatures without an increase in number [47,49]. It should be noted that there are two types of crystallization; one based on bulk nucleation and the other based on surface nucleation [38].

In the case of bulk nucleation, the variation of crystal volume fraction is expressed [50] by

$$\frac{dx}{dt} = 4\pi n r^2 (1-x)\frac{dr}{dt} \qquad \textbf{(3.8)}$$

where n is the number of crystal nuclei per unit volume of the sample formed in the course of heating and r is the radius of crystal particle. In deriving equation (3.8), the impingement of crystal particles and reduction of the glass phase are taken into account [50]. (1-x) is the correction factor for the impingement of crystal particles and reduction of the glass phase. This factor is also used to derive the Johnson-Mehl-Avrami (JMA) equation [51]. The rate of crystal growth, U, was derived by equation (3.3). The radius of crystallite, r, is expressed as follows,

$$r = \int U_0 \exp(-E/RT)dt = \frac{U_0}{\alpha}\int \exp\left(\frac{-E}{RT}\right)dT \qquad \textbf{(3.9)}$$

where α is the heating rate (α = dT/dt). This integral can not be expressed by any elementary function and the following approximation is made,

$$r \cong r_o \exp(-E/RT) \qquad \textbf{(3.10)}$$

From equations (3.3), (3.8) and (3.10),

$$\frac{dx}{dt} = 4\pi n r_o^2 U_o (1-x)^k \exp\left(\frac{-mE}{RT}\right) \qquad \textbf{(3.11)}$$

$A = 4\pi n r_o^2$ = constant and $U_o = \alpha^{-(n-1)}$ are taken,

$$\frac{dx}{dt} = A\alpha^{-(n-1)}(1-x)^k \exp\left(\frac{-mE}{RT}\right) \qquad \textbf{(3.12)}$$

where R is the gas constant and n, m and k are numerical factors which depend on the crystallization mechanism (m depends on the dimensionality of crystal growth). The parameters n, m and k can take on various values, as summarized in Table 3.1[52-55].

In the case of interface controlled growth where U is independent of time, m has the values of 1, 2 and 3 for one-, two- and three-dimensional growths, respectively. For diffusion controlled growth where U is dependent of time, m is assumed to be 1/2, 1 and 3/2 for the respective dimensionalities of growth [56].

Table 3.1: Values of n and m for different crystallization mechanisms in the heating process [52-55]

Crystallization Mechanism	n	m	k
Bulk crystallization with a constant number of nuclei (i.e. the number of nuclei is independent of the heating rate)			
Three-dimensional growth of crystals	3	3	1
Two-dimensional growth of crystals	2	2	1
One-dimensional growth of crystals	1	1	1
Bulk crystallization with an increasing number of nuclei (i.e. the number of nuclei is inversely proportional to the heating rate)			
Three-dimensional growth of crystals	4	3	1
Two-dimensional growth of crystals	3	2	1
One-dimensional growth of crystals	2	1	1
Surface Crystallization	1	1	2/3

The rate of increase of x reaches its maximum at a temperature T_p. Solving equation (3.12) for d(dx/dt)/dt =0, the following equation is derived:

$$\frac{\alpha^n}{T_p^2} = \frac{AKR}{mE}(1-x_p)^{k-1}\exp\left(\frac{-mE}{RT_p}\right) \qquad \textbf{(3.13)}$$

where x_p is the fraction crystallized at T_p. According to the Table 3.1 k is equal to 1 for bulk crystallization. Therefore $(1\text{-}x_p)^{k-1}$ is equal to 1 for all cases. For surface crystallization (k = 2/3), usually, the change of $(1\text{-}x_p)^{k-1}$ is negligibly small compared with the exponantional term and $(1\text{-}x_p)^{k-1}$ can be taken as constant. Therefore, equation (3.13) is rewritten as

$$\ln\left(\frac{\alpha^n}{T_p^2}\right) = \left(\frac{-mE}{RT_p}\right) + \text{constant} \qquad \textbf{(3.14)}$$

The activation energy is found from the slope (-mE/R) of a plot of $\ln(\alpha^n/T_p^2)$ against $1/T_p$, on substitution of the appropriate values for n, m and R [38,55].

Activation energy for crystallization

Many different methods can be used for estimating the activation energy of a process, e.g. crystallization of a glass, but care is required in the choice of method and in the interpretation of data obtained. It should also be noted that values determined for activation energy may be compound values (corresponding, for example, to nucleation and growth processes or overlapping of two or more crystalline phases) rather than specific to a single process. Techniques can be broadly classified into isothermal and non-isothermal methods [57]. In the isothermal method, glass samples are quickly heated up and held at a temperature above the glass transition temperature. Crystallization occurs at a constant temperature. In the non-isothermal method, glass samples are heated up at a fixed heating rate and crystallized during the thermal analysis scan. Generally, an isothermal experiment takes longer than a non-isothermal experiment. On the other hand, non-isothermal experiments themselves are rather simple and quick, but assumptions are usually required for data interpretation due to the deficiency of uniquely accepted equations for non-isothermal analysis [58].

Isothermal Methods

In general, isothermal methods are related through application of the Johnson-Mehl-Avrami (JMA) transformation kinetic equation [43,59-62]:

$$x = 1 - \exp(-kt^n) \qquad \textbf{(3.15)}$$

where x is the fraction crystallized at a given temperature in time t; k is the reaction rate constant and n, the Avrami exponent, is a dimensionless constant which is related to the nucleation and growth mechanisms. The reaction rate constant, k, is related to the activation energy for the process, E, through the Arhenius temperature dependence

$$k = \nu \exp(-E/RT) \qquad \textbf{(3.16)}$$

where ν is frequency factor and T is the (isothermal) absolute temperature. Taking logs, equation (3.16) may be rewritten as:

$$\ln(k) = \ln(\nu) - E/RT \quad \textbf{(3.17)}$$

Appropriate values of k are found experimentally by plotting the fraction crystallized, x, against the isothermal hold time for a range of different temperatures. From these plots, the time to reach a given x can then be found for a range of x values. Values for k and n are then determined using the relationship (derived from equation (3.15) by taking logs and rearranging)

$$\ln [- \ln(1-x)] = n \ln k + n \ln t \quad \textbf{(3.18)}$$

The above equation indicates that a plot of ln [- ln(1-x)] against lnt for different temperatures is expected to be linear and gives the values of n and k. A plot of ln k against 1/T for different isothermal temperatures is also expected to be linear according to the equation (3.17). From these plots, the values of E and ν can thus be obtained by isothermal method [57].

Non-isothermal methods

Several equations have been proposed, attempting to interpret the non-isothermal data [63-69]. Most of these equations assume that the variation of peak crystallization temperature, T_p, on non-isothermal analysis curves is directly related to the heating rate, α. Apparent activation energies for crystallization may be determined employing non-isothermal methods to the crystallization peak. For example, in the Kissinger method [70], the crystallization peak temperature is monitored as a function of the heating rate; the following relationship is then applied

$$\ln\left(\frac{\alpha}{T_p^2}\right) = \left(\frac{-E_{ck}}{RT_p}\right) + \text{constant} \quad (3.19)$$

where E_{ck} is activation energy for crystallization, determined by the Kissinger method. A plot of ln (α/T_p^2) vs $1/T_p$ should be straight line, from the slope of which E_{ck} can be determined. Matusita-Sakka[38, 54, 71] have stated that equation (3.19) is valid only when crystal growth occurs on a fixed number of nuclei. Incorrect values for the activation energy are obtained if a majority of the nuclei are formed during the DTA measurement, so that the number of nuclei continuously varies with α. They have proposed a modified form of the Kissinger equation as given before (equation (3.14))

$$\ln\left(\frac{\alpha^n}{T_p^2}\right) = \left(\frac{-mE_c}{RT_p}\right) + \text{constant} \qquad \textbf{(3.14)}$$

where E_c is the correct activation energy for crystallization. When surface crystallization predominates, m = 1 and when the crystallization is predominantly bulk, m = 3(from Table 3.1). The value of m is related to n as m = n when crystallization at different heating rates occurs on a fixed number of nuclei (i.e., the number of nuclei is constant during DTA runs at different values of α), and m = n-1 when nucleation occurs during DTA and the number of nuclei in the glass is inversely proportional to α.

In addition, when surface crystallization predominates, m = n = 1 and equation (3.14) essentially reduces to the Kissinger equation will yield the correct value for the activation energy, i.e., $E_{ck} = E_c$.

In the presence of bulk crystallization, E_{ck} does not necessarily to be equal to E_c. Rather, a close inspection of equations (3.14) and (3.19) shows that

$$E_c = (n/m)\, E_{ck} - 2\,((n-1)/m)RT_p \qquad \textbf{(3.20)}$$

For most oxide glass systems, $E_c \geq 20\ RT_p$ typically [56]. Therefore, the neglect of $2\ ((n-1)/m)RT_p \leq 2\ RT_p$ in equation (3.20) will result in an error less than only 10 % in the value of E_c. This error is within the error range of the DTA experiment. Then we obtain

$$E_c \cong (n/m)\, E_{ck} \qquad \textbf{(3.21)}$$

For m = n, i.e., when crystallization occurs on a fixed number of nuclei, $E_{ck} = E_c$. Thus, for predominantly surface crystallization or for crystal growth that occurs on a fixed number of nuclei, the analysis of DTA data by the Kissinger model (equation (3.19)) yields the correct value of E_c. When the number of nuclei changes during the DTA measurements, either, equation (3.14) should be used or E_{ck} determined from equation (3.19) should be multiplied by the term (n/m) to obtain the correct activation energy [72].

From the exothermic peak, the Avrami parameter,n, can be obtained by using the modified Ozawa equation[73]:

$$\left|\frac{d(\ln(-\ln(1-x)))}{d\ln\alpha}\right|_T = -n \qquad \textbf{(3.22)}$$

where x is the volume fraction crystallized at a fixed temperature T with the heating rate of α. x is the ratio of the partial area at a certain temperature to the total area of a crystallization exotherm (Figure A.1). The value of n close to 1 means that surface crystallization dominates overall crystallization while the value of 3 implies a significant contribution of the bulk crystallization process [74].

3.4 Glass-ceramic Process

The preparation of glass-ceramic involves a number of steps, the first one of which, as the name implies, is the preparation of a glass. The mixture of raw materials that will form the desired composition is melted in a suitable container at a temperature generally in the range 1273 to 1973 K (depending on the composition). After refining and homogenization to provide a good quality glass, the molten glass is worked by the usual methods employed in the glass industry, for example, casting, pressing, drawing or chilling to form glass frit that can subsequently be reduced to glass powder.

Many, although not all, of the compositions that form glass-ceramics are silicate based and the ranges of compositions that can be melted and which can then be converted to the polycrystalline structure of a glass-ceramic are now extensive. The earliest glass-ceramics were based on lithium silicate and lithium aluminosilicate compositions but many alkali free materials now available that are more refractory and with improved mechanical and electrical, particularly dielectric, properties. The fabrication routes for all these materials can take advantage of bulk glass shaping techniques or the materials can be processed via powder routes similar to those employed for sintered ceramics[14].

3.4.1 Bulk glass-ceramics

For any given bulk glass, the tendency and ability to crystallize can be expressed in terms of the nucleation and crystal growth curves given in Figure 3.2, which illustrate rates of homogeneous nucleation and crystallization in a glass. Below the equilibrium melting temperature there exists a temperature interval, referred to as the metastable zone, in which nuclei do not form at a detectable rate, owing to the fact that the very small crystal nuclei have melting temperatures significantly below that of the bulk material. Crystals can grow in this region, if nuclei of a sufficient size are provided by seeding (heterogeneous nucleation). At temperatures below this region the crystallization process is governed by the rate of formation of nuclei and the crystal growth rate. As the temperature falls the nucleation and crystallization rates increase, as shown in Figure 3.2, passing through maxima as the increasing viscosity of the glass hinders the atomic rearrangements and diffusion processes necessary for nucleation and crystal growth. Eventually, at still lower temperatures, the viscosity becomes so high that the nucleation and crystallization processes cease [14].

Generally, the nucleation and crystallization curves overlap to some extent, as shown in Fiure 3.2, and this permits crystal growth to start when a large number of nuclei are present, thus enabling the desired fine crystal structure to be obtained. It is clear that if the aim is to produce the largest number of small crystals than the greatest number of nuclei, on which crystal growth can commence simultaneously, temperature and holding time are very important. It has been demonstrated that the greatest number of nuclei are not necessarily developed by heating at the temperature of the maximum nucleation rate, but rather at a lower temperature and maintaining that temperature for extended periods of time [75]. Under these conditions, a long induction period may be observed before nucleation starts, although the subsequent number of nuclei formed is high.

The preparation of a satisfactory glass-ceramic from a bulk glass thus depends on crystallizing the glass composition under strictly controlled conditions, determined by previous experimentation, in order to provide the desired closely interlocking, microcrystalline structure and a smooth surface, free from cracks and other blemishes. In order to achieve this, it has usually been necessary to include a

constituent in the glass that will provide the nuclei for subsequent crystal growth or influence the structural reorganization in the glass in such a manner that many crystals of the desired types grow in the glass. Table 3.2 lists some of the nucleating agents that have been used by different workers [76]. Oxide nucleants such as TiO_2, P_2O_5 and ZrO_2 have been employed and are preferred to give better results than any one of the individual nucleants used in the same total proportion [14,58,59].

Table 3.2: Nucleating agents used in glass-ceramics [76]

Metals	Au, Ag, Cu, Pt
Single nucleating agents	TiO_2, P_2O_5, ZrO_2, Fe_2O_5, V_2O_5
Complex nucleants	P_2O_5+TiO_2, P_2O_5+ ZrO_2, P_2O_5+MoO_3, P_2O_5+ WO_3, TiO_2+P_2O_5, ZrO_2+TiO_2

3.4.1.1. The heat treatment process

The object of the heat treatment process is to convert the glass into a microcrystalline ceramic having properties superior to those of the original glass. It is especially important to achieve a high mechanical strength and since this is favored by a fine-grained microstructure, the aim is to produce a glass-ceramic containing crystals of small dimensions which are closely interlocked.

A clear idea of the various stages of the heat treatment process will be obtained by reference to Figure 3.3 which represents an idealized heat treatment schedule for a glass-ceramic. It is proposed to consider the different parts of the heat treatment schedule in further detail so that the various factors of importance may be emphasized.

The crystallization of the desired phases at controlled grain sizes is achieved by carrying out two step heat treatment sequences causing first the copious nucleation of crystallites, followed by crystal growth. The object is formed from the glass at a working range viscosity of about 10^4 poise, corresponding to a temperature range near the liquidus at 1523 K. The glass object is then heated from room temperature to the nucleation temperature [21]. Generally, speaking, the rate of heating employed

here is not critical so far as the crystallization process is concerned. It is limited mainly by the requirement that dangerously high stresses which might cause cracking shall not be generated due to temperature gradients within the glass articles. The thickness of the glass ware will chiefly determine the rate of heating which can be employed, although the thermal expansion coefficient of the glass will also play a part since glasses with low expansion coefficients can withstand higher temperature gradients without cracking than can the glasses with high expansion coefficients. Normally heating rates between 2 and 5 K/min will be employed, although for thin glass ware rates as high as 10 K/min can safely be used.

The optimum nucleation temperature generally seems to lie within the range of temperatures corresponding with viscosities of 10^{11} to 10^{12} poises. The temperature within this range which gives optimum nucleation temperature is determined by experimentation. As a first approximation, the optimum nucleation temperature lies between the glass transition temperature and a temperature 50 K higher than this. A more exact determination of the optimum nucleation temperature may be carried out by the following method. A droplet of glass is melted in a furnace provided with means for measuring the temperature of the glass droplet accurately and rapidly and arranged so that the droplet can be under microscopic observation. The droplet is cooled to an arbitrarily chosen temperature, held at this temperature for a minute or so and then reheated to the lowest liquidus temperature of the glass (when several different crystal phases can be produced by the devitrification of a glass it will posses a corresponding number of liquidus temperatures). If on reheating to the lowest liquidus temperature no crystallization occurs, the glass droplet is completely remelted and cooled to a slightly lower temperature than before and is again reheated to observe crystal formation, if any. This procedure is continued until the temperature of maximum nucleation has been determined. The period of time for which the glass is maintained at the nucleation temperature will usually change from 0.5 to 2 hours, although longer periods may not have a detrimental effect. Although nucleation can occur at any temperature between the temperature of nucleation and the annealing point, the use of lower temperatures for nucleation can greatly increase the time for nucleation to be completed since the rapid increase of viscosity as the temperature falls leads to great reduction of the nucleation rate. For example, at the annealing point corresponding to a viscosity of $10^{13.4}$ poises, a period of 100 hours

may be required to achieve satisfactory nucleation of glasses containing TiO_2 as the nucleating agent. An important point to note in connection with the nucleation process is that to achieve a glass-ceramic of optimum strength, the glass must be cooled below the maximum nucleation temperature before the nucleation heating stage. This will often occur in the natural course of events, since the material will be cooled in the glassy state and annealed at a temperature below the nucleation temperature, followed by slow cooling to room temperature. In some cases, however, the crystallization heat treatment process may follow immediately from the shaping of the glass ware and in these cases it is necessary to cool the glass substantially below the nucleation temperature and in some cases the temperature interval necessary may be as much as 373 K to 573 K.

As an alternative to the procedure outlined in the preceding paragraph, the optimum temperature for nucleation may be determined by heat treating specimens for a fixed period (eg. 1 hour) at various temperatures in the nucleating range and then transferring them to a furnace held at a crystal growth temperature. After a pre-determined time the specimens are removed from the furnace. The specimens are effectively quenched, therefore the crystal growth process is arrested. By means of optical and electron microscopy, the number of growth centers and mean crystal diameters can be established and shown to be strongly dependent upon the nucleation temperature used.

Following the nucleation stage, the temperature of the glass is increased at a controlled rate sufficiently slowly to permit crystal growth to occur so that deformation of the glass article will not take place. Crystallization occurs increasingly rapidly as the liquidus temperature of a predominant crystalline phase is approached but, to prevent deformation in the early stages when the glass phase predominates, as a heating rate not usually exceeding 5 K/min is employed. The permissible heating rate can readily be determined by experiments in which rods supported two knife edges are subjected to the nucleation heat treatment stage and are then heated at various rates. The sag occurring at the center of the rod is afterwards measured and used as a guide to decide upon an acceptable rate of heating.

The upper crystallization temperature for a glass-ceramic is chosen so that maximum crystallization can be achieved without leading to excessive deformation of the material. The temperature at which the final product will deform appreciably will correspond to the liquidus temperature of the predominant crystal phase since increasing the temperature above this liquidus will cause the phase to redissolve. The upper crystallization temperature will be lower than the temperature at which the predominant crystalline phase will redissolve by a suitable interval, usually 298 to 323 K.

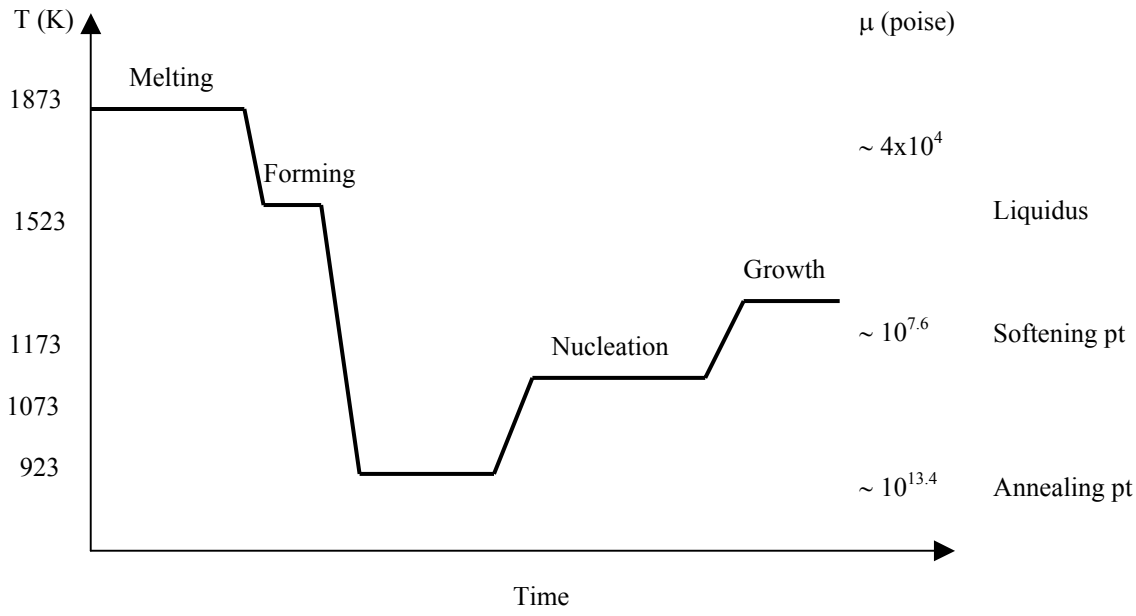

Figure 3.3: Heat treatment schedule for a glass-ceramic [21]

The upper crystallization temperature, determined by one of the foregoing methods, is maintained for a period of at least one hour, but longer holding periods may be employed if this is necessary in order to achieve the desired degree of crystallinity in the glass-ceramic. After completion of the holding period the glass-ceramic is cooled to room temperature. Cooling can be quite rapid since the glass-ceramic can withstand fairly high temperature gradients because of their high mechanical strengths. A certain amount of care is exercised in cooling materials of high thermal expansion coefficient although, cooling rates as high as 10 K/min can often be employed and for the low expansion materials faster cooling still is quite safe. Unlike glasses, glass-ceramics do not require annealing to prevent the generation of permanent strains in the materials.

Some of the crystalline phases present may exhibit structural changes in certain temperature zones and these changes are accompanied by alterations of density and thermal expansion coefficient. In a conventional ceramic, structural changes of this type can cause breakage unless the ceramic is cooled slowly though the critical temperature zone. For glass-ceramics, this limitation is not found to the same degree since quite rapid cooling through critical temperature zones does not cause fracture of the material. The superiority of glass-ceramics in this respect may be due to the very small sizes of the crystals present, since the stresses generated as a result of volume changes would be small [18].

3.4.2 Bulk glass-ceramics via powder techniques

This method of combining the powder particles to form a bulk material follows essentially the principles of conventional sintered ceramic technology. The difference lies in that the starting powder is a glass, sintering and crystallization processes occur in the one firing cycle.

The advantages of this method are essentially that relatively thin films of the dielectric material can readily be obtained as described below in a process which is likely to be cheaper than the bulk approach where a significant proportion of substrate cost can result from machining operations. A problem is that, in common with other sintered materials, closed pores are present in the fired product, which reduce dielectric properties, dielectric breakdown
strength, mechanical strength and capability of obtaining a high quality surface finish.

A number of types of glass-ceramic have been examined by the authors for the preparation of bulk materials via the powder route, including materials of the LiO_2-Al_2O_3-SiO_2, ZnO-Al_2O_3-SiO_2 and MgO-Al_2O_2-SiO_2 types. Nucleation and crystallization phenomena in the materials differ from those experienced in the bulk glass-ceramics. This arises in part from the nature of the particle surface which results in a greater predominance of surface crystallization processes rather than bulk nucleated crystallization.

Glasses of the various types are prepared in a similar manner to those for bulk materials. Following refining the glasses are cast into cold water or on to cold metal plates to provide frit. After drying (if necessary), the glass frit is reduced to powder by milling. It is essential to determine the particle size distribution required for the preparation of the sintered glass-ceramic body, which is controlled in subsequent batches of the powder as part of quality assurance procedures.

The required sintering conditions vary to some extent with the method of forming the green state body, requiring that each case be treated individually in the final iterations of process development. The powder processing routes for the preparation of glass-ceramic substrates are:

1. Compacting by means of die pressing or isostatic pressing
2. Screen printing
3. Tape casting

Compacting by pressing

This involves incorporation into the powder of a binder such as diethylene glycol monostearate (DGMS) or polyvinyl alcohol (PVA) which will hold the powder particles together in the desired shape prior to further processing.

Screen printing

This process is utilized for the build up multilayers on a previously prepared substrate, which can be a suitable organic film from which the screened material can be separated. The powder and organic binder are mixed to form an ink which can be screened through a suitable mesh. This method offers the advantage of preparing thin layers in selected patterns.

Tape casting

This process is again involves mixing powder and suitable organic liquids to form a viscous substance which can be applied via a doctor blade process on to a suitable organic carrier film to form a continuous tape. The ceramic/binder mix sets

sufficiently to form a flexible tape which can be used to form multilayer structures after pre-processing such as punching holes through the tape. This method has been used with ceramics such as alumina and $BaTiO_3$ (capacitors) but it is only recently that glass-ceramics have been investigated and utilized in this context.

Firing

Following the preparation of green state glass-ceramic body the material has to be sintered to maximum density. As a first stage the binder has to be burned out at temperatures in the region of 773 K and during this process sufficient oxygen must be maintained in the furnace atmosphere to enable this to occur without leaving any deleterious deposits (e.g. carbon). Subsequently, as the temperature is raised to promote sintering, the furnace atmosphere is not necessarily oxidizing and in some cases is advantageously neutral. The firing continuous to temperature in the range 1073 to 1473 K, depending on composition. In this stage of the process sintering occurs by solid reactions between the particles and by flow as the glass particles soften. At the same time crystallization in the particles is progressing by a combination of bulk and surface processes, particularly latter in fine powders. By this means, the loosely bounded initial glass powder is converted to a dense, glass-ceramic material [77].

3.4.3 Changes in physical characteristics of glass-ceramics brought about by the heat treatment process

An obvious change brought about by the heat treatment is to conversion of the transparent glass to an opaque polycrystalline material. The opacity of the glass-ceramic is due to scattering of light at interfaces between adjacent crystals and between crystals and the residual glass phase due to the differences in refractive indices of the phases. In certain instances, where the crystals are small and the refractive indices of the various phases are fairly closely matched, the glass-ceramic may be transparent or translucent.

In addition to obvious change in appearance, there is another, more subtle change which is only apparent when the materials are examined under high magnifications.

To the eye and to the touch glass-ceramics appear perfectly smooth, but examination by the electron microscope reveals that their surfaces are not so smooth as those of the parent glasses. Clearly, the result of heat treatment is to produce a generally undulating surface made up of rounded crystal boundaries and occasionally there are angular crystals which project above the mean surface level. Even though the surface of glass-ceramic is less smooth than that of a glass, this difference is not significant in most practical applications. A further point is that glass-ceramic surfaces will be considerably smoother than those of unglazed conventional ceramics.

The specific gravity of a glass-ceramic is very often different from that of the parent glass because small volume changes may occur during the heat treatment process. These changes may involve either a slight contraction or a slight expansion of the material but they would not usually exceed a 3% volume change. This may be contrasted with the large volume changes which occur during the drying and firing of conventional ceramics which may quite often total as high as 40 to 50%. The volume changes in glass-ceramics are a result of the overall differences in specific gravity of the crystalline phases which are formed as compared with those of the parent glasses. The crystal phases formed may have higher or lower densities than the glass so that the net effect of crystallization can be to cause a contraction or an expansion of the material.

The relatively small dimensional changes which take place during heat treatment constitutes one of the advantages of the glass-ceramic process over conventional ceramic manufacturing techniques, since it enables articles to be produced to much closer dimensional tolerances.

The thermal expansion coefficients of glass-ceramics are generally markedly different from those of the parent glasses. Devitrification of the glass may result in raising or lowering of the thermal expansion coefficient depending on the types of crystals which are formed. The formation of cristobalite, for example, will give materials with high expansion coefficients, especially for the temperature range 293 to about 473 K. On the other hand, the formation of the lithium aluminosilicate type crystals such as beta spodumene or beta eucrptite can give materials having very low thermal expansion coefficients.

Another change in physical characteristics brought about by devitrification is the increase in refractoriness of the material.

Perhaps the most striking and important change in characteristics is the increase of the mechanical strength.

Generally speaking, the electrical properties of glass-ceramics are superior to those of the parent glasses and in particular the electrical resistivities are higher and dielectric losses are lower. This improvement in properties can to a large extent be attributed to the tighter binding of ions, especially alkali metal ions within the regular crystal lattices as compared with the disordered glass structure [18].

3.5 Glass Compositions for Glass-ceramic Production

In any given part of a glass forming system, one crystal phase is likely to predominate on conversion to glass-ceramic. Typical examples of the principal crystal phases that develop in a number of glass-ceramic forming systems are given in Table 3.3. The phases that are produced are influenced not only by the major constituents in the composition of the material, but minor constituents in the glass-ceramics can also have a profound effect. For example, the presence of large ions such as K_2O and BaO, in proportions up to about 5% in a high expansion Li_2O-SiO_2 (low Al_2O_3) based material, favor the silica crystal phase appearing as quartz rather than cristobalite. Another interesting phenomenon is associated with the presence of small proportions of ZnO (about 1%) in glass-ceramics which can prevent their discoloration in neutral or reducing atmospheres resulting from the presence of iron in the materials. This is thought to arise from the capability of ZnO to release oxygen at elevated temperatures [14]. Phase composition may also be affected by the heat treatment given to the glass, particularly for glasses of high silica contents [78,79]. These, in turn, will have a significant effect on the properties of the glass-ceramics. Thus, it is important to appreciate that the crystal phases derived by the glass-ceramic process do not necessarily correspond with those which might be anticipated from the study of phase diagrams. This is to be expected in view of the different

methods involved in developing crystal phases in glass-ceramics and those used to produce crystal phases in phase diagram construction [14].

3.6 The Properties of Glass-ceramics

Glass-ceramic materials can be considered as a non-porous matter consisting of fine crystals uniformly distributed throughout a residual glass phase. As glass-ceramic materials contain arbitrarily oriented crystals, their properties are independent of direction. The extremely fine and uniform structure, even distribution throughout the bulk of the material, and the absence of pores are important characteristics in the structure of glass-ceramic materials [36].

Table 3.3: Examples of crystal phases developing in glass-ceramics [14]

Glass-ceramic systems	Crystal phases
Li_2O-Al_2O_3-SiO_2 (low Al_2O_3)	Quartz, Cristobalite, Lithium disilicate, Lithium metasilicate
Li_2O-Al_2O_3-SiO_2 (low Al_2O_3)	Beta spodumene, Beta eucryptite
Li_2O-MgO-SiO_2	Quartz, Cristobalite, Lithium disilicate, Lithium metasilicate, Enstatite, Forsterite
Li_2O-ZnO-SiO_2	Quartz, Cristobalite, Lithium disilicate, Lithium metasilicate, Willemite
MgO-Al_2O_3-SiO_2	Quartz, Cristobalite, Enstatite, Forsterite, Cordierite
ZnO-Al_2O_3-SiO_2	Quartz, Cristobalite, Willemite, Gahnite

The properties of glass-ceramic materials depend primarily on the physico-chemical properties of the main crystalline phase and the size of the crystal, residual glass, the amount and morphology of glass phase present in the total bulk material and the interface formed between the crystalline and glass phase. A review of some of the more important properties are summarized below [18]:

3.6.1 General physical and chemical properties

3.6.1.1 Microstructure and porosity

One of the notable characteristics of glass-ceramics is extremely fine grain size and it is likely that this feature is responsible in a large measure for the valuable properties of the materials. It is true to say that a glass-ceramic can have an almost ideal polycrystalline microstructure since, in addition to the fine texture, the crystals are fairly uniform in size and they are randomly oriented.

In general, the average crystal size in useful glass-ceramics is not greater than a few microns and materials with mean crystal sizes as small as 200 to 300 Å are known. For some material prepared by the crystallization of the glasses, however, greater mean grain sizes are obtained especially where the nucleation density is low and the crystal growth is spherulitic in nature but such materials do not have good mechanical strengths.

In addition to the crystalline phases, there is usually a residual glass phase. It should be noted that this phase does not normally have the same chemical composition as the parent glass since it will be deficient in those oxides which have taken part in crystal formation.

In contrast to the fine microstructure characteristic of glass-ceramics, the average crystal size of sintered alumina ceramics is in usually in the vicinity of 10 to 20 microns and that in mineral based ceramics such as an electrical porcelain may be up to 40 microns.

Although ceramics made by conventional techniques can often be quite impermeable to liquids or gases so that their apparent porosity is zero and they are vacuum tight, they are rarely, if ever, completely free from closed pores. In a sintered high alumina ceramic the percentage of closed porosity is usually in the region of 5 to 10% and in a feldspathic porcelain of the type used for electrical insulators it is about 10%. In contrast with conventional ceramics, glass-ceramics are entirely free from any type of porosity, providing the glass from which they are prepared is free from gas

bubbles. Porosity does not develop during the conversion from the glass to ceramic state since the overall volume changes are very small. Quite often the volume change is a shrinkage but even when the conversion is accompanied by a volume increase, voids do not develop within the interior of the material, the volume increase being due to the production of crystals of lower density than the original glass. The complete absence of pores in glass-ceramics is a characteristics which favors the development of good properties since pores will reduce the mechanical strength by diminishing the useful cross-section and the material [18].

3.6.1.2 Density

The density of a glass-ceramic will be an additive function of the various crystal and glass phases present. Since the volume change which occurs during conversion from the glass state to the glass-ceramic is usually small, it would be expected that the effects of various oxides on the densities of glass-ceramics would be similar to those observed with conventional glasses. Broadly speaking, it is true because this oxides, such as barium or lead oxides, which tend to confer high densities on glasses also result in glass-ceramics with high densities. Similarly, glass-ceramics having lithia as a major constituent have low densities, as do glasses containing this oxide. It is also found that increases of the proportions of MgO, CaO, ZnO, BaO or PbO at the expenses of Al_2O_3 or SiO_2 in the glass-ceramics lead to higher densities and that BaO and PbO exert the most marked effects. In some glass-ceramics, oxides present in minor amounts may exert a significant influence on the density because they affect the types of major crystal phases which are present [18].

3.6.1.3 Chemical durability

The resistance of a material to chemical attack by water or other reagents is of considerable practical importance. The processes involved are often very complex and methods of studying chemical durability usually involve subjecting a sample of carefully controlled surface area to closely specified test conditions. Often, the process of attack is accelerated, as compared with anticipated service conditions, by employing conditions of increased temperature and, in some cases, pressure.

Tests of this nature have indicated that glass-ceramics in general posses good chemical stability and that they compare favorably in this respect with other ceramic type materials.

In many cases, it is likely that when a glass-ceramic is chemically attacked the initial effect is on the glass phase present. This occurs because the early stages of attack involve ion exchange between hydrogen and mobile cations (usually alkali metal ions) in the glass. Subsequently the silica network structure can be attacked by a process hydration. The greater mobility of alkali metal ions in the glass phase as compared with that of similar ions incorporated in crystal phases, will lead to greater reactivity of the glass phase and hence to inferior resistance to chemical attack.

Certain types of glass-ceramics have good resistance to attack by corrosive chemical reagents. Low expansion glass-ceramics derived from lithium aluminasilicate glasses are only slightly inferior to borosilicate chemically resistant glass with regard to attack by strong acids. They are also more resistant to attack by alkaline solutions. Even at high temperatures, certain types of glass-ceramics can be resistant to attack by corrosive gases [18].

3.6.2 Mechanical properties

Mechanical properties such as strength, elasticity, hardness and abrasion resistance are influenced by particle size and volume fraction of the crystalline phase, interfacial bond strength and differences in elastic modulus and differences in thermal expansions. Increased strength over the parent glass is a result of fine grain and uniform microstructure.

3.6.2.1 Mechanical strength

The mechanical strength of a material is one of the most important property since it is often the major factor in determining the suitability of the material for a particular application. In addition, other important characteristics, such as the ability of a material to withstand sudden temperature changes without failure, are strongly influenced by mechanical strength. Not only it is desirable to have a high mechanical

strength at normal ambient temperatures but also to retain high strengths at elevated temperatures since quite often the material may be required to operate under such conditions. For these reasons it is necessary to know how the strength of a glass-ceramic is influenced both by its constitutions and by external factors. Composition, heat treatment processes, temperature and surface conditions affect the mechanical strength of glass-ceramics.

Interpretations of the results of mechanical strength investigations on glasses have relied very heavily on the well known expression for mechanical strength, σ, derived by Griffith (1920):

$$\sigma = \sqrt{\frac{2E\gamma}{\pi c}} \qquad \textbf{(3.23)}$$

where E is the elastic modulus, γ is the fracture surface energy and c is the length of the critical flaw. From this it is evident that increase of strength would occur only if E or γ were increased or if c were reduced. It is of interest to consider the relative importance of these parameters with regard to the mechanical strength of glass-ceramics.

The mechanical strength, σ, of a glass-ceramic is related to the mean grain diameter, d, by the well known Hall-Petch relation:

$$\sigma = Kd^{-1/2} \qquad \textbf{(3.24)}$$

where K is tensile factor. The implication of this relationship is that the crack length, c, in the Griffith equation is proportional to the grain diameter.

The mechanical strengths of glass-ceramics are higher than those of many conventional ceramics and glasses when comparison is made using specimens that have received the same abrasion treatment. The complete absence of pores has already be mentioned as factor contributing to high strength. This, however, does not provide a sufficient explanation for the observed strengths and it seems that a combination of factors may be responsible. The various possibilities are as follows [18]:

1. The elastic moduli of glass-ceramics are significantly greater than those of glasses and thus theories of mechanical strength based on a critical strain concept would predict a higher strength for glass-ceramics. This explanation is insufficient, however, since glass-ceramics are often stronger than glasses by a greater factor than the ratio of the elastic moduli.
2. Glass-ceramics are harder and more abrasion resistant than glasses and surface damage leading to loss of strength is likely to be less severe for a given abrading condition.
3. The combination of crystal and glass phases having different thermal expansion may lead to a system of microstresses that favors high mechanical strengths. Where the crystal has a higher thermal expansion coefficient than the surrounding glass, the radial stresses in the glass will be tensile. Where the crystal posses the lower expansion coefficient, the signs of the stresses are reversed.
4. The presence of crystals in a glass-ceramic causes deflection and possibly blunting of the fracture tip. Thus the work of fracture is increased and the crack may be slowed down or even arrested as it traverses or crosses boundaries between crystalline or glass phases whereas in glass there will be an uninterrupted fracture path.
5. It is probable that the mechanical strengths of glass-ceramics are controlled by the severity and distributions of microcracks in the surface. These factors will be controlled by the surface microstructure of the glass-ceramics if, as seems likely, the microcracks are propagated across crystal glass boundaries with greater difficulty than through the intervening glass. In this case length of the microcracks will be related to the sizes and volume fractions of the crystal phases and it is probable that an optimum microstructure will exist which will result in a minimum average microcrack length and therefore in maximum mechanical strength [18].

The Young's modulus and bending strength of glass-ceramic materials can be compared with other materials. This is shown in Tables 3.4 and 3.5[36].

Table 3.4: Young's modulus of glass-ceramic materials compared with other materials [36].

Material	Young's modulus (MPa 10^{-4})
Glass-ceramic	8-14
Sodium-calcium glass	7.0
Boro-silicate glass	6.6
Ceramics (High Al_2O_3)	28-35
Marble	2.7-8.2
Granite	4.2-6.0

Table 3.5: Bending strength of glass-ceramic materials compared with other materials[36].

Material	Bending strength (MPa)
Glass	55-70
Glass-ceramic	70-350
Glass-ceramic with modified surface	Up to 1400
Electro porcelain (glazed)	86-140
Ceramics (High Al_2O_3)	212-353
Cast iron	140-320*
Steel	300-1400*

* Tensile strength

3.6.2.2 Elastic properties

The elastic properties of a material are of great importance in determining its behavior when it is subjected to deformation. For example, the modulus of elasticity fixes the levels of stress which are generated if a glass-ceramic is strained by the application of a temperature gradient. This can occur when the material is suddenly heated or cooled. In this case a low modulus of elasticity is desirable. Similarly, if the glass-ceramic is to be sealed to another material having a different coefficient of thermal expansion a low modulus of elasticity is useful since for a given strain the

stress will be lower. There are cases, of course, where a high modulus of elasticity may be desirable. This situation exists for glass used in fiber form for reinforcing plastics.

The moduli of elasticity for glass-ceramics are higher than those of ordinary glasses and of some conventional ceramics, but they are lower than those of sintered pure oxide ceramics. The moduli of elasticity of glass-ceramic materials compared with other materials is shown in Table 3.6. For glasses, the modulus of elasticity, E, shows a roughly additive relationship with chemical composition. The modulus of elasticity of a polyphase ceramic will also be an additive function of the individual characteristics of the crystalline and glassy phases. In a glass-ceramic it is to be expected that the modulus of elasticity will be determined primarily by the elastic constants of the major crystalline phases although the presence in the glass phase of oxides which promote the development of high values of E must be allowed for; in particular, calcium oxide, magnesium oxide and aluminum oxide appear to exert a marked influence on the elastic moduli of glasses [18].

Table 3.6: Bending strength of glass-ceramic materials compared with other materials[36].

Material	Elasticity modulus (MPa 10^4)
Glass	7.2
Sodium-calcium glass	6.9
Glass-ceramic	8.3-13.8
Electro porcelain (glazed)	6.6
Ceramics (High Al_2O_3)	36.6
Pyrex	6.6

3.6.2.3. Hardness and abrasion resistance

Hardness is not a fundamental physical characteristics of a material but rather it is a complex function of physical properties which are combined in differing degrees depending on the method of test. In a sense, we can equate the hardness of a material with its resistance to abrasion or wear and this characteristic is of practical interest

since it may determine the durability of a material during normal use and it may also decide the suitability of the material for special applications where abrasion resistance is of prime importance. Thus, the resistance of the material to abrasion under closely specified conditions may be taken as one measure of hardness. The resistance to scratching of the material by other materials represents another measure of its hardness and the depth of penetration of a loaded pyramid (usually a diamond) into the material under specified conditions represents yet another measure of hardness.

The maximum hardness corresponded approximately but not exactly with the maximum volume fraction of the crystal phase in the glass-ceramic suggesting that microstructural effects influence hardness. Researches have indicated that the nature of the crystal phases may play a highly significant role in determining hardness. Some crystal phases, even when present in only a small volume fraction seem to result in marked enhancement of hardness. Phases of the spinel type appear to be particularly effective in this respect.

It is thought that a more practical and reliable method of studying the relative hardnesses of glass-ceramics would be to abrade them under standard conditions and to measure the amount of which occurs. In considering the wear occurring between glass-ceramic parts which are moving in contact with one another due to sliding or rotation, the extent to which friction occurs becomes important. For this reason, it is of interest to know the values for coefficients of friction between glass-ceramic surfaces [18].

3.6.3 Electrical properties

3.6.3.1 Electrical resistivity

If a glass-ceramic is to be used for electrical insulation, its resistivity should be as high as possible. In many cases the insulating material is required to operate at or near to normal ambient temperatures but in some devices the insulator may be required to operate at elevated temperatures and for these applications the variation of electrical resistivity with temperature is important.

Depending on chemical composition and on the nature of the crystal phases present, the electrical resistivities of glass-ceramics can vary widely. Values of resistivity at 573 K, for example, range from 10^6 to 10^{12} ohm cm.

3.6.3.2 Dielectric loss

The dielectric losses for glass-ceramics is more complicated than glasses. It is difficult to assess the exact effects of the various crystal phases and of the residual glass phase, since the precise chemical composition of glass is not usually known. The dielectric losses for single crystals are small and mainly determined by minor impurities and it is likely that the glass phase of the glass-ceramic is the main contributor to dielectric losses. This means that to achieve low losses the amount of residual glass phase must be as small as possible. In addition to the effects of chemical constitution, the dielectric losses of a glass-ceramic, like a glass, are related to the frequency which is measured at a specific temperature. The general effect for the losses is to increase the temperature, although the temperature dependence of dielectric losses become less marked as the frequency increases.

3.6.3.3 Dielectric strength

If an insulating material is subjected to a large voltage gradient, failure of the material may occur due to puncture. This possibility is one of the important factors which govern the design of high voltage insulators. Dielectric breakdown strength is also of importance in the design of capacitors required to operate at high voltages such as those used for energy storage applications.

Glass-ceramics have high dielectric breakdown strengths compared with conventional ceramics. It may be partly due to the complete absence of closed pores in the former materials. Porosity tends to give variations in the local electrical field thus giving rise to low measured values. The very homogeneous and fine grained nature of the glass-ceramics may be another factor which favors high breakdown strengths [18].

3.6.4 Thermal Properties

3.6.4.1 Thermal expansion coefficient

The dimensional changes which occur with change of temperature are of great importance from a number of points of view. For example, if a glass-ceramic is required to have high thermal shock resistance, the thermal expansion coefficient should be as low as possible to minimize strain resulting from temperature gradients within the material. Also if the glass-ceramic is to be sealed or otherwise rigidly joined to another material such as a metal, close matching of the thermal expansion coefficients is necessary to prevent the generation of high stresses when the composite article is heated or cooled. In some applications, dimensional stability with change of temperature may be important and a glass-ceramic of near zero thermal expansion coefficient would be required for this.

Glass-ceramics are remarkable for the very wide range of thermal expansion coefficients. At one extreme, materials having negative thermal expansion coefficients are available while for other compositions very high positive thermal expansion coefficients are observed. Between these two extremes there exists glass-ceramics having thermal expansion coefficients practically equal to zero and others whose thermal expansion coefficients are similar to those of ordinary glasses or ceramics or to those of certain metals or alloys.

The thermal expansion coefficient of a glass-ceramic can be markedly different from that of the parent glass. The glass-ceramic may have a higher or lower thermal expansion coefficient depending on the crystal phases formed. While the development of crystal phases usually causes the major changes in the thermal expansion coefficient, crystallization will alter the composition of the residual glass phase from that of the parent glass and this must be taken into account when attempting to analyze the thermal expansion coefficients in glass-ceramics in relation to their constitution. In certain cases, the changes in composition of the residual glass phase result in changes of the thermal expansion coefficient of a sufficient magnitude to counterbalance the effects of the development of the crystal phase.

An extremely wide range of thermal expansion coefficients is covered by the different crystal types and the development of these phases in appropriate proportions forms the basis of the production of glass-ceramics having controlled thermal expansion coefficients. Thus a low thermal expansion coefficient glass-ceramic may contain beta-eucryptite, beta-spodumene or cordierite as major phases while at the other extreme, a high thermal expansion coefficient glass-ceramic contain major proportions of crystals such as lithium disilicate, quartz or cristobalite.

3.6.4.2 Refractoriness

The temperature to which a glass-ceramic can be heated without exhibiting deformation can be important if the material is required to operate or to be processed at high temperatures. For this reason, it is necessary to know how glass-ceramics compare with other ceramic type materials with regard to refractoriness and it is also useful to relate this characteristic to the glass-ceramic type.

The factors which govern the deformation of a glass-ceramic are complex, since there are one or more crystal phases present together with a residual glass phase; this phase is probably distributed fairly uniformly between the crystals. It is very likely that it is the characteristics of the glass phase which largely govern the refractoriness of a glass-ceramic since most of the crystal phase have high melting temperatures. Obviously, the proportion of glass phase present will have a strong bearing on the refractoriness of the glass-ceramic and from this point of view it is desirable to limit the glass phase to the smallest possible proportion. In addition, the composition of the glass phase is of great importance and it is necessary to ensure that oxides which will lower the softening temperature of the glass phase are present only small proportions. Oxides which would have this effect include the alkali metal oxides, boric oxide and lead oxide.

Glass-ceramics are more refractory than most conventional glasses since, although some aluminasilicate glasses may have dilatometric softening temperature of 1073 K or so, and fused silica glass is even more refractory, commonly available glasses have dilatometric softening points not exceeding 773 to 873 K. Thus glass-ceramics are more suitable for high temperature applications than most glasses. Comparison

with conventional ceramics is not too easy since the methods of assessing refractoriness often differ from those which have been used for glass-ceramics. Nevertheless a qualitative comparison can be made and it appears that glass-ceramics are generally less refractory than high alumina ceramics.

3.6.4.3 Thermal conductivity

A glass-ceramic may be required for use as a thermal conductor or as a thermal insulator and its suitability for these applications will be largely determined by the rate of heat transfer through it under a given temperature gradient. A reasonably high thermal conductivity is desirable if the material is to be used for cooking vessels. In addition, the thermal shock resistance of the material is influenced by the thermal conductivity. The thermal conductivities of glass-ceramics are somewhat higher than those of glasses but lower than those of pure oxide ceramics [18].

3.6.5 Optical Properties

The most important optical property is radiation transmission. Although some glass ceramic materials are translucent or transparent or transmit infrared radiation. Most of the materials are opaque. The passage of light is affected primarily by the crystal size and if the crystals are smaller than the wavelength of visible light, then the glass-ceramic material is transparent. Transparent glass-ceramic materials with high permittivity show good electro-optical properties [36].

3.7 Applications of Glass-ceramics

The applications can, in broad sense, be termed as engineering and thus glass-ceramic may be considered to fall within the general class of materials referred to as engineering ceramics. Increasingly, ceramics, including glass-ceramics, are being used for critical components outside their traditional engineering areas of electrical insulation and in domestic applications. They are used because of their properties that are quite unlike any other group of materials and nothing else can fit the requirements. These properties include; hardness and wear resistance, resistance to oxidation and to high temperatures, resistance to chemical attack, dimensional

stability, optical and other transmission characteristics and specific electrical properties.

Of course, not all glass-ceramics can be expected to posses all these characteristics. Each material, each proprietary product has both advantageous and disadvantageous properties when it comes to engineering performance. It is the function of the glass-ceramic experts, in collaboration with design engineers, to develop materials and component designs to fulfil the needs of specific applications. Examples of the ways in which this has been achieved with glass-ceramics, often in competition with other ceramic materials, are given below, which covers the principal uses of glass-ceramics at the present time.

3.7.1 Engine applications

The use of ceramic materials in engines is seen as a way towards increasing engine efficiency and allowing engines to operate at higher temperatures than can currently be realized because of limitations imposed by the metals and alloys that are presently available. The general properties of glass-ceramics suggest that they could be potentially useful in engine applications, both for diesel and gas turbines. Interestingly, in spite of the useful combinations of properties available, together with their capabilities of providing adherent coatings or strongly bonded composite structures, little work has been carried out in this field with glass-ceramics [14]. One of the most important glass-ceramic developments has been as rotary heat exchangers in which a low expansion lithium aluminosilicate fabricated to a honeycombe section with through channels, was employed. The hot gases from the engine heated a section of the device which rotated continuously so that the hot sections were able to heat incoming air [80]. Ceramic seals and bearings were developed for these applications.

A limited amount of work has also been carried out to investigate low expansion and cordierite glass-ceramics for cylinders [81] and to examine the possibilities of providing coatings onto nickel based turbine blades with the aim of enhancing corrosion resistance. Glass-ceramics are more likely to be used in diesel engines to increase resistance to corrosion and act as thermal barriers. In addition, the glass-

ceramic processing capabilities suggest that these materials offer a high potential for thermal expansion matching and high quality bonding to the various metals and alloys employed in the engine [14].

3.7.2 Pumps, valves and pipes

The high hardness and excellent abrasion resistance of glass-ceramics suggest their use for the construction of pumps, valves and pipes for handling abrasive slurries. In addition, the good chemical durabilities of many glass-ceramics enable them to be used in contact with corrosive liquids under conditions where many metals would undergo unacceptable deterioration. Stainless steel components can be used in some applications but the superior resistance to wear of glass-ceramics would be advantageous. The low thermal expansion coefficient confers high thermal shock resistance rendering the components suitable for handling hot fluids. The use of techniques which enable metal parts to be firmly attached to the glass-ceramic or the cladding of metal components with an abrasion resistant coating gives the potentiality for great flexibility of design [18].

3.7.3 Machinable glass-ceramics

The materials that have been described so far can be further shaped after forming and heat treatment by means of suitable machining. This requires the use of diamond tipped and occasionally silicon carbide tooling because of the hardness of the materials. It would be useful, in some instances, if post shaping were made easier and this has been achieved in the case of glass-ceramics in which mica flakes of the phlogopite and fluorophlogopite types have been precipitated during heat treatment [82,83]. A number of mica containing glass-ceramics are available that can be shaped using more conventional metal working tooling. This offers considerable advantages for the preparation of certain complex shapes and for the development of prototypes, but the cost of these materials limits their more general use [14].

3.7.4 Refractory glass-ceramics

The ability of a ceramic type material to withstand high temperatures is important in a number of applications in which either processing and/or usage temperatures are necessarily high. Resistance to temperature in the region of 1173 K is needed. Other potential applications include engines where even higher temperature capability will be essential. Glass-ceramics that are capable of withstanding temperatures well in excess of 1273 K are now well established. Materials of the magnesium aluminosilicate and zinc aluminosilicate types, together with barium silicate materials fall into this category. However, the biggest advance which has been made in this direction has been the introduction of nitrogen, replacing some of the oxygen in selected compositions.

Study of nitrogen containing glass-ceramics originated from the need to make the glassy phase in sialon (Si-Al-O-N, made by firing silicon nitride with alumina added essentially as a sintering aid) ceramics more refractory in order to improve the high temperature capabilities of these materials. Following studies on the ceramic systems the glass and glass-ceramic compositions were prepared independently and the overall range extended [84]. Incorporation of nitrogen into to the glasses influences their properties significantly, essentially as a result of the nitrogen producing a more tightly bonded glass structure [85]. Properties such as density, hardness, Young's modulus and glass transition temperature all increase with increasing nitrogen content, whereas the thermal expansion of the glass decreases [14].

3.7.5 High dielectric constant materials

Ceramic materials possess high dielectric constants. They can be used in infrared sensors, as capacitors, as pizoelectrics, as magnetic materials and in optoelectronic devices [86]. Sintered ceramic materials based on barium, strontium or lead titanates are predominant in this field and can possess dielectric constants in excess of 20000. There are some advantages, however, to be gained by fabricating materials via glass-ceramic routes, particularly where very high dielectric constants are not required and where the dielectric can be produced in thin section using bulk fabrication routes. Although it has been demonstrated that glass-ceramics possessing dielectric

constants up to 11500 are possible [87]. In practical terms the highest dielectric constant that can usefully be realized in a barium titanate in the range 2000-2500 measured at a frequency of 1 MHz. The advantage of glass-ceramic over the sintered material is that it can be made in a pore free condition via bulk processing routes, which provides much higher dielectric breakdown strength, about ten times greater than can be achieved with the sintered material. Thus the glass-ceramic is more suitable for the high voltage applications [88]. It can also be readily made in a thin film form and this form possesses greater strength than the sintered material [14].

3.7.6 Storage of radioactive wastes

A number of solutions have been put forward to this difficult problem. Clearly, any material used for the storage of radioactive wastes must be impervious to attack not only by the wastes but also by any surrounding medium. Glasses and ceramics have been considered for uses where the waste material forms one of the constituents of the glass and ceramic. Glass-ceramics also offer considerable potential in this fields and materials can be prepared that will meet the exacting requirements. Glass-ceramics of the Na_2O-Al_2O_3-CaO-TiO_2-SiO_2 type have been prepared containing up to 20% by weight of simulated nuclear fuel recycle waste. Sphene ($CaTiSiO_5$) was the principal crystal phase developed and the uranium was found to be concentrated in the glassy phase [89,90].

3.7.7 Low and zero expansion glass-ceramics

Materials of this type are suitable for use in applications where dimensional stability with change in temperature is required, often in combination with good electrical , transmissive and mechanical properties. A number of approaches is possible. An attractive way to produce materials of very low expansion is to prepare glass-ceramics of the lithium aluminasilicate type in which the principal crystal phase developed is β-spodumene ($Li_2O.Al_2O_3.4SiO_2$) or β-eucryptite ($Li_2O.Al_2O_3.2SiO_2$). The presence of these crystals enables glass-ceramics with the thermal expansion coefficients in the range $–4x10^{-6}$ to $4x10^{-6}$ K^{-1}. Control of the nucleation/crystallization procedures [91] can enable materials that also possess high

transparency in the visible and near infrared to be obtained [92,93] combined with the low or nearly zero thermal expansion characteristics.

The low expansion transparent glass-ceramics have received most attention in recent years in two principal applications, namely telescope mirrors and laser envelopes [94] where their dimensional stability with change in temperature is of considerable value in reducing optical distortion (mirrors) and ensuring frequency stability (lasers). The high transparency enable this type glass-ceramics to be used as windows in the laser applications. An application that is well developed, is in ring lasers, where the laser is in the form of a triangle with mirrors at the truncated apices, used for gyroscopic guidance systems in aircraft etc, where the laser body contains a helium gas discharge [94,95].

A further development of a lithium alimunasilicate, low expansion, transparent type of glass-ceramics, with which the general public is more familiar, is in domestic cooker hot plates and cooking utensils. The hot plate and cooking dishes made in these materials must possess high strength and be resistant to thermal shock and to mechanical shock, which, it has been amply demonstrated, they do. The domestic area represents a large volume output of this type of glass-ceramic worldwide in the cooking dish field and in the cooker hob field. Large number of both items are produced annually [14].

3.7.8 Windows

Glass-ceramics that can transmit over a wide range of frequencies/wavelengths are needed. For transmission in near infrared, in the 3-5 μm wavelength, it is likely that aluminate materials will be preferred although others are possible. This may impose some penalties for dual mode operation in the near infrared and at milimeterwaves owing to the dielectric constant of these materials being in the region of ten but dual mode operation at microwave and in the near infrared may be possible.

Glass-ceramics of the magnesium aluminosilicate type have been seen earlier to provide windows for applications requiring transmissions at frequencies in the range

10-20 GHz [93]. In addition, their dielectric properties at higher frequencies suggest that they could be useful at milimetrewaves frequencies.

The high transmission, together with refractoriness, that can be achieved with certain glass-ceramics, particularly those of the magnesium aluminosilicate type, indicates their potential usefulness in the lighting applications [91]. Aluminate based materials may be more suitable for lighting uses involving sodium based discharge lamps, because of their expected higher resistance to attack by sodium vapor- although this would have to be proved [14].

3.7.9 Joining

3.7.9.1 Vacuum envelopes

The developments of glass-ceramics to join to further metals and alloys, particularly cheap and readily available ones, would clearly be of advantage, always with the essential thermal expansion matching being achieved. Further developments utilizing more refractory glass-ceramics are likely and necessary in order to meet competition from such materials as alumina and where higher vacuum bake-out temperature and/or higher operating temperature capability is required.

3.7.9.2 Coatings

Class-ceramic coating materials, for application to metals, that possess higher electrical resistivity, greater resistance to corrosion and with improved thermal dissipation characteristics are required. A possible way forward is by the use of sol-gel procedures. An alternative, that has some merit for a number of applications, is the modification of the properties of present coating materials in fine powder form and it is anticipated that more will be made of this aspect in the future [96].

3.7.9.3 Bonding media

Further development of nonmetallic bonds to join sintered ceramics such as SiC, Si_3N_4 and ZrO_2 to themselves and to appropriate metals is needed. At present, metallic bonding media are considered to be the most successful of the various

joining technologies available but vitreous joining systems have a lot to offer, particularly in terms of their stability and resistance to oxidation at elevated temperatures [14].

3.7.10 Superconducting materials

Any discussion on the potential uses of glass-ceramics would not be complete without mention of the preparation of superconducting materials by this technique. The discovery, in the mid 1980s, of ceramic materials that could exhibit a state of zero electrical resistivity at temperatures above the boiling point of liquid nitrogen (77 K), had considerable impact and a great deal of effort and resources were expended through out the world on these materials. This effort has now decreased as the enormity of problems to be overcome, particularly in high voltage, high current electrical applications and where high magnetic fields are present, has been appreciated. Present forecasts indicate that the successful and profitable use of these materials in power electrical engineering applications is a long way away [97]. However, more immediate applications in light current fields appear to be possible and real.

It has been realized that considerable advantage would ensure if glass-ceramic technology could be used, particularly for the preparation of fibers for use as conductors. Success with this has been realized with compositions of bismuth strontium calcium copper oxide (BiSCCO) type incorporation lead oxide (PbO) into the composition. Successful preparation of flexible fiber, rods, tapes and tubes has been achieved by redrawing from a cast boule (in a manner analogous to that used for the preparation of optical fibers)[98,99].

3.7.11 Glass-ceramics in biomedical applications

Ceramic materials find extensive use in biomedical applications. The most widely used has been high purity alumina (>99.5%) which is strong, highly resistant to attack by body fluids and which is very resistant to wear [100]. The areas in which glass-ceramics have been considered are as bone implants and as fillings for teeth. Glass-ceramics can be classed as either bioinert (not reacting with bone or other

tissue) or bioactive reaction occurs with the bone so that an integral structure is developed.

3.7.11.1 Bone replacements

The principal advantage of glass-ceramics in this field is in their potential as bioactive materials. Little advantage may accrue from their use as bioinert materials where they are likely to be less strong and less wear resistant than alumina. Those that have been studied have crystal phases, such as apatite, present so that bioactivity with the living bone can take place and developments have been directed towards improving the strength of the material and ease of forming to a near net shape product. Strengths comparable to those of human arm and leg bones have been achieved with glass-ceramics of the Na_2O-CaO-P_2O_5-SiO_2 type in which the principal crystal phases were $Ca_2P_2O_5$ and $Na_2Ca_3Si_6O_{16}$ with a mean crystal size of about 30 μm 101]. The presence of silicon has been established as increasing bone mineralising rates and shown to be useful for normal skeletal development.

Another approach has been to include constituents in the composition that will provide mica type crystals in the glass-ceramic. The presence of the mica crystals means that the glass-ceramics are readily machinable and adjustments can be carried out during the course of an operation, by the surgeon, if necessary. These glass-ceramics have been used successfully in a number of replacement situations, particularly in the spine and as tooth root implants.

Another approach has been to prepare composite structures comprising two interlocking crystal phases of $Ca_3(PO_4)_2$ and $MgAl_2O_4$ spinel [102]. As an implant, the phosphate phase is bioresorbable and is largely replaced by bone so that it acts as a means of stimulating bone growth.

3.7.11.2 Dental applications

This application of glass-ceramics is probably the best suitable area in biomedical usage. It would clearly be useful if the glass-ceramic could be made to be of a similar appearance to that of natural teeth., with which it will be placed adjacent and this can vary from person to person. A number of different compositions have been studied

for use as crowns including; potassium aluminasilicates applied onto a metallic dental prosthesis, lithium calcium aluminasilicates that are made by the powder technology route and which can readily be colored to match natural teeth, mica containing glass-ceramics for which the shaping of the article is carried out using a lost wax investment casting process, and calcium magnesium phosphorus silicate type, also made by a lost wax process, but only applied as a thin veneer to the tooth rather than as a full crown [103].

Filling of teeth, after decayed material has been removed, is one of the most important aspects of dentistry. For many years metal amalgams have been used, but use is now being made of glass and glass-ceramic materials in this application. These materials are usually in the form of a glass ionomer material which powder glass being mixed with an organic resin. Glass-ceramics of the above types may be used, the resin gripping the tooth cavity and the glass-ceramic providing wear resistance and color matching. In cases where higher strength is required in order to provide longer term resistance to chewing stresses the glass ionomer cement can be further strengthened by filling with amalgam in finely divided form [14].

3.8 Glass-ceramic Materials Obtained by Industrial Wastes

3.8.1 Glass-ceramics by Bulk Crystallization

The vitrification process to obtain glass-ceramics is a well established technique which improves the properties of a parent glass produced by using pure raw materials, as in the case of low thermal expansion glass-ceramics or industrial residues such as paving tiles or wall covering panels produced by vitrification and crystallization of foundry slags and thermal power plant fly ashes [104].

The more recent studies and applications are aimed at finding a recycling process for the huge amount of fly ashes generated from coal and oil fired electric power stations i.e. and industrial gaseous effluent purification, by producing marketable products for the building industry. Besides fly ashes and slag or mud from metallurgy, other quantitatively consistent industrial residues are the mud and scraps of the caving and sawing of natural rocks [105].

For the recycling and exploitation of coal fly ash, several approaches have been taken over half a decade to develop a glass-ceramic from coal fly ash produced by thermal power plants. Typically, glass-ceramics obtained from fly ash have been produced by a combination of melting the fly ash and a one or two stage heat treatment for crystallization, nucleation and crystal growth. Other approaches involving a sintering process have also been used.

The properties of glass-ceramics differ according to the make up of components and heat treatment conditions. In general the major component found in the ash is CAS (CaO-Al_2O_3-SiO_2), with minor components such as MgO, Na_2O present in order to form crystalline phase. In order to devitrify fly ash glass after melting, the composition of the ash is modified in terms of composition for internal crystallization. There are several ways to modify the composition of the fly ash [106]:

Some of the researchers used nucleating agents in the production of glass-ceramic materials from coal fly ash [107]. Cumpston et al. [108] produced glass-ceramic materials from coal fly ash with adding 1 wt.% TiO_2 to study the effect of nucleating agent on the microstructure of the samples. SEM studies showed that the use of these additives had little effect on the degree of crystallization, but it did improve the definition of the crystal shape and morphology. Kim et al. [106] used TiO_2 and CaO (using arc shell as the source of the CaO) as nucleating agents and also to decrease the melting temperature of the coal fly ash, meaning a more economical process. The obtained glass-ceramic samples showed sufficiently high wear resistance and fracture toughness to be used in building materials requiring good mechanical properties.

Another approach that can be found in the literature is to add different industrial wastes as minor constituent to coal fly ash to produce glass-ceramic. The addition of inorganic wastes such as SiO_2, CaO and Na_2O as a glass cullet and CaO and MgO as a float dolomite promote the formation of amorphous and semicrystallized materials. Glasses and glass-ceramics were obtained by mixing up to 50 % of Italian coal fly ash with glass cullet and float dolomite [109]. The behavior of ten compositions was investigated by differential thermal analysis and x-ray diffraction and microstructural

(SEM) characterization. It was verified that the contribution of the alkaline earth elements in the original composition was fundamental to obtaining glass-ceramics with a fine microstructure that improves mechanical properties. With a small addition of dolomite slag and glass cullet into the coal fly ash, very stable glass-ceramic materials were obtained [11,110]. Results showed that the properties of glass-ceramic samples were better than the commercial glass-ceramic materials. Mendez et al. [111] mixed industrial wastes (coal fly ash, dolomite slag) with quartz sand to produce glass-ceramic. Glass-ceramic with a surface crystallized pyroxene type phase was obtained from those wastes. Another example mixing different industrial wastes to obtain glass-ceramic material was reported by Barbieri et al.[112]. Several compositions were formulated with mixing in different percentages of coal fly ashes, municipal solid waste (MSW), glass cullet and float dolomite from mineral extraction operations. It was reported that all the glass-ceramic samples showed a good crystallization tendency with the formation of pyroxene and wollastonite. Coal fly ash is also rich in iron and Francis et al. [113,114] mixed the waste with borosilicate or sodalime glass powders to promote the densification and to directly produce glass-ceramic products containing magnetic phases.

Some of the researchers obtained glass, glass-ceramic materials by adding Na_2O to decrease the melting point of fly ash and CaO, Na_2O as fluxing additives. Sheng et al.[115] added 10 wt.% of Na_2O to the coal fly ash and the melting point of fly ash decreased to 1473 K. Peng et al.[116] produced glass-ceramic samples from coal fly ash with Na_2O + CaO and BaO + CaO as fluxing additives. XRD and SEM studies showed that the main crystalline phase in the both glass-ceramic samples was wollastonite and the average crystalline size was below 300 nm. Another example of adding fluxing additives was reported by Leroy et al.[117]. 10 wt. % CaO and 10 wt.% Na_2O were added to the coal fly ash however, the melting temperature of 1793 K for 2 h was found to be too high.

Coal fly ashes were transformed into glass-ceramics without any additives or nucleating agents. Erol et al. were reported that coal fly ash can be used as a raw material to produce glass-ceramic materials and obtained glass-ceramic materials were good candidates for industrial use in construction, tiling and cladding applications [118-120].

More recently, a wide range of other industrial wastes, leading to very different glass compositions, has been used to produce glass-ceramics for building industry or other applications. Glass-ceramics from MSW fly ash can be obtained mainly by controlling the temperature of the vitrified product during the cooling down stage [10,121]. The resulting product presents better mechanical and technical properties than those of the amorphous product. According to Boccaccini et al.[10], obtained glass-ceramic samples have higher hardness, better workability and increased fracture toughness, strength (almost three fold) and thermal shock resistance. From the mechanical point of view, it is desirable to maximize the number of nuclei formed to produce microcrystalline ceramics. In another study Boccacccini et al.[8] showed that almost three fold increase of bending strength (from 90 to 240 MPa) and fracture toughness (from 0.6 to 1.7 MPa $m^{0.5}$) for a glass-ceramic with respect to the parent glass, produced from vitrification of MSW ash. Chemical durability tests should be conducted on all glass-ceramics produced from MSW ash. MSW ashes were vitrified by heating at 1773 K by Park et al. [122], with the addition of at least 10 wt.% of silica and MgO (10 wt.%) to avoid heavy metal leaching and obtain an inert glass-ceramic. They indicated that the main problem of this type of waste lies in the relevant chlorine content, particularly high in this case if compared with other reported compositions, due to a high concentration of salty food waste and plastic materials in the MSW. Up to 70 wt. % MSW ash corrected with waste from feldspar production were transformed to glass-ceramic materials by Karamanov et al.[123,124], obtaining a chemically inert glass-ceramic.

A mixture of different fly ashes has been sometimes used with the aim of obtaining a composition more suitable for glass-ceramic production, as reported by Cheng [125] in the melting and ceramization of dust generated in an electric arc furnace for stainless steel making and MSW fly ashes (in the weight ratio 1:9, respectively). However, the resulting glass-ceramic product showed a certain leachability for Cr ions, depending on the temperature of the ceramization treatment. The same approach was followed also by Barbieri et al., with the production of glass-ceramics from different fly ashes melted at 1773 K after correction with glass cullet and dolomite [110,126,127]. Glass-ceramics are also produced from slags obtained from different metallurgical industries. Öveçoğlu [128] recently produced slag-based glass-ceramics with a high bending strength (> 300 MPa) and excellent fracture

toughness (5.2 MPa $m^{0.5}$). Ferreira et al. [129] produced several glass-ceramics from basic oxygen furnace (BOF) slag and found that an optimal composition was 60% BOF slag, 35% sand and 5% Na_2O. Steelwork slag was also used in the glass-ceramic production and Gomes et al.[130] proposed the addition of residues of bauxite extraction, limestone, sand and TiO_2 as nucleating agent.

Knowledge of nucleation and crystallization kinetic parameters such as, activation energy for crystal growth and crystal growth mechanism is important in the preparation of glass-ceramics with desired microstructure and properties. Although a number of studies have been reported on examining the crystallization behavior of glasses produced from industrial wastes[110,111,131-133], only a few researchers have done investigations on coal fly ash based glasses. The activation energy of the glasses produced from coal fly ash was calculated as 370 kJ/mol by Cioffi et al. [134]. Erol et al.[135,136] determined the kinetic parameters that describe the crystallization process of coal fly ash based glasses. Studies showed that the activation energies of the fly ash based glasses were between 283-320 kJ/mol and the bulk nucleation occurred in the glasses by three dimensional growth. The crystallization behavior of glasses made of mixture of coal ash and soda lime glass cullet was investigated by Francis et al.[137]. Obtained results showed that the crystallization mechanism is diffusion controlled crystallization with a decreasing nucleation rate.

Table 3.7 presents a literature survey of the main studies carried out on the topic of glass-ceramic materials produced from industrial wastes. The main compositions and heat treatment conditions do not differ greatly, however there are a variety of types of crystalline phases in the final product according to the presence of any of the minor components.

Table 3.7: Literature survey of the glass-ceramic materials obtained by industrial wastes

Waste	Crystalline phase	Main property	Application	Ref.
Slag	Wollastonite, anorthite, mellite, diopside	Wear, chemical resistance, mechanical strength	Tiles, pipes, wall cladding, floor tile	121,138, 139,140
Slag and shale	Wollastonite, diopside	Erosion resistance	Pipes	141
Oil shale and mining residues	n.r.	Crystallization study, Wear, chemical resistance, mechanical strength	n.r.	142,143
Fly ash, fluorine Flotation, clay	n.r.	Appearance, chemical resistance	Decorative panels	144
Slag, copper industry, fly ash	Wollastonite, anorthite, diopside	Chemical resistance, mechanical strength	Wall covering	105
Fly ash	Wollastonite, anorthite, diopside, esseneite, nepheline	Chemical resistance, mechanical strength	Building industry, refractory materials	107,108, 117,145
Fly ash	Mullite, anorthite	Crystallization study	n.r.	111
Zinc hydrometallurgy	Magnetite, pyroxenes	Chemical resistance, mechanical strength	Building industry	146,147
Ash and slag from fertilizer industry	Quartz, feldspar, mullite	Bending strength and low porosity	Tiles, bricks	148
Steel slag, fly ash, slurry	Pyroxenes	Mechanical strength and alkali resistance	Building materials	149
Ash, glass cullet and clay	Mullite, anorthite	n.r.	Facing tiles and panels	150
Ash and slag	Augite, wollastanite, alumino-silicate, magnetite	Thermal and acid resistance	Refractories, light filling materials, bricks	151

Table 3.7: Literature survey of the glass-ceramic materials obtained by industrial wastes

Steel slag, ash, gangue	Nepheline, illite	Machinability	n.r.	152
Steel fly ash, municipal incinerator fly ash	Wollastonite, anorthite, diopside	Crystallization study, chemical resistance	n.r.	125,153
Municipal incinerator fly ash, glass cullet, $Mg(OH)_2$	Pryroxene, akermanite, gehlenite, augite	Crystallization study, mechanical strength, chemical resistance	Building materials, engineering and construction applications	10, 130, 132,154, 155

n.r. : not reported

3.8.2 Glass-ceramics by Sinter Crystallization

A drawback of the typical glass-ceramics manufacturing route is requiring a nucleation/crystal growth step that may be difficult to control and economically expensive. Moreover, defects in the glass articles, like pores, remain in the glass-ceramic, causing a decrease in the mechanical properties. This problem is particularly pressing when waste glasses are used as starting material; in order to obtain good glass-ceramics the present glasses should be extensively refined, so that gas bubbles may evolve from the glass melt. The refining treatment requires high temperatures and long holding times, especially when the glass, due to the content in heavy metals, is dark and its thermal conductivity by radiation is consequently low. In addition, the visual appearance of glass-ceramics obtained by the traditional route is inferior to that of natural stones and traditional ceramics. In order to avoid these problems, another glass-ceramic production route was developed in the 1950s, that of sintered glass-ceramics, which led to marble like materials for architectonic applications [156]. This approach has been reevaluated since the early 1990s, in the treatment of wastes, mainly due to the work of Karamanov et al.[157].

The advantage, when applying the sintering route to the production of glass-ceramics from wastes, is that only a short time vitrification treatment can be used and there is no need to refine the melt before casting into a frit, thus reducing cost and gaseous emissions. The ground glass powder is subsequently heated to a certain temperature,

at which sintering occurs together with crystallization. The simultaneous sintering and crystallization treatment is known as sinter-crystallization. Glass surface is a preferred site for crystallization and thus ground glass is easier to devitrify than bulk glass with the same composition and nucleating agents are not needed [158-161]. Karamanov et al. [162] recently exploited this process to produce sintered glass-ceramics for building applications starting from iron rich wastes. The heating conditions during sinter crystallization were also found to be of importance. Karamanov et. al.[123] reported that the balance between surface crystallization and bulk crystallization is strongly affected by the heating rate. Low heating rates favor bulk crystallization and sintering may be inhibited by the crystal phase, causing incomplete densification. High heating rates favor sintering so that low porosity remains in the material; however the degree of crystal phase formation is lower, because crystallization occurs only at the surface. Other recent works confirmed the feasibility of sinter crystallization as a way to obtain glass-ceramics exhibiting good mechanical properties from wastes. Cheng et al.[163] manufactured glass-ceramics compacts from MSW fly ashes (with porosity in the range 12 to 26%) with good compressive strength (from 30 to 50 MPa) and acceptable durability. Brusatin et al.[164] obtained by cold pressing of fine powders and heating at 1213 K for 5 h, highly dense sintered glass-ceramics, exhibiting a remarkable modulus of rupture (>7 GPa) and fracture toughness (>2 MPa $m^{0.5}$).

A comprehensive literature survey showed that any research which has been conducted on to the sintered glass-ceramics produced from coal fly ash can not find. Table 3.8 presents a literature survey of the main studies carried out on the topic of sintered glass-ceramic materials produced from industrial wastes.

Table 3.8: Literature survey of sintered glass-ceramic materials produced from industrial wastes

Waste	Crystalline phase	Main property	Application	Ref.
Municipal incinerator fly ash	Pryroxene, gehlenite, diopside	Physical properties, mechanical strength, chemical resistance	Building materials	163,165
Municipal incinerator fly ash, glass cullet	Pryroxene	n.r.	n.r.	166
Fly ash from domiciliary solid waste	Diopside, wollastonite	n.r.	n.r.	123,124
The incinerator fly ash, from domestic waste incinerator	Gehlenite	n.r.	n.r.	167

4 Sintering

4.1 Definition and History of Sintering

Sintering is a thermal treatment for bonding particles into a coherent, predominantly solid structure via mass transport events that often occur on the atomic scale. The bonding leads to improved strength and a lower system energy [168]. In other words, sintering is the bonding together of particles at high temperatures. It can occur at temperatures below the melting point by solid state atomic transport events, but in many instances involves the formation of a liquid phase [169].

Powders exhibit a fluidlike character that allows shaping over a wide range of stresses. Consequently, powders are beneficial in forming many objects, ranging from automotive connecting rods to pottery. A variety of shaping processes can be applicable to powders, including die compacting, slip casting, tape casting, extrusion, injection molding, isostatic pressing and rolling. In each case, to maintain the strength in the shaped powder requires a firing treatment known as sintering. Upon heating, the particles bond to one another giving a higher strength. Thus, particulate materials are attractive because they allow net-shaping, but sinter bonding is necessary to attain desirable final physical properties. This is the reason for widespread interest in sintering in terms of both the available materials and of applications.

It is typical for particles to sinter bond together when heated to relatively high temperatures. Sintering is usually evident at temperatures in excess of approximately half of the absolute melting temperature. Materials melt over a wide range of temperatures; accordingly, sintering is performed over an equally wide range of conditions.

The sintering process has been known for thousands of years. Some of the first sintered products were bricks heated in open pit fires to add strength. Even today

sintering is a primary operation in the production of the most common ceramics; whitewares, refractories, bricks, abrasives, porcelain and construction materials. Many sintered ceramic structures are known around the world, including porcelain, a glass-bonded ceramic formed by sintering. Other examples include gold-platinum jewelry sintered by the Incas; and Egyptian uses of sintered materials (metal and ceramic) date back to 3000 BC. During the nineteenth century the need for platinum laboratory equipment led to the development of chemically precipitated Pt powder that was hot pressed to form dense structures. Other historical uses of sintered materials include coins from sintered copper, silver and lead powders.

The modern era of sintering is traced to Coolidge, who used tungsten powder to develop a durable lamp filament for Edison. Subsequently, spark plugs, cemented carbides, porous bronze bearings, electrical insulators and copper graphite electrical contacts were developed in the 1930s. By the 1940s, sintering was used in fabrication of tungsten alloys, uranium dioxide nuclear fuel elements, electrical contacts, ferrous structural alloys and many refractories. In the latter part of the twentieth century there has been enormous growth in sintering practice, especially for the creation of technical ceramics. Particular attention has been directed to materials with high temperature strength, high fracture toughness, high wear resistance or novel electronic properties. Today, sintering is employed in a diverse range of products that includes dental implants, rocket nozzles, aircraft wing weights, ultrasonic transducers, turbochargers, semiconductor substrates and golf clubs. Many of the modern applications reflect factors that include manufacturing economy, improved properties and novel compositions [168,170].

4.2 The Sintering Process

A basic characteristic encountered in sintering is a transformation of the particles into a solid object consisting of bonded particles. Usually, the particles are smaller than 1 mm in size and can be spheres, cubes, wires, flakes, disks, snowflakes, or other small solids that flow and pack as a powder. At small particle sizes the high surface area/volume ratio ensures that surface forces are relatively large.

Sintering lowers the surface energy by reducing surface area with the connection of the interparticle bonds. The bonds grow by various mechanisms that occur at the atomic level. For many metals and ceramics, bonding is by solid state diffusion. Alternatively, particle melting occurs during liquid phase sintering, resulting in a solid-liquid mixture during the thermal cycle. The liquid phase provides bonding, contributes a capillary force and usually enhances the rate of mass transport as compared to solid-state processes. Other sintering techniques apply pressure to enhance particle deformation and bonding simultaneously. Hot isostatic pressing is a popular form of pressure assisted sintering, where yielding and diffusion can both occur. Newer techniques involve reactions between mixed powders, leading to the synthesis of a new composition by sintering under the conditions of an exothermic reaction.

Particle shapes and the application of pressure can give higher densities, but usually there is always porosity between particles. Thus, all powder structures are initially porous. The initial structure is termed the green state, reflecting the unfired condition of the powder. The shaped, but unfired powders are often termed a compact, to reflect the pressed condition. Most compacts are prepared by applying pressure to the powder to increase density and invoke shape to the powder. A green compact is usually weak; vitamin pills and aspirin are common examples of pressed powders. These shapes are sintered to improve strength and other properties.

The stage of sintering refer to geometric categories for analyzing the mass from process is outlined in Table 4.1. For most cases the starting point is an assembly consisting of contacting particles. Depending on the fabrication of the particle compact, the initial bonds range from points contacts to highly deformed interfaces. With sintering the contacts grow in size and in the initial stage there is extensive loss of surface area. As the pore structure becomes rounded the discrete particles are less evident and the intermediate stage of sintering occurs. This characterized by a tubular, rounded pore structure that is open to the compact surface. Gas can permeate through the open pore space. Consequently, many sintered structures are sintered to this stage only to preserve desired pore structures.

In a crystalline solid the grain boundaries are usually attached to the open pore structure. As the pore shrink, a final stage of sintering occurs. Now as the density increases the pores spheroidize and are no longer connected to the compact surface. These are termed close pores and any gas trapped in the pores proves difficult to remove. Since open pores are more effective in retarding grain growth, the transition to final stage sintering gives less grain boundary pinning and usually results in rapid grain growth. There are many variants to this basic progress, but the three stages provide a convenient definition for the morphology progression. For some structural materials all three stages are encountered, while for porous structures sintering is usually terminated in the intermediate stage [168].

4.3 Development of Microstructure

Accompanying particle bonding during sintering cause significant changes in the pore structure. Additionally, many properties, including strength, ductility, conductivity, magnetic permeability and corrosion resistance undergo dramatic improvements during sintering. These property changes are primary concerns in industrial sintering cycles. To understand the evaluation of various properties, it is important to study the microstructure changes. One negative consequence of microstructure coarsening is the occurrence of oversintering, where the properties peak and then decline with continued heating for longer times or at higher temperatures.

In many cases, sintering is accompanied by an increase in compact density due to dimensional shrinkage. The particles actually attract each other and self compress to eliminate pores. This is common in ceramics. On the other hand, zero dimensional change is desired in many components. The key is to use the forming pressures to control density and to use lower sintering temperatures to minimize shrinkage. Although the essentials seem simple, there is complexity because of the large number of events that occur in sintering. Of special concern is evolution of microstructure, since microstructure is primary factor in determining properties [168].

Although opinions vary somewhat concerning that exact events constituting each stage, it is important to realize that this description is at best very qualitative and that

these stages may occur virtually simultaneously within the compact. Nevertheless, the concept does help to introduce the physical nature of the sintering process. Sintering is divided into six stages[171]:

- Interparticle bonding
- Neck growth
- Closure of pore channels
- Rounding of pores
- Pore shrinkages (densification)
- Pore coarsening.

Table 4.1: Classic stages of sintering [168]

Stage	Process	Surface area loss	Densification	Coarsening
Adhesion	Contact formation	Minimal unless compacted at high pressures	None	None
Initial	Neck growth	Significant, up to 50% loss	Small at first	Minimal
Intermediate	Pore rounding and elongation	Near total loss of open porosity	Significant	Increase in grain size and pore size
Final	Pore closure, final densification	Negligible further Loss	Slow and relatively minimal	Extensive grain and pore growth

Interparticle Bonding: Transport of atoms at particle contact points leads to the establishment of physical bonding and grain boundaries at these points. These initial bonds are developed very rapidly even as the compact is being heated to temperature.

Neck Growth: Continuing mass transport leads to the development of distinct necks between particles, growing from the initial bonds. This stage greatly increases the strength of the compact but does not involve any densification.

Pore Channel Closure: Continued neck growth can cause pore channels within the compact to be closed, leading to isolated porosity. It is very important to control this event in sintering powder metallurgy products, which utilize interconnected porosity for example, filters, self lubricating bearings, etc.

Pore Rounding : As neck growth reaches an advanced stage, the material transported from the general particle surfaces to the neck regions results in a smoothing of the pore walls (reduction of pore area). This can be an important structural change with respect to improving to ductility and toughness of the sintered compact. This stage of sintering is illustrated by the idealized three sphere models in Figure 4.1 [172].

Pore Shrinkage: As sintering progresses, the pores in the compact may begin to shrink in size and decrease in number, resulting in densification. This stage must involve extensive diffusion and annihilation of vacancies. Not all porosity can be eliminated during this stage of sintering; some residual pores will be left (particularly inside of grains) even after very long sintering times.

Pore Coarsing: This stage is not considered to be very important in most commercial sintering operations. When it occurs, it involves in increase in size of some of the larger pores and concurrent elimination of some smaller pores. No net change in the pore volume fraction is involved, so the average distance between pores is increased. In many respects, this microstructral change is analogues to the precipate coarsing, which occurs during severe overaging of conventional age-hardening alloys[172].

4.4 Sintering Techniques

Theory is most accurate for the case of single phase powders sintering by solid state diffusion. Unfortunately, this is only a small portion of actual sintering practice. Many sintering systems consists of multiple phases, possibly forming a liquid and may even be subjected to an external pressure to enhance densification. The diagram in Figure 4.2 helps relate the key sintering techniques. This chart is a conceptual map to the various processes. In a general categorization, pressure is the first consideration. However, most sintering is performed without an external pressure (pressureless sintering). Pressure assisted sintering techniques are newer and

represent a hybrid between high density approaches such as hot isostatic pressing and pressureless sintering. These approaches involve sintering a material to a low residual porosity level, then using gas pressure to squeeze out the remaining pores. Pressurezation during sintering is most useful in processing materials that are unresponsive to traditional sintering cycles; for example, composites and high temperature intermetallics. The pressure can be low, giving densification controlled by diffusional creep. Alternatively, densification at high pressures is rapid if the effective stress exceeds the yield strength of the material. Pressure is usually hydrostatic (hot isostatic pressing) or uniaxial (forging and hot pressing).

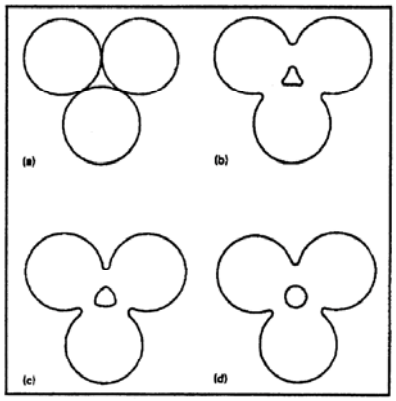

Figure 4.1: Three sphere sintering models. (a) Original points contacts. (b) Neck growth. (c) and (d) Pore rounding[172].

A major distinction among pressureless sintering techniques is between solid state and liquid phase processes. Single phase solid state sintering has received the greatest consideration from a theoretical standpoint. Several reviews [173-180] give details on solid state sintering theory. The classic treatments are applicable to pure substances such as nickel, alumina or copper. Among the solid state processes, there are options involving second (solid) phases. These include compact homogenization (such as occurs with sintering mixed powders that are soluble in each other), activated sintering and mixed phase sintering in the solid state. The latter process is the basis for sintering composites. Activated sintering is a solid state process where a second solid phase contributes to rapid particle bonding. In such a situation, sintering occurs in a equilibrium two phase field, such as high carbon steels at temperatures where ferrite and cementite coexists. Homogenization occurs during sintering of

mixed powders that form a single phase product, such as with alumina and chromia, which form a solid solution.

Many sintering cycles generate a liquid. It may be present momentarily or may persist during much of the sintering cycle. The liquid improves mass transport rates. It also exerts a capilarly pull on the particles that are equivalent to a large external pressure. Because of cost and productivity advantages, the greatest level of industrial sintering is performed in the presence of a liquid phase. It is estimated that over 70% of the sintered products are processed in the presence of a liquid phase. This includes stainless steels, superalloys, aluminides, tool steels,
titinates, TiC-Fe, WC-Co, Fe-P, Mo-Cu, W-Ag, Cu-Sn, W-Ni-Fe and Fe-Cu-C as common examples.

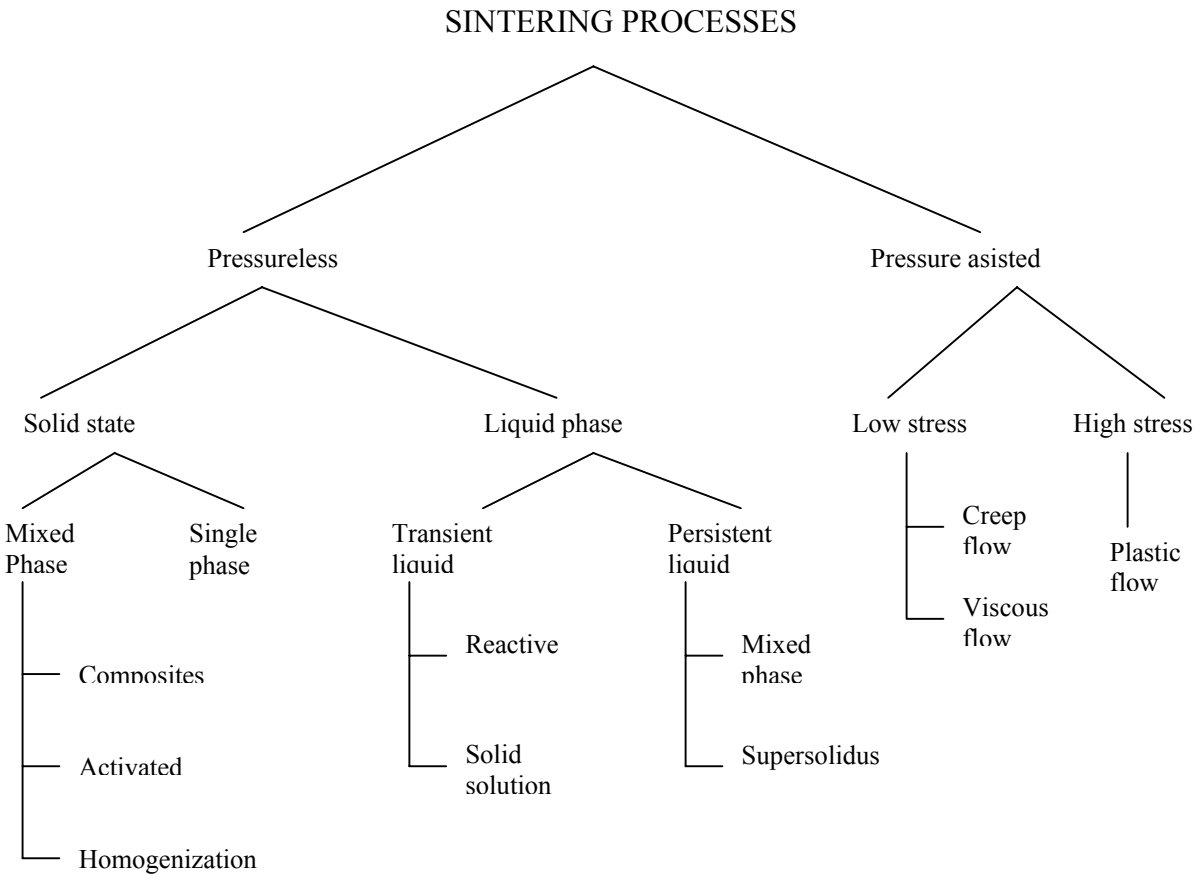

Figure 4.2: Map to sintering processes [168]

There are similarities between solid state and liquid phase sintering, but the presence of a liquid in the sintering cycle accelerates mass transfer, densification and

microstructure coarsening. There are two main forms of liquid phase sintering. Persistent liquid phases exists throughout the high temperature portion of the sintering cycle and can be formed by use of prealloyed powder (supersolidus liquid phase sintering) or by inducing melting in a mixture of powders. Alternatively, transient liquid phase sintering has a liquid that disappears during the sintering cycle, due to dissolution into the solid (solid solution) of formation of a new phase. The latter process is reactive liquid phase sintering and is employed in the generation of high temperature compounds, including $MoSi_2$, Ni_3Al, WC and TiB_2 [168].

4.5 Goals in Sintering Studies

Since particles are fluidlike prior to consolidation, various shaping techniques have evolved for placing the particles into desired geometries. Sintering preserves the compact shape while bonding the particles to one another, a process referred to as net shaping. The ability to control product shape, properties and defects are important to sintering. Sintered products are usually more precise than castings but less precise than machined components. However, the lower fabrication cost makes sintered objects very desirable for a wide range of components. Because the green powder compacts are weak, sintering proves to necessary to attain the needed final properties. In cases where the particles have a high level of compressibility, sintering can be performed at a low temperature with zero dimensional change. Thus, bonding occurs without shrinkage or densification, leading to high precision [169].

To understand the evolution of the final microstructure, attention is given to particle size, initial density and pore microstructure, heating rate, maximum temperature, hold time and atmosphere. With such understanding it is possible to evaluate processing alternatives. Table 4.2 outlines some of the key processing changes and their effects.

Sintering is irreversible, so once defects are formed, they persist. Although sintering is sensitive to many factors, the basic kinetics are sufficiently slow that considerable control can be exercised during the process. It is critical to several industries, including ore processing, powder metallurgy, nuclear fuel processing, ceramics, filtration, catalysis and refractories. Sintered products can be tailored for a wide

range of engineering properties. Examples of sintered products are all around us in automobiles, airplanes, bathroom fixtures, appliances, wristwatches, musical instruments and sporting equipments. Further, sintering is often used to bond objects into assemblies or to put protective coatings in place. This diversity of applications often clouds the fundamental unifying technology.

In the fabrication of bearings, filters, catalysts, heat wicks, batteries, capacitors and other devices requiring high surface areas, it is desirable to obtain strength without densification. Here sintering cycles are designed to obtain desirable pore structures, with minimal loss of surface area. Alternatively, in ceramic materials, poor compressibility inhibits pressing to high densities; thus, it is necessary to sinter at high temperatures where shrinkage occurs. Further, in ceramics the residual pores act as incipient cracks to degrade strength substantially. Consequently, full density is most useful for competitive mechanical properties. Similarly, powders are used in the fabrication of high performance components for jet engines, automobile engines, metal cutting tools, biomedical implants, sputtering targets and magnetic recording sensors. It is necessary to densify these structures fully, so that external pressure applied during sintering to ensure closure of all pores. Such a diversity in processing routes makes sintering a useful option in materials processing, especially since all common engineering materials can be sintered to net shape [168].

Table 4.2: Sintering processing effects [168]

Change to aid sintering	Effects
Decrease in particle size	Faster sintering, Greater expense, Higher impurity level, Increased hazards
Increase in time	Greater expense, Grain growth and coarsening Reduced productivity
Increase in temperature	Greater shrinkage, Grain growth, Greater expense, Less precision, Higher properties, Furnace limitations, Pore coarsening
Increase in green density	Less shrinkage, Smaller pores, Higher final density, Uniform dimensions, Density gradients
Increase in alloying/additives	Higher strength, Homogeneity problems, Higher sintering temperatures
Use of sintering aids	Faster sintering, Lower sintering temperatures, Embrittlement, Distortion, Grain growth control

5. Experimental Procedure

5.1 Introduction

In this study, the production of glasses, glass-ceramics and sintered materials from industrial wastes has been investigated. For this purpose, coal fly ash samples were obtained from 7 different thermal power plants which are located in Afşin-Elbistan, Çan, Çatalağzı, Çayırhan, Orhaneli, Seyitömer and Tunçbilek. Beside coal fly ashes, red mud from Seydişehir alumina plant and silica fume from ferrosilicon alloy production were used as additives. To accomplish this study, different techniques such as differential thermal analysis (DTA), x-ray diffraction (XRD), mercury porosimeter, inductively coupled plasma spectrometry (ICP) and scanning electron microscopy (SEM) have been used. Determination of chemical, physical and mechanical properties of the waste materials and the produced samples have been made according to internationally accepted standards.

5.2 Starting Materials

5.2.1 Fly ash

Fly ash is the particulate very fine matter removed from the stack gas of thermal power plants as a waste product and constitutes ecological and disposal problems. Fly ash is basically a silicous and aluminous combustion waste product, occurring as a result of burning pulverized bituminous coal or lignite at high temperatures.

ASTM identifies two classes of fly ash based on the coal source; Class F fly ash originating from butimunous coal and Class C from subbituminous coal or lignite [181,182]. In general fly ash consists of glassy spheres of sizes varying from under 1 μm to as large as 100 μm, although typical particle size distribution shows that most of the material is under 20 μm. According to Luke [183], the specific gravity of fly ash particles range from 1.97 to 3.02, but is normally in the range of 2.2 to 2.8.

Fly ash generally comprises the following mineral phases bound to glassy matrix: Quartz (SiO_2), mullite ($Al_6Si_2O_{13}$), magnetite (Fe_3O_4), hematite (Fe_2O_3), anorthite ($CaAl_2Si_2O_8$) and enstatite ($(Mg, Fe)SiO_3$). Wide ranges exists in the amounts of the three principle constituents of fly ash, namely silica (SiO_2, 25 to 60%), alumina (Al_2O_3, 0 to 30%) and iron oxide (Fe_2O_3, 5 to 25%). The magnesium oxide (MgO) content of fly ash is generally not greater than 5%. Class F fly ashes usually contain less than 5% whereas Class C ones contain 15 to 35% calcium oxide (CaO). The level of alkali oxides expressed as Na_2O and K_2O equivalant is generally less than 5% in Class F fly ashes , but it may range up to about 10% in Class C fly ashes[184].

5.2.2 Red mud

Red mud is a waste material generated by alumina production from bauxite. Producing one ton of metallic aluminum requires two tons of alumina, which in turn takes about four tons of ore (bauxite), due to the presence of iron oxides and other impurities. This means that about two tons of red mud is generated per ton of metallic aluminum. World production of red mud is roughly 30 million tons per year (dry basis)[185].

The red mud consists of alumina, iron oxide, titanium oxide and small quantities of silica, calcium oxide and alkali oxides. It also contains trace elements such as P, V, Mn, Cr, Mg, Zn and Ga. The pH value of red mud changes in the range of 10-12 and they may have a very fine particle size (sometimes less than 1 micron) [186].

5.2.3. Silica fume

Silica fume is a by-product resulting from the production of silicon or ferrosilicon- or other silicon-alloys. Silica fume is light or dark gray in colour containing high content of amorphous silicon dioxide. Silica fume powder as collected from waste gasses without further treatment is some times referred to as undensified silica fume to distinguish it from other forms of treated silica fume. Undensified silicon fume consists of very fine vitreous spherical particles with average diameter about 0.1μm, which is 100 times smaller than the average cement particle. The undensified silica

fume is almost as fine as cigarette ash and the bulk density is only about 200 - 300 kg/m^3 and relative density of typical silica fume particle is between 2.2 and 2.5. Because the extreme fineness and high silicon content, silica fume is a highly effective pozzolan[187,188]. Chemical composition of silica fume varies depending on the nature of the product from the manufacture process of which the silica fume is collected. The main constituent material in silica fume is silica (SiO_2), the content of which is normally over 90%[189].

5.3 Characterization of Industrial Wastes

In order to utilize as a raw material, the chemical, physical and mineralogical properties of the waste materials were firstly determined.

Table 5.1 shows the color of the waste materials. The colors of the waste materials depend on the chemical compositions of them. The appearence of fly ash samples was found to be much darker in color and in fine powder form. The dark color of the fly ash samples is the evidence of the high iron and unburned carbon residues.

Table 5.1: The colors of the waste materials

Waste Material	Color
Çayırhan Thermal Power Plant Fly Ash	Dark brown
Çan Thermal Power Plant Fly Ash	Light grey
Çatalağzı Thermal Power Plant Fly Ash	Grey
Seyitömer Thermal Power Plant Fly Ash	Dark brown
Tunçbilek Thermal Power Plant Fly Ash	Dark brown
Orhaneli Thermal Power Plant Fly Ash	Between dark red and brown
Afşin-Elbistan Thermal Power Plant Fly Ash	Light grey
Red Mud	Red
Silica Fume	Light grey

Waste materials were chemically analyzed using well established analytical methods [190-192] which are of ASTM (oxidies including SiO_2, Al_2O_3, CaO, MgO,...) and ICP (Zn, Pb, Cr, Mn). Chemical analysis of silica fume and fly ash samples were

determined in other studies by means of ASTM methods [193,194]. Chemical compositions of waste materials were given in Table 5.2 [193,194] and Table 5.3 (for ICP). It is clear that the major chemical components in fly ash samples are SiO_2, Al_2O_3, CaO. The amount of SiO_2-Al_2O_3-CaO varied in the range of 63.54-83.27 %. The chemical composition of fly ash samples, except Afşin-Elbistan fly ash, is typical of the most common glassy ternary systems. Significant amount of Fe_2O_3, which can be used as a nucleating agent, is also present especially in the Tunçbilek, Çayırhan, Seyitömer fly ash samples. Red mud and silica fume were composed of mostly Fe_2O_3 and SiO_2, respectively. Therefore, they can't be used as a raw material source in the production of glasses and glass-ceramics. They can be used as additives in fly ash batches. All other elements such as Cr, Mn, Zn and Pb were determined in the parts per million range.

Table 5.2: Chemical analysis of waste materials [193,194]

Waste Materials	SiO_2 (%)	Al_2O_3 (%)	CaO (%)	MgO (%)	Fe_2O_3 (%)	Na_2O (%)	K_2O (%)	LOI (%)
Çayırhan Fly Ash	41.53	17.77	12.52	4.46	9.93	2.57	2.43	0.68
Çan Fly Ash	49.07	30.80	1.46	2.46	6.13	0.63	3.86	0.83
Çatalağzı Fly Ash	48.88	27.63	6.16	2.71	6.68	0.45	2.39	1.41
Seyitömer Fly Ash	44.58	22.54	6.76	8.98	9.85	0.22	0.60	3.83
Tunçbilek Fly Ash	54.08	25.58	3.10	3.03	9.82	0.58	1.51	2.01
Orhaneli Fly Ash	32.83	13.34	30.35	4.51	5.61	2.15	1.37	3.67
Afşin-Elbistan Fly Ash	18.11	7.63	37.80	3.50	5.23	0.22	0.60	8.40
Silica Fume	90.80	1.02	2.55	0.94	1.93	-	-	1.57
Red Mud*	10.40	28.50	3.90	7.70	35.1	3.80	1.60	3.90

*Chemical composition was determined in this study

Table 5.3: Heavy metals detected in waste materials

Waste Materials	Cr (ppm)	Pb (ppm)	Mn (ppm)	Zn (ppm)
Çayırhan Fly Ash	15.70	10.20	9.70	25.8
Çan Fly Ash	19.40	15.20	11.30	30.20
Çatalağzı Fly Ash	18.27	14.43	12.41	29.82
Seyitömer Fly Ash	18.20	9.82	7.60	24.60
Tunçbilek Fly Ash	20.30	11.70	10.50	28.70
Orhaneli Fly Ash	14.70	9.20	7.90	21.40
Afşin-ElbistanFly Ash	13.80	8.60	6.30	23.20
Silica Fume	10.23	5.62	4.23	11.21
Red Mud	19.21	13.23	10.21	28.24

The average particle sizes of waste materials were determined using centrifugal particle size analyzer and their densities were determined by means of mercury porosimeter. Particle size and the densities of waste materials except red mud were obtained from previous studies [193,194]. As seen from Table 5.4 particle size of waste materials varied in a wide range. Particle size of fly ash samples was smaller than red mud. Density of fly ash samples ranged from 1.69 to 2.48 g/cm^3.

X-ray diffraction was utilized to determine the mineralogical properties of the waste materials. During the combustion process, temperature may exceed 1873 K. This temperature is sufficiently high to melt most of the inorganic materials present in the waste materials. The majority of the minerals formed were quartz, anorthite, mullite and enstatite. The following Table 5.5 shows the mineralogical composition of waste materials obtained in the prerious studies except red mud [193,194].

Table 5.4: Particle size and densities of the waste materials [193,194]

Waste Materials	Density (g/cm^3)	Average particle size (μm)
Çayırhan Fly Ash	1.80	139
Çan Fly Ash	1.69	29
Çatalağzı Fly Ash	1.72	12
Seyitömer Fly Ash	1.73	261
Tunçbilek Fly Ash	1.77	75
Orhaneli Fly Ash	2.48	84
Afşin-Elbistan Fly Ash	2.03	57
Silica Fume	1.06	20
Red Mud*	2.55	550

* Density and average particle size were determined in this study

Table 5.5: Mineralogical compositions of the waste materials [193,194]

Waste Materials	Mineral phases
Çayırhan Fly Ash	Quartz, mullite, anorthite, enstatite, hematite
Çan Fly Ash	Quartz, mullite, anorthite, enstatite
Çatalağzı Fly Ash	Quartz, mullite, anorthite, enstatite
Seyitömer Fly Ash	Quartz, mullite, anorthite, enstatite, hematite
Tunçbilek Fly Ash	Quartz, mullite, anorthite, enstatite, hematite
Orhaneli Fly Ash	Quartz, mullite, anorthite, enstatite
Afşin-Elbistan Fly Ash	Quartz, mullite, anorthite, enstatite
Silica Fume	Quartz
Red Mud*	Quartz, mullite, anorthite, enstatite, hematite

* Mineralogical phases were determined in this study

As seen from Table 5.5 Çayırhan, Seyitömer and Tunçbilek fly ash samples contain hematite phase in addition to other phases present in the all fly ash samples, due to their high Fe_2O_3 content. Quartz is the main phase present in the silica fume as it is expected. Figure 5.1 is a x-ray diffraction pattern of the red mud. As seen in Figure 5.1, red mud comprised the mineral phases : Mullite, enstatite, hematite, quartz and

anorthite. The number and the intensity of the hematite and enstatite peaks were more than the other peaks present in the x-ray pattern of the red mud. This result is in well agreement with the chemical analysis of red mud.

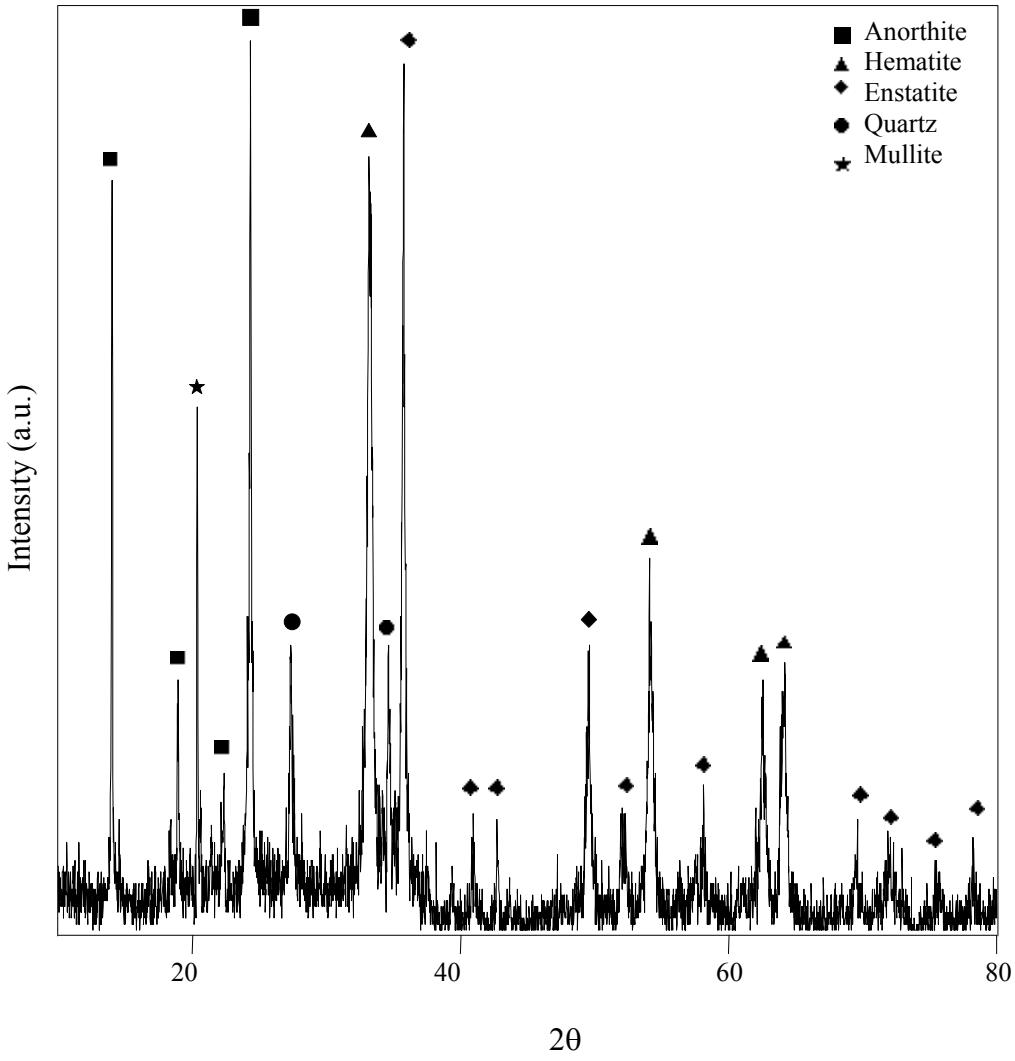

Figure 5.1: X-ray diffaction pattern of red mud

5.4 Glass Preparation

Glass samples were prepared from the fly ashes without or with the addition of red mud and silica fume in different percentages. In each batch 20 g of fly ash was melted in platinum crucible for 2 hours in an electrically heated furnace (Protherm PLF 1600 Model) at 1773 K. To ensure homogeneity, the melt was poured into water. The cast glasses were crushed, pulverized and remelted at the same temperature for 3 h to remove the air bubbles from the melt. Following this

procedure, the refined melt was cast in a preheated graphite mould (673 K) to form cylinders of approximately 0.8 to 1 cm in diameter and 1 to 4 cm in length. The cylinders were cooled to room temperature. To remove thermal residual stress, the cast glasses were annealed in a furnace at 873 K for 2 h followed by slow cooling to room temperature. The annealing temperature was chosen as 873 K since 70-100 K below the glass transition temperature is appropriate for the annealing temperature as reported in the literature [11,195]. The annealing time of 2 h was determined as an optimum time in a previous study [135]. Annealed glass samples were subjected to a heat treatment process. As it is known, some glass structures have no crystallization tendency. So, any significant crystalline phase could not occur when a heat treatment process apply to the glasses which show no crystallization tendency. These glasses could not be transformed to the glass-ceramic materials, but their mechanical, physical and chemical properties could change. Therefore, produced glass samples were heated at a rate of 10 K/min to 1423 K and held at this temperature for 2 h to determine the effect of heat treatment process on the properties of glasses. The heat-treated glass samples were then cooled in the furnace.

5.5 Differential Thermal Analysis

DTA scans of annealed glass specimens were carried out using two different thermal analyzers. Rigaku (Model Thermoflex) thermal analyzer was used to detect the glass transition (T_g) and the crystallization peak temperatures (T_p). The crystallization behavior of glasses was determined by using a Perkin Elmer (Model TAC7/DX) thermal analyzer. The glasses were ground to a coarse particle size (800-1000 μm) to be a representative of a bulk sample. The particle size of fine glasses used in DTA experiments is about 180 μm. DTA experiments were performed by heating 20 mg glass samples in a Pt-crucible and using Al_2O_3 as a reference material in the temperature range between 293 and 1373 K at the heating rates of 5, 10, 15 and 20 K/min. DTA measurements were applied to the produced glass samples to determine the glass transition temperature (Tg), the maximum nucleation temperature, maximum nucleation time and crystallization temperature at a heating rate of 10 K/min. For the determination of the maximum nucleation temperature, the as-quenched glass samples were held for 4 h at different nucleation temperatures, that is above the Tg temperature, in 5 K intervals. To estimate the maximum nucleation

time, the glass samples were heat treated isothermally at the maximum nucleation temperature for 1, 2, 3 and 4 h.

The variation of the crystallization peaks with different heating rates can be used to estimate the activation energy for crystallization and to determine the crystallization mechanism. The crystallization behavior of glasses was determined by using the both isothermal and non-isothermal methods. DTA was performed on both coarse and fine glass samples in each method to determine the particle size effect on the crystallization mechanism. Johnson-Mehl-Avrami (JMA) method has been widely used as an isothermal method for the interpretation of the crystallization experiments and for the determination of the crystallization mechanisms from the results of DTA curves. In the JMA method, the as-quenched glass samples were heated to the maximum nucleation temperature at a heating rate of 20 K/min and nucleated at this temperature for the maximum nucleation time. Fully nucleated samples were then heated to the selected temperature at a heating rate of 20 K/min and held at this temperature for 15, 30 and 60 min. Then the temperature was raised to the crystallization temperature without being removed the samples from the DTA.

Kissinger, Matusita-Sakka and Ozawa methods were used as non-isothermal methods. Crystallization mechanisms and activation energies were calculated in each method from the heating rate dependence of the crystallization peak temperature. In order to investigate the crystallization behavior of glass samples by using the Kissinger equation, the glass samples were heated to the maximum nucleation temperature and held at this temperature for the maximum nucleation time for complete nucleation to prevent the increase in the number of nuclei during the DTA scans. The temperature was then raised to the maximum working temperature of DTA. DTA scans of fully nucleated glass samples were performed at the heating rates of 5, 10, 15 and 20 K/min. In this method, the number of nuclei is independent of the heating rate. Assuming that the nucleation had occurred in glass samples during the DTA measurements, DTA data were analyzed by Matusita-Sakka and Ozawa methods. The glass samples were heated at a heating rate of 5, 10, 15 and 20 K/min to 1373 K without being removed from the DTA. In this method, the number of nuclei is inversely proportional to the heating rate. The reason that all of these

methods were used in the present study is to obtain more accurate kinetic parameters for the glasses produced from waste materials.

5.6 Glass-ceramic Forming

To produce the glass-ceramic samples, both classical and sintering methods were applied to the bulk and powder glass samples to understand the particle size effect on the crystallization mechanism. Since the objective was to produce bulk and sintered glass-ceramics, two batches were made for each composition. In the first case produced glasses were cut by diamond saw blade in identical pieces with a disc shape of about 10 mm diameter and 5 mm height suitable for microstructural and mechanical characterizations. In the second case, glass samples were milled until they passes through a sieve of 180 μm. The grounded powder was subsequently humidified at 5 wt % with distilled water without any additives. 5 wt % polyvinil alcohol (PVA) water solution was also added to the grounded powder to determine the effect of the binder on the properties of sintered glass-ceramics. Glass powders were than cold pressed using 40 MPa in a disc shape (10 x 5 mm). Cylindrical samples were dried in an electric oven at 383 K for 2 h. Finally, both bulk and pressed glass samples were crystallized by suitable nucleation and crystal growth heat treatments on the basis of DTA results. For this purpose, glass samples were placed in an alumina brick and heated at a rate of 10 K/min to the maximum nucleation temperature and held at this temperature for maximum nucleation time. Following the nucleation, the temperature was raised to the crystallization temperature and held at this temperature for 15, 30 and 60 min to examine the effects of holding time at the crystallization stage on the microstructural, mechanical, physical, and chemical properties of the produced glass-ceramic samples. The crystallized samples were then cooled in the furnace. Heat treatments were carried out in an electric muffle furnace. Flow chart of glass-ceramic production can be seen in Figure 5.2

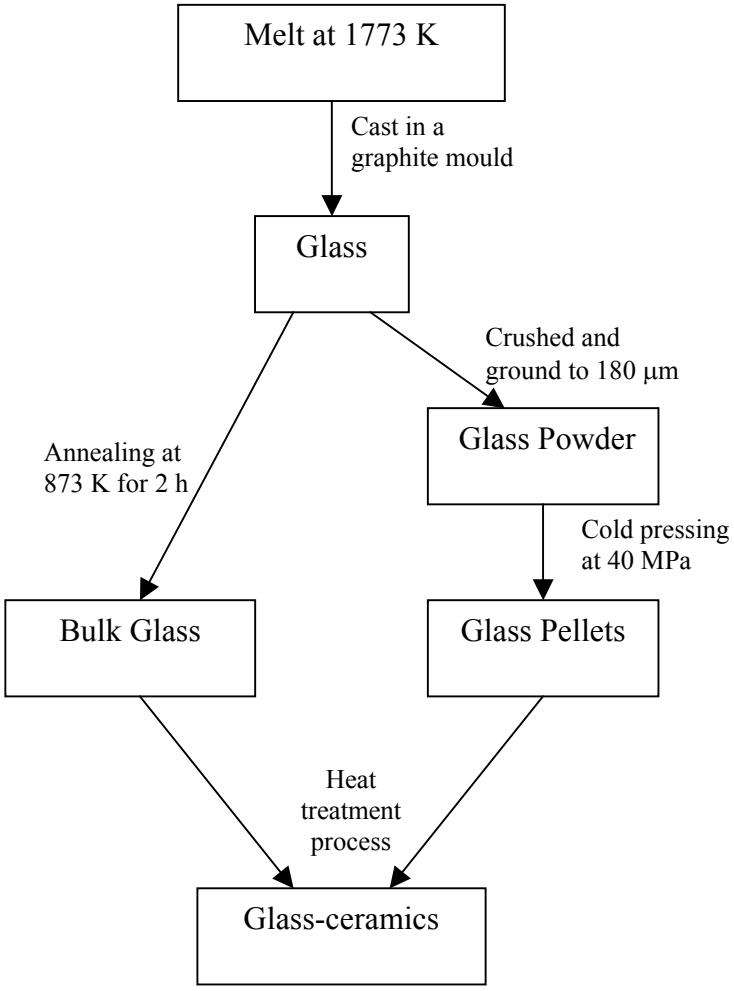

Figure 5.2: Flow chart for glass-ceramic production

5.7 Preparation of Sintered Materials from Fly Ash Samples

Afşin-Elbistan, Çan, Çatalağzı, Çayırhan, Orhaneli, Seyitömer and Tunçbilek thermal power plant fly ashes were sintered to form ceramic materials using conventional powder processing technique based on powder compaction and firing, without the addition of organic binder or inorganic additives. In sample preparation, a small amount of water was used to humudify the fly ash before compaction. 1.5 g of fly ash was mixed in a mortar with water at the water/solid ratio of 0.1 for each pellet. The circular pellets of 10 mm diameter were uniaxially pressed at 40 MPa to achieve a reasonable strength. The powder compacts were sintered in air. The sintering temperature varied between 1298 K and 1523 K to determine the effect of

firing temperature on the properties of sintered fly ash samples. Firing experiments were carried out in the Protherm PLF 1600 furnace equipped with a small chamber and a programmable controller (the internal PID constants were adjusted to obtain a maximum deviation of 7 K). Before every sintering operation the samples were pre-heated to 573 K for 60 min to derive off adsorbed gasses and moisture. After that, the temperature was raised to the firing temperature. The heating rate was 10 K/min and the sintering time was 120 min for all samples. All samples were cooled down in the furnace.

5.8 Characterization of the Produced Glass, Glass-ceramic and Sintered Materials

5.8.1 X-ray diffraction studies

X-ray diffraction was utilized to determine the crystalline phases occurred in the glass-ceramic and sintered materials and also the amount of amorphous glass present in the samples. The initial glass compositions were analyzed to check for any crystalline phases that may have formed during annealing process. The crystallized samples were analyzed to determine which crystalline phases were present and also to determine if the sample had fully crystallized.

In all cases, samples which were analyzed by x-ray diffraction were ground to fine powder form. A Siemens diffractometer Model D 5000 operated at 40 kV and 30 mA utilizing CuKα radiation was used for the measurements. The detector was scanned over a range of 2θ angles from 10 to 80 ^{0}, at a step size of 0.02 ^{0} and a dwell time of 2 seconds per step. The resulting powder diffraction patterns were analyzed utilizing a software package program. The crystalline phases were identified by comparing the peak positions and intensities with those in the Joint Committee on Powder Diffraction Standards (JCPDS) data files.

5.8.2 Scanning electron microscopy (SEM) analysis

SEM is a versatile instrument capable of producing an image with high resolution. Images displayed on the monitor can result from secondary electrons or

backscattered electrons captured by the detector. In this study, Jeol Model JSM-5410 and Amray Model 1830 both operated at 20 kV were used to observe the microstructure of the produced samples. Samples were mounted (using Buehler Model Simpliment II) in epoxy resin and their surfaces were ground flat by 400, 800, 1000 and 1200 grit abrasive papers. Then the samples were polished with diamond paste to achieve a mirror-smooth surface. The polished samples were etched with HF solution (5 volume %) for 1.5 min, immediately rinsed with excess distilled water and then cleaned in ethanol for 2 minutes. The samples were coated with carbon prior to examination. The microstructures of the samples were examined by SEM and the photographs were taken.

5.8.3 Mechanical tests

5.8.3.1 Vickers microhardness

Vickers microhardness measurements were done on the produced glass and glass-ceramic samples. The microhardness tester used in this study was a Leco Model M-400-G. Samples were ground and polished with diamond paste. A load of 0.5 kg was selected and the time of indentation was fixed as 15 seconds. The diamond indenter was a Vickers indenter ground in a shape of a square based pyramid with an angle of 136 ^{0} between the faces. The surface of the samples must be completely normal to the indenter to ensure a symetrical indentation. For this reason, the mounted sample was placed in an universal clamp. The size of the indentation was precisely measured with a microscope having a good resolving power. The average value of indentation diagonals was used for hardness calculation in the following equation [196].

$$H_V = 1.854\ (P/d^2) \qquad \textbf{(5.1)}$$

Where H_V is the Vickers hardness, P is the test load (kg), d is the arithmetic mean of the two diagonals (mm). For each condition an average value was calculated.

5.8.3.2 Rockwell hardness

Rockwell hardness measurements were done on the sintered materials produced from fly ashes to determine the effects of different heat treatment processes on the mechanical properties of the samples. The Rockwell hardness tester used in this study was a Wilson Model 4J. A Rockwell hardness test is a hardness measurement based on the net increase in the depth of impression as a load is applied. Rockwell hardness numbers have no units and commonly given in the B, C, R, L, K, M and E scales. The higher the number in each of the scales means the harder the material. This test proceeds in two steps. At first the penetration start point (zero) under a minor or preliminary load is determined, and the second step happens under a major load. The latent deformation measured after releasing the major load, is a direct measure of the Rockwell hardness, which is given on the scale of the dial gauge. [196]. The hardness of sintered materials were determined by the Rockwell hardness test, according to the specifications of ASTM E-18 [197]. This test measures the difference in depth caused by two different forces, using a dial gauge. Using standard hardness conversion tables, the Rockwell hardness value is determined for the load applied, the diameter of the indentor, and the indentation depth [197].

A superficial Rockwell Hardness tester (Wilson) was employed with 1.588 mm ball indenter (B scale) to the sintered materials loading at a minor load of 0.5 kg and major load of 1 kg. Ten indentations were performed on each sample and the results averaged.

5.8.4 Measurements of the density and the porosity

Density and the porosity of the produced glass, glass-ceramic and sintered materials were measured by using a Quantachrome Autoscan-33 mercury porosimeter. Mercury intrusion porosimetry measurements of the samples were carried out pressurizing up to 227 MPa with a Hg contact angle of 140^0. Samples were weighed, placed in the penetrometer and loaded in the filling apparatus (low pressure port of the porosimeter). The penetrometer was sealed with high vacuum grease. Samples were evacuated of residual air in the low-pressure port where initial mercury intrusion subsequently takes place. The penetrometer assembly was then transferred

to autoclave (high-pressure port). Mercury intrusion to the samples takes place with the increase of pressure. Data on density and percent porosity were acquired through a microcomputer data acquisition system interfaced with the porosimeter.

5.8.5 Toxicity characteristic leaching procedure (TCLP)

Toxicity evaluation was made by application of standard leaching procedures. Leaching test methods are used in order to asses: i) whether a waste should be classified as hazardous, ii) the waste treatment process effectiveness and iii) whether land disposal of a specific waste is an appropriate method of management. Due to the variations in the numerous applicable leaching tests, the choice of the most appropriate ones should be carefully considered. The number of vitrified samples produced did not allow the use of some other leaching tests. Consequently, attention was focused on single batch leaching tests (equilibrium based).

Toxicity characteristic leaching procedure (TCLP) was selected as the most appropriate method for the determination of leachability of the produced samples. TCLP is a relatively simple method. Furthermore, TCLP has acceptable limits so that it is extensively used for comparison to results of analogous studies. In order to asses the stabilization of the wastes (fly ash, red mud and silica fume) into a glass and glass-ceramic materials, the produced glass and glass-ceramic samples were subjected to TCLP test.

The experimental procedure according to TCLP is summarized as follows [198]: One leaching solution (extraction fluid) was used in the experiments. Extraction fluid consists of 5.7 ml of acetic acid diluted in 500 ml of distilled water, in which 64.3 ml of NaOH (1 N) were added and the resulting solution was diluted with distilled water to the volume of 1 l giving a final pH value of 4.93±0.05. The produced samples were manually crushed (< 9.5 mm) and placed in a conical flask. Extraction fluid was added in order to keep a liquid to solid ratio of 20 (L/S=20). The flask is tightly closed and stored at 298 K for 18 h. The resultant solutions were filtered through a 0.6-0.8 μm filter and the concentrations of heavy metals in the leachate were determined by using ICP. A Perkin Elmer Model Optima 3000 XL ICP operated at 13.56 MHz (using Ar and N_2 gases) was used for the measurements.

5.8.6 Determination of the chemical resistance and water adsorption of the produced materials

The chemical resistances of the glass, glass-ceramic and sintered materials were estimated in 10 % HNO_3 and 10 % NaOH solutions. In these experiments, 2 g of grained samples with average particle sizes between 0.3 and 0.5 mm were treated at 373 K for 2 h in 70 ml solutions. After washing and drying, the grained samples were weighed and the percentages of weight losses were calculated.

The water adsorptions (%) of the produced materials were determined using the procedure outlined in the ASTM standards [199]. For this purpose, the samples were dried to constant weight at 383 K, cooled to room temperature in a desicator and weighed accurately (W_1). The samples were immersed in distilled water and boiled for 2 h. The heating was then removed and the samples were taken out and excess water from the surfaces was removed by wiping with damp cloth. The sample was again weighted accurately (W_2) and the water adsorption (%) was calculated using the following formula:

$$(W2-W1/W1)*100 \quad \textbf{(5.2)}$$

6. Experimental Results and Discussions

6.1 Glass Production

Glass formulation optimization for coal fly ash is constrained by product control (chemical durability, homogeneity and thermal stability), process control (viscosity, melting temperature and waste solubility) and overall economics. The chemical durability and viscosity are highly dependent on the glass composition. The viscosity of a glass melt, as a function of temperature, is the most important variable affecting the melt rate and pourability of the glass. The viscosity determines the rate of melting of the raw feed, the rate of glass bubble release (foaming and fining), the rate of homogenization and thus, quality of the final glass product. As a possible industrial material, glass product should have good chemical durability and enough mechanical strength. Another factor that effects the glass production is the release of heavy metals or other hazardous elements into environment. Less additives is the major factor that influences the overall economics. In general, chemical durability and viscosity are the main initial factors used to determine the acceptability of a glass formulation.

The glass structure is usually considered as a random network. The elements are generally classified into three types:

1. Network forming atoms: such as Si, B, P, Ge;
2. Network modifiers (or glass fluxes): such as Na, K, Li, Ca, Mg;
3. Intermediates: such as Al, Fe, Zn, Ti, Mo, etc.

The chemical durability of glass is mainly influenced by the chemical composition. There has been much research focused on the composition-durability relationships of glass made of waste. Some general rules can be extracted from these studies, such as the following [115,200]:

1. The components that form the strongest bonds in glasses results in the greatest improvement to glass durability, whereas those that form the weakest bonds generally prove the greatest detriment to glass durability;
2. Adding SiO_2, Al_2O_3, B_2O_3, ZrO_2 may improve durability;
3. Adding alkali metal oxides may decrease the durability.

The glass formers are the major constituents of all waste glasses. If the inorganic oxides from the waste have insufficient glass formers to fall within an accepted glass formulation range, additional glass formers must be added through the process. Although the network modifiers (such as alkali metals) may decrease the durability, they are important to control melted glass viscosity. The addition of fluxes to the glass melt is controlled as increased flux composition generally lowers melting temperature, glass viscosity and leaching resistance. Of the glass forming oxides, SiO_2 is the most important in glass making and used as the major ingredient in most glasses because of its good chemical durability. According to the current knowledge, the coal fly ash contains high amounts of SiO_2 and Al_2O_3, but has insufficient glass network modifiers. The most effective glass modifier is Na_2O. Other than CaO or MgO, adding Na_2O does not increase the crystalline tendency [115]. On the other hand, Fe_2O_3 as an intermediate network oxide increases the crystalline tendency. It is generally used as a nucleating agent in the waste glass compositions.

According to the above discussions, it can be estimated from Table 5.2 that Çayırhan, Tunçbilek, Orhaneli, Çan, Çatalağzı and Seyitömer fly ashes are the most appropriate candidates for the production of glasses; however Afşin-Elbistan fly ash is not suitable for the glass production because of the low SiO_2 - Al_2O_3 content and high CaO content of it. As can be seen from chemical composition of the silica fume and red mud, both of them are not suitable for glass production. On the basis of these observations, all coal fly ash samples used for the glass production starting from the Çayırhan fly ash. Glasses were obtained from Çayırhan, Tunçbilek, Orhaneli, Afşin-Elbistan and Seyitömer fly ashes without any additives according to the procedure described in section 5.4. However, the glass production from Çan and Çatalağzı fly ashes cannot be achieved because of the very high viscosities of them at the melting temperature of 1773 K. The higher SiO_2 and Al_2O_3 content of those fly ashes led to higher viscosity. The viscosity is mainly depending on the amount of network

formers and can be decreased with the addition of Na_2O, K_2O and CaO. The literature surveys showed that Na_2O content higher than 15% could lead to adequate melts, since this modifier tends to lower the viscosity of the batch fluid increasing the workability of the melts [117,201]. However, this indication was not followed, because Na_2O rich glasses are usually very unstable and exhibit low chemical durability. Glass formation with good chemical durability achieved with using the combined addition of fluxes Na_2O and CaO [117]. With the aim of lowering the viscosity of the batch fluids, different amounts of modifier oxides were added by trial and error, essaying firstly the effect of Na_2O content and then the effect of Na_2O+CaO. Na_2CO_3 $CaCO_3$ were used as raw materials for Na_2O and CaO sources, respectively. Table 6.1 shows the effect of additives on the melting behavior of fly ashes. As seen from Table 6.1, the addition of Na_2O cannot be enough to decrease the viscosity. On the basis of these results, both Na_2O and CaO were added to the Çan and Çatalağzı fly ashes.

Table 6.1: Effects of different amounts of additives on the melting behavior of Çan and Çatalağzı fly ashes

	Amount of added oxides (wt %)		Effect on melting behavior
	Na_2O	CaO	
Çan fly ash	5	-	Melt is very viscous and couldn't be poured into water
	5	5	Melt is very viscous and hardly poured out of crucible
	10	7	A small amount of melt could be poured out of the crucible
Çatalağzı fly ash	5	-	Melt is very viscous and couldn't be poured into water
	5	5	Melt is very viscous and hardly poured out of crucible
	10	7	A small amount of melt could be poured out of the crucible

Since the compositions of the Çan and Çatalağzı fly ashes are not significantly different from each other, it was decided to add the same amount of 5 wt% Na_2O + 5 wt% CaO to those fly ashes. The obtained melts for both fly ashes couldn't be poured to the water due to their high viscosities. Glass production from Çan and

Çatalağzı fly ashes tried again with the increase in the amount of Na_2O + CaO content. 10 wt% Na_2O + 7 wt% CaO were added to fly ashes to decrease the viscosity of the melt. But, only a small amount of melt could be poured into the water. This amount was not sufficient for the glass production. Therefore, it was decided to quit the glass production from Çan and Çatalağzı fly ashes. The glass samples produced from Çayırhan, Tunçbilek, Orhaneli, Afşin-Elbistan and Seyitömer fly ashes were deep brown to black in color. The color of the glasses produced from Çayırhan, Tunçbilek and Seyitömer fly ashes were deep black because of their high Fe_2O_3 content of them. Iron is the coloring ion in ashes caused the formation of dark colored glasses. The produced glasses were homogeneous and free from bubble. Codes were given to the produced glass samples obtained from fly ashes (Table 6.2).

6.2 Experimental Results on Glass Production

6.2.1 DTA results of the produced glasses

DTA was utilized to measure the glass thermal properties by heating 20 mg glass sample with a heating rate of 20 K/min (Figures 6.1-6.5).

As a glass is heated, its heat capacity changes within a narrow temperature range called the glass transition temperature (Tg), which corresponds to the temperature at which the glass network acquires sufficient mobility to change from a rigid to a plastic solid. It was observed that the endothermic peaks that show the glass transition temperature took place in all glass samples. The glass transition temperatures of the glass samples varied in the temperature range of 964-1023 K. As the crystallization takes place, the heat of crystallization is evolved and an exothermic peak that shows the crystallization peak temperature (Tp) occurs. Table 6.3 shows the Tg and Tp values of the produced glasses. As seen from Table 6.3, only TG sample has one crystallization peak temperature at 1166 K. This result can be seen from Figure 6.5 as well. Any exothermic peak was not observed in the other glass sample's DTA scans. According to DTA results, it can be said that only one glass sample obtained from Tunçbilek fly ash is suitable for the glass-ceramic production and glass-ceramic samples can't be produced from Çayırhan, Orhaneli, Afşin-Elbistan and Seyitömer fly ashes without any additives.

Table 6.2: Codes of the produced glass samples

Glass	Code
Obtained from Çayırhan Fly Ash	CG
Obtained from Seyitömer Fly Ash	SG
Obtained from Tunçbilek Fly Ash	TG
Obtained from Orhaneli Fly Ash	OG
Obtained from Afşin-Elbistan Fly Ash	AEG

Table 6.3: DTA results of the produced glasses

Glass	Tg(K)	Tp(K)
CG	988	-
SG	985	-
TG	964	1166
OG	1003	-
AEG	1023	-

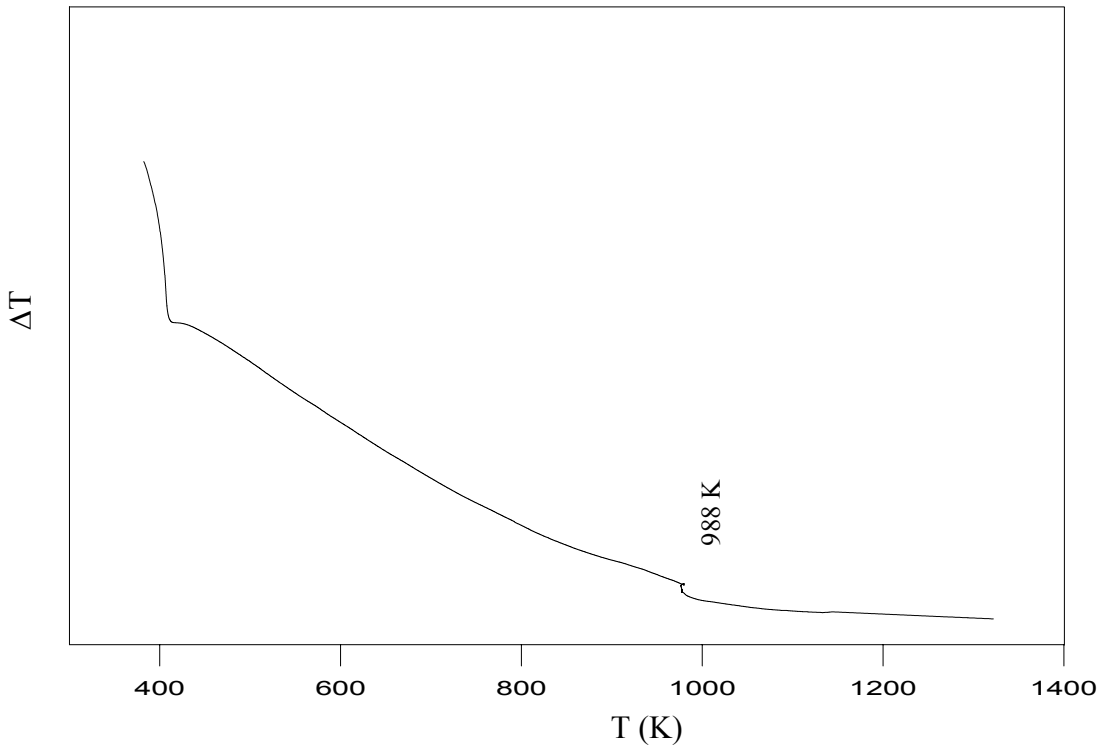

Figure 6.1: DTA Graph of the CG sample

6.2.2 XRD studies of the produced glasses

XRD pattern of the TG sample shown in Figure 6.6 indicated the amorphous state of the sample. No significant crystalline phase could be detected by the XRD in tested CG sample. XRD patterns of the SG, CG, OG, AEG samples were given in Appendix A Figure A.2. In all cases, the spectra show presence of a non-crystalline material and absence of any distinct crystalline species, as it was expected.

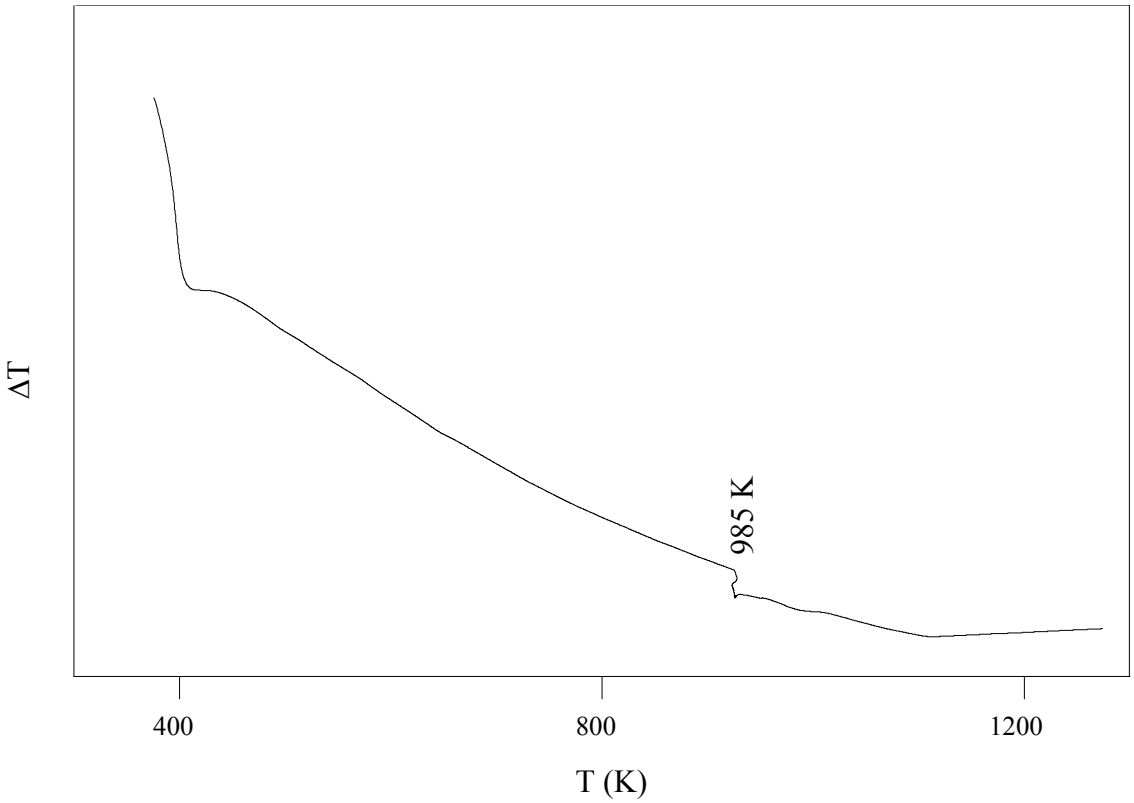

Figure 6.2: DTA Graph of the SG sample

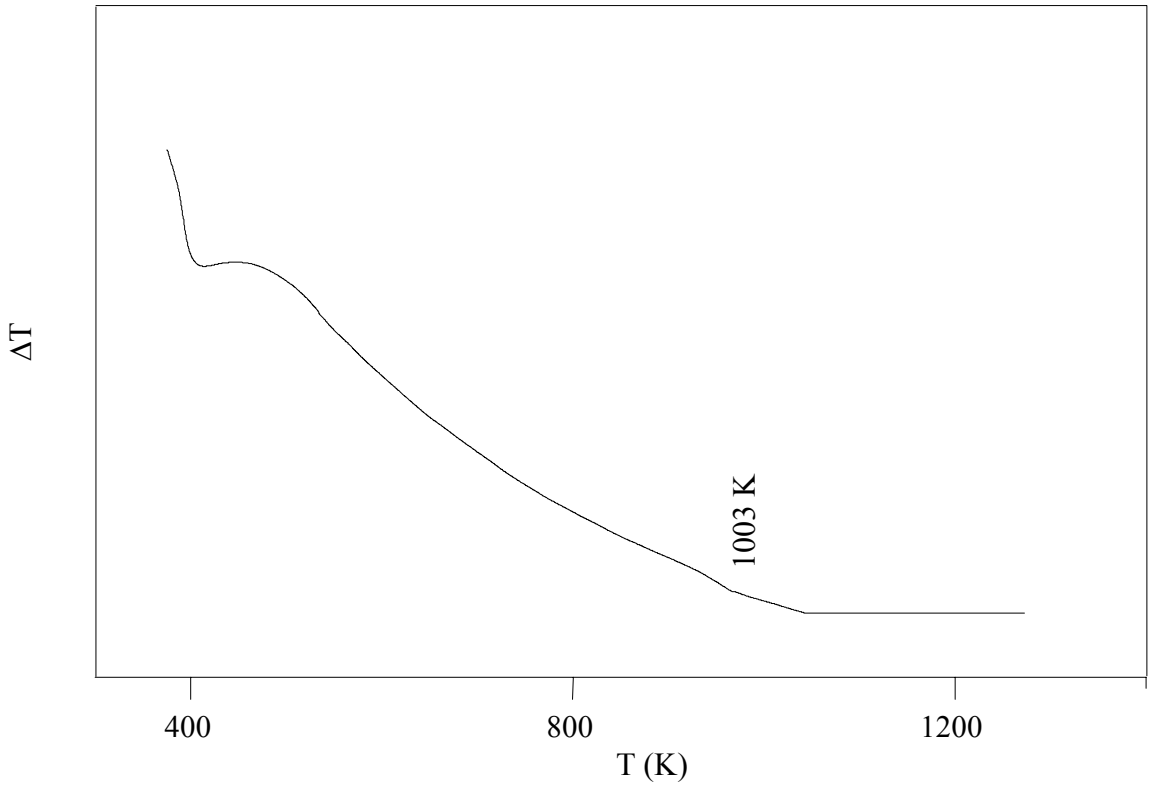

Figure 6.3: DTA Graph of the OG sample

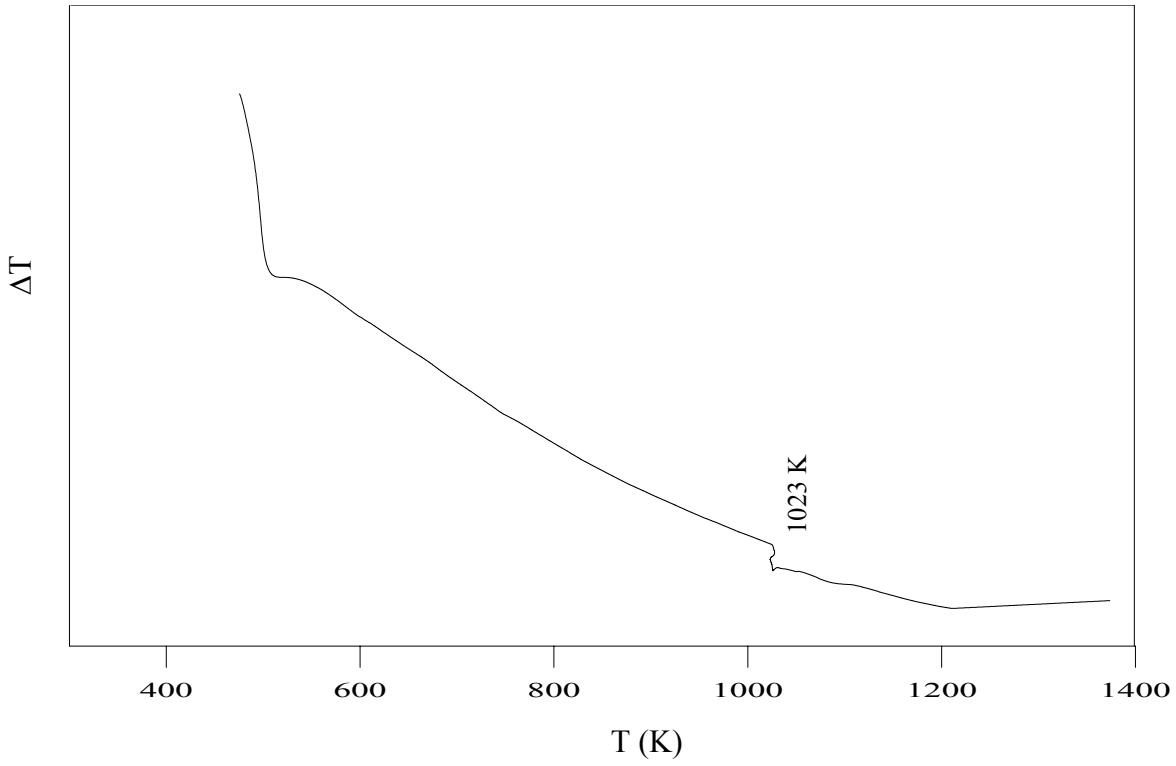

Figure 6.4: DTA Graph of the AEG sample

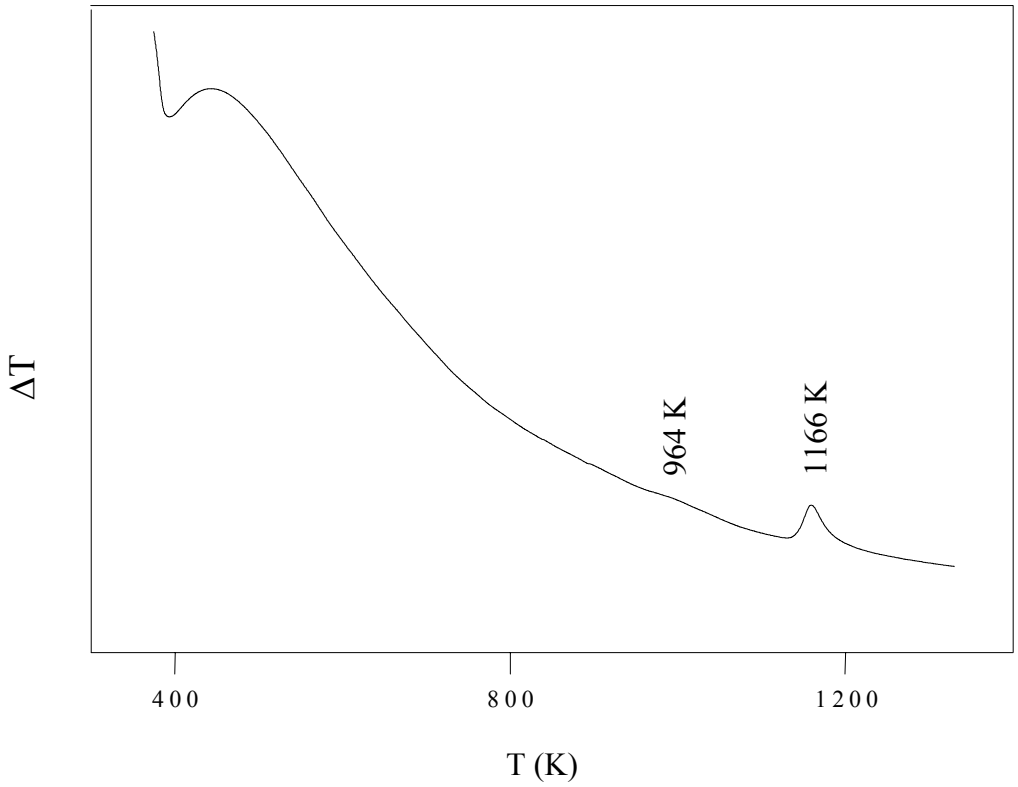

Figure 6.5: DTA Graph of the TG sample

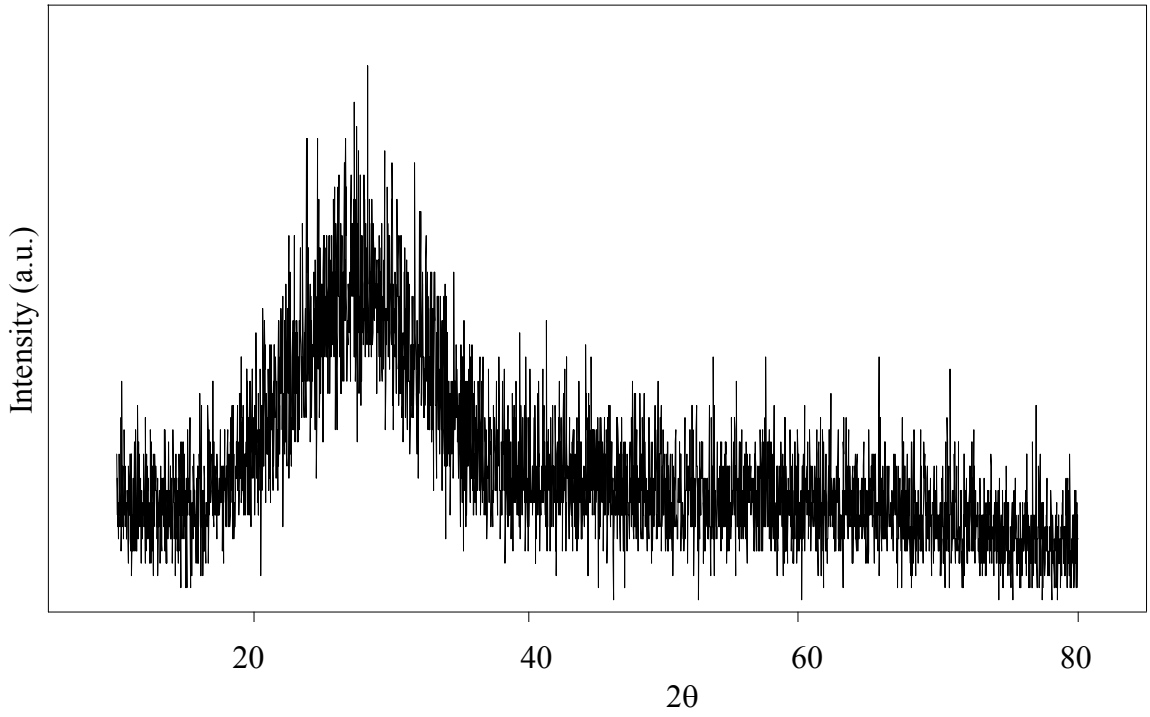

Figure 6.6: X-ray diffraction pattern of TG sample

6.2.3 SEM studies of the produced glasses

The microstructural studies were performed on the obtained glass samples using SEM. The knowledge homogeneity of waste glass was obviously related to the performance of the production process. SEM investigations confirmed their homogeneous nature of all glass samples. Figure 6.7 indicates the SEM micrographs of the CG, SG, TG, OG and AEG samples. All the produced glass samples had shiny surfaces and were bubble free except AEG sample. A significant volume of approximately spherical pores in the glass matrix can be seen in Figure 6.7 (e). These are believed to result from softening of the glassy phase present in the ash, together with simultaneous evaluation of gas at this temperature.

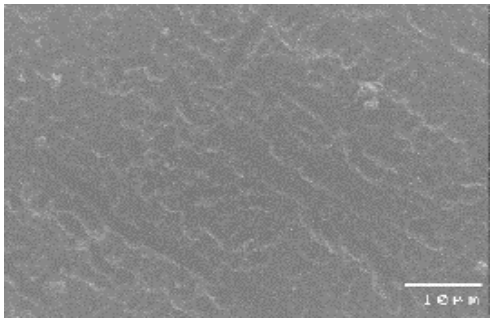

(a)

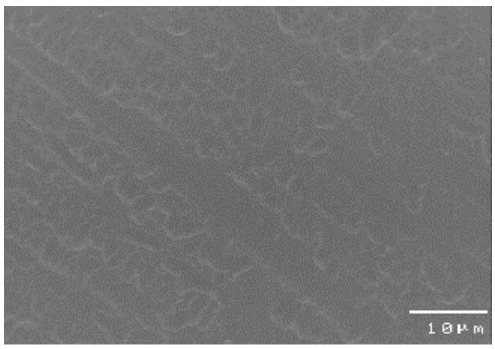

(b)

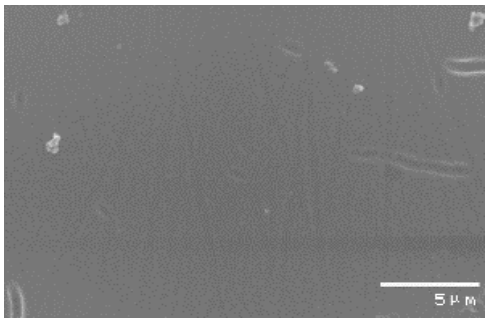

(c)

Figure 6.7: SEM micrographs of the CG (a), SG (b) and TG (c) samples

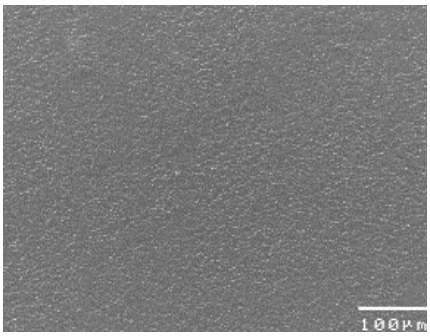

(d)

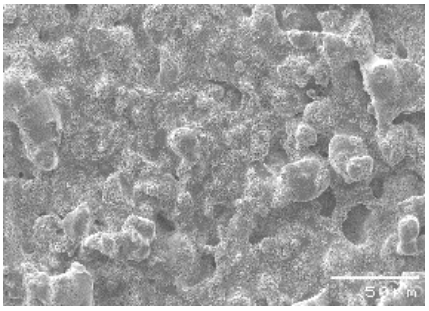

(e)

Figure 6.7: SEM micrographs of the OG (d) and AEG (e) samples

6.2.4 Physical and mechanical properties of the produced glasses

Density, porosity, water adsorption and Vickers microhardness values of glasses were given in Table 6.4. Densities of the glasses were in the range of 1.29-2.91 g/cm^3. Density of AEG sample has the lowest value due to Afşin-Elbistan fly ash has the lowest SiO_2 - Al_2O_3 and highest CaO content. Of the glass forming oxides, SiO_2 is the most important in glass making and used as the major ingredient in most glasses because of its good chemical durability. The results also indicated that Al_2O_3 had the same effect as SiO_2 on the properties of glass materials. Higher SiO_2 - Al_2O_3 content makes the glass structure more rigid. CaO, Na_2O and K_2O which form the weakest bonds generally prove the greatest detriment to glass durability. Similar results were shown in the microhardness values. Decrease in density also resulted in decrease of microhardness. As seen from Figure 6.8, Vickers microhardness of glasses obtained from fly ashes increased from 317 to 511 kg/mm^2 as SiO_2 - Al_2O_3 content increases. This indicates that SiO_2 - Al_2O_3 acts as a network former, which enhances the network connectivity of the glass matrix. In addition, bond energy of a

network former is much higher than that of a network modifier [202]. Microhardness values of CG, SG and TG samples are high in comparison with window glass (418.1 kg/mm^2), silica glass (476.7 kg/mm^2)[203], glasses produced from coal fly ash in another study (410 kg/mm^2)[204] and glasses produced from municipal solid waste (MSW) incinerator fly ash (482.3 kg/mm^2)[205]. Both water adsorption and porosity correlated well with each other and decreased with the increase of the density values of the produced glasses. AEG sample has the highest porosity value of 8.6%. This result is in well agreement with the SEM observations.

Table 6.4: Physical and mechanical properties of the produced glass samples

Glass	Density (g/cm^3)	Vickers Microhardness (kg/mm^2)	Porosity (%)	Water adsorption (%)
CG	2.81	485	0.38	0.6
AEG	1.29	317	8.60	3.2
OG	2.76	455	0.50	1.7
SG	2.85	498	0.35	0.3
TG	2.91	511	0.31	0.1

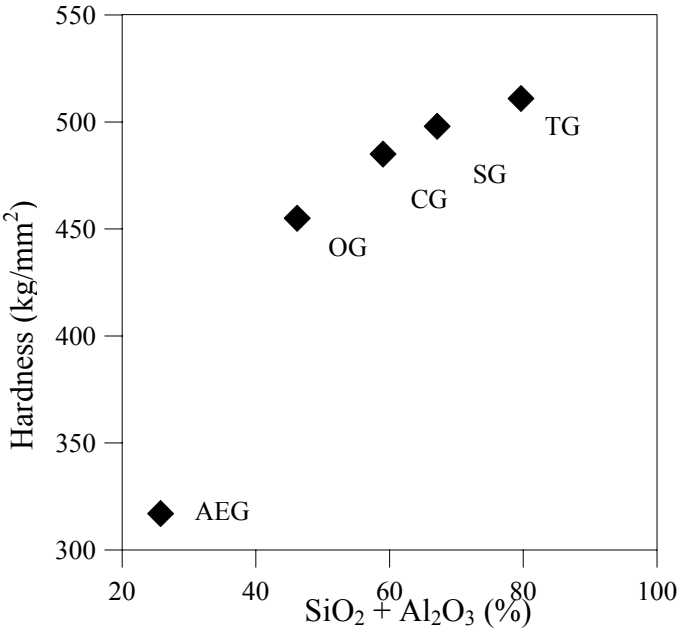

Figure 6.8: The effect of $SiO_2 + Al_2O_3$ content on the hardness of the glass samples

6.2.5 TCLP results of the produced glasses

The TCLP test was conducted to study the heavy metals migration. The dissolution of the silica matrix can release heavy metals from the glass structure [115]. In this study, the TCLP analyses were limited to the main hazardous heavy metals of Zn, Pb, Mn and Cr. TCLP results of the glasses produced from fly ashes were given in Table 6.5. The results were compared with the US EPA limits. It was found that the extracted amounts of heavy metals are lower than the limits required by the US EPA. It should be noted that the volatile metals such as Zn and Pb may evaporate to the atmosphere before or during melting stage. Therefore, to treat fly ashes by using thermal melting technology, a secondary air pollution control system should be designed to catch volatile metals [155]. Another reason for the lower leachability is due to the heavy metal ions replaced with other ions and successfully solidified into the glass matrix. The percentage of leachable fraction of heavy metals is different. Among the studied heavy metals, Zn showed the highest percentage of leachable fraction than others, since Zn is unstable in acidic solutions and also Zn concentration is the highest in all fly ash samples. As seen from Tables 5.2, 6.5 and Figures 6.9, 6.10, leaching of heavy metal ions decreased with the increase in SiO_2 and decrease in CaO and MgO content. In general, chemical stability is consistent with the progressive formation of a more compact and interconnected glass network structure with the addition of the glass formers [205]. Therefore, increase in the ratio of SiO_2 strengths the chemical stability of the glasses. On the other hand, the network modifiers (such as CaO, Na_2O) may decrease the durability. They lower melting temperature and glass viscosity but also lower leaching resistance since they weaken the network structure. Therefore, AEG and OG samples have the lowest leaching resistances. The glasses produced in this work showed high leaching resistance than the glasses obtained from coal fly ash by Sheng et al.[115] and incinerator fly ash by Park et al.[205]. TCLP results showed that the glasses produced from coal fly ashes could be taken as non-hazardous, which showed the potential application as useful materials.

Table 6.5: TCLP results of the produced glass samples

Glass	Cr^{3+} (ppm)	Mn^{2+} (ppm)	Zn^{2+} (ppm)	Pb^{2+} (ppm)
CG	BDL	BDL	0.006	BDL
AEG	0.06	0.03	0.22	0.09
OG	0.01	0.01	0.11	0.02
SG	BDL	BDL	0.001	BDL
TG	BDL	BDL	0.005	BDL
US EPA limit	5	5	500	0.5

BDL: Below Detection Limit

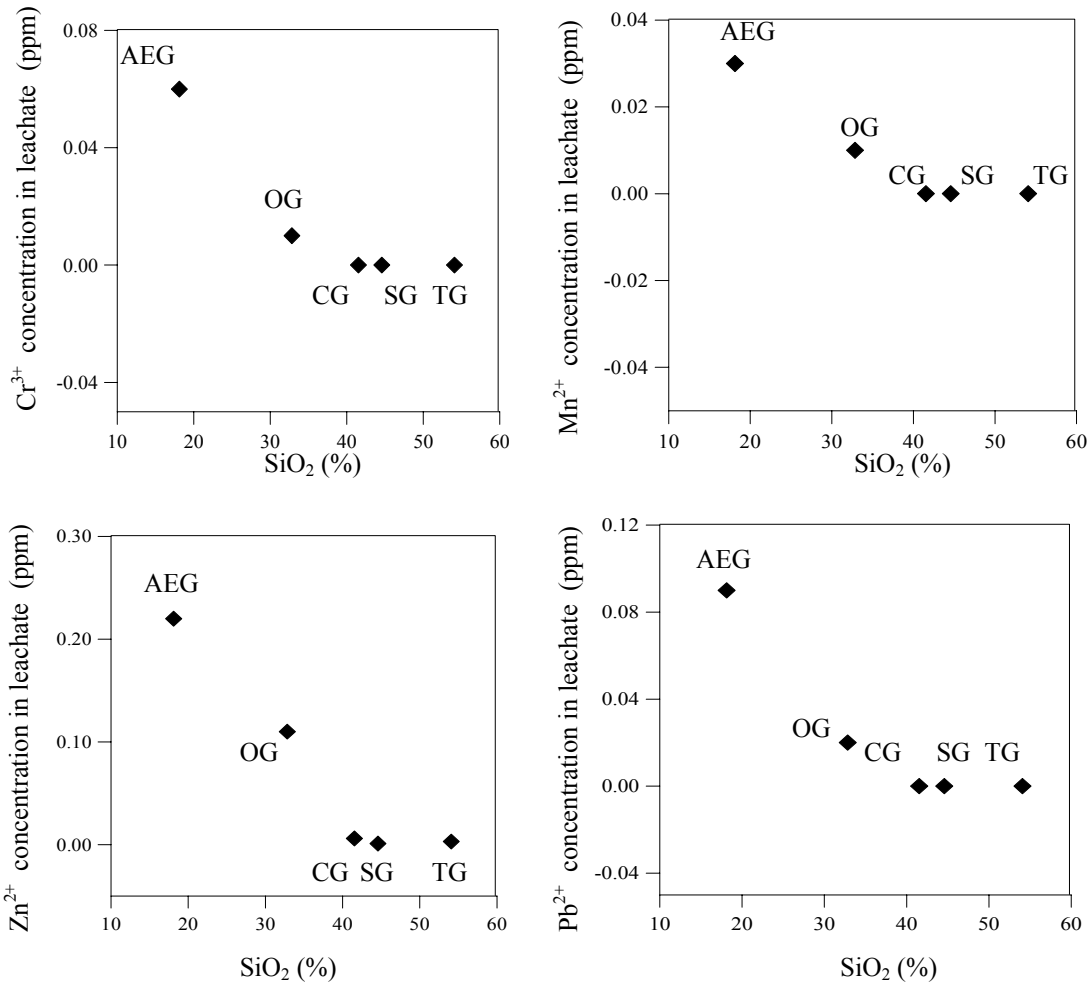

Figure 6.9: The relationship between the heavy metal concentrations in the leachate of the produced glasses and SiO_2 content of the fly ash samples

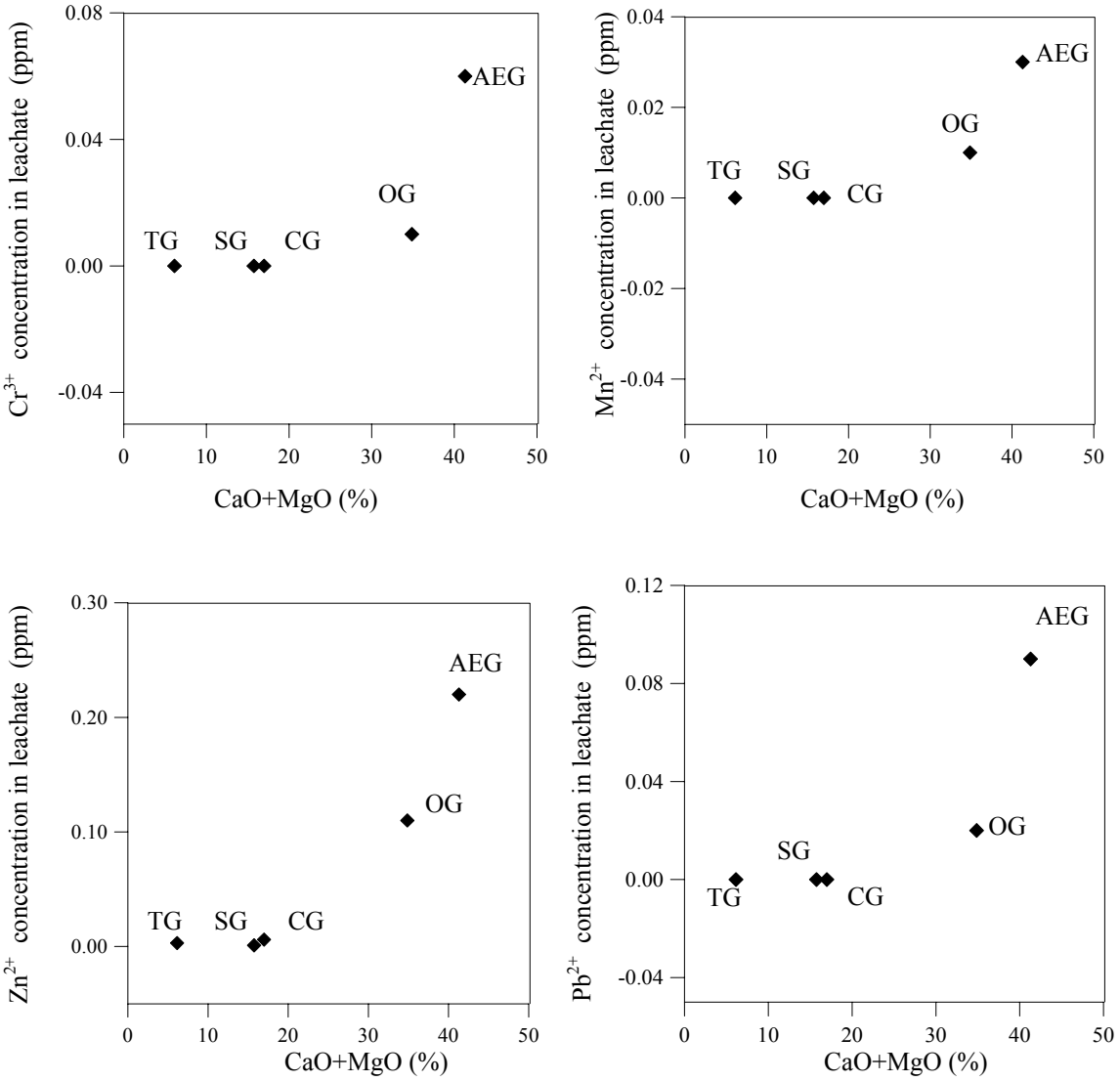

Figure 6.10: The relationship between the heavy metal concentrations in the leachate of the produced glasses and CaO-MgO content of the fly ash samples

6.2.6 Chemical resistance of the produced glasses

Chemical resistance of glasses was listed in Table 6.6. Chemical resistance of glasses increased with the increase in SiO_2 + Al_2O_3 content of fly ashes (Figure 6.11(a)). Same results were obtained and discussed in the Sections 6.1, 6.2.4 and 6.2.5. Furthermore, Fe_2O_3, which is found in the initial ash is a serious candidate to take part in the construction of the vitreous network of the stabilized product. It has been found that Fe_2O_3 can be incorporated into a silicate glass and increase the number of polyhedra taking part in the vitreous network [206]. It can thus act as an intermediate

rather than a modifier. The higher Fe_2O_3 content leads to a more chemically stable product. Therefore, chemical resistance of the glass samples also increased with increasing in Fe_2O_3 content of fly ash (Figure 6.11(b)). The chemical durability of glasses shows acceptable behavior. However, they have relatively high weight losses for HNO_3 durability compare to NaOH durability. It is apparent that the produced glasses show high resistance to alkali solutions.

Table 6.6: Chemical resistance of the glass samples

Glass	HNO_3 (%)	NaOH(%)
CG	1.3	0.05
AEG	31.3	0.1
OG	13.2	0.08
SG	2.8	0.14
TG	1.11	0.05

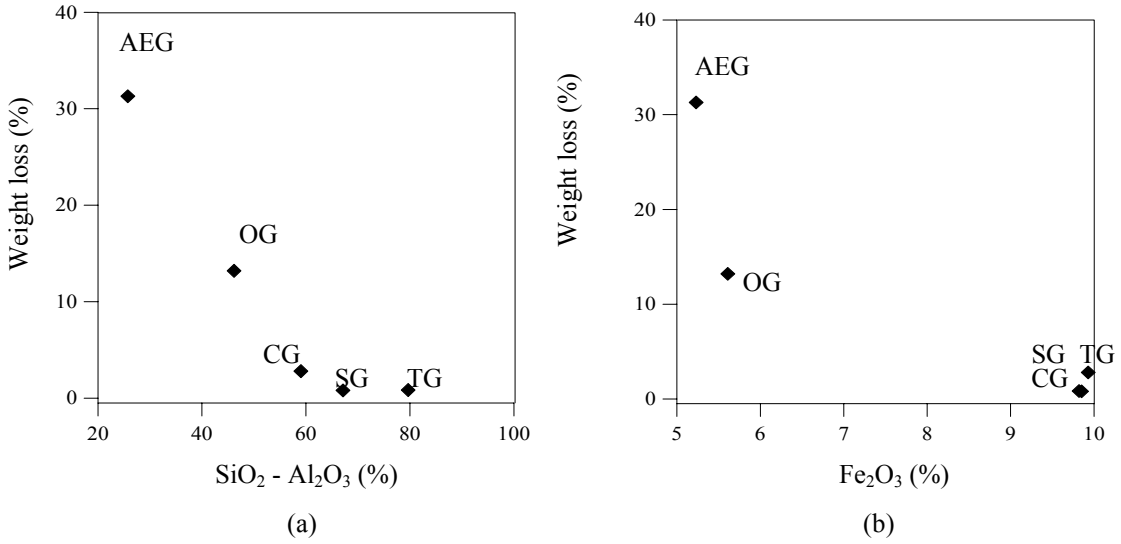

Figure 6.11: The effect of SiO_2 - Al_2O_3 (a) and Fe_2O_3 (b) contents on the chemical resistance of the glass samples

6.3 Experimental Results on Heat-Treated Glass Samples

It was concluded from the DTA results that the glasses produced from fly ashes except Tunçbilek fly ash showed no crystallization tendency since any exothermic peak couldn't be seen on the DTA curves. However, physical, microstructural, mechanical and chemical properties of the glass samples can be changed when a heat treatment process conducted on the produced glasses. One of the objectives of this study was to determine whether or not the glasses could be transformed to a crystalline structured material by means of heat treatment. Therefore, to investigate the effect of heat treatment on the properties of glass samples, SEM and XRD, TCLP test, density, porosity, water adsorption, microhardness and chemical resistance measurements were performed. Some codes were given to the heat-treated glass samples which are shown in Table 6.7.

Table 6.7: Codes of the heat-treated glass samples

Heat Treated Glass	Code
Obtained from Çayırhan Fly Ash	CG1000
Obtained from Seyitömer Fly Ash	SG1000
Obtained from Tunçbilek Fly Ash	TG1000
Obtained from Orhaneli Fly Ash	OG1000
Obtained from Afşin-Elbistan Fly Ash	AEG1000

6.3.1 XRD studies of the heat-treated glasses

In order to identify the crystalline phase(s), x-ray scans were carried out on samples which had been heat-treated up to 1423 K followed by slow cooling in the furnace to the room temperature. The XRD analysis of OG1000 sample is shown in Figure 6.12. XRD patterns of CG1000, SG1000, TG1000 and AEG1000 samples were given in Appendix A in Figure A.3. There is no doubt that crystalline phases coexist since the XRD patterns show that the amorphous phase has practically disappeared and augite, diopside, wollastonite and gehlenite crystalline phases occurred in the samples. On the XRD pattern of the AEG1000 sample the characteristic broad peak of amorphous material and some small peaks which correspond to diopside phase

($CaMg(SiO_3)_2$) are present. AEG1000 sample has the most amorphous material in all samples because of the chemical composition of it. As it was discussed in the previous sections Afşin-Elbistan fly ash has the lowest SiO_2 - Al_2O_3 content and therefore, it is not suitable for glass and glass-ceramic production. Furthermore, it has the lowest Fe_2O_3 content among the fly ash samples. So, only a small amount of diopside phase occurred in the microcrystalline structure. Diopside phase (Ca (Mg, Fe, Al)(Si, $Al)_2O_6$) was also determined in the SG1000 and CG1000 samples. Diopside structure occurred in this samples is the same since the chemical composition of these samples are very similar. It is important to note that Fe_2O_3 known to be a nucleating agent and presented in reasonable amounts in those samples. Only a small proportion of glassy phase detected in the XRD patterns of those samples. XRD result of TG1000 sample revealed that the main crystalline phase was aluminum augite ($Ca(Mg, Fe^{3+}, Al)(Si, Al)_2O_6$). Although it is usually considered as an intermediate glass network ion, the Fe^{3+} could act as a modifier of the TG glass structure, breaking the Si-O-Si bonds to form the augite phase. Mg and Ca ions have also effects on the formation of crystalline structure as network modifiers [12]. However, Fe^{3+} plays an important role in the crystalline structure as the network modifier since the content of Fe^{3+} is high enough compared to the Ca and Mg ions. Ca and Mg contents of the Çayırhan and Seyitömer fly ashes are higher than that of the Tunçbilek fly ash. Therefore, diopside phase ($Ca(Mg,Al)(Si,Al)_2O_6$) occurred in the CG1000 and SG1000 samples instead of aluminum augite phase($Ca(Mg, Fe^{3+}, Al)(Si, Al)_2O_6$) which was obtained in the TG1000 sample. However, diopside and augite phases belong to the same group. XRD pattern of the OG1000 sample shows the presence of wollastonite ($CaSiO_3$) and gehlenite ($Ca_2Al_2SiO_7$) phases. The high Ca and Si content, which are essential elements for wollastonite formation ($CaSiO_3$) on the surface, may enhance the crystallization probability of this phase. Since CaO content of Orhaneli fly ash is high, wollastonite and gehlenite phases occurred in the microcrystalline form in contrast to the SG1000, CG1000 and TG1000 samples.

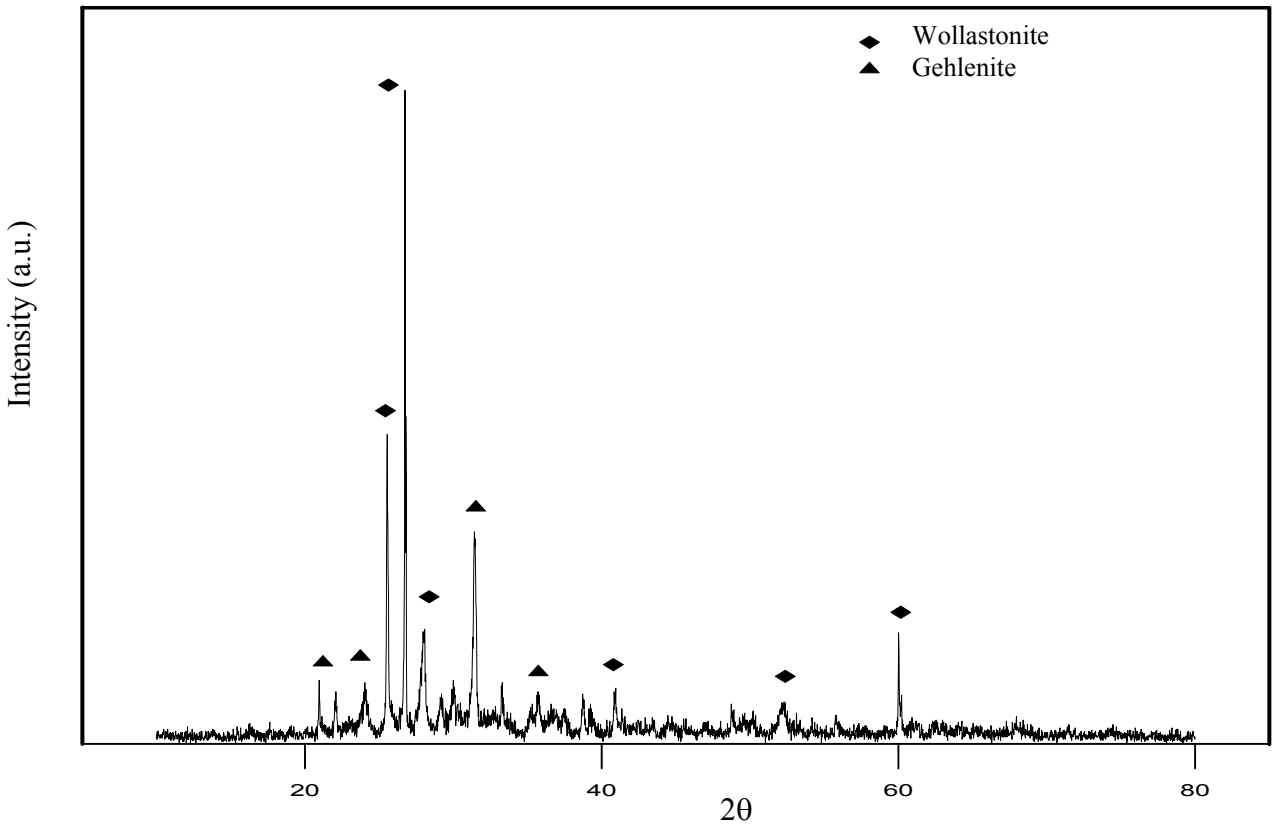

Figure 6.12: XRD pattern of the OG1000 sample

6.3.2 SEM studies of the heat-treated glasses

SEM investigations were conducted in order to obtain better understanding of the morphology and size of the resultant microstructure. SEM micrograph of the TG1000 sample (Figure 6.13) shows the presence of strongly interlocked tiny crystals of about 0.15-0.30 μm size embedded in a glassy matrix and the absence of pores. Figures 6.14 and 6.15 are representative SEM micrographs of SG1000 and CG1000 samples, respectively. As seen from these figures, diopside crystals formed in a very irregular shape and orientation were observed in the SEM micrographs of the SG1000 samples. Their size ranges from 0.5 to 1 μm. The holes in the crystals are probably due to preferential etching in HF solution. The crystals were formed randomly in the microstructure and still a large amount of glassy phase remained between the crystallites. As seen from Figure 6.15, small diopside crystallites were dispersed in the microstructure of the CG1000 sample. There are also extensive cracks on the surface of the sample. These cracks may occur due to the thermal

residual stress of the glass during the cooling of the melt to the room temperature. The microstructure of the OG1000 sample corresponded well with the crystal phases found by XRD as seen in Figure 6.16. A network of wollastonite and gehlenite crystallites were formed with perpendical branching. Irregular shaped crystallites dispersed randomly in the microstructure of the OG1000sample. Some small pores with a diameter of 1 μm or less than 1 μm can also be observed on the surface of the sample. Figure 6.17 shows SEM micrgraph of the AEG1000 sample. It is seen from this figure that, high content of glassy phase still remained in the volume of the sample, as it was expected from the XRD result. Only a few glassy droplets were converted into diopside crystals. Their size and shape are irregular and crystallites randomly distributed in the glassy microstructure. XRD and SEM results of the AEG1000, SG1000, OG1000 and CG1000 samples revealed that small amount of crystallites occurred in the microstructure of the samples in contrast to the DTA results. DTA results were showed that those glass samples had no crystallization tendency because of the absence of crystallization peak. However, maximum working temperature of DTA is 1373 K and above this temperature there may be an exothermic peak that we couldn't detect. Crystallization peak temperatures of glasses produced from fly ashes generally change between 1073-1273 K [116,118,135,207]. However, several authors reported that crystallization peak temperatures of glasses produced from waste materials are in the range of 1293-1414 K [131,204]. If there had been exothermic peaks of those glass samples we could not have detected since the maximum working temperature of DTA is limited. Therefore, glass samples were heated to the temperature of 1423 K, which is above the maximum working temperature of DTA to determine the effect of heat treatment process. The controlled nucleation and crystallization of glasses is of prime importance in the formation of glass-ceramics, because the properties are influenced by the manner in which crystallization occurs. Accordingly, the conventional process to produce a glass-ceramic involves two steps: a low temperature heat treatment of glasses, to induce nucleation, followed by heating to a second, higher temperature, to allow crystal growth of the nuclei as we knew. However, in this case the controlled heat treatment process couldn't be applied to the glass samples since the crystallization peak temperatures were not known. This is one of the reasons for the poor microcrystalline structure obtained in the AEG1000, CG1000, OG1000 and SG1000 samples. But, TG1000 sample has the best microcrystalline structure. Tiny

crystallites dispersed in the microstructure of the sample since iron oxide content of Tunçbilek fly ash is high. Some authors have reported on the influence of Fe_2O_3 and Al_2O_3 in the nucleation and crystallization of silicate glasses. Thus, Rogers et al.[208] found that iron oxide has a large influence on the nucleation of glasses if Fe_2O_3 content higher than 5 wt%. In this study, TG1000 sample has one of the highest Fe_2O_3 and Al_2O_3 content and AEG1000 has the lowest Fe_2O_3 content. Therefore, tiny crystallites dispersed in the microstructure increased with the increasing Fe_2O_3 and Al_2O_3 content of sample. Furthermore, the another reason for better microcrystalline structure for TG1000 sample is the chemical composition of it. Thus, TG sample is the most appropriate candidate for glass-ceramic production because of the chemical composition of it and DTA results, as it was discussed in the previous sections.

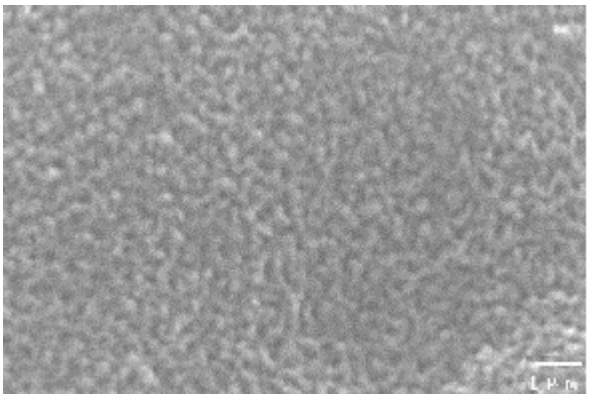

Figure 6.13: SEM micrographs of the TG1000 sample

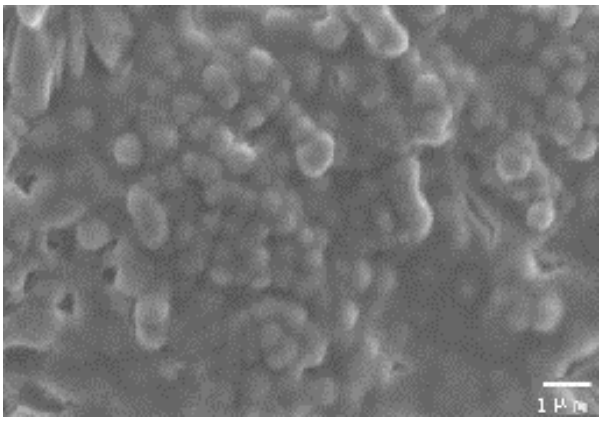

Figure 6.14: SEM micrographs of the SG1000 sample

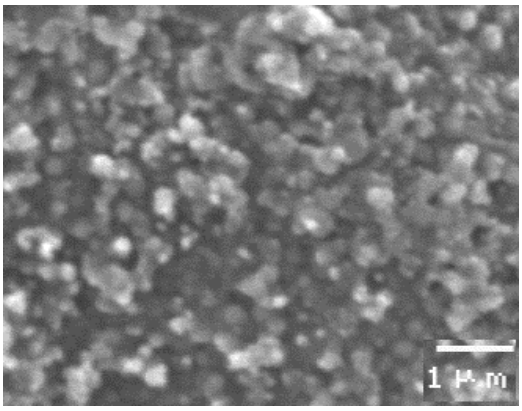

Figure 6.15: SEM micrographs of the CG1000 sample

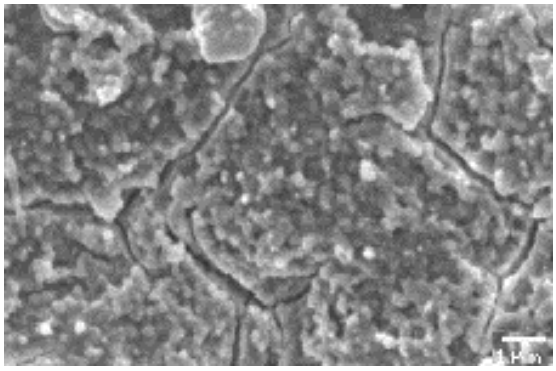

Figure 6.16: SEM micrographs of the OG1000 sample

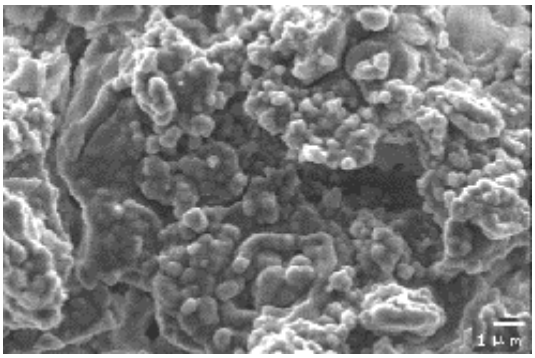

Figure 6.17: SEM micrographs of the AEG1000 sample

6.3.3 Physical and mechanical properties of the heat-treated glasses

Density, porosity, water adsorption and Vickers microhardness values of the heat-treated glass samples were given in Table 6.8. Densities of the heat-treated glass samples are changed in the range of 2.03-3.19 g/cm^3 and increased with increasing

crystalline volume in the glassy matrix. Density values are functions of both the crystalline sizes and the crystalline volume in the glassy matrix. Both porosity and water adsorption are correlated well each other and decreased with the increase of the crystalline sites. The Vickers microhardness values increased with increasing amount of crystallites and decreasing the average crystalline sizes. The factors which effect the hardness values are crystal type, crytallization rate and homogeneity of crystal size. As discussed above, the main crystalline phases were augite for TG1000, diopside for CG1000, AEG1000 and SG1000 and wollastonite+gehlenite for OG1000. SEM results revealed that the amount of crystallites increased and the average crystalline size decreased in the sequence of TG1000, SG1000, CG1000, OG1000 and AEG1000. From Table 6.8, it is obvious that TG1000 sample has highest hardness value with the best microcrystalline structure. It is reported that fine grained crystalline materials posses better microhardness [116]. However, the crystallization rate is also an important factor deciding hardness. From the XRD and SEM results it can be said that some glassy phase was remained AEG1000, SG1000, CG1000 and OG1000 samples and only TG1000 sample reached complete crystallization. From the SEM investigations, it can be observed that average crystal size of TG1000 sample was smaller than the other samples and the sphereletic crystallites dispersed in the microstructure homogeneously. The crystal size of other samples ranges greatly and the shapes of the crystallites were irregular. This inhomogeneity of crystal size and shape may also cause a decrease in the hardness of the samples. Similar to hardness results, as the samples became more crystalline, the density increased, the porosity and water adsorption decreased. By comparing the physical and mechanical properties of the heat treated glasses, it was obvious that AEG1000 sample has the lowest values due to its lower ratio of glass formers and intermediate elements (here considering: Si+Al+Fe) to the modifier elements (in this case: Ca+Mg+Na+K). Properties of heat-treated glasses were compared with the properties of glasses and glass-ceramics produced from industrial wastes. These properties of the SG1000, OG1000, CG1000 and TG1000 samples are better than the properties of glass-ceramic materials produced from incinerator fly ash [155,163]. According to Cheng et al., the highest hardness value of the gehlenite glass-ceramic was 479 kg/mm^2 [163]. Hardness values of TG1000, OG1000, SG1000 and CG1000 are higher than that value. Density and hardness values of TG1000 sample are higher

than the values of the glasses produced from domiciliary incinerator fly ash measured by Romero et al.[209].

Table 6.8: Physical and mechanical properties of the heat-treated glass samples

Heat Treated Glass	Density (g/cm^3)	Vickers Microhardness (kg/mm^2)	Porosity (%)	Water adsorption (%)
CG1000	2.98	542	0.11	0.30
AEG1000	2.03	398	1.40	2.10
OG1000	2.86	512	0.21	0.90
SG1000	3.08	522	0.10	0.20
TG1000	3.19	792	0.00	0.03

6.3.4 TCLP results of the heat-treated glasses

TCLP tests were performed to all heat-treated glass samples and the experimental results are presented in Table 6.9. Mn concentration of all samples was found to be below the detection limit of analytical method, which is 0.001 ppm. All extracted amounts of heavy metals are lower than the limits required by US EPA. Each sample analyzed has insignificant leachibility characteristics for all heavy metals, suggesting that the heavy metal ions replaced other ions, such as Ca^{2+} and Al^{3+} and were held in the framework of the samples. In order to interpret the TCLP results, on the first place, the strong effect of microcrystalline structure formed in the samples, on the second place, the structural role of the main oxide should be taken into consideration. It was reported that crystalline structure affects leaching resistance [206]. After formation of crystalline phases in the heat-treated glass samples, the products become more resistant to leaching comparing to the produced glass samples. It was obvious that the leaching resistance of the glass samples were lower than the heat-treated glass samples. The heavy metal ions were strongly bonded inside the structure of the crystalline phases (diopside, wollastonite and gehlenite). The bonds in the glass structure are weaker than the crystalline phases since the glasses are amorphous materials. In that way heavy metal ions in the heat-treated glasses seemed to become non-leachable. Leaching resistance is also affected from microstructure of

the samples. The better microcrystalline structure results the better leaching resistance. Therefore, TG1000 sample had the highest leaching resistance. The structural role of the main oxides was discussed in the previous sections. TCLP results of the heat-treated glass samples are better than the results of the glass-ceramic materials produced from incinerator fly ashes. Cr-ion content in the resultant leachate solutions measured by Cheng et al.[125] is higher than the content of the leachate solutions in this study. TCLP results of the all heat treated glass samples are better than the TCLP results of the glasses and the heat-treated glasses produced from incinerator fly ash reported by Kavouras et al.[210].

Table 6.9: TCLP results of the heat-treated glass samples

Heat Treated Glass	Cr (ppm)	Mn (ppm)	Zn (ppm)	Pb (ppm)
CG1000	BDL	BDL	0.006	BDL
AEG1000	0.006	BDL	0.08	BDL
OG1000	BDL	BDL	0.009	0.002
SG1000	BDL	BDL	0.006	BDL
TG1000	BDL	BDL	BDL	BDL
US EPA limit	5	5	500	0.5

BDL: Below Detection Limit

6.3.5 Chemical resistance properties of the heat-treated glasses

Results for chemical resistance of the heat-treated glass samples were given in Table 6.10. As seen from Table 6.10 chemical resistance of heat-treated glass samples to the alkali solutions is relatively high compared to the acidic solutions. However, both HNO_3 and NaOH durability is better than the glass-ceramic produced from coal fly ash according to the study which was reported by Leroy et al.[117]. It can be seen from Table 6.10 that the durability of the samples correlates well with the crystallization tendency of the glass samples. Chemical resistance of TG1000 sample is the highest among all heat-treated glass samples due to its better microcrystalline structure. Chemical resistance increased with decreasing amount of glassy matrix surrounding the crystalline grains. Since weight losses are usually attributed to the

dissolution of the glassy matrix, this would lead to lower weight losses for TG1000 sample than AEG1000 sample. Chemical resistance of the heat- treated glass samples is better than the produced glass samples. This result was expected since the other properties of the heat-treated glass samples were much improved than the glass samples. The improved properties are attributed to the crystalline structure formed in the heat-treated glass samples.

Table 6.10: Chemical resistance of the heat-treated glass samples

Heat Treated Glass	HNO_3 (%)	NaOH(%)
CG1000	0.14	0.04
AEG1000	9.8	0.08
OG1000	0.29	0.07
SG1000	0.19	0.05
TG1000	0.05	0.02

6.4 Fly Ash Capability to Produce Glass-ceramics

The tendency of the fly ash based-glasses to transform to glass-ceramics was examined theoretically before initiating experimental work. The final product should comprise a high crystalline phase volume fraction containing finely textured crystals. The controlled vitrification process is a versatile method, allowing for a wide range of crystalline materials because of the variety of compositions for the manufacture of glass-ceramics from waste materials. Oxide compositions varied in a limited range for glass-ceramic production from waste materials which is given in the literature as [11]: 40-55 % SiO_2, 10-25 % Al_2O_3, <25 % CaO, 2-13 % MgO, 2-5 % Na_2O, 0.7-2 % K_2O and 4-11 % Fe_2O_3. In principle, depending on the chemical compositions of these materials, the following phases could be obtained in glass-ceramic production: Anorthite ($CaO-Al_2O_3-2SiO_2$), calcium ferrite (Fe-O-CaO), wollastonite ($CaO-SiO_2$), gehlenite ($CaO- Al_2O_3-2SiO_2$), diopside ($CaO-MgO-2SiO_2$), and/or augite ($CaO-MgO-FeO-SiO_2$). According to the above discussions, it can be estimated from Table 5.2 that CG, TG and SG samples are the most appropriate candidates for the glass-ceramic production. The silica contents of these samples are within the glass forming

region of the CaO-Al_2O_3-SiO_2 (CAS) ternary and fall between the silica content of the fly ash used by Boccaccini et al. [211] and that of the As Pontes fly ash used by Barbieri et al. [11] to form glass and glass-ceramics. CAS system glasses which belong to one of the fundamental silicate systems have been used widely in many fields of industry. Although glass production was achieved by using Orhaneli fly ash, it is not suitable for glass-ceramic production because of its low Fe_2O_3 content. AEG sample is not suitable for glass-ceramic production since it has low Al_2O_3-SiO_2 and high CaO content. On the basis of these interpretations that are based on chemical composition of fly ashes, only TG, CG and SG samples can be used for glass-ceramic production.

Initially the theoretical approach used for glass-ceramic production was applied in order to study the capability to devitrify the different glasses. The Ginsberg method uses a ternary diagram to represent the composition of the original glasses; Sal (Al_2O_3-SiO_2), Cafem ($CaO + (FeO + Fe_2O_3) + MgO$) and Alk ($Na_2O + K_2O$) [212]. Basically, only glasses located between the 60-70 % Sal band are considered suitable for producing glass-ceramics with the best properties. The glass compositions below this zone contain excessive modifiers that destabilize the glass network. Those with higher SiO_2 content have a very rigid structure, making processing operations difficult. Experimental data (Figure 6.18 (a)) show that only CG and SG glasses are located in the Sal band and TG sample is close to the ideal band. OG and AEG samples are far from the Sal band so they don't have acceptable compositions for producing glass-ceramics.

Another well-known method is the Rashin-Tschetveritkov [213] method modified by Kanazirsky and Tetzo in 1972 [214]. In this case, the triangular diagram corresponds to the corners of: Q, L and M, where Q is SiO_2, L is $Al_2O_3 + Na_2O + K_2O$ and M is $CaO + (Fe_2O + Fe_2O_3) + MgO + TiO_2$. This diagram is divided into three zones limited by tie lines : pyroxene-feldspar and pyroxene-Tschermark molecule (Tsch(a well-known calcium excess pyroxene from the geochemical basalt process), $CaALSi_2O_6$)[215]. The pyroxene (P) and feldspar (Fd) positions corresponds to their theoretical compositions. The glasses located in the Q-P-Fd region have excess SiO_2 causing high viscosity on molding. More suitable glasses are located inside or near the line P-Tsch and inside the triangle P-Fd-Tsch. The compositions under the P-

Tsch line are inadequate, because they precipitate olivine crystals [110,112]. Glasses obtained from fly ashes in this study are far away from this ideal triangle (Figure 6.18(b)). TG and SG samples are close to the quartz corner, which is related to higher viscosity on melting and controlled crystallization. AEG sample is under P-Tsch line, which indicates inadequate composition for glass-ceramic production.

Finally, Lebedeva modified the diagram (Figure 6.18(c)) by considering the role of modifier cations (Ca^{2+}, Mg^{2+} and Fe^{2+}) in the crystallization process [216]. Thus the Lebedeva diagram considers the following corners: MG, CA andFE, where MG = Mg^{2+}, CA = Ca^{2+} and FE = Fe^{2+}. This ternary diagram is divided into six zones according to the appearance of crystalline phases. Consequently, glasses located in zone I give rise to magnetite (Fe_3O_4) surrounded by spherulitic pyroxene crystals. Inside zone II, magnetite is not the primary phase, giving rise to materials where pyroxene could coexist with secondary magnetite. Zones III to V are very similar in microstructural composition (Diopside, augite and anorthite). Finally, zone VI produces olivine ($MgO.SiO_2$), which is not adequate for glass-ceramic production [112]. Because of SG, TG and CG compositions fall into region V of the diagram, diopside or augite can be crystalline phase occurred in this samples. As seen from Figure 6.18 (c), it is particularly evident for OG and AEG glasses that they experimentally could not be adequate for glass-ceramic production as suggested by Lebedeva diagram.

According to the above discussions, TG, SG and CG samples are suitable for glass-ceramic production. The three methods are complementary, because we are not allowed to define what is the best composition for glass-ceramic production. Thus, the Ginsberg method gives us an idea of the role played by cations in the crystallization precess. Similarly, the Raschin and Lebedeva methods give us information about the nature and sequence of crystallization [110]. It is important to note that, only experimental thermal behavior can give the actual trend for crystallization in these complex glasses as it was given in the following section.

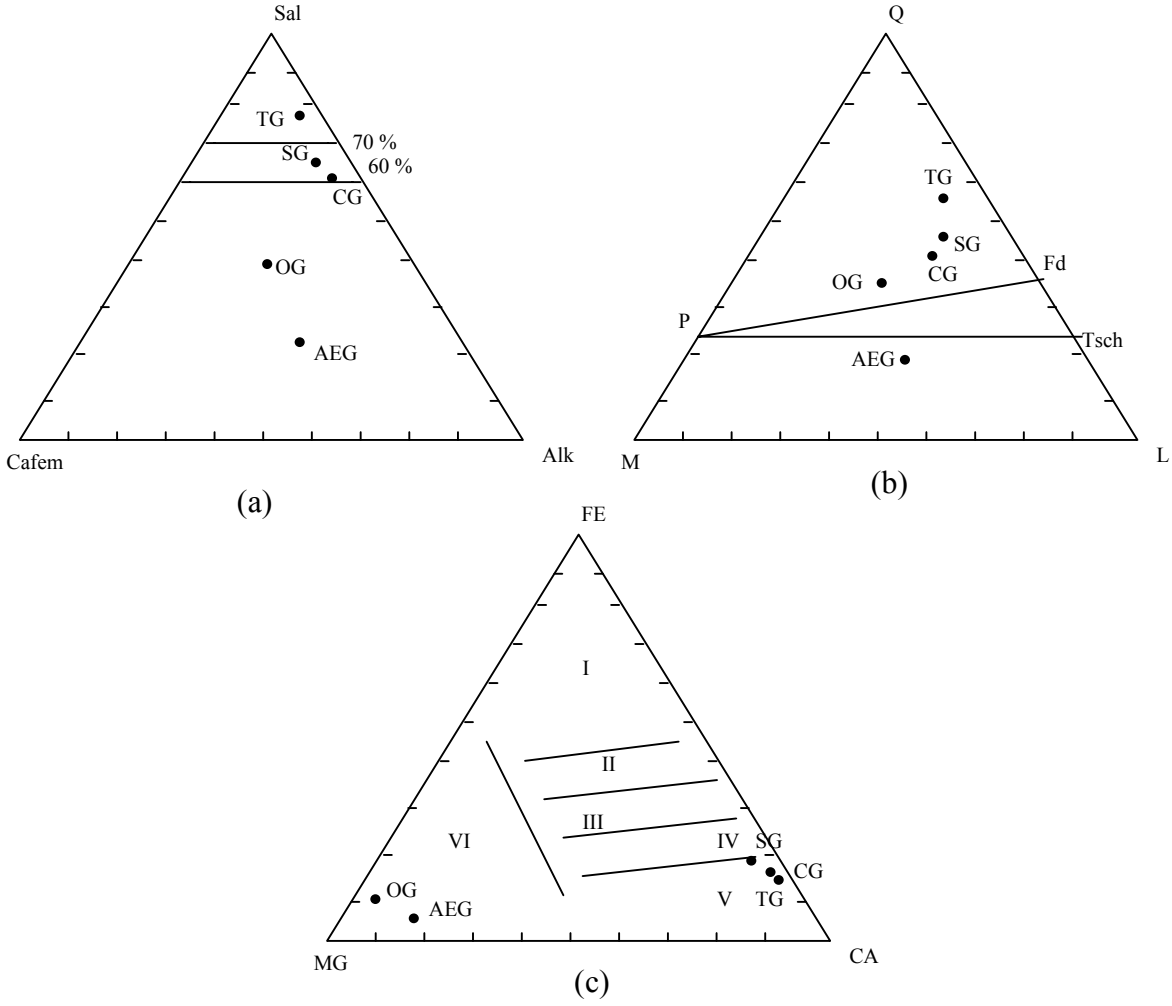

Figure 6.18: Diagrams used to study glasses' capability to transform into glass-ceramic materials. (a) Ginsberg, (b) Raschin-Tschetveritkov and (c) Lebedeva diagrams.

6.5 Re-production of Glasses from Waste materials to Obtain Better Crystallization Tendency

DTA experiments conducted on the all glass samples and the results were given in Section 6.2.1. As it was mentioned in Section 6.2.1, only TG sample had an exothermic peak, which shows the crystallization tendency of this glass. To be able to produce glass-ceramic materials from other glass samples, the composition of those glasses must be changed. Therefore, silica fume and red mud were added to Çayırhan, Seyitömer, Orhaneli and Afşin-Elbistan fly ashes as additives to obtain

new compositions of their glasses suitable for glass-ceramic production. First of all, Çayırhan fly ash was selected for the glass re-production since its composition is more convenient than the others compositions according to the discussion given in Section 6.4. If the chemical composition of Çayırhan fly ash is examined, it will be seen that only the addition of nucleating agent will be enough for the glass production. Therefore, 5 % of red mud was added to the Çayırhan fly ash because of the high Fe_2O_3 content of it. High Fe_2O_3 content plays an important role in the glass-ceramic production as it was discussed in the Sections 6.3.1 and 6.3.2. Glass samples were produced from Çayırhan fly ash with the addition of 5 % of red mud according to the procedure described in Section 5.3. The new composition of Çayırhan fly ash with the addition of 5 % red mud is 39.97 % SiO_2, 12.09 % CaO, 4.43 % MgO, 11.18 % Fe_2O_3, 18.30 % Al_2O_3, 2.63 % Na_2O and 2.39 % K_2O. DTA experiment was performed on 20 mg of the glass sample produced from Çayırhan fly ash and red mud at a heating rate of 20 K/min and the observed DTA graph was given in Figure 6.19. As it was seen from Figure 6.19, an endothermic peak at 968 K and an exothermic peak at 1222 K were detected. Therefore, the studies continued with Seyitömer fly ash to re-produce glass samples with the addition of 5 % red mud. DTA was conducted on the produced glass samples at a heating rate of 20 K/min up to the temperature of 1373 K. On the DTA thermogram of the produced glass sample, one small endothermic peak at 980 K was observed, but there was no exothermic peak (Figure 6.20 (a)). Therefore, 10 % red mud was added to Seyitömer fly ash and the new glass sample was produced. However, only a small amount of glass could be obtained because of the high viscosity of the melt. DTA thermogram of the produced glass sample from Seyitömer fly ash showed only one endothermic peak at 978 K (Figure 6.20(b)). As seen from Figure 6.20 (b), there is no evident for the exothermic peak. The studies on the re-production of glass from Seyitömer fly ash with the addition of red mud was finished since the high viscosity of the melt and the unsuitableness of red mud as a nucleating agent for this composition. The composition of Seyitömer fly ash and 10 % red mud mixture is 41.16 % SiO_2, 6.47 % CaO, 8.85 % MgO, 12.38 % Fe_2O_3, 23.13 % Al_2O_3, 0.58 % Na_2O and 0.7 % K_2O. This composition is not suitable for glass-ceramic production because of the high Fe_2O_3 and Al_2O_3 content. Studies showed that more than 11 % of Fe_2O_3 is not suitable for glass-ceramic production [11,110,112]. High Al_2O_3 content causes the higher viscosity of the melt. Therefore, studies continued with the re-production of

glass from Orhaneli fly ash. 20 % red mud and 20 % silica fume were added to the Orhaneli fly ash since both SiO_2 and Fe_2O_3 contents of it was not enough for the glass-ceramic production. The new composition of Orhaneli fly ash, red mud and silica fume mixture were given as: 39.94 % SiO_2, 19.5 % CaO, 4.43 % MgO, 10.77 % Fe_2O_3, 13.9 % Al_2O_3, 2.05 % Na_2O and 1.14 % K_2O. The DTA curve of the produced glass sample given in Figure 6.21 indicates that one endothermic peak at 983 K and one exothermic peak at 1254 K were appeared at the heating rate of 20 K/min. Lastly, 10 % red mud and 30 % silica fume were added to the Afşin-Elbistan fly ash to produce glass samples. Since the SiO_2 content of the Afşin-Elbistan fly ash is very low, the percentage of silica fume was increased and red mud percentage was decreased. Figure 6.22 (a) shows the DTA graph of the produced glass sample. There is one endothermic peak at 976 K but there is no evidence for any exothermic peak. Therefore, red mud percentage was increased to 20 % to improve the crystallization tendency. The new glass samples were produced with the addition of 20 % red mud and 30 % silica fume into the Afşin-Elbistan fly ash. The new composition of the waste is 38.87 % SiO_2, 20.44 % CaO, 3.57 % MgO, 10.21 % Fe_2O_3, 11.41 % Al_2O_3, 0.87 % Na_2O and 0.62 % K_2O. However, any exothermic peak could not be observed in DTA graph as it was seen from Figure 6.22 (b). There is only one endothermic peak at 1056 K. The new composition of waste glass is not suitable for glass-ceramic production because of its high CaO content. The high CaO content decreases the crystallization tendency [115]. Therefore, any exothermic peak could not be obtained. Afşin-Elbistan fly ash is not suitable for glass-ceramic production because of the high CaO, low SiO_2 and Fe_2O_3 content of it. It was also noted that the red mud and silica fume are not suitable additives for Afşin-Elbistan fly ash. The new codes were given to the re-produced glasses from waste materials. The new codes of the re-produced glass samples are; CRG: Re-produced glass sample obtained from Çayırhan fly ash and red mud, SRG: Re-produced glass sample obtained from Seyitömer fly ash and red mud, ORSG: Re-produced glass sample obtained from Orhaneli fly ash, silica fume and red mud, AERSG: Re-produced glass sample obtained from Afşin-Elbistan fly ash, silica fume and red mud.

These glasses showed different tendencies toward crystallization. SRG and AERG glasses were more thermally stable, showing the glass transition peak without any exothermic peak at high temperatures. Above the glass transition temperature, TG,

ORSG and CRG samples, conversely, showed very clear exothermic peaks that correspond to the formation of a crystalline phase. Therefore, TG, ORSG and CRG glasses were used in the glass-ceramic production and the crystallization behavior of those glasses were investigated. In addition to those glasses, thermal and sintering behavior of the glass sample produced from Çayırhan thermal power plant fly ash (obtained in 1997) were also investigated in this study. Altough the crystallization behavior of glasses produced from Çayırhan fly ash (obtained in 1997) was determined in a previous study [118], some of the properties of these glasses could not be determined. Chemical composition of Çayırhan thermal power plant fly ash obtained in 1997 was different from Çayırhan thermal power plant fly ash obtained in the year 2000. Therefore, crystallization behavior of those glasses and glass-ceramics produced from those glasses were also different. The code of CG-97 was given to the glasses produced from Çayırhan thermal power plant fly ash obtained in 1997.

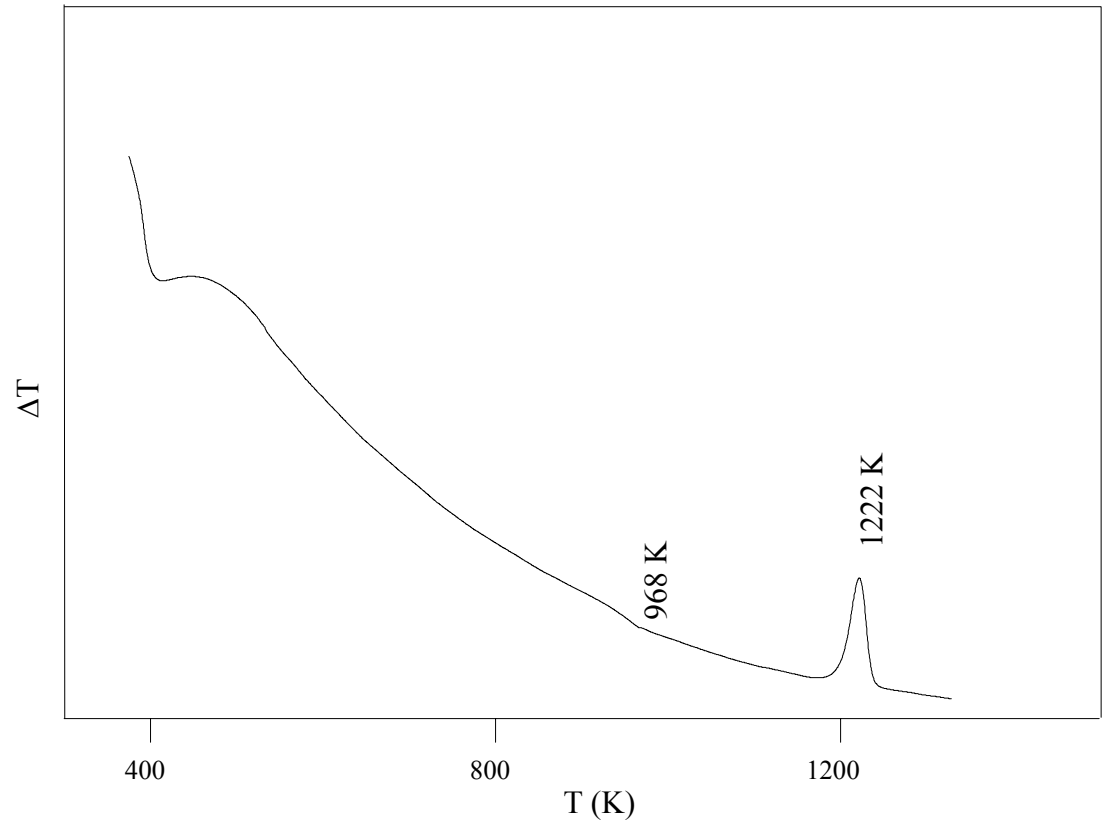

Figure 6.19: DTA graph of the CRG sample

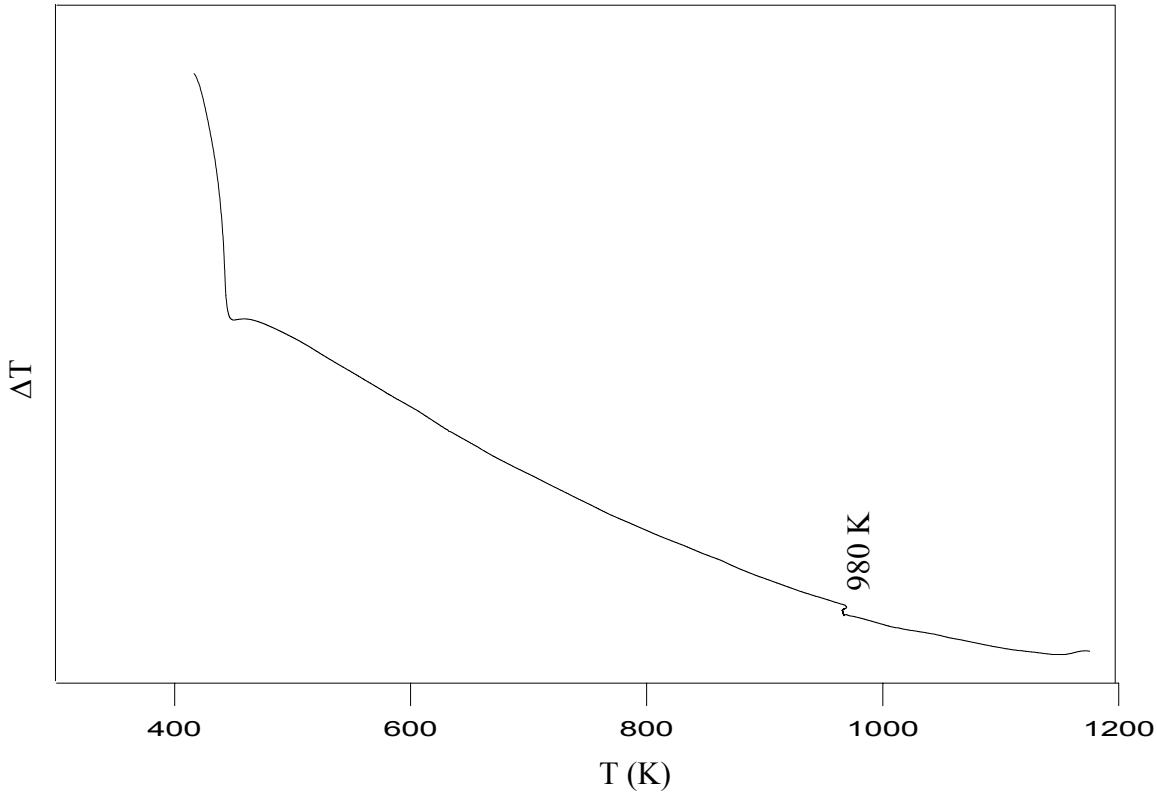

(a)

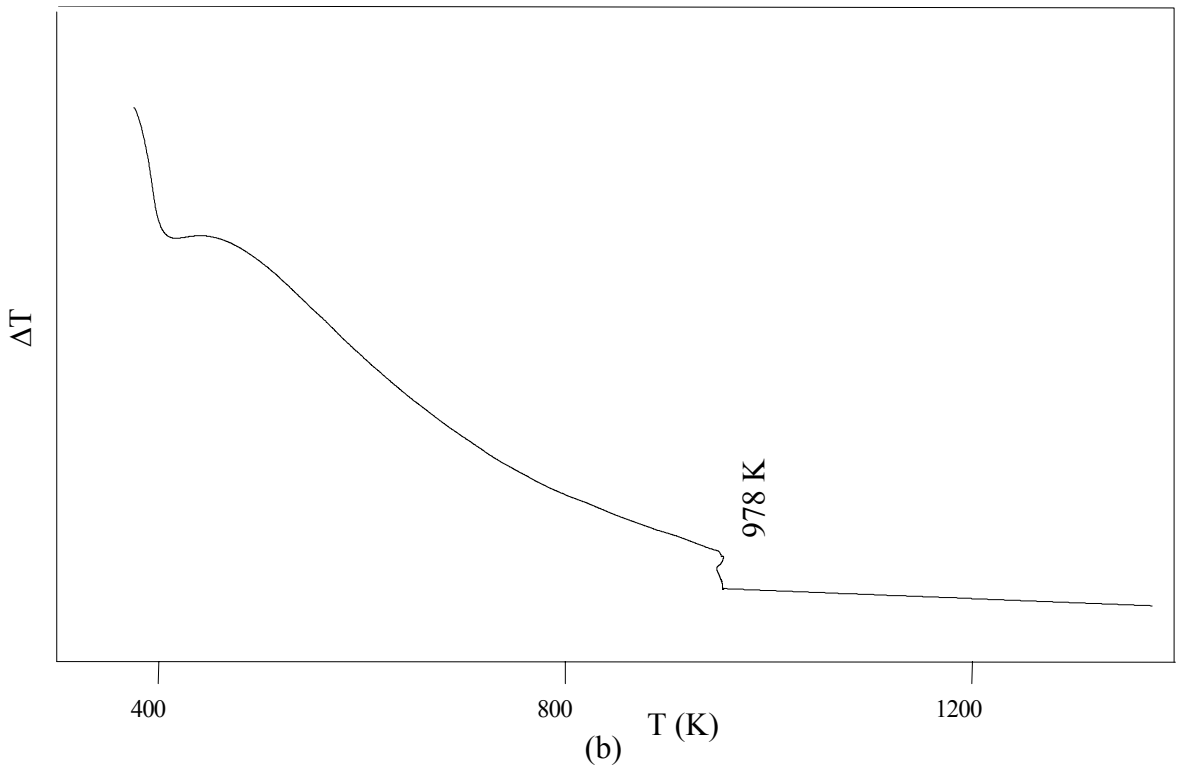

(b)

Figure 6.20: DTA graphs of the SRG samples((a) 5 % red mud; (b) 10 % red mud)

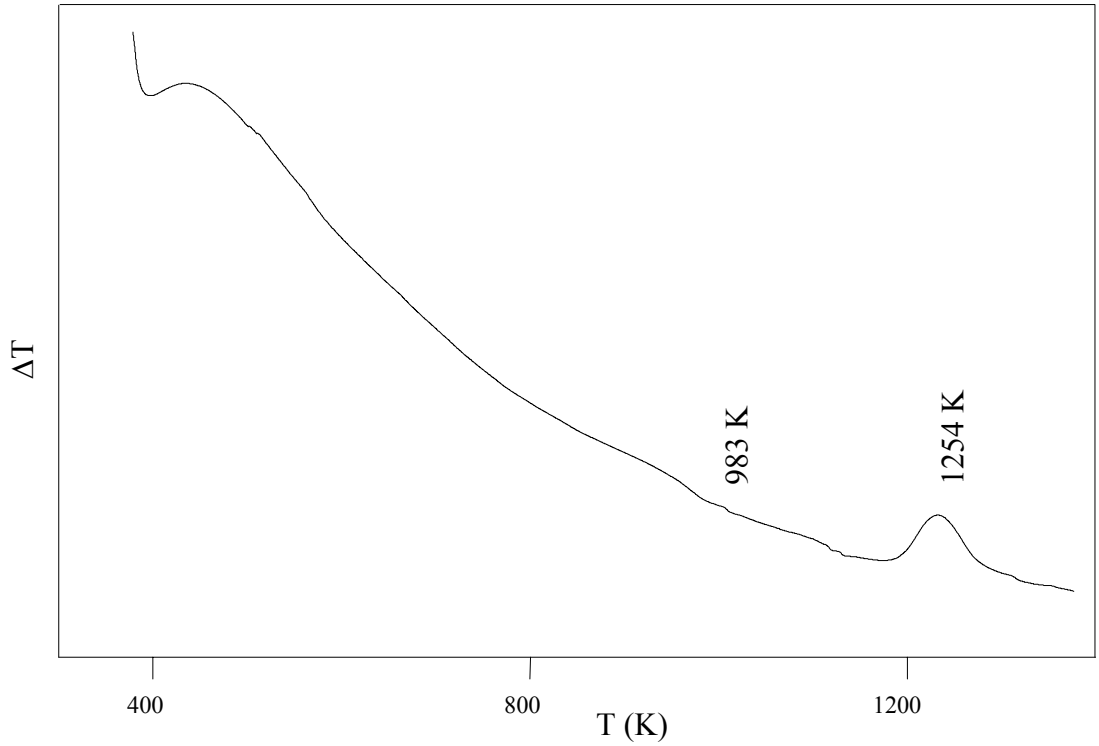

Figure 6.21: DTA graph of the ORG sample

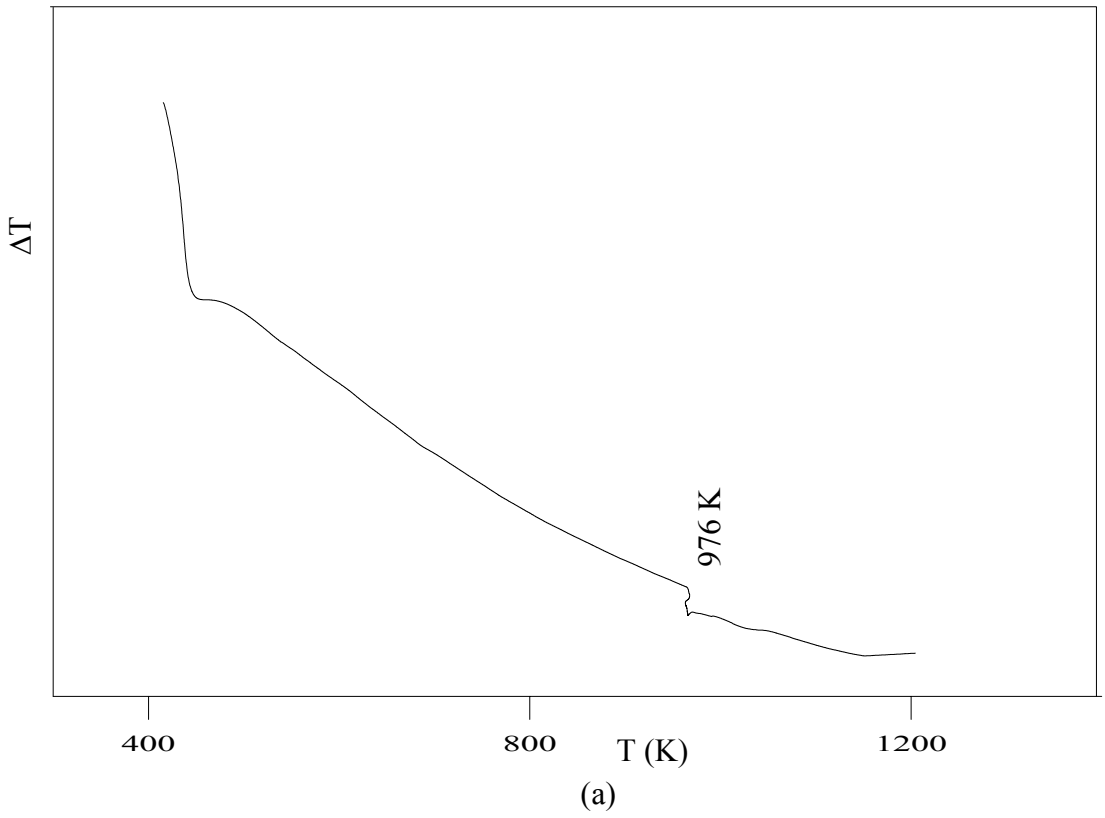

(a)

Figure 6.22: DTA graph of the AERSG sample (a) 10 %red mud, 30 % silica fume

6.6 Thermal Behavior of Glasses Produced from Waste Materials

DTA investigations were conducted on all samples at the heating rates of 5, 10, 15 and 20 K/min to determine the thermal behavior of the produced glasses. To perform the heat treatment schedules on the glass samples maximum nucleation temperature, maximum nucleation time and crystallization peak temperatures were obtained on the basis of DTA scan results. Kinetic parameters of crystal growth were determined by using both isothermal and non-isothermal methods.

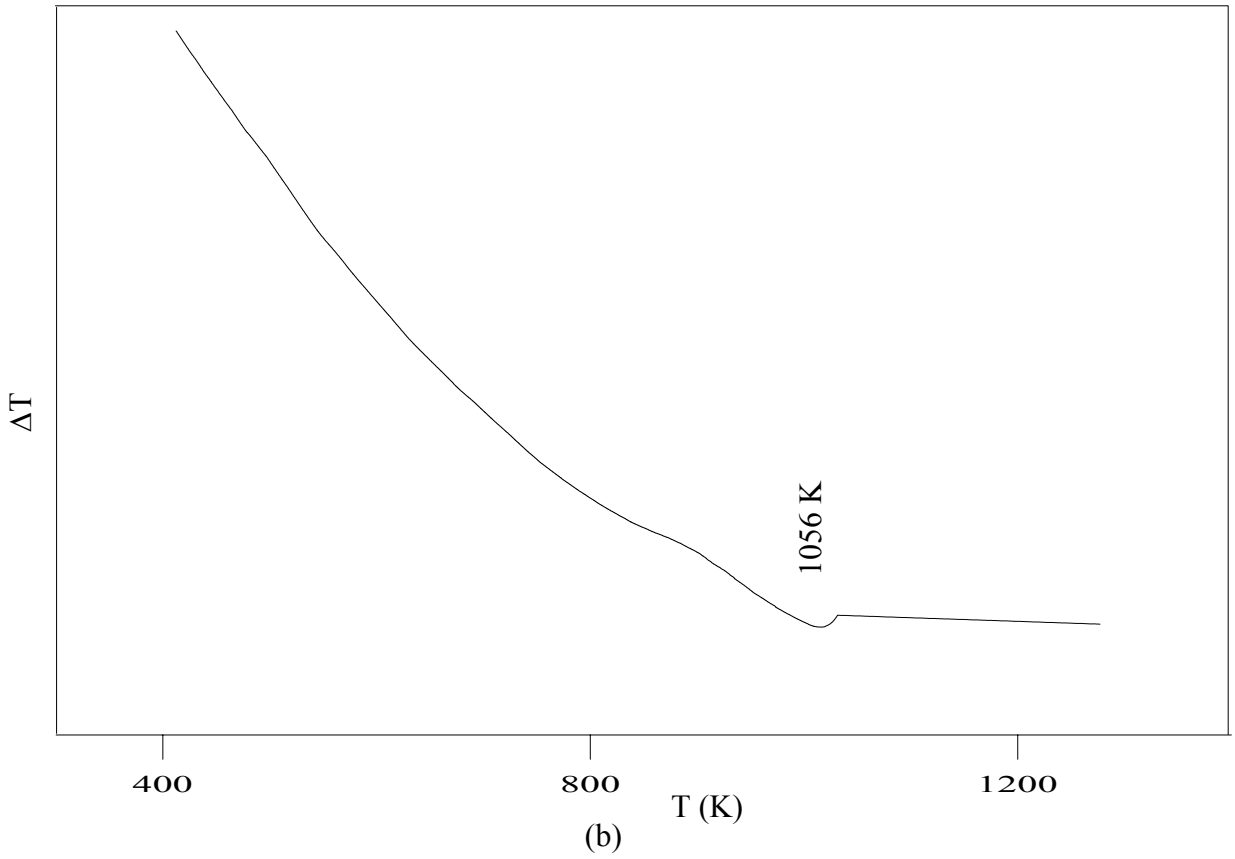

Figure 6.22: DTA graph of the AERSG sample (b) 20 % red mud, 30 % silica fume

6.6.1 Determination of maximum nucleation temperature and time

As reported by Marotta et al. [66] and Xu et al.[72], the DTA technique can be used to determine the maximum nucleation temperature and time. In the DTA technique, the crystallization peak temperature, T_p, is determined as a function of the nucleation temperature, Tn, using a constant sample weight and heating rate. The crystallization peak in the DTA analysis occurs because of the heat evolution during crystal growth

from the nuclei present in the glass. The number of nuclei in a glass can be expressed as

$$N = N_q + N_i + N_h \quad \textbf{(6.1)}$$

where N_q is the concentration of quenched in nuclei, N_i the number of nuclei formed per unit volume during the isothermal heat treatment and N_h is the number of nuclei per unit volume that form during non-isothermal heating in the DTA. For a high heating rate, the glass spends a relatively shorter time in the temperature range for nucleation and N_h can be neglected [217]. Furthermore, using a constant heating rate for all the measurements means that N_h is constant (even if it is small) in all the samples of the same composition. Likewise, N_q for all samples should be the same if the samples are prepared in the same manner from the same glass melt. Consequently, any change in DTA peaks for the glass samples nucleated at different temperatures for the same time should result solely from the contribution of N_i, which is proportional to the nucleation rate (I) at the temperature for nucleation (T_n). For glasses with the same composition, the following relationship [72] is applied between the number of nuclei, N and the crystallization peak temperature, T_p, when the heating rates are the same for the DTA runs.

$$\ln N = \frac{E}{RT_p} + cons\tan t \quad \textbf{(6.2)}$$

Thus, the greater the number of nuclei, the lower the crystallization temperature. Therefore, the change in T_p with T_n is primarily due to a change in the glass type [53]. The height of the crystallization peak, $(\delta T)_p$, is also proportional to N. Although no definite relationship has been established between $(\delta T)_p$ and N, experimental studies [72,218] showed that the concentration of nuclei in the glass increases with the increase in $(\delta T)_p$. For the determination of maximum nucleation temperature, the glass samples were held for 4 h at different nucleation temperatures that is above the glass transition temperature, Tg, in 5 K intervals. To estimate the maximum nucleation time glass samples were heat treated isothermally at the maximum nucleation temperature for 1, 2, 3 and 4 h. The obtained Tp and $(\delta T)_p$ values for all glass samples were summarized in Tables 6.11-6.14 and the DTA graphs of these glass samples were given in Figures B1-8 in Appendix B. In all DTA scans, the heating rate was 10 K/min.

It is well known that the nucleation rate (number of nuclei formed per unit volume per second) is a function of temperature and becomes maximum at a temperature near the middle of the temperature range where nucleation can occur. As seen from Table 6.11, T_p values reached the lowest value at 963 K while $\delta(T)_p$ values reached a maximum at this temperature for CRG glass. Therefore, maximum nucleation temperature was selected as 963 K. As seen in Table 6.11, T_p values decreased and $\delta(T)_p$ values increase with increasing nucleation times. With increasing holding time at the nucleation temperature (963 K), the concentration of nuclei in the glass increases, which increases the crystallization rate as indicated by the larger $\delta(T)_p$ and lower T_p values. The increase in $\delta(T)_p$ and decrease in T_p, which are considered to be the direct result of increasing concentration of nuclei in the glass, are expected to continue until the glass becomes saturated with nuclei. If the crystallization temperature does not vary with the nucleation time, this case shows that the nucleation stage is fully completed [72,219]. On the basis of these interpretations, the nucleation time that is necessary to achieve optimum conditions was selected as 4 h. In previous studies [118,135], it was determined that 10 K above the T_p value was sufficient for crystal growth in the microstructure of the glass sample. Therefore, crystallization temperatures were chosen 10 K above the T_p values in this study. Consequently, maximum nucleation temperature, maximum nucleation time and crystallization temperature of CRG glass were determined as 963 K, 4 h and 1135 K, respectively. As seen from Table 6.12, T_p values decreased and $\delta(T)_p$ values increased with increasing nucleation temperature until 988 K for ORSG sample. On the other hand, $\delta(T)_p$ values reached a maximum at 2 h of nucleation time and then decreased gradually with the increase in the nucleation time. Therefore, for ORSG sample maximum nucleation temperature and time were selected as 988 K and 2 h while the crystallization temperature was 1188 K. The same observations were detected at the DTA results of TG glass (Table 6.13). On the basis of DTA results and the interpretations mentioned above, maximum nucleation temperature, maximum nucleation time and crystallization temperature were determined as 948 K, 2 h and 1140 K, respectively. In a previous study [118], maximum nucleation temperature and time were detected by more time consuming methods instead of DTA technique. Maximum nucleation temperature of CG-97 glass was selected as 10

K above the T_g temperature (953 K) according to the literature survey of glass systems that have the similar compositions. Maximum nucleation time was determined as 5 h on the basis of microstructural studies and the mechanical properties of the produced glass-ceramics nucleated at different holding times. In this study, maximum nucleation temperature and time for CRG sample were selected as 958 K and 4 h on the basis of DTA results that are given in Table 6.14. These results are very close to the results obtained in a previous study [118], however DTA technique is more convenient and shorter. The crystallization temperature of CG-97 glass was determined as 1142 K which is lower than the crystallization temperature of 1190 K obtained in the previous study [118].

Table 6.11: T_p and $\delta(T)_p$ values of CRG sample

T_p and $\delta(T)_p$ values for different nucleation temperatures				T_p and $\delta(T)_p$ values for different holding times at 963 K			
Nuc. temp. (K)	Hold. time (h)	T_p (K)	$\delta(T)_p$	Nuc. temp. (K)	Hold. time (h)	T_p (K)	$\delta(T)_p$
953	4	1128	2.301	963	1	1132	2.503
963	4	1125	2.572	963	2	1127	2.542
968	4	1136	2.512	963	3	1126	2.558
973	4	1141	2.428	963	4	1125	2.572

Table 6.12: T_p and $\delta(T)_p$ values of ORSG sample

T_p and $\delta(T)_p$ values for different nucleation temperatures				T_p and $\delta(T)_p$ values for different holding times at 963 K			
Nuc. temp. (K)	Hold. time (h)	T_p (K)	$\delta(T)_p$	Nuc. temp. (K)	Hold. time (h)	T_p (K)	$\delta(T)_p$
978	4	1188	0.714	988	1	1187	0.718
983	4	1185	0.725	988	2	1178	0.794
988	4	1183	0.753	988	3	1180	0.773
993	4	1192	0.614	988	4	1183	0.753

Table 6.13: T_p and $\delta(T)_p$ values of TG sample

T_p and $\delta(T)_p$ values for different nucleation temperatures				T_p and $\delta(T)_p$ values for different holding times at 963 K			
Nuc. temp. (K)	Hold. time (h)	T_p (K)	$\delta(T)_p$	Nuc. temp. (K)	Hold. time (h)	T_p (K)	$\delta(T)_p$
943	4	1138	0.654	948	1	1143	0.621
948	4	1136	0.669	948	2	1130	0.706
953	4	1141	0.646	948	3	1134	0.682
958	4	1142	0.634	948	4	1136	0.669

Table 6.14: T_p and $\delta(T)_p$ values of CG sample

T_p and $\delta(T)_p$ values for different nucleation temperatures				T_p and $\delta(T)_p$ values for different holding times at 963 K			
Nuc. temp. (K)	Hold. time (h)	T_p (K)	$\delta(T)_p$	Nuc. temp. (K)	Hold. time (h)	T_p (K)	$\delta(T)_p$
958	4	1133	1.015	958	1	1141	0.882
963	4	1138	0.908	958	2	1137	0.912
968	4	1145	0.825	958	3	1133	1.018
973	4	1146	0.802	958	4	1133	1.015

6.6.2 Kinetic parameters of crystal growth

The crystallization kinetics of glasses produced from waste materials was investigated by using both isothermal and non-isothermal methods. Coarse (particle size is about 1 mm) and fine (particle size is less than 180 μm) glasses with sample weight of ≈20 mg were used in all DTA experiments. There were three main aim for conducting these experiments: 1) to determine more accurate value for the Avrami exponent, n, and activation energy for crystallization, E., 2) to examine the effect of particle size on crystallization mechanism and 3) to compare the results of kinetic data as determined by isothermal and non-isothermal methods.

6.6.2.1 Non-isothermal analysis

The kinetic parameters of the glass-crystallization transformation were estimated under non-isothermal conditions applying three different equations, namely, Kissinger[70], Matusuta-Sakka[38,54,71] and Ozawa[73]. Non-isothermal DTA curves were obtained with selected heating rates (5, 10, 15 and 20 K/min) using both coarse and fine glass samples. Typical DTA graphs for coarse and fine samples of CRG, ORSG and TG glasses recorded at 4 different heating rates were shown in Figures B9-10, B11-12 and B13-14 in Appendix B, respectively. The characteristic temperature and the heights of the crystallization peaks of CRG, ORSG and TG glasses of both coarse and fine particles measured by DTA were given in Tables 6.15, 6.16 and 6.17, respectively. As can be seen in Figures B9-14 and Tables 6.15-17, crystallization peak temperatures of all glass samples increased with the increase in heating rates. T_p for coarse particles was significantly higher than that for fine particles and this difference in T_p increased consistently with increasing heating rate.

Table 6.15: DTA results of coarse and fine CRG sample

Heating rate (K/min)	Coarse Particles	Fine Particles
	Crystallization temp. (K)	Crystallization temp. (K)
5	1157	1080
10	1187	1091
15	1205	1108
20	1222	1113

Table 6.16: DTA results of coarse and fine ORSG sample

Heating rate (K/min)	Coarse Particles	Fine Particles
	Crystallization temp. (K)	Crystallization temp. (K)
5	1200	1082
10	1222	1097
15	1237	1108
20	1254	1110

Table 6.17: DTA results of coarse and fine TG sample

Heating rate (K/min)	Coarse Particles	Fine Particles
	Crystallization temp. (K)	Crystallization temp. (K)
5	1134	1043
10	1149	1046
15	1161	1050
20	1166	1060

At a particular heating rate, the T_p for a glass depends on the total concentration of surface and bulk nuclei present in the glass and decreases with increasing concentration of nuclei. Since the surface area increases with decreasing particle size, the concentration of surface nuclei is expected to be higher for fine particles. If a glass is not initially saturated with internal nuclei, the concentration of nuclei will be higher for lower heating rates, since the glass spends longer time in the temperature range where nucleation can occur. The effect of these internal nuclei on crystallization is more pronounced in coarse particles, as they provide larger effective volumes for internal nucleation. It is expected that at low heating rates, all the different particle sizes are highly nucleated (surface or bulk). At high heating rates, the concentration of nuclei in the coarse particles is less than that in the fine particles so that crystallization for coarse particles occurs at a higher temperature. This is due to the particle size effect on heat transfer. Temperature gradients developed between the surrounding air and the surface of the glass sample and inside the glass sample. Temperature gradients can arise when the glass samples dimensions or the heating rate are relatively high. At a given heating rate, coarse particles have greater heat transfer resistance, so it takes longer for the center of the particle to reach the furnace temperature and a higher observed crystallization temperature results. The concentration of nuclei in coarse particles is expected to decrease with increasing heating rate (less time in the nucleation range), so the difference in nuclei concentration between coarse and fine particles will increase with increasing heating rate. This will cause the difference in T_p between coarse and fine particles with increasing heating rate. This case has also been observed by several researchers [111,217,220-222].

Matusuta-Sakka [54] mentioned that the Kissinger equation is valid only when the number of nuclei is fixed during crystal growth. If most of the nuclei are formed during the DTA scan, the activation energy values from the Kissinger equation are incorrect. Therefore, CRG, ORSG and TG glasses were completely nucleated at the transition temperature and the crystallization behavior of these nucleated glasses was also examined by using DTA scans. For this purpose, , CRG, ORSG and TG glass samples were heated at different heating rates of 5, 10, 15 and 20 K/min, until the maximum nucleation temperature and nucleated at this temperature for the maximum nucleation time determined in the previous section. Then the nucleated samples were crystallized at these heating rates without being removed from DTA. DTA scans of the completely nucleated CRG, ORSG and TG glasses of coarse and fine particles were shown in Figures B15, B16-17 and B18-19 in Appendix B, respectively. Tables 6.18-6.20 list the crystallization peak temperatures of the CRG, ORSG and TG glasses according to the heating rates. However, DTA results of CRG glasses of fine particles could not be given since T_p values were found same for all heating rates. In this case, it is impossible to determine the activation energy of fine CRG glasses by using Kissinger equation. As can be seen from Figures B15-19 and Tables 6.18-20, T_p values increased with the increasing in particle size as it was observed in the glasses which were not nucleated at T_g. If we compare the DTA results of as-quenched and fully nucleated glasses of both coarse and fine particles, we can see that there is a small difference in each of the T_p values of the quenched and nucleated glasses. The decreased T_p values in the nucleated glasses would result from the increased number of nuclei as it was discussed in the previous sections. The variation of crystallization peaks of as-quenched glasses with different DTA heating rates can be used to estimate the activation energy for crystallization and to determine the crystallization mechanism. In comparison with the fully nucleated CRG, ORSG and TG glasses, as-quenched glasses that were not heat treated, were expected to be initially unsaturated with nuclei. Therefore, internal nuclei could form in as-quenched glass samples during the DTA measurements, and the number of nuclei formed during the DTA run will be a function of α. This means that crystal growth in as-quenched glass samples could occur on a different number of nuclei when crystallized at different values of α. Since the number of nuclei available for crystal growth decreases with increasing α (less time in the nucleation temperature range),

T_p shifts to a progressively higher temperature with increasing heating rate [72]. This temperature is higher than what it would be if the crystal growth occurred on a fixed number of nuclei as it was observed in the fully nucleated glasses.

Table 6.18: DTA results of the CRG glasses held at nucleation temperature for 4 h

Coarse Particles		
Heating rate (K/min)	Nuc. temp. (K)	Crystallization temp. (K)
5	943	1129
10	958	1149
15	963	1160
20	968	1168

Table 6.19: DTA results of coarse and fine ORSG glass samples held at nucleation temperature for 2 h

Heating rate (K/min)	Coarse Particles		Fine Particles	
	Nuc. temp. (K)	Crystallization temp. (K)	Nuc. temp. (K)	Crystallization temp. (K)
5	973	1170	983	1059
10	978	1190	985	1073
15	980	1198	990	1083
20	983	1205	993	1084

Table 6.20: DTA results of coarse and fine TG glass samples held at nucleation temperature for 2 h

Heating rate (K/min)	Coarse Particles		Fine Particles	
	Nuc. temp. (K)	Crystallization temp. (K)	Nuc. temp. (K)	Crystallization temp. (K)
5	940	1130	930	1020
10	943	1140	935	1026
15	944	1151	941	1031
20	964	1159	953	1038

Assuming that the nucleation and growth processes had occurred simultaneously in as-quenched samples during the DTA measurements, the data for as-quenched glasses were analyzed by Matusita-Sakka model (Eq. (3.14)) to determine E_c. Since Eq. (3.14) includes the parameters of n and m, their values first determined using Ozawa model (Eq.(3.22)). Plots of ln(-ln(1-x))- (x values were determined according to the Figure A.1) vs. lnα for CRG glass of coarse and fine particles are shown in Figure 6.23 and the values of n determined from the slopes of these plots are found as 3.42 for coarse particles and 1.36 for fine particles. These values indicate that bulk and surface crystallizations are dominant in the coarse and fine particles, respectively. The m value for the coarse particles should be equal to n-1, i.e. 2.42 from Table 3.1. Fine particles have a larger effective surface area so that the number of internal nuclei formed during the DTA run could be neglected. This means that crystal growth for glasses of fine particles should have occurred on a fixed number of nuclei during the DTA measurements. Therefore, we can assume that n is equal to m for the fine glasses. n = m =1.36 for CRG glass of fine particles and these value is very close to 1 which means surface crystallization is dominant. By substituting the appropriate values of n, m and R (R value was taken as 8.3144 J/molK) in Matusita-Sakka equation (Eq.(3.14)), the following equations can be obtained for both coarse and fine particles:

For coarse particles
$$\ln\left(\frac{\alpha^{3.42}}{T_p^2}\right) = \frac{-2.42E_c}{RT_p} + c \qquad \textbf{(6.3)}$$

For fine particles
$$\ln\left(\frac{\alpha^{1.36}}{T_p^2}\right) = \frac{-1.36E_c}{RT_p} + c \qquad \textbf{(6.4)}$$

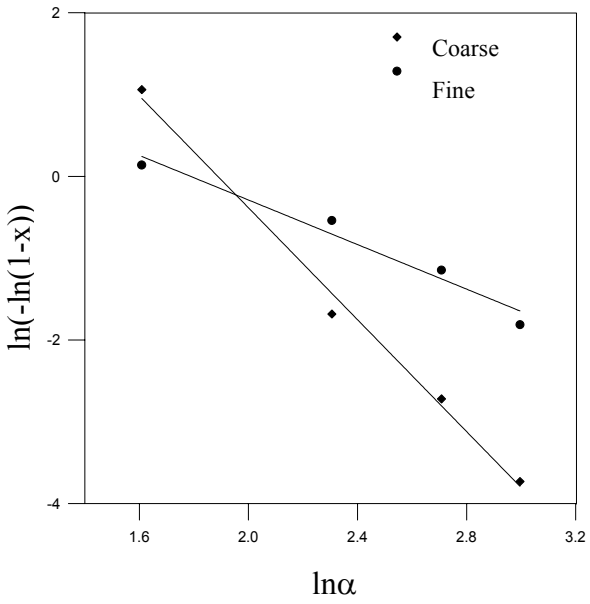

Figure 6.23: The Ozawa plots of the coarse and fine CRG glasses

Using n and m values, Matusita-Sakka plots, $\ln(\alpha^n/T_p^2)$ vs. $1/T_p$, for CRG sample yield E_c values as 350 and 372 kJ/mol for coarse and fine particles, respectively (Figures 6.24 and 6.25). Also using the Kissinger model (Eq.(3.19)), E_{ck} values of as-quenched glass of coarse and fine particles can be determined from the slope of the plots $\ln(\alpha/T_p)$ vs. $1/T_p$(Figure 6.26). For coarse particle E_{ck} is equal to 233 kJ/mol that is lower than the E_c value determined by Matusita-Sakka model. By using Eq.(3.21), i.e., multiplying E_{ck} value for coarse particles by the factor n/m (=3.42/2.42) yields E_c value of 330 kJ/mol. For fine particles E_{ck} value is equal to 369 kJ/mol that is close to E_c value determined from the Matusita-Sakka model. For n=m, i.e., when crystallization occurs on a fixed number of nuclei, $E_{ck} = E_c$. This case shows that the crystal growth for fine particles occurred on a fixed number of nuclei during the DTA measurements, so that all models gave similar results for activation energy of fine glasses (allowing for experimental errors, E_c values of all models are close to each other).

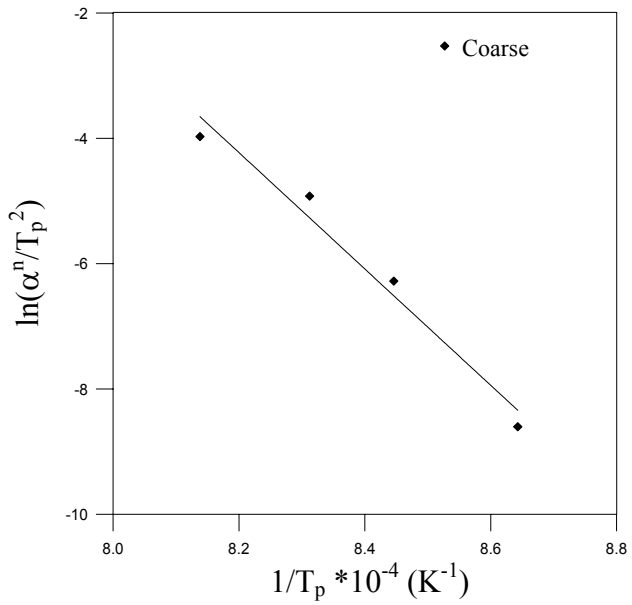

Figure 6.24: The Matusita-Sakka plot of the coarse CRG glass

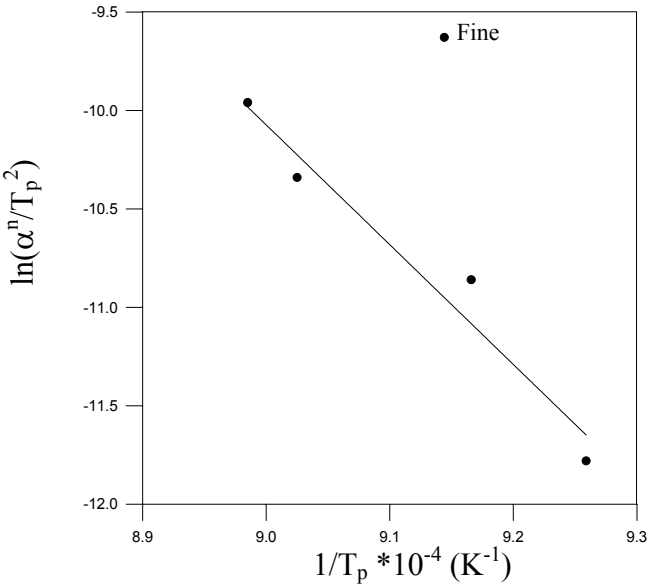

Figure 6.25: The Matusita-Sakka plot of the fine CRG glass

In order to determine the activation energy value for crystallization of completely nucleated CRG glass the Kissinger model (Eq.(3.19)) was applied. Figure 6.27 shows the Kissinger plot of the fully nucleated glasses of coarse particles. From the slope of the plot the activation energy for crystallization, E_{ck}, was determined as 370 kJ/mol. This activation energy is more closer to the E_c value determined by using Matusita-Sakka method than the E_{ck} value which was estimated for as-quenched CRG glass by

using Kissinger model (Eq.(3.19)). If we consider the experimental errors, E_c values of CRG glass of coarse particles determined from all models are close to each other.

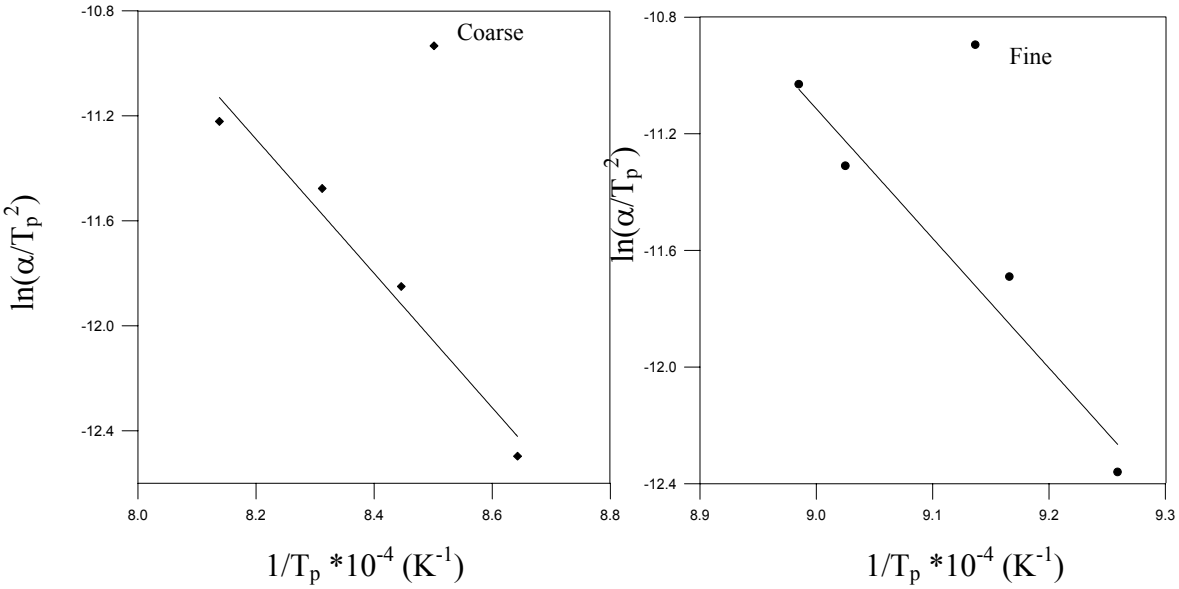

Figure 6.26: The Kissinger plots of the coarse and fine as-quenched CRG glasses

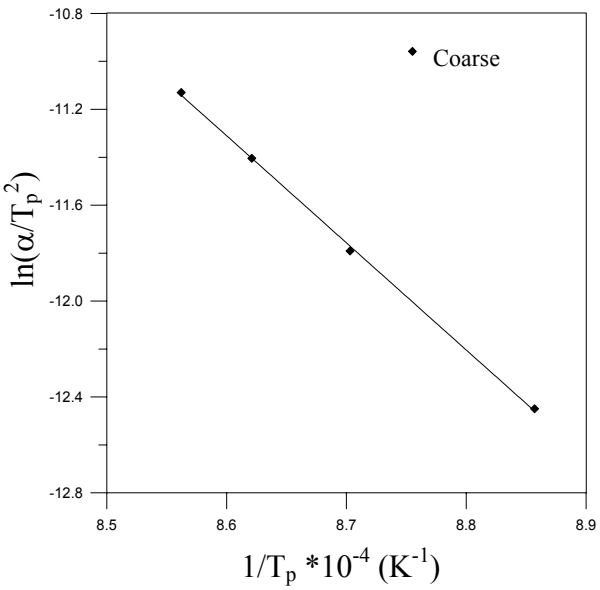

Figure 6.27: The Kissinger plot of the fully nucleated coarse CRG glass

The Ozawa plots of ln(-ln(1-x)) vs. $1/T_p$ for the coarse and fine particle sizes for ORSG glass are linear according to Eq.(3.22) with n = 3.68 and n = 1.24, respectively (Figure 6.28). n = 3.68 value for coarse particles indicates the bulk crystallization while n = 1.24 value for fine particles represents the surface crystallization. For coarse particles m is equal to 2.68 while m is equal to 1.2 for fine

particles. If we place the n and m values into Matusita-Sakka equation (Eq.(3.14)), following new equations for coarse and fine particles are obtained:

For coarse particles $$\ln\left(\frac{\alpha^{3.68}}{T_p^2}\right) = \frac{-2.68E_c}{RT_p} + c \qquad \textbf{(6.5)}$$

For fine particles $$\ln\left(\frac{\alpha^{1.24}}{T_p^2}\right) = \frac{-1.24E_c}{RT_p} + c \qquad \textbf{(6.6)}$$

By plotting $\ln(\alpha^n/T_p^2)$ vs. $1/T_p$, E_c values for coarse and fine particles were estimated from the slope of straight lines as 439 and 450 kJ/mol, respectively (Figures 6.29 and 6.30). Kissinger equation was used to determine the E_{ck} values of as-quenched ORSG glasses. Plot of $\ln(\alpha/T_p^2)$ vs. $1/T_p$, for coarse and fine particles is shown in Figure 6.31 and the values of E_{ck} obtained from the slopes of these plots are equal to 305 and 444 kJ/mol, respectively. The activation energy of fine glass obtained from Kissinger equation is close to the E_c value of fine glass estimated from Matusita-Sakka equation. n value of fine ORSG glass was found 1.24 which indicates the surface crystallization. We know that Kissinger equation (Eq. (3.19)) is valid only when the crystallization occurs on a fixed number of nuclei during the DTA runs or when the surface crystallization mechanism is dominant in the glass. Therefore, E_{ck} value of fine ORSG glass is more accurate than the E_{ck} value of coarse ORSG glass. If we multiply E_{ck} value of coarse particles with n/m (=3.68/2.68) we obtained E_c value as 414 kJ/mol by using the Eq. (3.21).

The activation energies of fully nucleated ORSG glasses were also determined by using Kissinger equation (Eq. (3.19)). By substituting α values and corresponding T_p values into Eq. (3.19), the Kissinger plots of coarse and fine particles were obtained as given in Figure 6.32,. The values of E_{ck} for coarse and fine particles estimated from the slope of Kissinger plots are 446 and 469 kJ/mol, respectively. If we compare the E_c values determined by using all models for coarse particles, it can be seen that the E_c values are very close to each other. The same situation can be observed in the E_c values of fine particles.

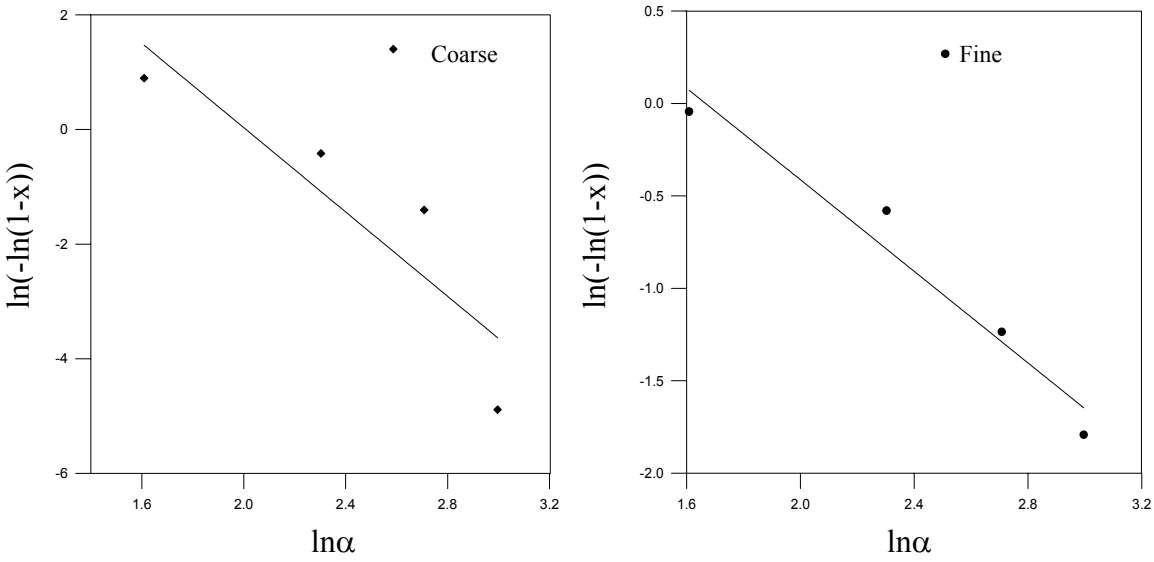

Figure 6.28: The Ozawa plots of the coarse and fine ORSG glasses

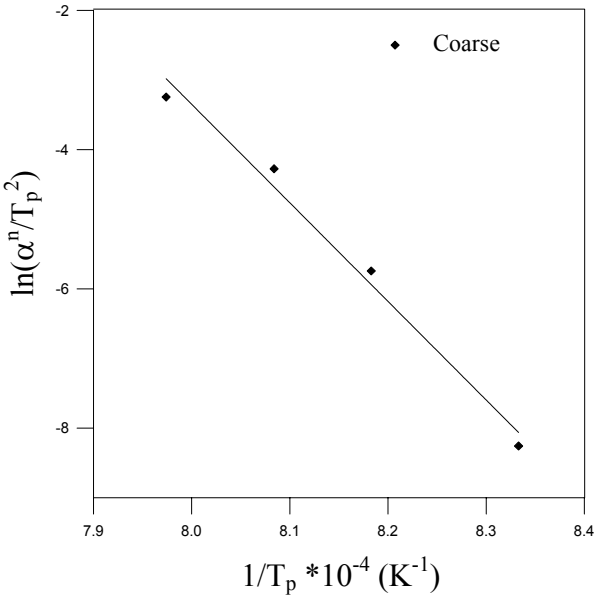

Figure 6.29: The Matusita-Sakka plot of the coarse ORSG glass

Plots of ln(-ln(1-x)) vs. $1/T_p$ (Eq.(3.22)) for crystallization of coarse and fine TG glasses are presented in Figure 6.33. n values of coarse glasses were estimated from the slope of Ozawa plot as 4.84 (m = n-1 = 3.84) which indicates the bulk crystallization, while n value of fine glasses is 1.7 (m = n= 1.7) which indicates that primary crystallization started from the surface of the sample.

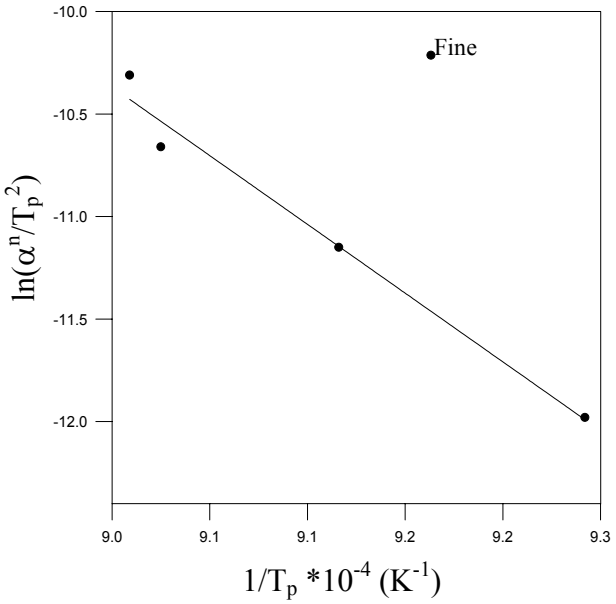

Figure 6.30: The Matusita-Sakka plot of the fine ORSG glass

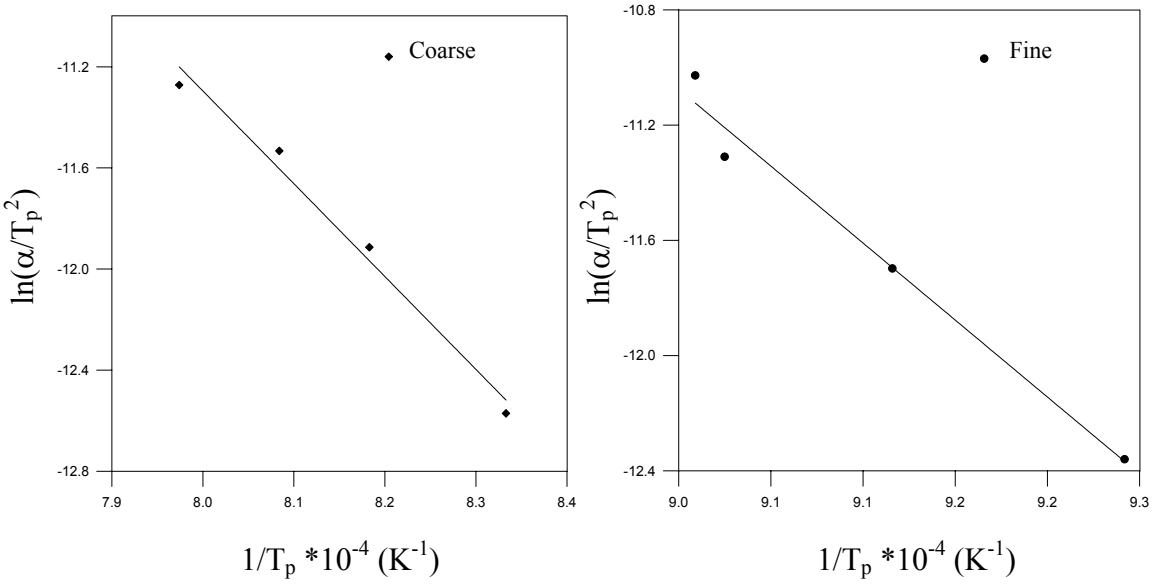

Figure 6.31: The Kissinger plots of the coarse and fine as-quenched ORSG glasses

By substituting n and m values into Eq.(3.14), the following equations were obtained for coarse and fine particles:

For coarse particles $$\ln\left(\frac{\alpha^{4.84}}{T_p^2}\right) = \frac{-3.84E_c}{RT_p} + c \qquad \textbf{(6.7)}$$

For fine particles $$\ln\left(\frac{\alpha^{1.7}}{T_p^2}\right) = \frac{-1.7E_c}{RT_p} + c \qquad \textbf{(6.8)}$$

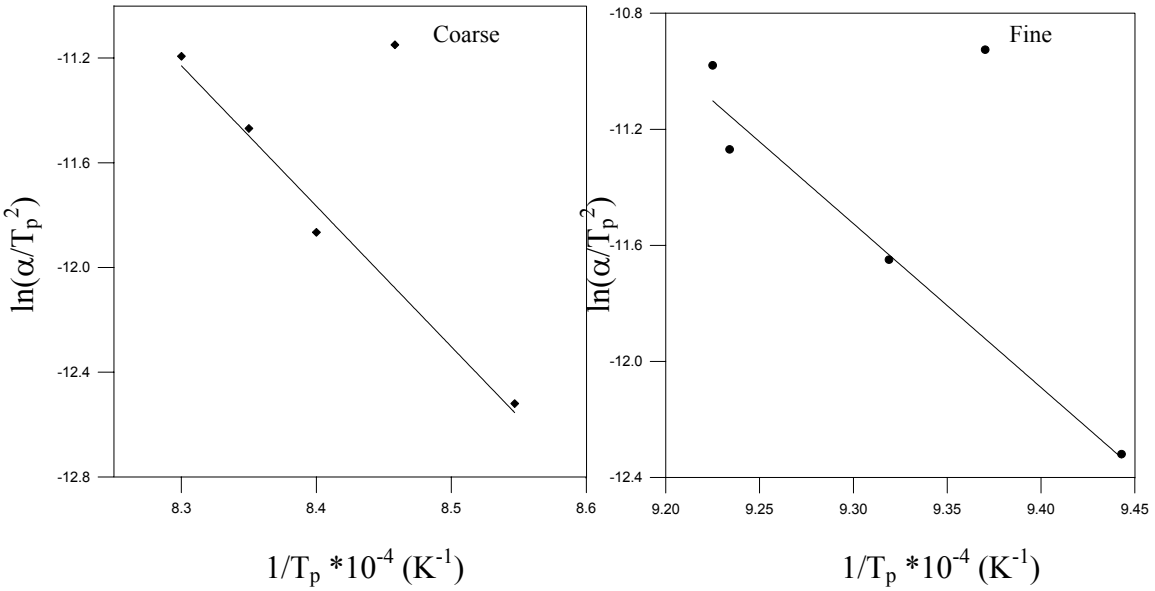

Figure 6.32: The Kissinger plots of the coarse and fine fully nucleated ORSG glasses

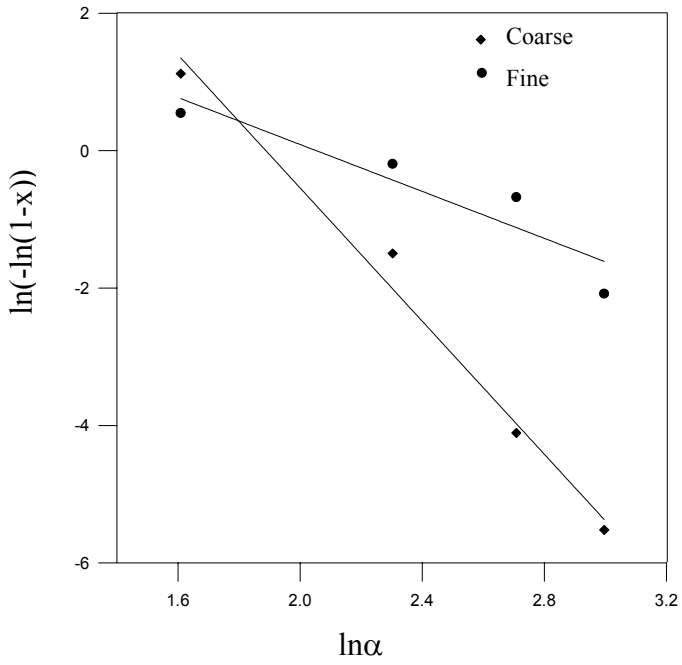

Figure 6.33: The Ozawa plots of the coarse and fine TG glasses

From the slopes, $\ln(\alpha^n/T_p^2)$ vs. $1/T_p$, in Figures 6.34 and 6.35 , we obtained the E_c values as 578 kJ/mol for coarse glasses and 654 kJ/mol for fine glasses. From the Figure 6.36 the corresponding E_{ck} values from the Kissinger method were obtained as 444 kJ/mol for coarse glasses and 645 kJ/mol for fine glasses. Also, by multiplying E_{ck} for coarse TG sample determined from Kissinger method (444 kJ/mol) by the factor n/m (=4.84/3.84) gives E_c value of 560 kJ/mol that is close to the other E_c values of coarse TG glasses. By applying Kissinger equation (Eq. (3.19))

on fully nucleated coarse and fine glasses, E_{ck} values were obtained. The Kissinger plot, $\ln(\alpha/T_p^2)$ vs. $1/T_p$, for the data given in Table 6.20 is shown in Figure 6.37. E_{ck} values of coarse and fine particles determined from the slopes of Kissinger plots are 544 and 662 kJ/mol, respectively. It's clearly seen that the data of fully nucleated glasses gave more accurate results for E_c value than the data of as-quenched glasses when Kissinger method (Eq. (3.19)) was applied on the DTA results of these glasses.

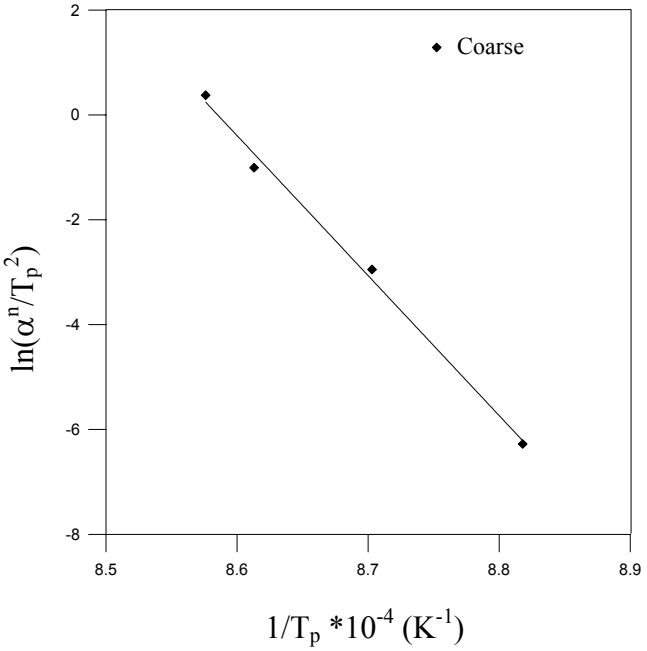

Figure 6.34: The Matusita-Sakka plot of the coarse TG glass

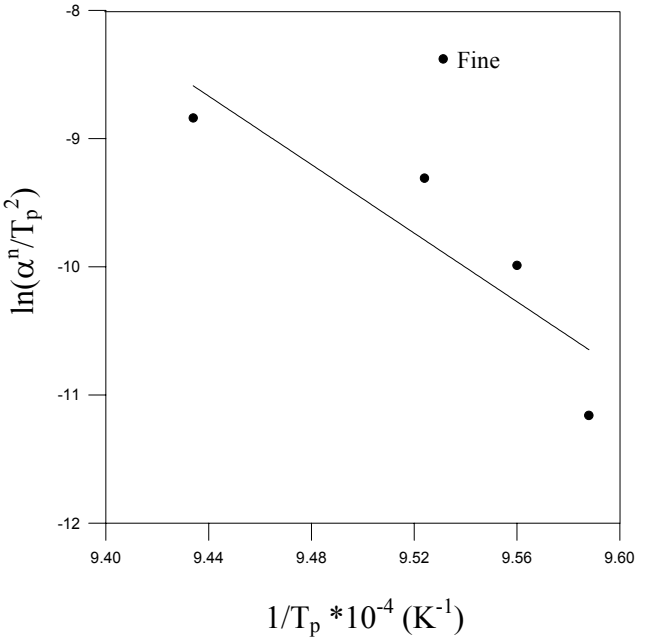

Figure 6.35: The Matusita-Sakka plot of the fine TG glass

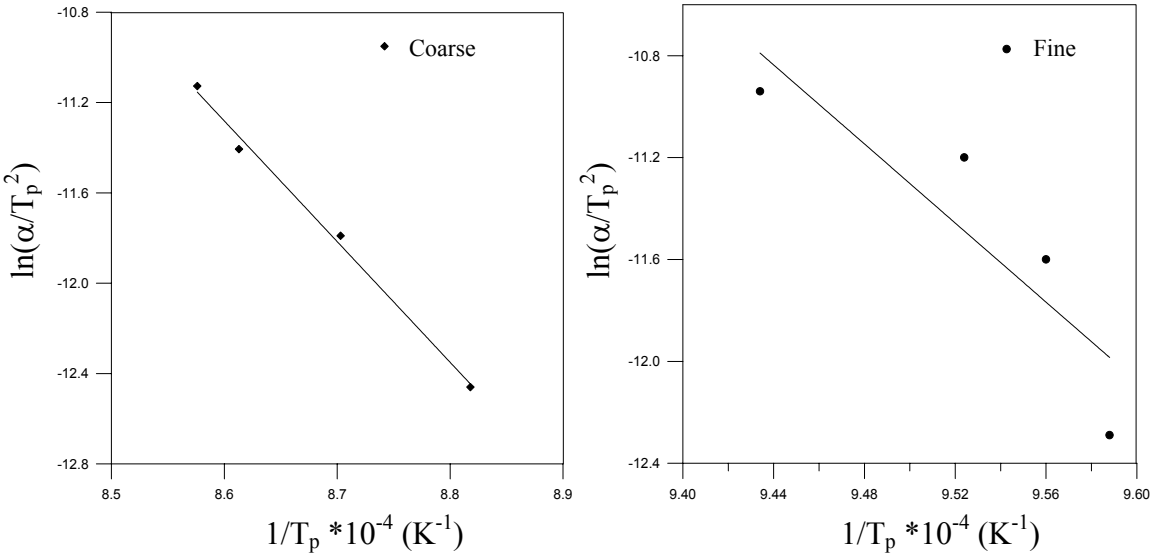

Figure 6.36: The Kissinger plots of the coarse and fine as-quenched TG glasses

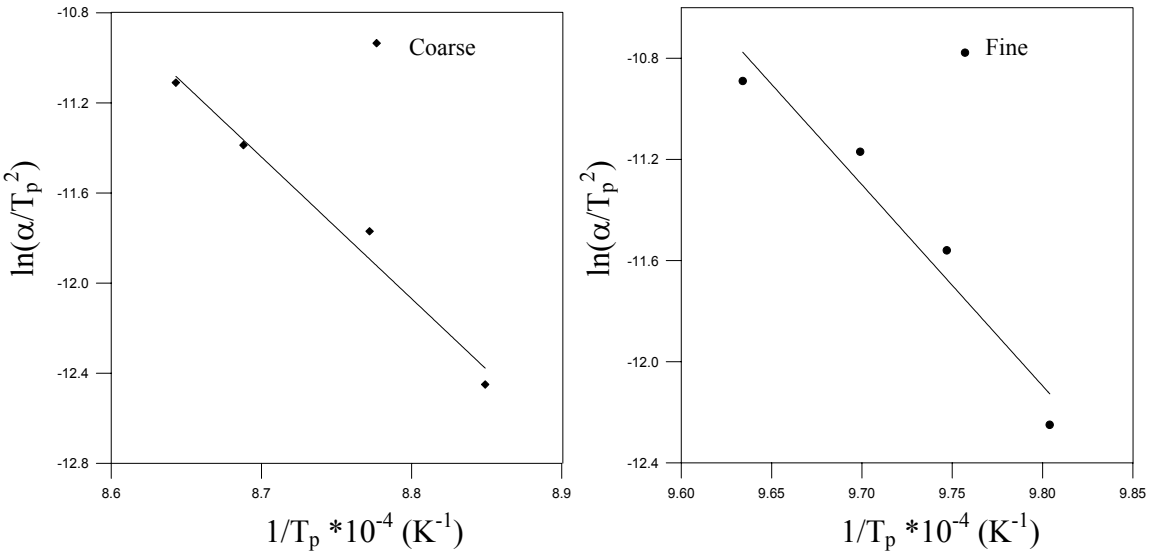

Figure 6.37: The Kissinger plot of the fully nucleated coarse TG glass

For all as-quenched glass samples, the E_{ck} values of coarse particles obtained from Kissinger method are lower than the E_c value of coarse particles determined from Matusita-Sakka method. However, activation energy values of fine glasses estimated from all methods are close to each other. The difference observed in activation energy values for coarse glasses is discussible when the Kissinger equation is used for the estimation of activation energy, E. Matusita-Sakka stated that Kissinger equation can only be used when crystallization occurs on a fixed number of nuclei as in the case of fine glass samples. Therefore, this result confirms that E_c value will be acceptable if the crystallization is made to occur on a fixed number of nuclei.

However, the analysis of crystallization data by using the Kissinger method will yield unacceptable values for E_c if nucleation and crystallization occur simultaneously. This result further confirms the necessity of using Matusita-Sakka model in determining E_c if the glass is initially unsaturated with nuclei. The Kissinger method can only be used to determine E_c values if the glass is fully nucleated with surface or bulk nuclei prior to crystallization so that crystal growth at a different α occurs always on a fixed number of nuclei.

Tables 6.21 and 6.22 show E_c, n and m values of CRG, ORSG and TG glasses of coarse and fine particles, respectively. As seen from these tables, n and m values are different for coarse and fine glasses. It is important to note that during the DTA run, surface and bulk crystallization may proceed simultaneously but if there is a control of particle size in glass, the crystallization may be governed by particle size. The differences in activation energies obtained in this study could result from a different crystallization mechanism, which is strongly influenced by the particle size in glasses. As it was also observed in all glass samples high E_c value is associated with surface crystallization while small E_c value is associated with bulk crystallization in the same glass.

The differences in n and m values obtained for coarse and fine glasses can be explained in terms of glass particle size. Large particles have much less surface area and few nuclei are formed. In this case, the dominant process would be the growth of nuclei. On heating above T_g, the nuclei are surrounded by liquid and their growth would be three-dimensional. As seen from Table 6.21, n values of all coarse glasses indicate the three-dimensional bulk crystallization. The larger surface area of smaller particles will contain larger numbers of nuclei. Supposing that glass surface is completely crystallized, crystal growth proceed one-dimensionally from surface to interior of the glass [223]. This statement can be clearly seen from Table 6.22. n values of fine samples showed that the crystallization mechanism is one-dimensional surface crystallization. The values of n obtained experimentally are changed in the range of 1.24 -1.7 for fine glasses. Table 6.23 shows the theoretical values of n at zero nucleation rate at crystal growth [224]. Comparing the experimental n values with those of the theoretical, it is found that the controlling mechanism may be either two-or three-dimension diffusional (n=1.0-1.5) or one-dimensional interfacial growth

(n =1)for the crystalline phase of fine glass-ceramic samples. n values of coarse glasses could not be compared with the theoretical values of n, since the crystal growth of coarse glasses did not occur on a fixed number of nuclei. The value of m coefficient depends on the mechanism for the formation of nuclei as summarized in Table 6.24 [225]. The m and n values determined for the coarse CRG and ORG glasses means that the nucleation growth occurred two- and three-dimensional interfacial controlled growth, respectively. m value of coarse TG sample is close to 4 which means the constant rate of nucleation with a three-dimensional interfacial controlled growth. However, nucleation and crystal growth processes occurred with an increasing number of nuclei as it was determined previously. n = 4.84 and m = 3.84 values are too high for coarse TG glasses assuming with the experimental errors. Actually, experiences show that obtaining n value of higher than 4 is very difficult and sometimes impossible for glasses [224]. m value of fine CRG, ORSG and TG glasses are changed in the range of 1.24–1.7. These values indicated that the crystallization growth occurred by three-dimensional diffusional controlled mechanism. These results showed that bulk crystallization with a three-dimensional interfacial controlled growth occurred in the coarse glass samples while the surface crystallization mechanism was dominant in the fine glasses with a one-dimensional growth.

The crystallization mode of a glass has a practical importance in the usage of it and also in the fabrication of a glass-ceramic since the surface crystallization mode may introduce huge thermal expansion difference at the boundary between the glass phase and crystallized phase, building up high tensile stress. This high tensile stress at the interface mostly causes total failure of the glass. On the other hand, in the case of the bulk crystallization mode where the crystal growth occurs at the finely distributed precursor nuclei in the glass, the huge thermal expansion coefficient gradient across the whole body does not occur and the glass body is safe against the thermal failure [219]. Therefore, from this perspective the bulk crystallization is desirable compared to the surface crystallization.

Table 6.21: E_c, n and m values of the coarse glasses

Sample Name	Activation Energy (kJ/mol)			n	m
	Matusita-Sakka Method	Kissinger Method	Isothermal Kissinger Method		
CRG	350	233	370	3.42	2.42
ORSG	439	305	446	3.68	2.68
TG	578	444	544	4.84	3.84

Table 6.22: E_c, n and m values of the fine glasses

Sample Name	Activation Energy (kJ/mol)			n	m
	Matusita-Sakka Method	Kissinger Method	Isothermal Kissinger Method		
CRG	372	369	-	1.36	1.36
ORSG	450	444	469	1.24	1.24
TG	654	645	662	1.70	1.70

As seen from Tables 6.21 and 6.22, crystallization of fine glasses requires with higher activation energy than coarse glasses for all glass samples. This result may be understood that the surface strain of the grain boundaries of the glasses effects on the nucleation and growth of crystals inside the glass. The applied energy from DTA may be exhausted in the part for the crystallization inside the glass and the other part for the surface strain from the grain boundaries of the glass particles. Since the small sized glasses have large surface grain energy compared with the large sized glass particles, thus the more energy is needed relatively for the crystallization in the small sized glass sample. It can be clearly seen that activation energy is dependent on temperature, i.e., the higher crystallization temperature is correlated with lower activation energy. In the case of surface nucleation, smaller particle size with its relatively large specific surface area helps the occurrence of crystallization and thus decreases the crystallization temperature. Consequently, E_c is larger for fine glass samples than that observed for coarse glasses. These observations were reported by several authors [133,220,221,223,226]. The crystallization activation energies of

coarse CRG, ORSG and TG glasses are changed in the range of 233-370 kJ/mol, 305-446 kJ/mol and 444-578 kJ/mol, respectively while the activation energies of fine CRG, ORSG and TG glasses are changed in the range of 369-372 kJ/mol, 444-469 kJ/mol and 645-662 kJ/mol, respectively. The activation energy determined from Matusita-Sakka and isothermal Kissinger methods are close to each other in each glasses of both coarse and fine particles. These results showed the accuracy of the applied methods.

The studied glasses are in the SiO_2-Al_2O_3-Fe_2O_3-CaO quartet system since the mixed wastes are mainly composed of SiO_2, Al_2O_3, Fe_2O_3 and CaO. With the solid-state reactions and the rearrangement of these structures, crystalline phases occur in the glassy matrix when the heat treatment process was applied on the glass samples. This must require breaking and reforming of the Si-O, Al-O, Fe-O and Ca-O bonds. The single bond strength of the Si-O, Al-O, Fe-O and Ca-O bonds are 445, 423, 335 and 128 kJ/mol, respectively [224,226,227]. The crystallization activation energies of ORGS and CRG glasses are close to Si-O, Al-O and Fe-O bond strengths while the E_c value of TG glass is higher than those of the bond strengths. This result is consistent with the mechanism requiring the breaking of Si-O, Al-O and Fe-O bonds and also rules out their possibilities as a reaction controlling kinetics in forming crystalline phases in the glassy matrix. The E_c value of TG glass is higher than the E_c values of CRG and ORSG glasses. Since the SiO_2 and Al_2O_3 contents of TG glasses are so high these E_c values are relatively high. It was also observed that the increase in Fe_2O_3 content in the glass compositions caused a decrease in the activation energies of the glasses. Since the CRG glass has the highest Fe_2O_3 content, its E_c value is the lowest one. This result was also observed in the other studies [126,228]. Iron oxides caused to lower glass viscosity and crystallization temperatures consequently increase the crystal growth rate. Despite that it is usually an intermediate glass network ion, the Fe^{3+} could act as a modifier of the glass structure, breaking the Si-O bonds. Therefore, the E_c value of TG glass is the highest one in all glass samples.

Only a few researchers studied the crystallization kinetics of coal fly ash based glasses. Crystallization activation energy values of glasses produced from coal fly ashes were found 283 and 318 kJ/mol in the previous studies [135,136] which are

lower than the E_c values obtained in this study since the chemical composition of the studied glassy systems are different from each other. The calculated crystallization activation energy value of CRG glass is close to the value of 370 kJ/mol found by Cioffi et al. [134] for a glass produced from coal fly ash while the E_c values of ORSG and TG glasses are higher than that value. The activation energy values for crystallization are lower for the incinerator fly ashes than for coal fly ash containing glasses, which are in the SiO_2-Al_2O_3-Fe_2O_3-CaO quartet glassy systems. The crystallization activation energy values for incinerator fly ashes are changed in the range of 379-468 kJ/mol [131,133,209], while the E_c values of glasses produced from industrial wastes (such as coal fly ash, glass cullet and soda-lime) are changed in the range of 534-545 kJ/mol [111,137]. These values are close to the E_c values of CRG and ORSG glasses obtained in this study.

Table 6.23: Theoretical values of Avrami exponent, n, at zero nucleation rate[224]

	Diffusion-controlled	Interface-controlled
3-dimension	1.5	3.0
2-dimension	1.0	2.0
1-dimension	0.5	1.0

Table 6.24: Physical meaning of Johnson-Mehl-Avrami kinetic coefficient, m[225]

Type of nucleation and geometry of growing	Law of growing nuclei	
	Interface-controlled	Diffusion-controlled
Instantaneous nucleation and one-dimensional growth	1.0	0.5
Instantaneous nucleation and two-dimensional growth	2.0	1.0
Instantaneous nucleation and three-dimensional growth	3.0	1.5
Constant rate of nucleation and one-dimensional growth	2.0	1.5
Constant rate of nucleation and two-dimensional growth	3.0	2.0
Constant rate of nucleation and three-dimensional growth	4.0	2.5

6.6.2.2 Isothermal analysis

The crystallization kinetics of the as-quenched coarse and fine glasses were also examined using isothermal differential thermal analysis. The DTA results were analyzed with the equation derived by Johnson-Mehl-Avrami (JMA)[43,59-62]. There were two main aims for conducting these experiments: 1) to determine a more accurate value for the Avrami exponent and E_c, 2) to compare the results of kinetic data as determined by isothermal and non-isothermal methods. The isothermal experiments were conducted in accordance with procedures stated in section 3.3.2.1. The obtained crystallization peak temperatures of CG-97, ORSG and TG glasses as a function of particle size were given in Tables 6.25-6.27. DTA graphs of CG-97, ORSG and TG glasses can be seen in Figures B20-37 in Appendix B. All exothermic peak's shape and temperature were the same for the CRG glass. Therefore, JMA method could not be applied on CRG glasses of both coarse and fine glasses since the crystallized fraction, x, up to any time, could not be determined from the exothermic peaks in each DTA graph. The crystallization kinetics of CG-97 glasses obtained in a previous study [135] did not estimate from the isothermal methods so that isothermal DTA data of CG-97 glasses were obtained and examined in this study. As seen from Tables 6.25-6.27, coarse particles have higher T_p values than the fine particles in convenience with the non-isothermal methods. The increase in specific surface area of the glass samples would result in the decrease in T_p for the case of surface crystallization.

The isothermal heat treatments of the coarse and fine CG-97 glasses were carried out in the temperature range of 1023-1058 K. The variation of the crystallized fraction (x) as a function of the isothermal hold time for both glass samples is shown in Figure 6.38. It is clearly seen that to complete crystallization at lower temperatures for glass samples take longer time. Crystallized fraction, x, at the range of 0.1-0.95 was employed to coarse and fine glass samples to construct the ln(-(ln(1-x)) versus ln t plots shown in Fig. 6.39. Determined values of the reaction rate constant and Avrami exponent from these plots are given in Table 6.28. The values of n of the coarse samples are roughly close to the values determined by the non-isothermal method previously [135]. Although the crystallization of the coarse samples is

governed by two dimensional bulk crystallization, the Avrami exponent values of the fine samples indicate that the mechanism is surface crystallization. Since fine samples have larger surface area than the coarse samples, this result is expected. The effective volume to surface area ratio is larger for coarse samples than fine samples. Therefore, bulk crystallization as opposed to surface crystallization is expected for coarse samples [72]. A plot of lnk as a function of 1/T is given in Fig. 6.40. Activation energies of the crystallization for coarse and fine particles were determined as 297 and 348 kJ/mol, respectively. The activation energy value of the coarse particles is close to the value determined by the non-isothermal method previously [135]. Fine particles have higher crystallization activation energy values than coarse particles. The frequency factors for coarse and fine particles were calculated as 1.94×10^{13} and 1.36×10^{16}, respectively.

Table 6.25: DTA results of CG-97 sample obtained from isothermal method

Heating rate 20K/dak							
Coarse particles				Fine particles			
Samples nucleated at 973 K for 2 h				Samples nucleated at 983 K for 2 h			
Holding time (min)	Selected temperatures below the crystallization temperature (K)			Holding time (min)	Selected temperatures below the crystallization temperature (K)		
	1038	1048	1058		1023	1033	1043
	Crystallization peak temperatures (K)				Crystallization peak temperatures (K)		
15	1189	1166	1160	15	1161	1160	1159
30	1185	1160	1148	30	1157	1158	1155
60	1181	1156	1145	60	1155	1156	1153

Table 6.26: DTA results of ORSG sample obtained from isothermal method

Heating rate 20K/dak							
Coarse particles				Fine particles			
Samples nucleated at 1033 K for 2 h				Samples nucleated at 988 K for 2 h			
Holding time (min)	Selected temperatures below the crystallization temperature (K)			Holding time (min)	Selected temperatures below the crystallization temperature (K)		
	1073	1093	1113		1033	1053	1073
	Crystallization peak temperatures (K)				Crystallization peak temperatures (K)		
15	1252	1250	1248	15	1187	1182	1179
30	1251	1249	1248	30	1186	1181	1177
60	1251	1249	1247	60	1183	1180	1170

Table 6.27: DTA results of TG sample obtained from isothermal method

Heating rate 20K/dak							
Coarse particles				Fine particles			
Samples nucleated at 963 K for 2 h				Samples nucleated at 953 K for 2 h			
Holding time (min)	Selected temperatures below the crystallization temperature (K)			Holding time (min)	Selected temperatures below the crystallization temperature (K)		
	1033	1053	1073		1033	1053	1073
	Crystallization peak temperatures (K)				Crystallization peak temperatures (K)		
15	1171	1169	1156	15	1164	1155	1156
30	1171	1166	1153	30	1163	1154	1152
60	1169	1164	1152	60	1156	1154	1151

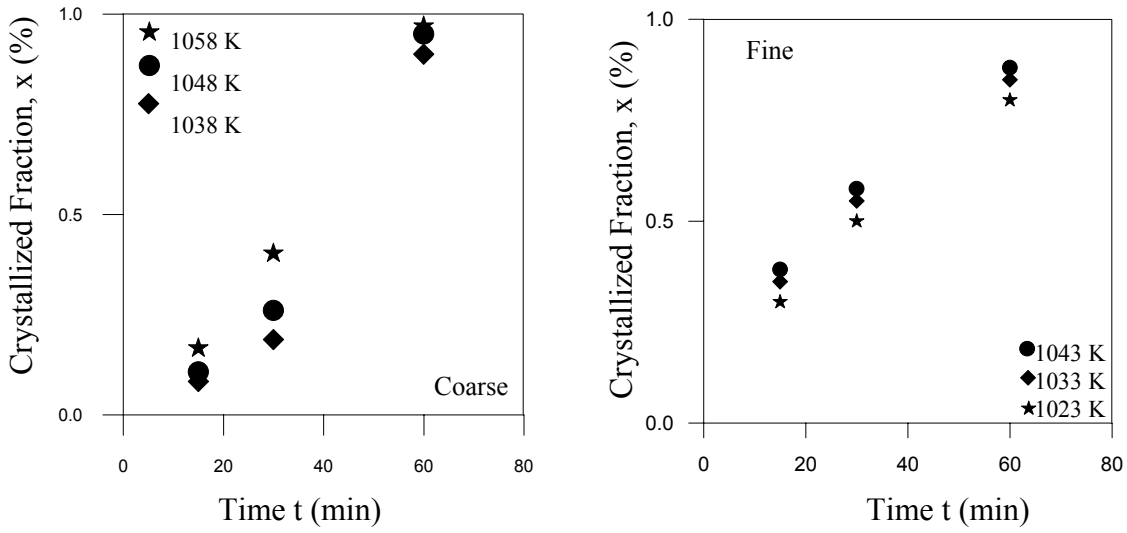

Figure 6.38: Plots of coarse and fine CG-97 glasses crystallized as a function of isothermal hold time

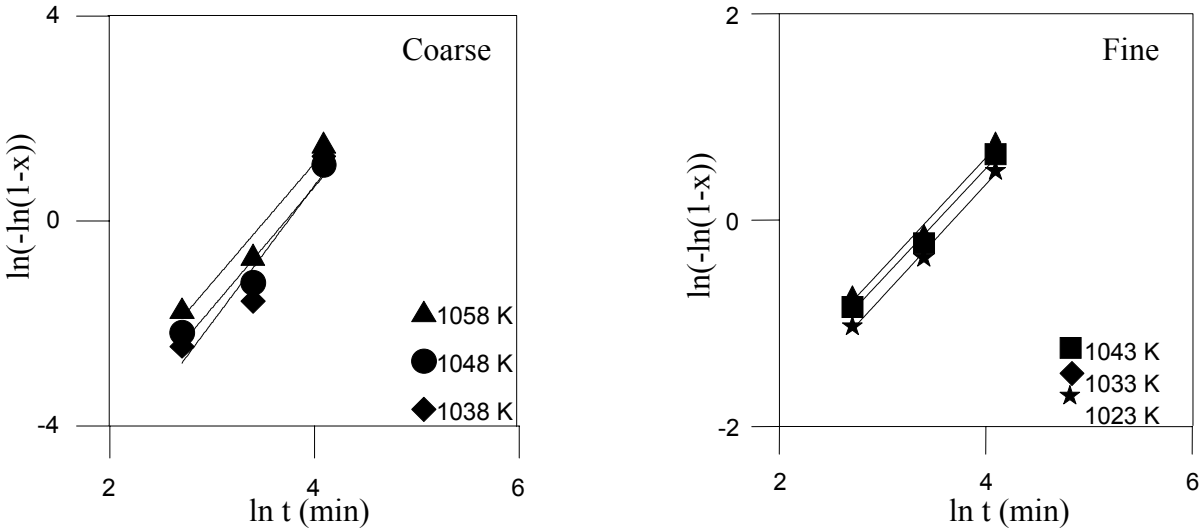

Figure 6.39: Plot of ln(-ln(1-x)) vs ln t for coarse and fine CG-97 glasses

Table 6.28: Avrami exponent and reaction rate values of coarse and fine CG-97 glasses

Coarse particles			Fine particles		
T (K)	ln k(min^{-1})	n	T (K)	ln k(min^{-1})	n
1038	-3.75	2.673	1023	-3.685	1.087
1048	-3.48	2.480	1033	-3.440	1.075
1058	-3.10	2.330	1043	-2.900	1.069

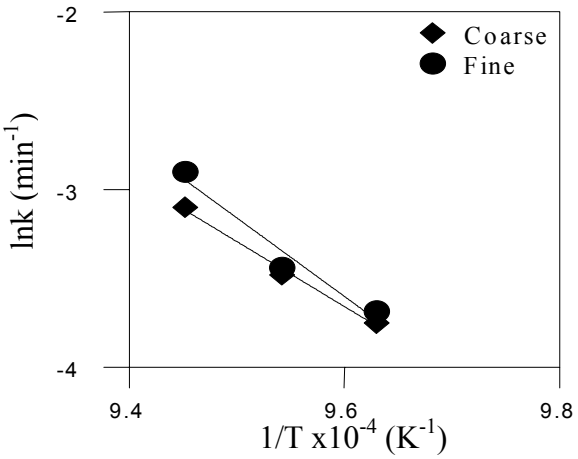

Figure 6.40: Plot of ln k vs 1/T for determining the values of E and A

The isothermal DTA measurements of coarse and fine ORSG glasses were performed between 953-1113 K since ORSG glasses showed reasonable peak shapes for data analysis in this range. The crystallized fraction as a function of time for both coarse and fine glasses can be seen from Figure 6.41. As it was observed from the Figure 6.41, it takes longer time for the ORSG glass to complete crystallization at lower temperature. Information derived from these plots over the range of x from 0.1-0.9 was employed to construct the ln(-ln(1-x)) vs. ln t plots shown in Figure 6.42. These plots were subsequently used to determine values for the reaction rate constant, k, and n in this range of temperature. The obtained data as summarized in Table 6.29 were then used to plot the graph of ln k vs. 1/T, shown in Figure 6.43 The average n value of coarse samples (n=3.37) indicates the three-dimensional bulk crystallization while the one-dimensional surface crystallization mechanism (n =1.71) is predominant for fine samples. Crystallization activation energies of coarse and fine glasses were estimated from these plots as 435 and 443 kJ/mol, respectively. As it was observed in non-isothermal methods, crystallization activation energy values increased with the decrease in particle size for the isothermal methods, too. The frequency factors for coarse and fine glasses were determined as 2.14×10^{14} and 6.13×10^{19} s^{-1}, respectively.

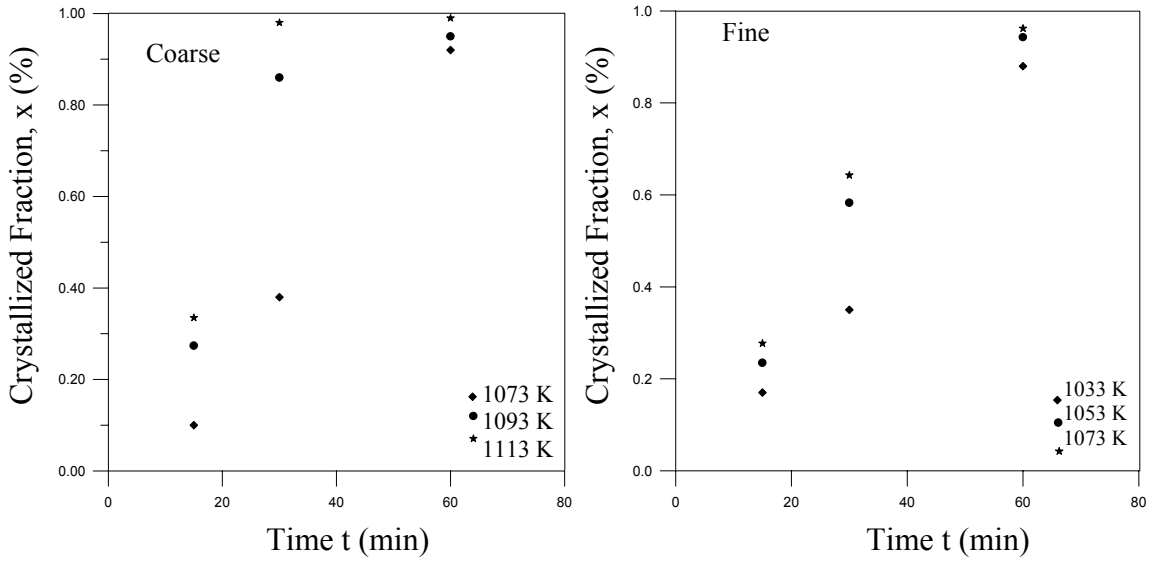

Figure 6.41: Plots of coarse and fine ORSG glasses crystallized as a function of isothermal hold time

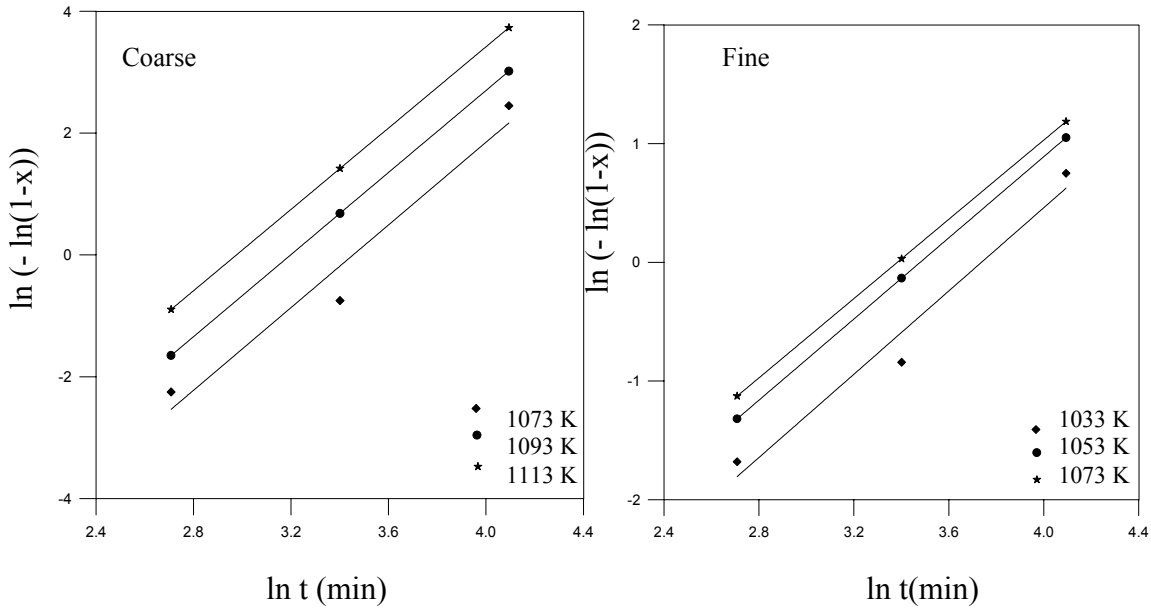

Figure 6.42: Plot of ln(-ln(1-x)) vs ln t for coarse and fine ORSG glasses

Table 6.29: Avrami exponent and reaction rate values of coarse and fine ORSG glasses

Coarse			Fine		
T (K)	ln k(min^{-1})	n	T (K)	ln k(min^{-1})	n
1073	-11.72	3.39	1033	-6.55	1.75
1093	-10.78	3.37	1053	-5.95	1.71
1113	-9.94	3.34	1073	-5.65	1.67

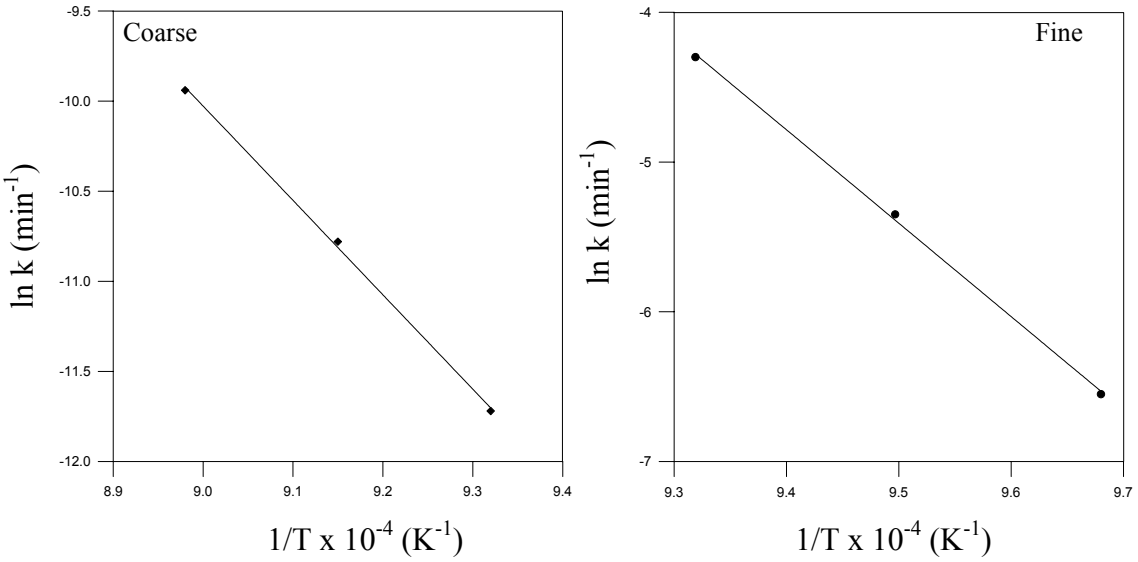

Figure 6.43: Plots of ln k vs 1/T for determining the values of E and A

Figure 6.44 shows the calculated results of the crystallized volume fraction of a coarse and fine TG glasses as a function of isothermal time at different temperatures which are in the range of 923-1073 K. As it was expected from the previous results, crystallization completed with the increase in holding time and the isothermal temperature. The kinetic parameters for crystallization, n and k, were determined at each temperature by using Eq. (3.18) as it was shown in Figure 6.45. The calculated values of n and k for each temperature were listed in Table 6.30 and the average values of n for coarse and fine glasses were 4.1 and 1.63, respectively. Avrami exponent of coarse glasses indicates three-dimensional bulk growth while the n value of fine glasses shows one-dimensional surface crystallization as it was observed in non-isothermal methods. Figure 6.46 is a plot of the reaction rate, k, vs. temperature, T obtained by using the data from Table 6.30. When the equation for reaction rate was applied to the plots in Figure 6.46, crystallization activation energy and frequency factor for coarse glasses were determined as 548 kJ/mol and 4.83×10^{18} s^{-1}, respectively. The crystallization activation energy and frequency factor of fine glasses is 610 kJ/mol and 5.65×10^{29} s^{-1}, respectively. n values of all coarse and fine glasses obtained from JMA model showed that the controlling mechanism was diffusion for fine glasses whereas the interface controlled mechanism was predominant for coarse glasses. These results were consistent with the results obtained in non-isothermal methods.

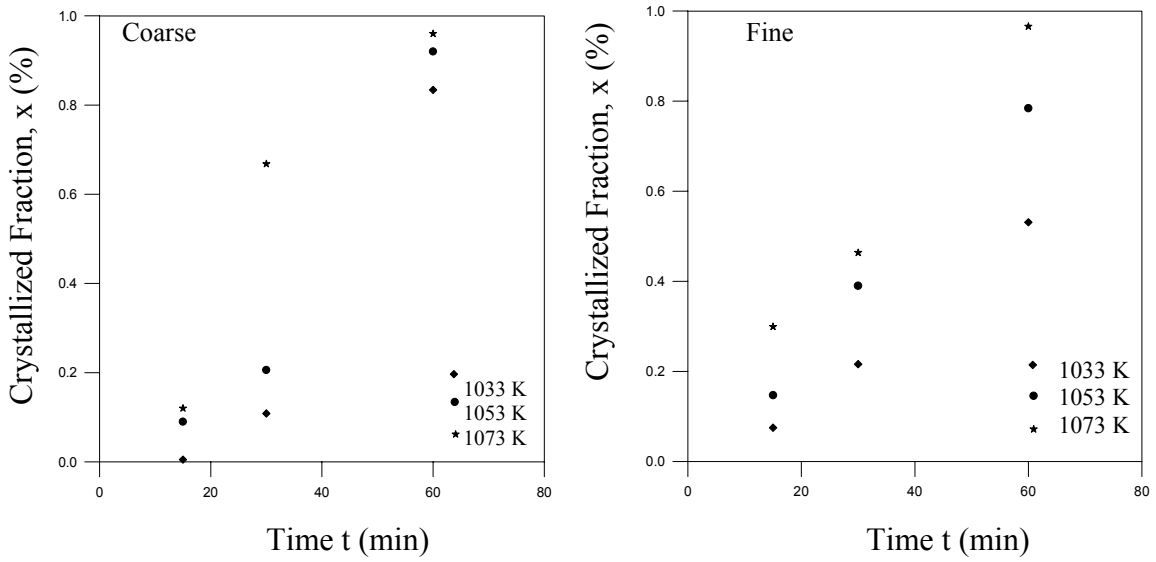

Figure 6.44: Plots of coarse and fine TG glasses crystallized as a function of isothermal hold time

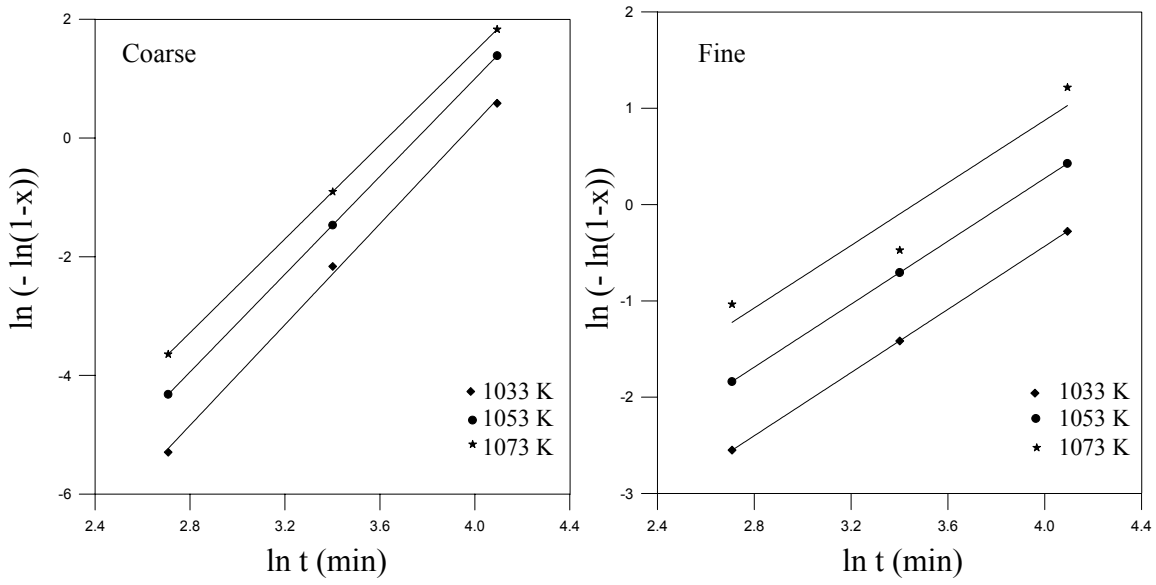

Figure 6.45: Plots of ln(-ln(1-x)) vs ln t for coarse and fine TG glasses

Table 6.30: Avrami exponent and reaction rate values of coarse and fine TG glasses

Coarse			Fine		
T (K)	ln k(min^{-1})	n	T (K)	ln k(min^{-1})	n
1033	-16.72	4.24	1033	-6.99	1.639
1053	-15.48	4.12	1053	-6.26	1.633
1073	-14.34	3.95	1073	-5.62	1.624

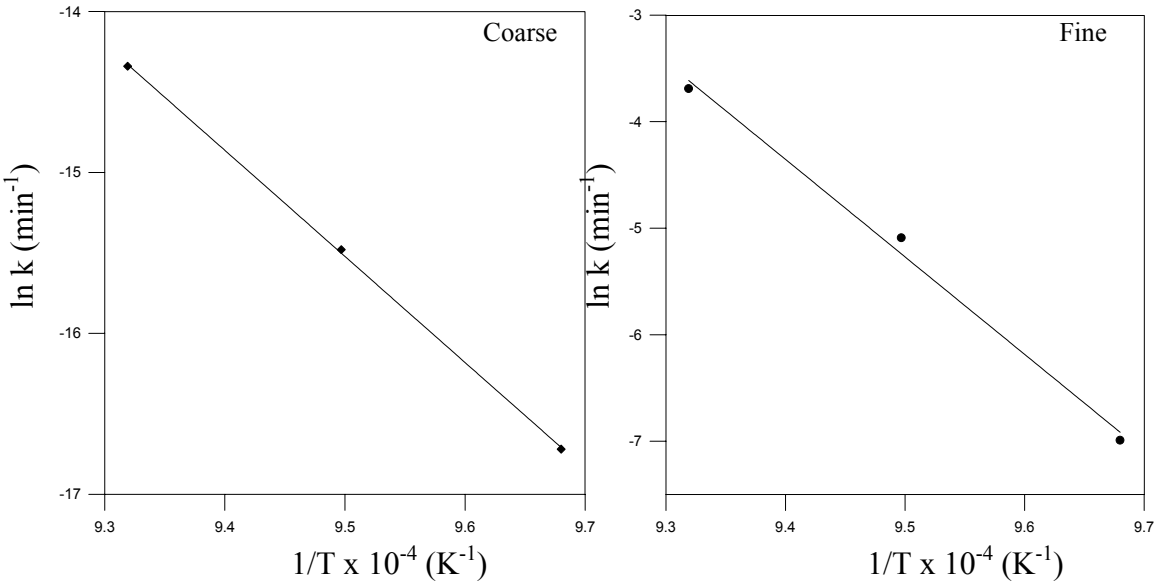

Figure 6.46: Plot of ln k vs 1/T for determining the values of E and A

A comparison of kinetic parameters of all coarse and fine glasses, as determined by isothermal and non-isothermal methods, is shown in Tables 6.31 and 6.32, respectively. The value of n for the isothermal data was computed directly from curve fits applied to the entire exotherm instead of by just a calculation based on T_p for non-isothermal data. Therefore, n as calculated by the isothermal experiments, was more accurate and more precise than that calculated by the non-isothermal experiments. The crystallization activation energy values of all coarse and fine glasses for the non-isothermal and isothermal methods are roughly close. However, E_c values obtained from non-isothermal methods were higher than that obtained from isothermal method. The discrepancy between the isothermal and non-isothermal results may be interpreted as the experimental error. It must be noted that this observation stated by the other authors for different glassy systems [58,229]. The isothermal experiments yield the lowest crystallization activation energy. Since the samples were heated at the highest rate (20 K/min) to the isothermal hold temperatures, it is possible that those conditions were able to force the very earliest stages of crystallization. The crystal growth occurred on a fixed number of nuclei for all coarse and fine glasses in isothermal methods since the isothermal heat treatments were applied to the glasses in every stage (at nucleation and below the crystallization temperatures). Consequently, the kinetic parameters determined by isothermal analysis were evaluated to be more accurate and more precise then those calculated by non-isothermal experiments for two reasons: 1) the JMA equation used for the

kinetic model was derived for isothermal transformations and hence no approximations, special conditions or assumptions were necessary, 2) the calculations were based on a curve fit applied to the exothermic peak, not just on T_p. This minimizes potential sources of errors that sometimes occur when using the JMA equation to model isothermal experiments. Some disadvantages of this technique, are that the experiments take longer time to perform the model and that very precise control of the furnace temperature is required.

Table 6.31: E_c, n and m values obtained from both isothermal and non-isothermal methods for the coarse glasses

Sample Name	Activation Energy (kJ/mol)				Non-isothermal		Isothermal	
	Matusita-Sakka Method	Kissinger Method	Isothermal Kissinger Method	JMA Equation	n	m	n	m
CRG	350	233	370	-	3.42	2.42	-	-
ORSG	439	305	446	435	3.68	2.68	3.37	3.37
TG	578	444	544	548	4.84	3.84	4.10	4.10
CG-97	-	-	-	297	4.00	3.00	2.50	2.50

Overall results showed that the results of isothermal and non-isothermal crystallization kinetics of glasses produced from coal fly ash and the other industrial wastes are in agreement within experimental error. These results indicate that the data of the crystallization mechanism and crystallization activation energy of glasses obtained in this study are accurate and reliable. Although a number of studies have been reported on examining the crystallization behavior of glasses produced from industrial wastes (such as incinerator fly ash, slag) by using isothermal and non-isothermal methods [111,112,131,133,162,230], only a few researchers have done investigations on glasses produced from coal fly ash [134-136]. The question to be addressed is whether or not these kinetic models that we used in this study can be applied to the fly ash based glasses by using DTA. The similar non-isothermal and isothermal results give us confidence that variable heating rate DTA techniques can be used to determine crystallization kinetics of glasses produced from coal fly ash and the other industrial wastes.

Table 6.32: E_c, n and m values obtained from both isothermal and non-isothermal methods for the fine glasses

Sample Name	Activation Energy (kJ/mol)				Non-isothermal		Isothermal	
	Matusita-Sakka Method	Kissinger Method	Isothermal Kissinger Method	JMA Equation	n	m	n	m
CRG	372	369	-	-	1.36	1.36	-	-
ORSG	450	444	469	443	1.24	1.24	1.71	1.71
TG	654	645	662	610	1.70	1.70	1.63	1.63
CG-97	-	-	-	348	-	-	1.08	1.08

6.7 Glass-ceramic Production

The ideal microstructure of glass-ceramics would be well-oriented and fine-grained crystallites extending the whole body in order to obtain the best microstructural, physical and mechanical properties. In addition, there should be a good bonding between crystallites, so that the glass-ceramic will have better properties. Glass-ceramics can be produced both by a traditional glass-forming technique starting from the melted glass, followed by a nucleation, crystallization heat treatment and by glass powders sintering thorough heating to high temperatures. One of the main aims of this study is to investigate the possibility of obtaining bulk and sintered glass-ceramics from coal fly ash and the other industrial wastes and to establish the best conditions to obtain a product with a high density and crystalline degree. For this purpose, bulk and sintered glass-ceramics produced from ORSG, CRG and TG glasses according to the procedure described in section 5.5. ORSG, CRG and TG glasses were the most appropriate candidates for the glass-ceramic production as it was determined previously. In this study, CG-97 glasses were also used to produce sintered glass-ceramics to compare the microstructural, physical, mechanical and chemical properties with the bulk glass-ceramics obtained in a previous study [118]. In all sintered glass-ceramics polyvinyl alcohol (PVA) used as a binder to determine its effect in the sintering technique. An idealized heat treatment schedule for

producing glass-ceramics from industrial wastes was determined by using the DTA results obtained in section 6.6.1. The applied heat treatment schedules to the all glasses were given in Table 6.33. CRGC, ORSGC, CGC-97 and TGC are corresponded to the glass-ceramics produced from CRG, ORSG, TG and CG-97 glasses, respectively. P, S and B letters indicate the sintering technique with using PVA as a binder, sintering and the bulk process, respectively. All the glass samples heat treated at the crystallization temperature for 15, 30 and 60 min to investigate the effect of holding time at the crystallization temperature on the properties of glass-ceramic samples. During all heat-treatment processes, heating rate was selected as 10 K/min since this rate is sufficiently slow to avoid any deformation of the glass samples and to permit crystal growth.

Table 6.33: Codes of the produced glass-ceramic samples

Glass	Nucleation Stage	Crystallization Stage	Code of the Glass-ceramic Samples
CRG	Nucleated at 963 K for 4 h	Crystallized at 1135 K for 15 min	CRGC-B15; CRGC-S15; CRGC-P15
		Crystallized at 1135 K for 30 min	CRGC-B30; CRGC-S30; CRGC-P30
		Crystallized at 1135 K for 60 min	CRGC-B60; CRGC-S60; CRGC-P60
ORSG	Nucleated at 988 K for 2 h	Crystallized at 1188 K for 15 min	ORSGC-B15; ORSGC-S15; ORSGC-P15
		Crystallized at 1188 K for 30 min	ORSGC-B30; ORSGC-S30; ORSGC-P30
		Crystallized at 1188 K for 60 min	ORSGC-B60; ORSGC-S60; ORSGC-P60
TG	Nucleated at 948 K for 2 h	Crystallized at 1140 K for 15 min	TGC-B15; TGC-S15; TGC-P15
		Crystallized at 1140 K for 30 min	TGC-B30; TGC-S30; TGC-P30
		Crystallized at 1140 K for 60 min	TGC-B60; TGC-S60; TGC-P60
CG-97	Nucleated at 958 K for 4 h	Crystallized at 1142 K for 15 min	CGC-B15; CGC-S15; CGC-P15
		Crystallized at 1142 K for 30 min	CGC-B30; CGC-S30; CGC-P30
		Crystallized at 1142 K for 60 min	CGC-B60; CGC-S60; CGC-P60

6.7.1 Experimental results on CRGC sample

6.7.1.1 Microstructural characterization of CRGC sample

X-ray diffractometry (XRD) scans were carried out on glass-ceramic samples produced by using different heat treatment schedules. In all XRD scans of CRGC samples produced using different heat treatment schedules, the d-values matched the card values of the diopside-alumina ($Ca(Mg,Al)(Si,Al)_2O_6$) phase. As seen in the representative XRD patterns of the CRGC-B samples (Fig. C.1 in Appendix C), all the diffraction peaks can be indexed as arising from the reflection planes of the diopside-alumina phase which has a monoclinic structure with lattice parameters a = 0.973 nm, b = 0.887 nm, c = 0.528 nm and $\beta = 105.92°$ [231]. This is in agreement with the reported literature on glass-ceramics produced from raw materials having similar chemical compositions to Çayırhan fly ash; either the diopside phase or phases belonging to the diopside group (melilite or akermanite) were reported [105,108]. Barbieri et al.[11], Cheng [155] and Boccaccini et al.[10] also reported the formation of the diopside phase during devitrification in the CaO-Al_2O_3-SiO_2 ternary system. XRD patterns of CRGC-S and CRGC-P samples were given in Figures C2-C3 in Appendix C. The main crystalline phase of all CRGC samples is diopside since the chemical compositions of those glass-ceramic samples are the same. The main crystalline phase cannot change when the production technique of glass-ceramic samples is different.

SEM gives very detailed information about the process of conversion of glass into a glass-ceramic material. In addition to qualitative evaluation of microstructural changes, it also permits quantitative measurements, especially on the number of particles, their size and distribution. To examine the microstructural evaluation of glass-ceramic samples, SEM investigations were conducted on all samples. Figures 6.47-6.49 show the SEM micrographs of the glass-ceramics produced by classical method. It is clearly seen that tiny crystallites dispersed in the microstructure of the samples. Figure 6.47 shows the SEM micrograph of the glass-ceramic sample crystallized at 1135 K for 15 min revealing tiny equiaxed crystallites uniformly dispersed in the microstructure. The average crystalline size is about 0.25 μm. Figure 6.48 is a respective typical SEM micrograph of the fly ash-based glass-ceramic

crystallized at 1135 K for 30 min. As seen in Figure 6.48, the crystallites are uniformly dispersed in the microstructure and the average crystalline grain size is about 0.5 μm. As a result of increase in the holding time at the crystallization temperature, the average crystalline size for the 30 min sample is larger than that for the 15 min sample. Figure 6.49 is a SEM micrograph of the glass-ceramic crystallized at 1135 K for 60 min showing the presence of a homogeneous dispersion of equiaxed crystallites about 0.5 μm in size. The crystallites are larger than those of the sample crystallized at 1135 K for 15 min.

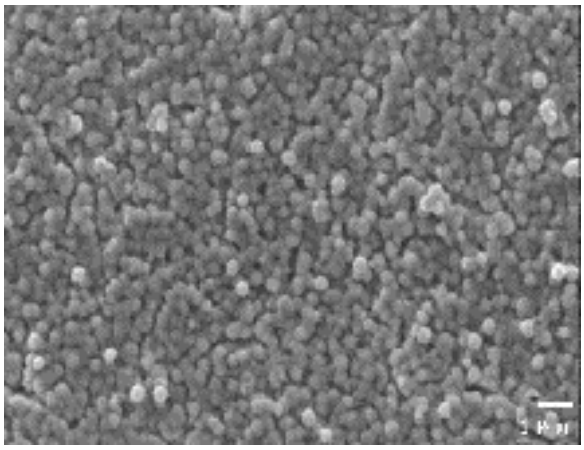

Figure 6.47: SEM micrographs of CRGC-B15

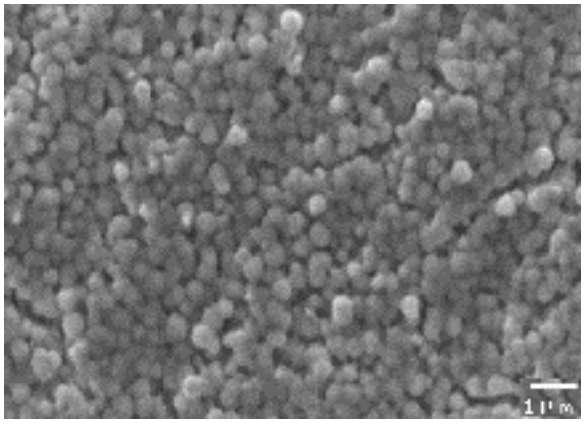

Figure 6.48: SEM micrographs of CRGC-B30

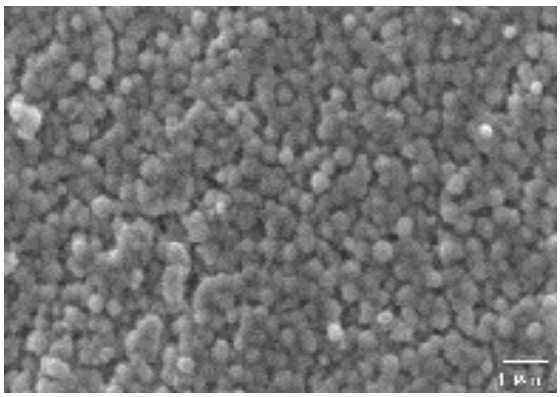

Figure 6.49: SEM micrographs of CRGC-B60

As seen in Figures 6.47-6.49, progressive increases in holding times at the nucleation temperature causes grain growth resulting in larger crystalline sizes in the microstructure. SEM micrographs have also shown that all glass-ceramic samples comprise uniformly dispersed crystallites with grain sizes varying between 0.25 – 0.5 μm with an overall mean grain size of 0.3 μm. This value is better than the mean crystalline size reported by Boccaccini et al.[132]. Further, since the controlled heat treatment procedure was applied to all glass-ceramic samples of the present investigations, the crystallites are more uniformly dispersed than those of the glass-ceramic sample (code : 4AP) reported by Barbieri et al.[11]. In addition, there are no surface cracks observed in the glass-ceramic samples of the present investigation contrary to the glass-ceramic reported by Boccaccini et al.[10].

Cross-sectional SEM investigations were also carried out to characterize the crystalline morphology in the bulk of the sample. Figure 6.50 shows the cross-sectional SEM micrograph of the CRGC-B30 sample. It can be seen from Figure 6.50 that the similar average crystalline size and morphologies were also detected in the cross-sectional SEM investigations. This confirms that bulk crystallization is predominant mechanism in the glass-ceramic samples as determined in Section 6.6.2.

Figures 6.51-6.53 show the SEM micrographs of sintered glass-ceramic samples. Fig. 6.51 shows the SEM micrograph of the glass-ceramic sample crystallized at 1135 K for 15 min revealing tiny crystallites dispersed in the microstructure. The average crystalline size is about 1.13 μm. It is also seen that some glassy regions are

still remained in the bulk of the sample. Fig. 6.52 is a SEM micrograph of the glass-ceramic sample crystallized at 1135 K for 30 min. The crystalline size of this sample varies between 1.5-1.7 μm. The crystallites are larger than that of the glass-ceramic sample crystallized at 1135 K for 15 min due to longer holding times at the crystallization temperature. It is also seen that the glassy region is smaller and the number of crystallites is greater. Fig. 6.53 is a representative SEM micrograph of the glass-ceramic sample crystallized at 1135 K for 60 min. As seen in Fig. 6.53, the crystallites have grain size between 1.85-2.2 μm and thus are larger than those of the samples crystallized at 1135 K for 15 and 30 min. The size and the number of crystallites occurred during the heat treatment processes increase with increasing holding time at the crystallization temperature. The similar crystalline shapes were observed in both sintered and bulk glass-ceramic samples. However, the number of the crystallites formed in all sintered glass-ceramic samples was less than the bulk glass-ceramic samples. The microcrystalline structures occurred in CRGC-S15 and CRGC-S30 samples are better than the microstructures of the sintered glass-ceramics reported by Boccaccini et al.[165] and Hong et al.[232].

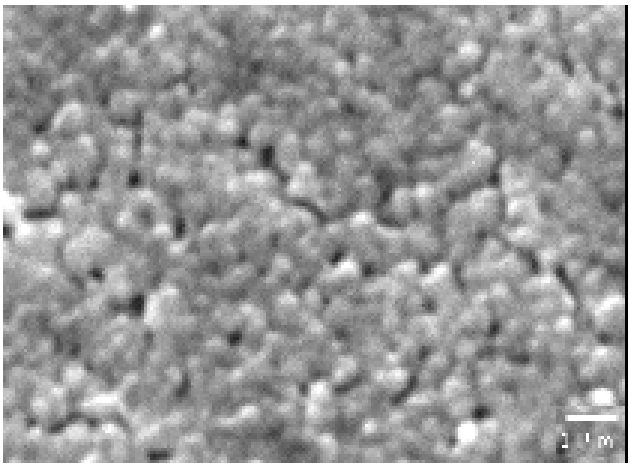

Figure 6.50: Cross-sectional SEM micrographs of CRGC-B30

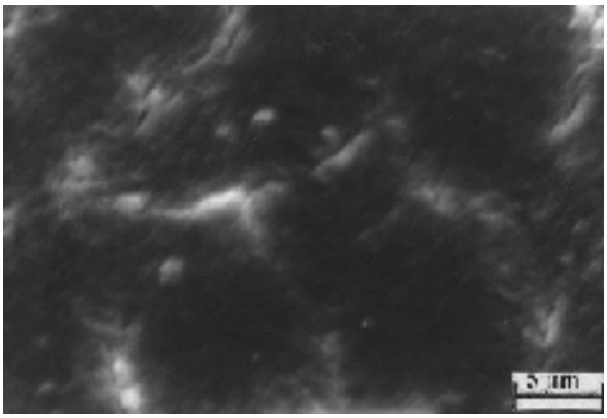

Figure 6.51: SEM micrographs of CRGC-S15

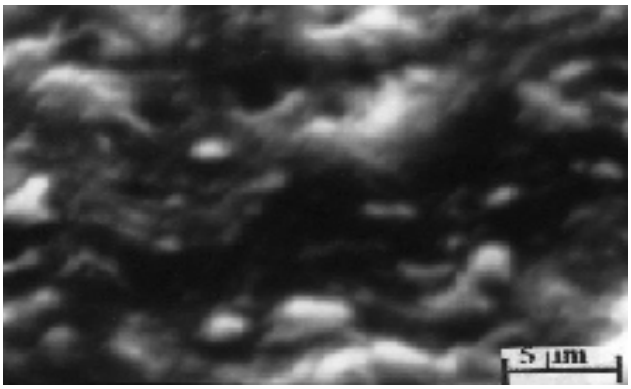

Figure 6.52: SEM micrographs of CRGC-S30

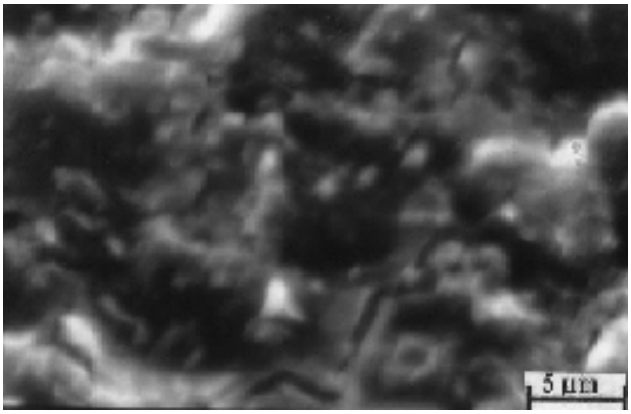

Figure 6.53: SEM micrographs of CRGC-S60

Fusing glass particles into a dense product occurs by viscous phase sintering at temperatures much lower than the melting temperatures of crystalline materials of the same composition. Sintering mechanism is controlled by glass composition, impurities, surface area, packing efficiency and crystallization behavior. The driving force for sintering of glass particles is to reduction of surface area. Increasing the surface area tends to promote sintering. The surface area is increased by decrease in the particle size. Another important parameter that affects sintering is how well the particles are initially packed together. Increasing the packing density promotes sintering. In the cold pressing technique, the sintering pressure is very important to get a better initially packed glass particles. Sintering can also be enhanced by additions of binders. Binders can promote sintering, but usually also increase the cost and complexity of the materials system. According to the above discussions, the presence of the glassy regions in the sintered glass-ceramic samples occurred since the selected sintering pressure and the particle size of the glass powders may not be suitable for this glass sample. And binderless working can also be another factor that resulted to the remained glassy regions. To see the effects of binders PVA was added to the glass powders and the glass samples were sintered according to the procedure described in Section 5.5.

Figures 6.54-56 show the SEM micrographs of the CRGC-P15, CRGC-P30 and CRGC-P60 samples. As seen from the SEM micrographs, tiny equiaxed crystallites uniformly dispersed in the microstructure of the samples. The crystalline size increased with the increase in holding time at the crystallization temperature as it was observed in the bulk and sintered samples. The average crystalline size changes in the range of 0.35-0.55 μm. Using of PVA as a binder in the CRG sample resulted better and denser crystalline structure without any glassy regions in the CRGC-P15, CRGC-P30 and CRGC-P60 samples contrary to the CRGC-S15, CRGC-S30 and CRGC-S60 samples. Using PVA in sintered samples as a binder resulted to stick the glass powders together and to promote the packing efficiency.

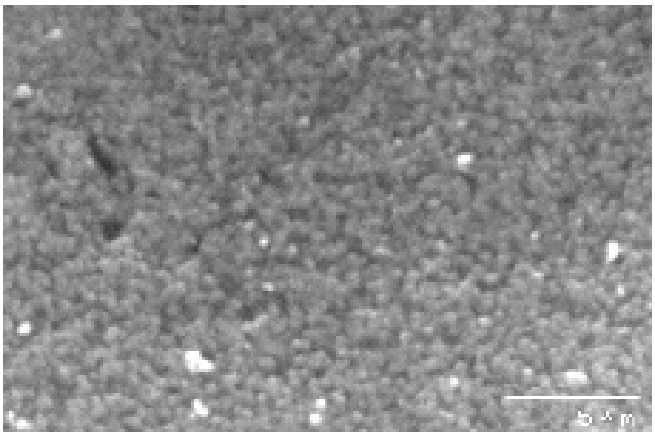

Figure 6.54: SEM micrographs of CRGC-P15

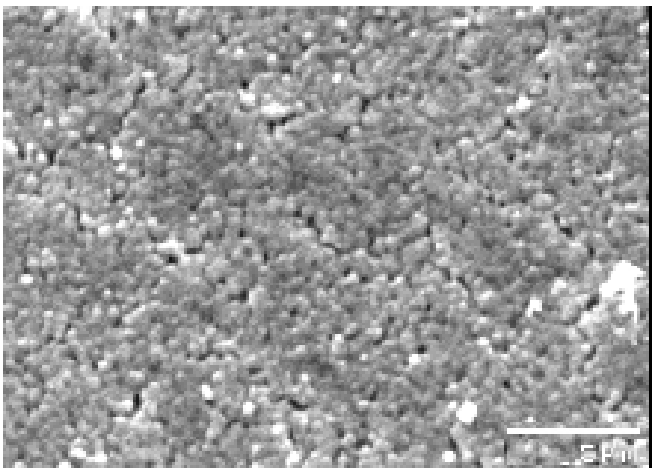

Figure 6.55: SEM micrographs of CRGC-P30

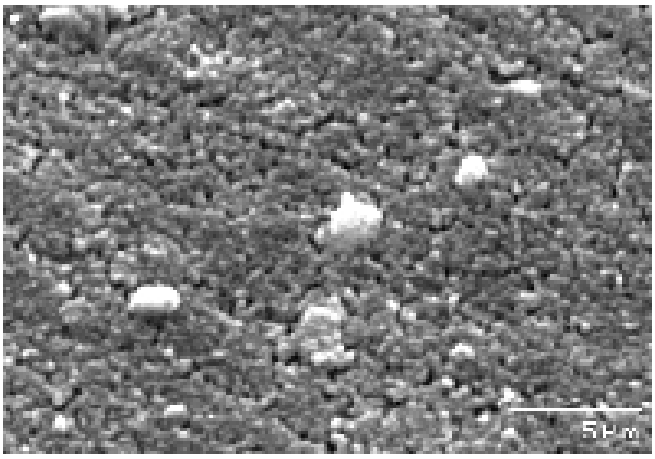

Figure 6.56: SEM micrographs of CRGC-P60

6.7.1.2 Physical and mechanical properties of CRGC samples

Table 6.34 summarizes the results of the hardness, density, porosity and water absorption tests of the bulk and the sintered glass-ceramic samples. It is clear that the microhardness value increases with the increasing holding times at the crystallization temperature. It can be concluded that with the increase in crystallinity, the hardness values of glass-ceramic samples were also increased as reported previously [119]. Similar to microhardness results, as the glass-ceramic samples become more crystalline, the density of the glass-ceramic samples increases. It is also noted that the density and hardness values of the CRGC-B15, CRGC-B30 and CRGC-B60 samples are higher than the CRGC-S15, CRGC-S30 and CRGC-S60 samples. This result was expected since the volume of the crystallized part of CRGC-S15, CRGC-S30 and CRGC-S60 samples was lower than the CRGC-B15, CRGC-B30 and CRGC-B60 samples. However, hardness and density values of CRGC-P15, CRGC-P30 and CRGC-P60 samples are very close to the bulk samples since the PVA results to denser microcrystalline structure in the sintering process. In compliance with the density and hardness results, porosity decreases when the glass-ceramics get more dense structures with the increase in holding times at crystallization temperature. Water absorption of all samples is so low that it can be negligible. This property is well correlated with the other properties especially with porosity. Since the porosity of all samples is so low even zero for CRGC-B60 and CRGC-P60 samples, water absorption is negligible. These properties are better than the physical and mechanical properties of the CG glass samples. Since the chemical compositions of CRG and CG glasses are close to each other we can compare the properties of CG glasses with CRGC glass-ceramics to investigate the transformation of glass to a glass-ceramic material. All the properties of CG sample improved with the increase of the crystalline volume in the glassy matrix. It is known that if fine grained crystallites homogeneously dispersed in the whole body of the glass-ceramic samples, this result will get better physical, mechanical and chemical properties for this material. Therefore, glass-ceramic samples possess better properties than the corresponded glass sample.

The properties of bulk and sintered samples are better than the samples produced from incinerator fly ashes as it was reported by Cheng et al.[163], Romero et al.[131]

and Karamanov et al.[124]. Boccaccini et al.[165] reported that the hardness value of the sintered sample produced from incinerator fly ash was 380 kg/mm^2 which was so low than the hardness values of the sintered samples produced in this study. However, density value of the sintered sample (2.74 g/cm^3) obtained by Boccaccini et al.[165] is higher than the density values obtained in this study. If we think from the point of hardness and density of the material, the harder the material the denser it is. The reason of this can be high heavy metal concentration of incinerator fly ash sample. Incinerator fly ash sample contains more heavy metals (such as Pb^{2+}, Zn^{2+}), which increase the density of the sample, then the coal fly ash and therefore incinerator fly ash has higher density value than the fly ash. Therefore, density of sintered glass-ceramics could be higher. The properties of CRGC-B60 sample are better than the bulk glass-ceramic samples produced from coal fly ash as reported by Barbieri et al.[11], Leroy et al.[117], Shao et al.[204] and Boccaccini et al.[10]. Porosity and water absorption values of all samples of this study are so low than the values reported by Cheng et al.[163].

Table 6.34: Properties of CRGC samples

Sample Name	Hardness (kg/mm^2)	Density (g/cm^3)	Porosity (%)	Water Absorption (wt. % loss)
CRGC-B15	594	2.62	0.73	Negligible
CRGC-B30	716	2.74	0.56	Negligible
CRGC-B60	852	3.03	0.00	Negligible
CRGC-S15	514	2.56	1.16	Negligible
CRGC-S30	677	2.65	0.95	Negligible
CRGC-S60	802	2.71	0.05	0.11
CRGC-P15	584	2.60	1.05	Negligible
CRGC-P30	708	2.70	0.82	Negligible
CRGC-P60	837	2.92	0.00	Negligible

6.7.1.3 TCLP results of CRGC samples

TCLP results of CRGC-B60, CRGC-S60 and CRGC-P60 samples were given in Table 6.35. As seen from Table 6.35, any heavy metal ions could not be detected in

the leachate solutions of those samples. This result is better than the TCLP results of CG sample. The crystalline phase occurred in the glass-ceramic samples affected the chemical stability. Crystalline phase makes the glass-ceramic materials more chemically stable and this results the resistance to leachability. Glasses show a much higher leachabilty with their amourphous phase. The higher leaching resistance of glass-ceramics indicated that the heavy metal ions replaced other ions, such as Ca^{2+} or Al^{3+} and were held in the crystalline phase. TCLP results of CRGC-B60, CRGC-S60 and CRGC-P60 samples are better than the bulk glass-ceramics produced from electric arc furnace (EAF) dust and incinerator fly ash as it was reported by Cheng [125] and Kavauras et al.[210]. Since the heavy metal concentration could not be detected in the leachates of CRGC-B60, CRGC-S60 and CRGC-P60 samples these are appropriate chemically stable products suitable for the production of safe structural materials.

Table 6.35: TCLP results of CRGC samples

Sample Name	Cr (ppm)	Mn (ppm)	Zn (ppm)	Pb (ppm)
CRGC-B60	BDL	BDL	BDL	BDL
CRGC-S60	BDL	BDL	BDL	BDL
CRGC-P60	BDL	BDL	BDL	BDL

BDL: Below Detection Limit

6.7.1.4 Chemical properties of CRGC samples

Table 6.36 shows the chemical resistance of CRGC samples. Glass-ceramics show higher chemical resistance than the CG glasses. As seen in Table 6.36, the chemical resistance of all glass-ceramic samples does not correlate with the heat treatment procedures but the CRGC-S15, CRGC-S30 and CRGC-S60 samples show lower resistance than the other glass-ceramic samples. Since weight losses are usually attributed to the dissolution of glassy matrix, this would lead to higher weight losses. It is also seen that the resistance to acids is relatively low for all glass-ceramic samples. Improvement of chemical durability especially for acid attacks, requires further investigation. The chemical resistance of CRGC samples is higher than the glass-ceramic samples produced from incinerator fly ash and coal fly ash reported by Cheng et al.[155,163] and Leroy et al.[117], respectively. Diopside phase is the main

crystalline phase in CRGC samples and may be a more chemically stable crystalline than the gehlenite, augite+anorthite and essenite phases occurred in the glass-ceramic samples produced from incinerator fly ash and coal fly ash, respectively.

It is desired to produce fine-grained crystalline structure with good mechanical properties in the glass-ceramic production. Overall results for CRGC samples showed that the properties of all samples are good enough for glass-ceramics produced from industrial wastes. CRGC-B60 sample had the best properties in all CRGC samples.

Table 6.36: Chemical resistances of the CRGC samples

Sample Name	HNO_3 (%)	NaOH(%)
CRGC-B15	0.13	Negligible
CRGC-B30	0.31	Negligible
CRGC-B60	0.13	Negligible
CRGC-S15	0.29	0.29
CRGC-S30	0.38	0.20
CRGC-S60	0.31	0.25
CRGC-P15	0.18	Negligible
CRGC-P30	0.11	Negligible
CRGC-P60	0.13	Negligible

6.7.2 Experimental results of ORSGC samples

6.7.2.1 Microstructural characterization of ORSGC samples

CaO-Al_2O_3-SiO_2 (CAS) system glasses are one of the fundamental silicate systems that have been used widely in many fields of industry. The crystallization of CAS system glasses produced from industrial wastes has been investigated by many researchers and it was reported that the main crystalline phases can be diopside, anorthite and wollastonite in this ternary system[10,11,126]. Chemical composition of ORSG samples are in the CaO-Al_2O_3-SiO_2 (CAS) ternary glassy system. Figure C.4 in Appendix C shows the x-ray patterns of ORSGC-B samples. X-ray diffraction analysis revealed that the main crystalline phase occurred in all ORSGC samples was

diopside ($Ca(Mg,Al)(Si,Al)_2O_6$). X-ray patterns of ORSGC-S and ORSGC-P samples were given in Figures C.5-C.6 in Appendix C. The addition of PVA to the ORSG glass samples to produce sintered glass-ceramics could not change the crystallization phase of ORSGC-P15, ORSGC-P30 and ORSGC-P60 samples as it was seen from Figure C.6. Altough the ORSG is a CAS type glass but Fe_2O_3 content of it is high enough compared to the CAS type glasses. For crystallization of CAS type glass Fe_2O_3 works efficiently as a nucleant to promote the speed of nucleation [9]. Iron oxide decreases glass viscosity and therefore, it increases the crystal growth rate since Fe^{3+} ion could act as a modifier of the structure, with breaking the Si-O-Si bonds. When the temperature was increased further to the maximum nucleation and crystallization temperatures to produce glass-ceramics diopside phase took place in the whole body of the ORSGC samples. This result is in well agreement with the Lebedeva diagram which indicates that the diopside phase can be the main crystalline phase in ORSGC sample. In ORSG glasses, not only the coal fly ash, but also the red mud and silica fume were used to produce glass samples. With the addition of red mud and silica fume, the chemical composition of ORSG glass was changed and became close to the chemical composition of CRSG glass. Therefore, diopside phase was also expected in the ORSGC samples. However, this result is quite different from the results of other researchers whose use coal fly ash as a raw material in the glass-ceramic production. They obtained anorthite, wollastonite and mullite phases in the CAS type coal fly ash-based glass-ceramics [110,116,117,204]. This phenomenon indicates the complexity and uncertainty of nucleation and crystallization in the CAS glass system.

SEM investigations were conducted in order to get a better understanding of the morphology of the microstructure. SEM micrographs of ORSGC-B15, ORSGC-B30 and ORSGC-B60 samples are shown in Figures 6.57-6.59. SEM observations revealed that both locally oriented dendritic crystalline growth and a significant number of leaf-shaped crystals occurred in the glass-ceramic samples. It was found that the volume of the crystalline phase increased after the holding time increased from 15 min to 60 min, as it was seen from Figures 6.57-6.59. This is due to higher driving force and increasing the crystal growth rate with the longer heat treatment process. The nuclei got more energy to achieve the crystal growth process when the holding time at crystallization increased. Pelino [233] reported that increasing the

crystallization time has a positive effect on the properties of glass-ceramic materials and the physical and mechanical properties of them yielded better characteristics. It was also observed that some pores with irregular shapes were found in the ORSGC-B15, ORSGC-B30 and ORSGC-B60 samples. The amount of pores decreased with the increase in the heating time. This is occurred since the number of the crystallites increased. Cross-sectional SEM investigations revealed that the similar average crystalline size and shape were observed in the Figure 6.60 of ORSGC-B60 sample. Surface and the cross-sectional microstructures of the ORSGC sample are the same and this result indicated that the bulk crystallization mechanism is the main crystallization mechanism in the ORGCS-B60 sample and also in all ORSGC samples. This result is in well agreement with the results obtained in Section 6.6.2.

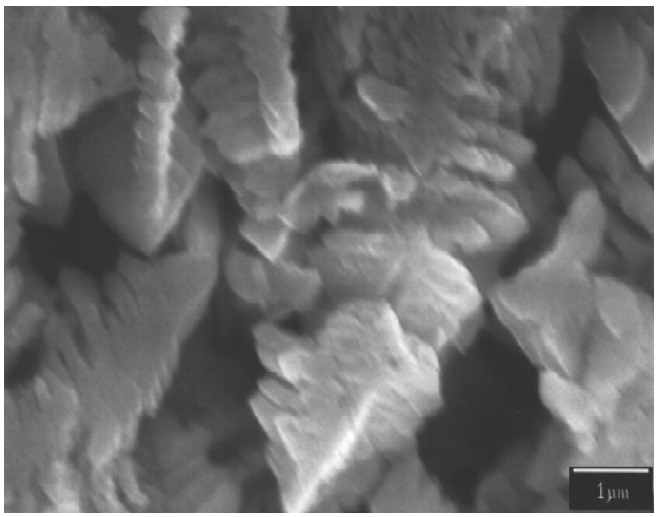

Figure 6.57: SEM micrographs of ORSGC-B15

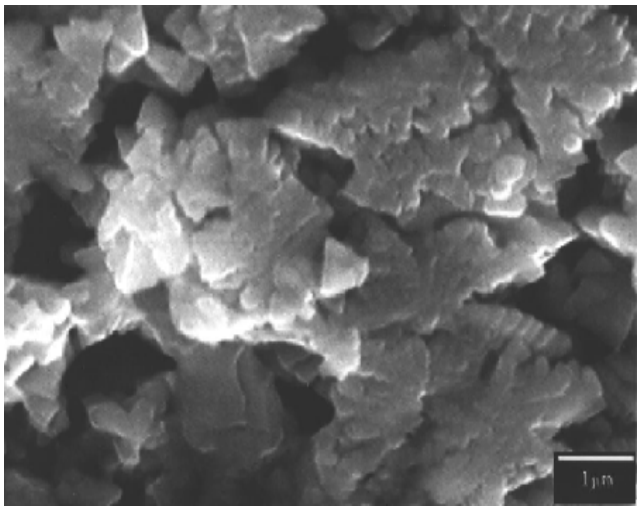

Figure 6.58: SEM micrographs of ORSGC-B30

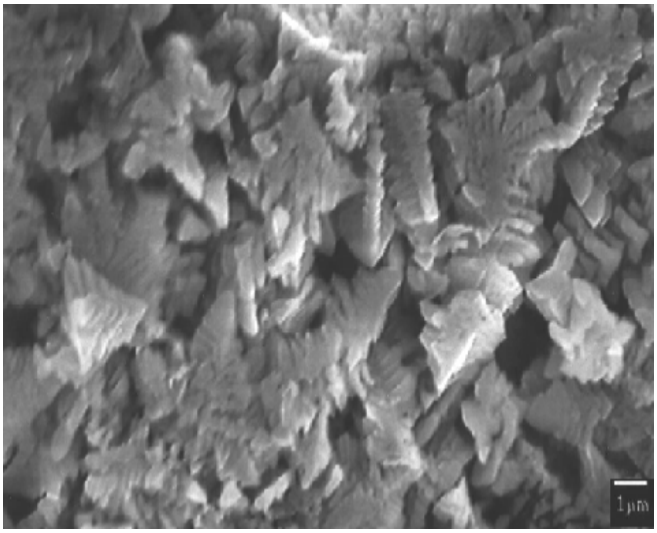

Figure 6.59: SEM micrographs of ORSGC-B60

Figures 6.61-6.63 are representative SEM micrographs of ORSGC-S15, ORSGC-S30 and ORSGC-S60 samples. As seen from Figures 6.61-6.63, the crystalline sizes of sintered samples are smaller than the crystalline size of the bulk glass-ceramics. The particle size has a great effect on crystallization of glass particles. The total effective surface area to the volume ratio increased with decreasing particle size for a fixed amount of sample [234]. Therefore, the number of nuclei occurred in the fine glasses is greater than bulk glasses having the same volume. The nuclei grow gradually to form crystallites when the heat treatment applied to the samples. The amount of

nuclei occurred in the bulk glass in the same volume is less than the fine glass, so the crystals grow more. Therefore, the crystalline size of the bulk samples is greater than the sintered samples. It was also observed that the shape of the crystallites was changed. The amount of leaf-shaped crystallites decreased with the increasing holding time. The crystalline shrinkage maintains a constant value and the crystallites do not maintain their shapes any more in the ORSGC-S60 sample. The number of the crystallites increased with the increase in holding time at crystallization temperature as it was observed in the bulk samples. The porosity also decreased in the sintered samples. Glass softening and flow is required for glass particles to sinter together into a dense product and to produce a smooth surface. In another words, for better microcrystalline structure and complete crystallization sintering must start before the crystallization process. The better microcrystalline microstructure of sintered ORSGC samples compare to bulk samples indicated that the sintering plays an important role in the crystallization of ORSG samples. This result is also revealed that the parameters for sintering process such as, particle size, firing temperature, sintering pressure and glass composition are suitable for ORSG glass samples to perform complete densification and crystallization. The sintered samples favor to bulk samples since all the samples show the maximum crystallization degree.

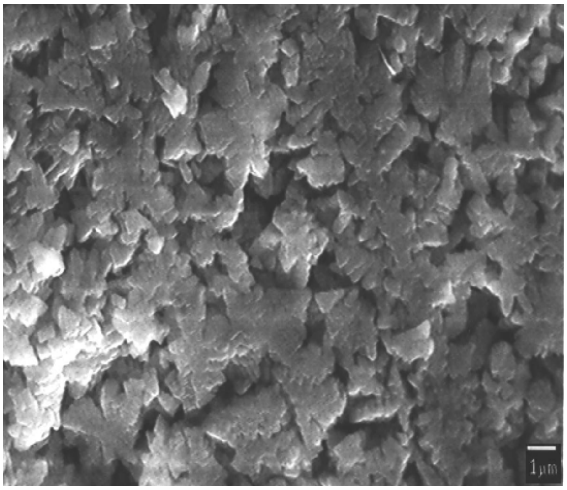

Figure 6.60: Cross-sectional SEM micrographs of ORSGC-B60

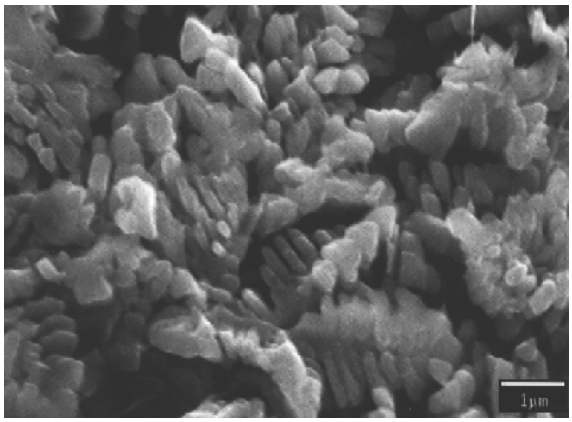

Figure 6.61: SEM micrographs of ORSGC-S15

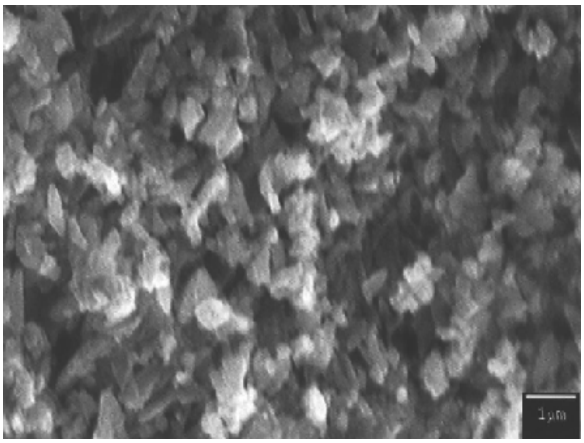

Figure 6.62: SEM micrographs of ORSGC-S30

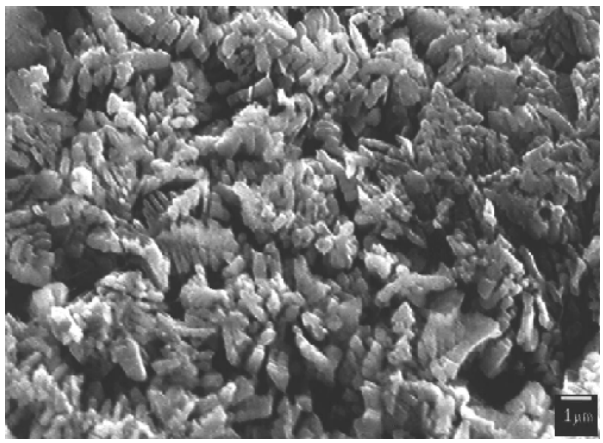

Figure 6.63: SEM micrographs of ORSGC-S60

Figures 6.64-6.66 show the SEM micrographs of ORSG-P15, ORSG-P30 and ORSG-P60 samples, respectively. It was clearly seen from these figures that the crystalline size and shape was completely different from the bulk glass-ceramic samples. The crystalline size and shape was also different from the ORSGC-S15, ORSGC-S30 and ORSGC-S60 samples. The crystalline size is getting smaller with the increasing holding time and the leaf-shaped crystallites disappeared from the

surface of the ORSG-P15, ORSG-P30 and ORSG-P60 samples. The addition of PVA to the glass powders increased the crystallization degree gradually by reducing the porosity formation as shown from Figures 6.64-6.66. The number of the crystallites occurred in the ORSGC-P60 sample is higher than the ORSGC-P15 sample. PVA bonds the glass powders together and with the sintering process denser product was obtained. The denser structure results in crystallization throughout the sample. Therefore, crystallization degree increased and the porosity decreased when the material became dense. The crystalline size and shape were changed since the PVA bonds glass powders to stick together. Using PVA in the sintering process resulted better microcrystalline structure for ORSGC samples.

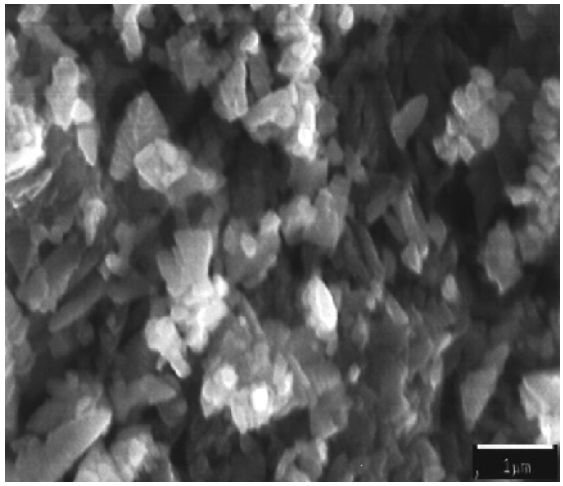

Figure 6.64: SEM micrographs of ORSGC-P15

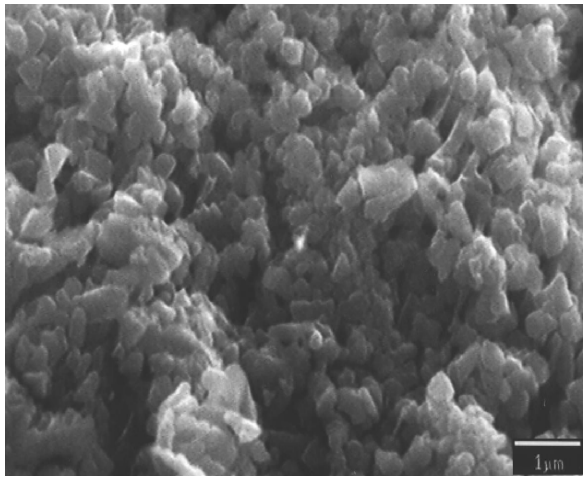

Figure 6.65: SEM micrographs of ORSGC-P30

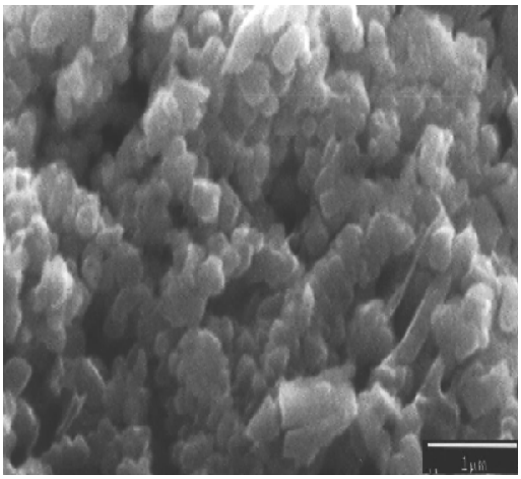

Figure 6.66: SEM micrographs of ORSGC-P60

6.7.2.2 Physical and mechanical properties of ORSGC samples

Table 6.37 gives values for the microhardness, density, porosity and water absorption of ORSGC samples. The general trend in microhardness found is that as samples become more crystalline, the average microhardness increases. The hardness values of sintered ORSGC samples are greater than the bulk ORSGC samples. The microhardness trend is consistent with what can be expected based on crystallization. The sintered ORSGC samples have more crystalline sites, whereas bulk ORSGC samples have less crystalline sites, as it was observed from the SEM micrographs. In compliance with the hardness values, density values of the glass-ceramic samples increased with the increase in crystallization degree. Density values of ORSGC samples are found in the range of 2.71-3.22 g/cm^3. The density of diopside is 3.39 g/cm^3. Therefore, it is expected that the density of the samples increased with the increase in crystalline phase occurred in the glass-ceramic samples. ORSG-P60 sample has the highest density value due to its highest crystalline degree. The porosity and water absorption values of sintered samples are lower than the bulk glass-ceramic samples since the crystallization degree is higher in the sintered samples. The presence of pores in the bulk samples was also confirmed by SEM observations. Both porosity and water absorption values correlated well each other and decreased with the increase of crystallinity. The factors regulating physical, mechanical and chemical properties are crystalline phase, crystallization degree, the size of the crysatallites and homogeneity of crystal size [116]. As it was determined

in the previous section, the main crystalline phase of all samples is the same (diopside). It was reported that fine-grained glass-ceramics possess better properties [235]. We can observe that although crystal size of samples grew larger along with crystallization time, the glass-ceramics obtained better properties. However, the crystallization degree is also an important factor which effects the hardness and the other properties of glass-ceramic samples. The closed porosity was observed in the bulk samples and only ORSGC-P60 sample reached complete crystallization. The closed porosity remained in the bulk samples for the shorter crystallization time damaged continuity of the crystal phase accounting for the decrease in hardness of the bulk glass-ceramic samples. ORSGC-P samples have higher crystallization degree with a smaller crystalline size and less porosity compared to ORSGC-B samples. Therefore, physical and mechanical properties of ORSG-P samples are better than the ORSGC-B samples. The physical and mechanical properties of all glass-ceramic samples are better than the OG sample because of the presence of the crystalline phase occurred in the glass-ceramic samples. The density values of ORSGC-S60 and ORSGC-P60 are higher while the porosity and water absorption values are lower than the values reported by Cheng [125]. Density and hardness values of ORSGC samples are higher than the glass-ceramic samples produced in different studies from coal fly ash and incinerator fly ash [131,204,209,235]. The density and hardness values of ORSGC-S60 and ORSGC-P60 sample are higher than the bulk glass-ceramics produced in different studies from coal fly ash [106] and the sintered samples produced from incinerator fly ash [124,165].

6.7.2.3 TCLP results of ORSGC samples

TCLP results of the ORSGC samples are given in Table 6.38. As seen from Table 6.38, any heavy metal concentration could not be detected in the extraction solutions of ORSGC-S30 and ORSGC-P30 samples, except ORSGC-B30 sample. But the extracted amount of Zn for ORSGC-B60 sample is lower than the limits required by US EPA. This result is better than the TCLP results of OG sample. Transformation of glass into a glass-ceramic material significantly improves the leachability characteristics of the materials. Heavy metal ions replaced other ions and held in the crystalline phase. Diopside has been shown to be an ideal crystalline matrix for the immobilization of wastes in the production of glass-ceramic materials. Chick et

al.[236] reported that the leachability of the glass-ceramic materials obtained from wastes is 4-10 times lower than the parent glass and the crystalline phase remains while the residual glass is dissolved away during leaching. It was also obtained in this study that the glass-ceramics are more chemically stable materials compare to the parent glasses. TCLP results of ORSGC samples is better than the TCLP results of bulk glass-ceramics produced by Cheng [125,155] and Kavaouras et al.[210]. TCLP results showed that the ORSGC samples are non-toxic materials.

Table 6.37: Properties of ORSGC samples

Sample Name	Hardness (kg/mm^2)	Density (g/cm^3)	Porosity (%)	Water Absorption (wt. % loss)
ORSGC-B15	577	2.71	1.08	0.21
ORSGC-B30	711	2.82	0.96	0.14
ORSGC-B60	827	2.91	0.61	Negligible
ORSGC-S15	589	2.92	0.92	Negligible
ORSGC-S30	705	3.10	0.69	Negligible
ORSGC-S60	838	3.17	0.32	Negligible
ORSGC-P15	592	3.03	0.88	Negligible
ORSGC-P30	728	3.11	0.25	Negligible
ORSGC-P60	842	3.22	0.15	Negligible

Table 6.38: TCLP results of ORSGC samples

Sample Name	Cr (ppm)	Mn (ppm)	Zn (ppm)	Pb (ppm)
ORSGC-B30	BDL	BDL	0.005	BDL
ORSGC-S30	BDL	BDL	BDL	BDL
ORSGC-P30	BDL	BDL	BDL	BDL

BDL: Below Detection Limit

6.7.2.4 Chemical resistance of ORSGC samples

Table 6.39 shows the chemical durability of glass-ceramic materials. Studying the chemical durability of glass-ceramics revealed that the weight loss decreased with the increase in the volume crystalline content. Comparing the chemical durability

results of OG samples with ORSGC samples, it can be seen that the weight loss percent is higher than those for the glass-ceramic samples in both HNO_3 and NaOH solutions. This seems to be due to the more bonding in glass-ceramic network rather than the parent glass, due to the formation of crystalline phases during heat treatment process. The achievement of high chemical durability in glass-ceramics indicates that the chemical composition of the crystalline phases obtained favor good stability. McMillan [18] had stated that the glass-ceramics, in general, possess good chemical stability and that they compare favorably in this respect with other ceramic type materials. Consequently, an increase in the content of the diopside phase results the higher chemical resistance in the glass-ceramic materials. Therefore, chemical resistance of sintered materials, especially of the PVA added samples are higher than the bulk glass-ceramic samples. It is apparent that the produced glass-ceramic samples show higher resistance to alkali solutions than the acidic solutions. Chemical resistances of glass-ceramics are better than those glass-ceramics produced in different studies from coal fly ash and incinerator fly ash [117,125,155,163]. Owing to its physical, mechanical and chemical properties, ORSGC-P60 sample has the best properties in all ORSGC samples.

Table 6.39: Chemical resistances of the ORSGC samples

Sample Name	HNO_3 (%)	NaOH(%)
ORSGC-B15	0.60	Negligible
ORSGC-B30	0.42	Negligible
ORSGC-B60	0.28	Negligible
ORSGC-S15	0.51	Negligible
ORSGC-S30	0.35	Negligible
ORSGC-S60	0.16	Negligible
ORSGC-P15	0.42	Negligible
ORSGC-P30	0.24	Negligible
ORSGC-P60	0.16	Negligible

6.7.3 Experimental results of TGC samples

6.7.3.1 Microstructural characterization of TGC samples

In order to identify the crystalline phases, XRD analysis was carried out on the produced glass-ceramic samples. XRD patterns of TGC-B, TGC-S and TGC-P samples were given in Figures C7-C9 in Appendix C, respectively. XRD results revealed that the main crystalline phase was aluminum augite (Ca(Mg, Fe^{3+}, Al)(Si, $Al)_2O_6$). Lebedeva diagram shows that the crystalline phase could be augite confirms this result. The main components of TG sample are SiO_2, Al_2O_3 and Fe_2O_3, whereas, CaO and MgO contents of TG sample are low compare to the other glass samples. In the structure of glass, O^{2-} is attracted to near Si^{4+} in the form of $(SiO_4)^{4-}$. At the same time the network modifiers also have a tendency to attract O^{2-} with a partial negative charge (non-bridge oxygen), so the network modifiers compete with Si^{4+} for O^{2-} [12]. When the surrounding temperature is equal to T_g, the structure of the glass becomes relaxed and diffusion of ions occurs easier. For glass with more network modifiers, non-bridged oxygens are concentrated in the area that contains more network modifiers and the glass separated into two phases, which are the phase with more Si^{4+} and the phase with more network modifiers. The conditions of nucleation are that ions diffuse together from the uniform glassy matrix and the ions are rearranged to give the structure of the crystals. Although it is usually considered as an intermediate glass network ion, the Fe^{3+} could act as a modifier of the TG glass structure, breaking the Si-O-Si bonds to form the augite phase. Mg and Ca ions have also effects on the formation of crystalline structure as network modifiers [12]. However, Fe^{3+} plays an important role in the crystalline structure as the network modifier since the content of Fe^{3+} is high enough compared to the Ca and Mg ions. Ca and Mg contents of the CRG and ORSG samples are higher than that of the TG sample. Therefore, diopside phase ($Ca(Mg,Al)(Si,Al)_2O_6$) occurred in the CRG and ORSG samples instead of aluminum augite phase(Ca(Mg, Fe^{3+}, Al)(Si, $Al)_2O_6$) which was obtained in the TG sample. The formation of augite has been reported during crystallization of coal fly ashes by Barbieri et al.[11]. Morover, augite crystals have also been observed in glass-ceramics obtained from other industrial wastes rich in Fe-ion such as, incinerator fly ash [131,165], and electric arc furnace dust(EAF)[125].

SEM micrographs of the TGC-B15, TGC-B30 and TGC-B60 samples were given in Figures 6.67-6.69, respectively. In all cases, SEM analyses show the presence of strongly interlocked crystals of about 100-500 nm size embedded in a glassy matrix. The morphology of the crystalline phase is composed of equiaxed or spherical networks forming a fully ordered microcrystalline mosaic that is mainly made up of augite. Microstructural observation clearly indicated that crystallization volume increases when the length of thermal treatment time increased. Figures 6.67-6.69 show the following features: Some of the equiaxed nano-crystals with a bright contrast were occurred in the glassy matrix; besides some of the nano-crystals exhibiting a grey contrast and making the most part of the crystalline phase and; areas of the amorphous residual glassy phase which appears in dark contrast were observed. To check the accuracy of the crystallization mechanism obtained from DTA results, cross-sectional SEM investigations were conducted on the TGC-B60 sample. Figure 6.70 shows the cross-sectional area of the TGC-B60 sample. The equiaxed nano-crystallites dispersed in the volume of the sample as it was expected. This result confirms the bulk crystallization of TGC samples determined in Section 6.6.2.

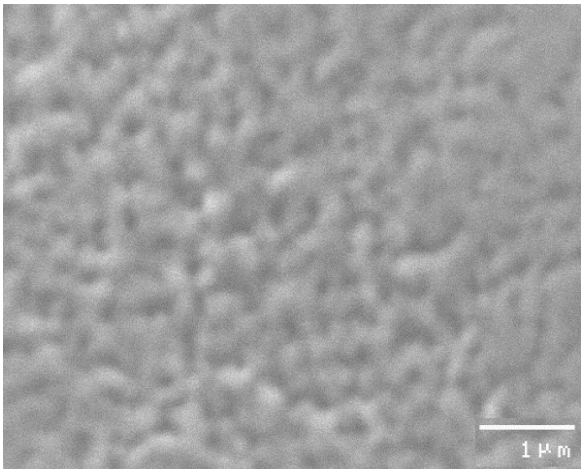

Figure 6.67: SEM micrographs of TGC-B15

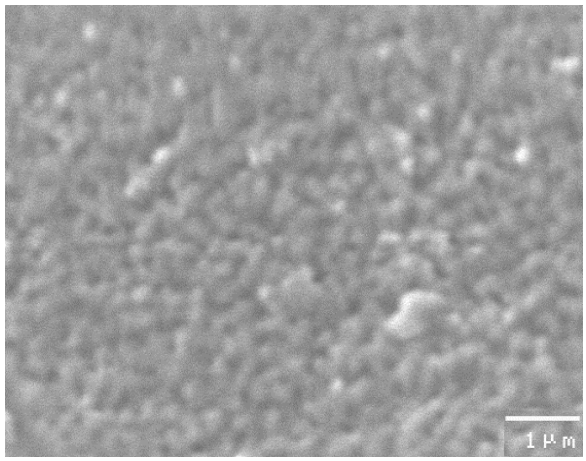

Figure 6.68: SEM micrographs of TGC-B30

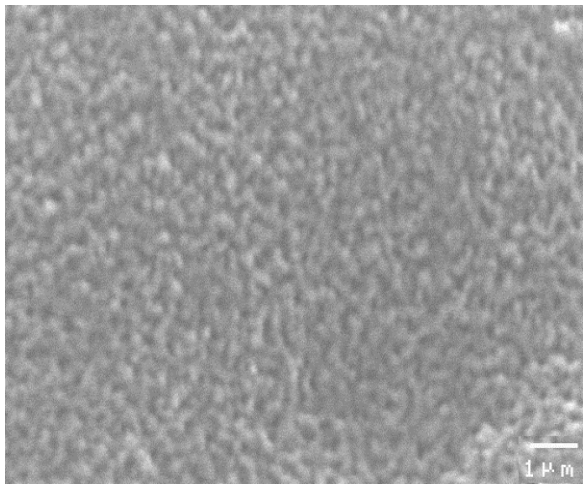

Figure 6.69: SEM micrographs of TGC-B60

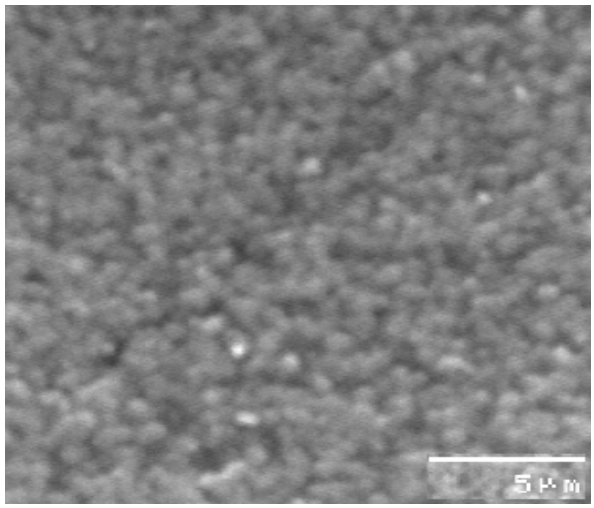

Figure 6.70: Cross-sectional SEM micrographs of TGC-B60

Figures 6.71-6.73 are representative SEM micrographs of the TGC-S15, TGC-S30 and TGC-S60 samples. As seen from Figures 6.71-6.73, there were only a few crystallites in the bulk of the samples. High content of the glassy phase still remained in the volume of the samples. Thus, only a few glassy droplets were converted into crystals. However, the number of the crystallites increased with the increase in holding time at the crystallization temperature, as it was observed in the bulk samples. The average crystalline size of sintered samples is bigger than the average crystalline size of the bulk samples. Glass softening and viscous flow are required for densification of glass particles. Some glass compositions densify easily by viscous phase sintering, while other compositions do not densify well. The viscosity has to decrease sufficiently for glass flow to occur densification process. The particle size of the glass powders is an important parameter in the sintering process. When the glass is milled into finer particles, the surface area greatly increased. The new surface area is covered with broken chemical bonds. This makes the surface highly reactive and thus it will react and bond to anything that will satisfy these broken bonds. Because of this highly reactive surface, variations in surface chemistry easily occur from changes in processing conditions. The surface chemistry can have a significant affect on particles crystallization and also on the sintering behavior. It is also known that as the particle size decreased the rate of crystallization increases and the crystallization temperature decreases. Because of this coarser particle size will reduce the tendency for crystallization [234]. However, the glass composition, sintering pressure, addition of any binders and firing conditions are also important parameters in the controlling of crystallization behavior of sintered glass-ceramics in addition to the particle size of the glass particles. It can be said that particle size of TG samples is coarse for this type of glassy system and thus reducing the glass particle size to a finer powder form may enhance the sintering and crystallization behavior. The heating rate applied to the TG samples is fast enough for this glass composition since it may cause a rapid decrease in the viscosity as it was observed in the CRG and ORSG samples. The sintering temperatures of 948 and 1140 K were also corresponded to the nucleation and crystallization temperatures of the bulk glass samples. Therefore, these temperatures may not be suitable for fine glass samples. As it was observed in Section 6.6.1, T_g and T_p values of the bulk samples were higher than the temperatures of the fine glass samples. However, nucleation and crystallization temperatures of the bulk CRG and ORSG samples which were also

selected as sintering temperatures gave better results for sintering of CRG and ORSG samples. SEM results revealed that the selected sintering temperatures, particle size of glass samples and sintering pressure may not be suitable for this glassy system.

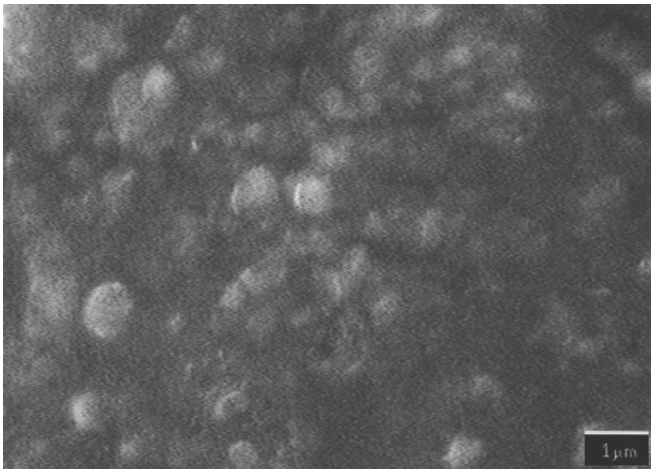

Figure 6.71: SEM micrographs of TGC-S15 sample

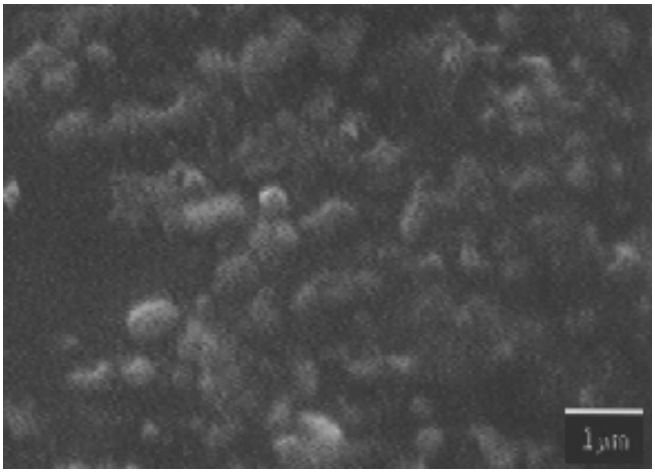

Figure 6.72: SEM micrographs of TGC-S30 sample

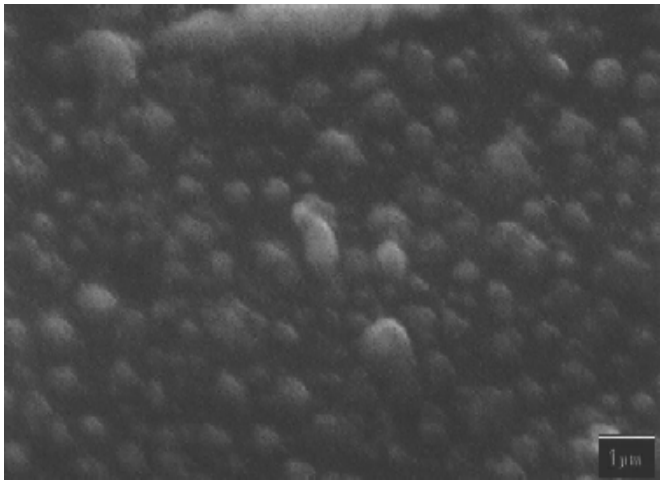

Figure 6.73: SEM micrographs of TGC-S60 sample

The SEM micrographs of TGC-P15, TGC-P30 and TGC-P60 samples were given in Figures 6.74-6.76, respectively. It can be clearly seen that the microstructure of the TGC-S15, TGC-S30 and TGC-S60 samples are better than the TGC-P15, TGC-P30 and TGC-P60 samples. There is a high glass phase in the TGC-P15, TGC-P30 and TGC-P60 samples. The number of crystallites is less than the TGC-S15, TGC-S30 and TGC-S60 samples. The crystalline volume increased with the increase in holding time at T_p as it was expected. Addition of PVA to the glass powders resulted to more remained glassy regions in the TGC-P15, TGC-P30 and TGC-P60 samples. PVA helps to obtain dense materials by sticking glass powders together. However, in this case sintering temperatures and particle size are very important parameters for this glassy system. Therefore, addition of PVA did not improve the microstructure of the sintered glass-ceramic samples. It can also be said that PVA is not an appropriate binder for this type of glassy system. SEM investigations showed that the crystalline degree is highest in the bulk samples and this result is in well agreement with the XRD results.

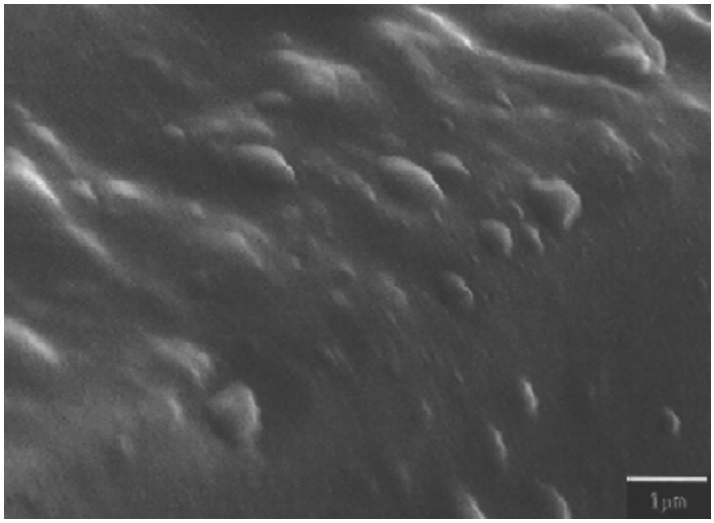

Figure 6.74: SEM micrographs of TGC-P15 sample

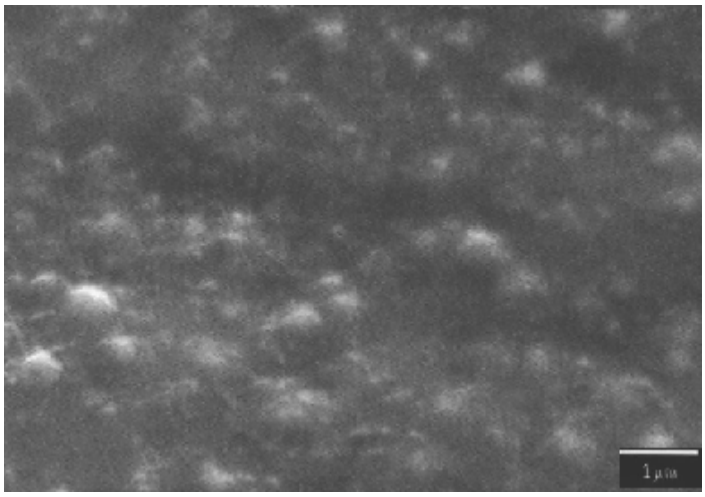

Figure 6.75: SEM micrographs of TGC-P30 sample

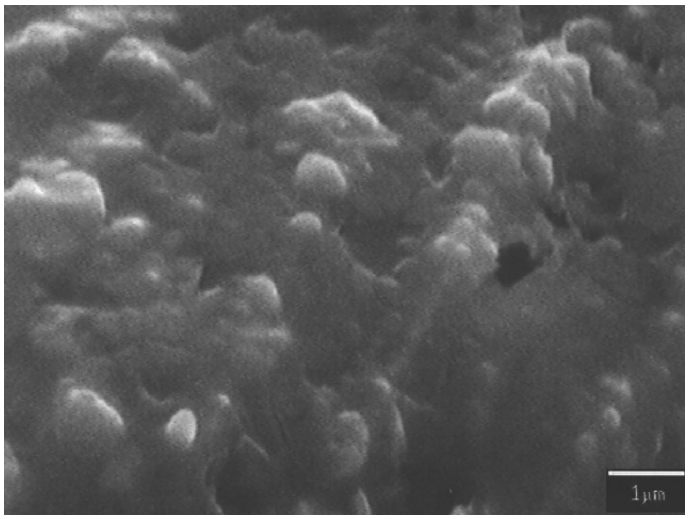

Figure 6.76: SEM micrographs of TGC-P60 sample

6.7.3.2 Physical and mechanical properties of TGC samples

Physical and mechanical properties of both bulk and sintered glass-ceramics were listed in Table 6.40. Densities of bulk samples are in the range of 2.96-3.32 g/cm^3 and increased with increasing crystallization degree and decreasing pore volume. The density values of bulk samples are higher than the TG sample since the amorphous glassy phase transformed to a dense crystalline material when the heat treatment process applied to the TG samples. In compliance with the SEM observations porosity decreased with the increasing holding time at the T_p as it was expected. TGC-B60 sample has almost zero porosity. However, TGC-S15, TGC-S30, TGC-

S60, TGC-P15, TGC-P30 and TGC-P60 samples have the lowest density and the highest porosity values. Density values of these samples are close to the density values of TG sample since the high volume of glassy phase still remained in the sintered glass-ceramic samples. Both porosity and water absorption values correlated well each other and decreased with the increase of the crystallization degree in all samples. We obtained the similar results in the hardness values of the glass-ceramic samples. Hardness values of the bulk samples are higher than the sintered sample's values, as it was expected. Increasing of crystallization degree also increased the hardness values of the glass-ceramic samples. Density and hardness values of TGC-B15, TGC-B30 and TGC-B60 samples are better than the values of the glass-ceramic samples produced in different studies from industrial wastes such as coal fly ash [117,204] and incinerator fly ash [124,131,155,165,209]. Porosity and water absorption values of bulk samples are lower than the values reported by Cheng et al.[163]. Hardness and density values of sintered samples are worse than the values of the sintered glass-ceramic samples produced from incinerator fly ash [124,165]. However, porosity and the water absorption values of the sintered samples in this study are better than the values of the sintered samples obtained from Cheng et al.[163].

Table 6.40: Properties of TGC samples

Sample Name	Hardness (kg/mm^2)	Density (g/cm^3)	Porosity (%)	Water Absorption (wt. % loss)
TGC-B15	628	3.03	0.71	Negligible
TGC-B30	776	3.14	0.17	Negligible
TGC-B60	867	3.32	0.10	Negligible
TGC-S15	326	2.81	8.05	4.11
TGC-S30	332	2.92	6.72	3.30
TGC-S60	339	2.98	6.74	3.10
TGC-P15	302	2.85	10.11	5.21
TGC-P30	319	2.89	9.72	4.21
TGC-P60	321	2.91	9.71	4.01

6.7.3.3 TCLP results of the TGC samples

TCLP results of TGC samples were given in Table 6.41. Any heavy metal concentration could not be detected in the extraction solution of the TGC-B15 sample. However, small concentrations of Zn and Cr ions were detected in the extraction solutions of the TGC-S15 and TGC-P15 samples since the solubility of amorphous glassy phase is higher than the augite crystalline phase. But these values are still lower than the limits of EPA. Only Cr and Zn ions were determined in the extraction solutions. The reason of this result may be the high Cr and Zn ion concentrations of Tunçbilek fly ash comparing to the Mn and Pb ion contents. Cr and Zn ion concentrations of extraction solutions are better than the values reported by Cheng [125] and Kavaouras et al.[210]. However, Cr ion content is higher than the Cr ion content of glass-ceramic sample produced from incinerator fly ash [155] while the content of Zn-ion is lower than the Zn-ion content of the same sample [167]. Consequently, the bulk and the sintered samples were sufficiently stabilized, according to the US EPA standards.

Table 6.41: TCLP results of TGC samples

Sample Name	Cr (ppm)	Mn (ppm)	Zn (ppm)	Pb (ppm)
TGC-B15	BDL	BDL	BDL	BDL
TGC-S15	0.002	BDL	0.008	BDL
TGC-P15	0.008	BDL	0.01	BDL

BDL: Below Detection Limit

6.7.3.4 Chemical resistance results of the TGC samples

Results for chemical resistance of the glass-ceramic samples are listed in Table 6.42. It can be seen that the durability of both bulk and sintered glass-ceramic samples correlate with volume of the crystalline phase and show acceptable chemical resistance behavior for all samples. However, chemical resistance of sintered materials is lower than the chemical resistance of the bulk samples, as can be predicted from the previous results. Sintered materials have relatively high weight losses for the acid attacks comparing to the alkali solutions. It is known that the glassy matrix is more easily leached in the acidic solutions. Chemical resistance of

bulk glass-ceramic samples is higher than the chemical resistance of the glass-ceramic samples produced in a different study from coal fly ash [117], while the chemical resistance of sintered samples obtained in this study is worse than the those samples. Chemical resistance of sintered samples are better than the values reported by Cheng et al.[125,155,163] but worse than the values reported by Karamanov et al.[124]. In any case, the chemical resistance is strongly influenced by the crystalline phase. Overall results showed that the TGC-B60 sample has the best microstructural, mechanical, physical and chemical properties of all glass-ceramic samples.

Table 6.42: Chemical resistances of the TGC samples

Sample Name	HNO_3 (%)	NaOH(%)
TGC-B15	0.100	Negligible
TGC-B30	0.033	Negligible
TGC-B60	0.015	Negligible
TGC-S15	4.770	1.12
TGC-S30	4.620	1.02
TGC-S60	4.120	1.07
TGC-P15	4.890	1.47
TGC-P30	4.720	1.46
TGC-P60	4.650	1.32

6.7.4 Experimental results of CGC samples

6.7.4.1 Microstructural characterization of CGC samples

XRD scans of the sintered glass-ceramic samples produced by using different heat treatment procedures were obtained. Interpretation the XRD scans of three sintered samples showed that the main crystalline phase is the diopside ($CaMgSi_2O_6$). CaO and MgO might modify the glass network by decreasing the relative proportion of bridging oxygen bonds to non-bridging oxygen bonds. Structural rearrangements might take place in the earlier stages of crystallization process. Octahedral magnesium groups ($[MgO_6]^{10-}$) tend to combine with $[CaO_6]^{10-}$ octahedrons and endless $[SiO_3]^{2-}$ groups, leading to diopside formation. This conclusion is in agreement with the reported literature on sintered glass-ceramics developed from

industrial wastes which belong to the diopside group [237]. XRD patterns of CGC-S and CGC-P were given in Figures C.10-C.11 in Appendix C.

The microstructures of the crystallized glass samples were examined by using SEM. Fig. 6.77 shows the SEM micrograph of the CGC-S15 sample. Fig. 6.77 reveals tiny crystals dispersed in the microstructure and the glassy regions still remained in the bulk of the sample. It is also seen that there are extensive cracks on the surface of the sample. Figs. 6.78 and 6.79 are the representative SEM micrographs of the CGC-S30 and CGC-S60 samples, respectively. As seen from the figures, same microstructures were detected in the bulk of the sample and also the number of crystallites increased with the increasing holding time at the crystallization temperature. It was determined that the number of crystallites occurred in the sintered glass-ceramic samples is less and the size of the crystallites is larger than that of the samples produced by the classical method. It was also detected that extensive cracks and glassy regions were observed in the microstructure of the sintered glass-ceramic samples, in contrast to the glass-ceramic samples obtained by the classical method. It was concluded that the microstructures of the glass-ceramic samples produced by the classical method which was reported in the previous study [118] are better than the glass-ceramic samples produced by the sintering method.

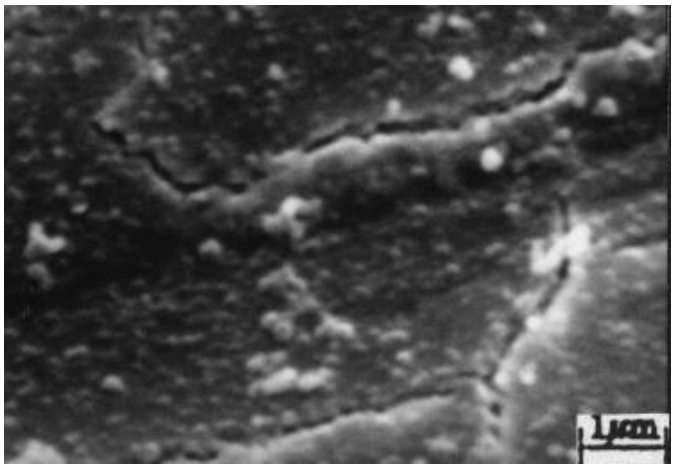

Figure 6.77: SEM micrographs of CGC-S15 sample

Figures 6.80-6.82 show the SEM micrographs of the CGC-P15, CGC-P30 and CGC-P60 samples, respectively. As seen from these figures, tiny equiaxed crystallites homogeneously dispersed in the bulk of the sample. The volume of the crystalline phase increased with the increase in holding time at T_p as it was expected. Furthermore, there is no cracks and glassy regions on the surface of the CGC-P15, CGC-P30 and CGC-P60 samples. It was observed that the microstructures of these samples are very similar to the microstructures of the bulk glass-ceramic samples obtained in the previous study [118]. PVA helps to bond to glass powders together and thus the more dense structure occurred in the glass-ceramic samples. Any cracks could not be observed on the surface of the PVA added samples. It was concluded that the addition of PVA as a binder to the CG-97 glass powder improved the microstructure of the sintered glass-ceramic samples.

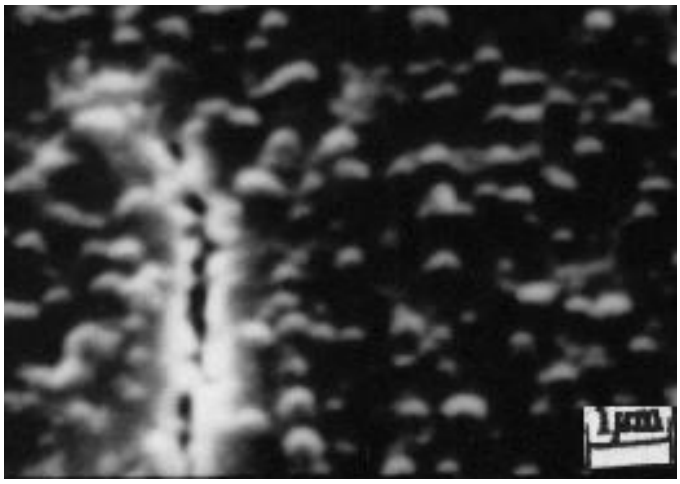

Figure 6.78: SEM micrographs of CGC-S30 sample

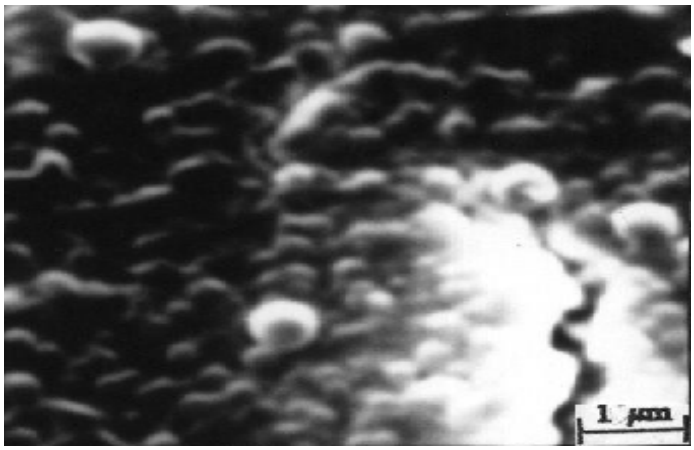

Figure 6.79: SEM micrographs of CGC-S60 sample

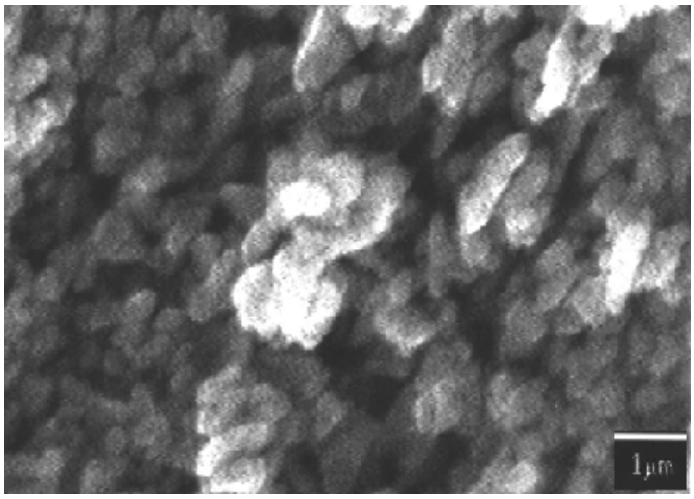

Figure 6.80: SEM micrographs of CGC-P15 sample

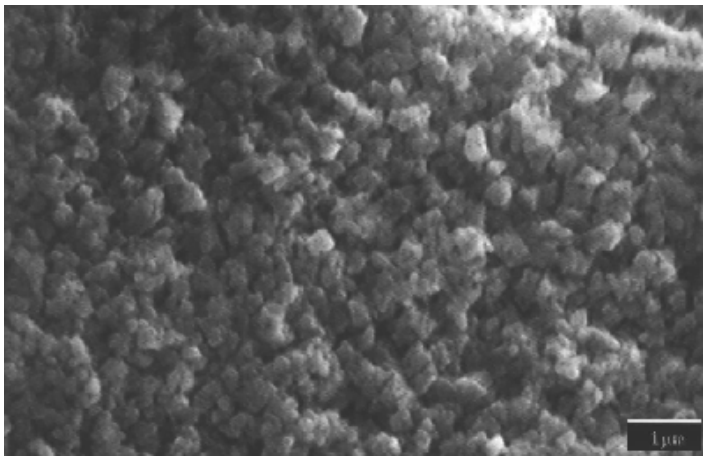

Figure 6.81: SEM micrographs of CGC-P30 sample

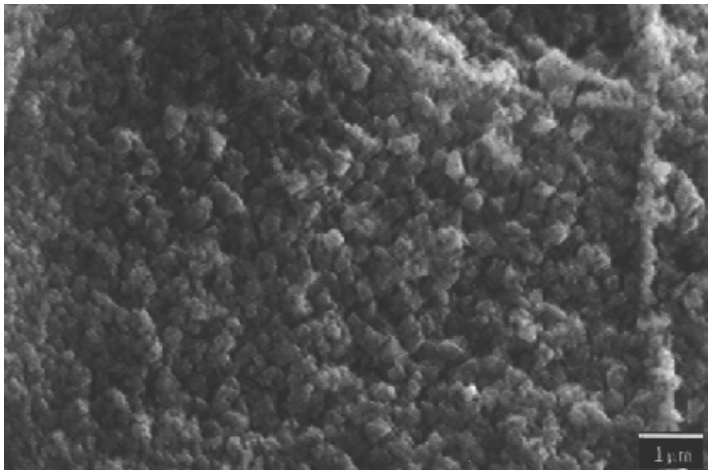

Figure 6.82: SEM micrographs of CGC-P60 sample

6.7.4.2 Physical and mechanical properties of CGC samples

Table 6.43 summarizes the Vickers microhardness, density, porosity and water absorption values of the sintered glass-ceramic samples. Hardness and density values increased with the increasing holding times at the crystallization temperature. It can be concluded that if the crystallinity increased, the hardness and density values of glass-ceramic samples increased and water absorption also decreased, which is also observed previously [119]. Although the CGC-P60 has the maximum hardness value of 887 kg/mm^2, the hardness values of glass-ceramic samples produced by classical method reported in the previous study [118] are better than this value. However, density and hardness values of CGC-P15, CGC-P30 and CGC-P60 samples are higher than the values reported by Shao et al.[204], Leroy et al.[117]. The extensive cracks on the surface of the CGC-S15, CGC-S30 and CGC-S60 samples caused to decrease the hardness values of those samples. The hardness value of CGC-S60 sample is higher than the value of sintered sample produced from incinerator fly ash [165]. Water absorption and porosity values decreased with the increase in crystallization degree. Cracks on the surface of the CGC-S15, CGC-S30 and CGC-S60 samples also resulted to increase the water absorption of these samples. Water absorption and porosity values of all samples are lower than the values of the incinerator fly ash based-glass-ceramic materials [155,163]

Table 6.43: Properties of CGC samples

Sample Name	Hardness (kg/mm^2)	Density (g/cm^3)	Porosity (%)	Water Absorption (wt. % loss)
CGC-S15	386	2.38	0.90	0.20
CGC-S30	403	2.66	0.85	0.17
CGC-S60	458	3.74	0.20	0.03
CGC-P15	598	2.98	0.40	Negligible
CGC-P30	653	2.89	0.15	Negligible
CGC-P60	887	3.32	0.00	Negligible

6.7.4.3 TCLP results of CGC samples

Table 6.44 shows the TCLP test results of CGC samples. As seen from Table 6.44, Cr and Zn ions were detected in the extraction solution of CGC-S60 sample. Their concentration values are under the limits of US EPA and are also better than the values reported by Cheng [155] and Kavaouras et al.[210]. The remained glassy phase and the extensive cracks on the surface of the CGC-S60 sample may lead to dissolution of heavy metal ions from bulk of the sample to the extraction solution. Any heavy metal ion concentration could not be detected in the extraction solutions of CGC-P60 sample since the heavy metal ions replaced Ca^{2+} and Al^{3+} and hold in the framework of the glass-ceramic samples. Therefore, CGC-P60 sample is more chemically stable than the CGC-S60 sample. However, according to the US EPA standards heavy metal ions were successfully hold in both CGC-P60 and CGC-S60 samples.

Table 6.44: TCLP results of CGC samples

Sample Name	Cr (ppm)	Mn (ppm)	Zn (ppm)	Pb (ppm)
CGC-S60	0.005	BDL	0.008	BDL
CGC-P60	BDL	BDL	BDL	BDL

BDL: Below Detection Limit

6.7.4.4 Chemical resistance of CGC samples

Chemical resistances of sintered glass-ceramic samples were given in Table 6.45. As seen in Table 6.45, the results for chemical resistance of the glass-ceramic samples do not correlate with the heat treatment procedures. CGC-P15, CGC-P30 and CGC-P60 samples showed more resistance to both acidic and alkali solutions than the CGC-S15, CGC-S30 and CGC-S60 samples since their crystallization degree is higher than the CGC-S15, CGC-S30 and CGC-S60 samples. And, there is not any crack on the surface of the CGC-P15, CGC-P30 and CGC-P60 samples. The CGC-P60 sample has the highest chemical resistance of all samples. These results indicated that the chemical resistance increased with the increase in crystallization volume as it was concluded before. However, it is apparent that the all samples show low resistance to acidic solutions. It was found that the chemical resistance of CGC

samples was higher than the chemical resistance of glass-ceramics produced from incinerator fly ash [163]. It can be concluded that the higher the crystallinity the better the chemical durability and the smaller the quantity of metals found in the leaching solutions.

Table 6.45: Chemical resistances of the CGC samples

Sample Name	HNO_3 (%)	NaOH(%)
CGC-S15	0.90	0.60
CGC-S30	1.00	0.70
CGC-S60	0.80	0.14
CGC-P15	0.71	Negligible
CGC-P30	0.61	Negligible
CGC-P60	0.32	Negligible

6.7.5 Overall results of the produced glass-ceramic materials

Overall results showed that CRGC-B60, ORSGC-P60, TGC-B60 and CGC-P60 samples have the best microstructural, mechanical, physical and chemical properties among all glass-ceramic samples produced from Çayırhan, Orhaneli, Tunçbilek fly ashes with or without the addition of red mud and silica fume at different heat treatment conditions. The obtained properties of these glass-ceramic samples are better than the most of the glass-ceramic samples produced from industrial wastes as it was discussed in the previous sections. Only the crystalline phase of TGC samples is different from the other glass-ceramic sample's crystalline phases since the chemical composition of TG sample is different from the other glass compositions. The chemical compositions of CG, CRG and ORG glasses are similar to each other. Al_2O_3 and SiO_2 contents of TG sample are higher while MgO and CaO contents are lower than the other glass compositions. Therefore, crystalline phase occurred in the TGC samples is different. However, diopside and augite phases belong to the same group. The properties of the sintered glass-ceramic samples are depending on the glass composition, particle size, the addition of the binder, heating rate, sintering pressure and the firing temperature. It was observed that, in all glass-ceramic samples, except TGC-P15, TGC-P30 and TGC-P60 samples, addition of PVA improved the properties of the samples.

The properties of the bulk glass-ceramic samples were influenced by the glass composition, glass production conditions and the heat treatment process. TGC-B60 sample has the best properties in all bulk glass-ceramic samples while ORSGC-B15 sample has the worst one. The crystalline size and the shapes of the ORSGC samples are different from the other bulk glass-ceramic samples. The crystalline size of the ORGC samples is the bigger than those of the other glass-ceramic samples. It was also observed that in all glass-ceramic samples the volume of the crystalline phase increased with the increase in holding time at T_p and this result caused to improve the physical, mechanical and chemical properties of the glass-ceramic samples. With the increasing of crystallization degree, crystallites were strongly interlocked together to form a more dense crystalline structure. Therefore, amorphous glassy phase deceased gradually and the properties of the samples were improved.

Overall results indicated that coal fly ash can be used as a raw material to produce glass-ceramic materials with or without the addition of red mud and silica fume and coal fly ash-based glass-ceramics have several desirable properties that would make them attractive to industrial use in construction, tiling and cladding applications.

6.8 Sintering Process

The sintering behavior of Seyitömer, Tunçbilek, Orhaneli, Çan, Çatalağzı, Çayırhan and Afşin-Elbistan thermal power plant fly ashes were investigated. The main aim of this investigation is to optimize a powder technology route for fly ash samples in order to maximize the sintered density of the products with the lowest possible sintering temperature. For this purpose, coal fly ash samples were sintered to form ceramic materials by using conventional powder processing based on powder compaction and firing, without the addition of any organic or inorganic binders. A number of preliminary experimental trials were conducted on fly ash samples at different temperatures and residence times in order to investigate the possibility of thermal treatment of fly ash alone. The firing temperature ranges and the residence time, which were selected on the basis of preliminary runs, are 1223-1473 K and 2 h, respectively. Fly ash samples were sintered at 4 different temperatures to determine the lowest sintering temperature. Some codes were given to the sintered products and these codes were listed in Table 6.46. To investigate the effects of firing

temperatures on the properties of the sintered materials, microstructural analysis, mechanical and physical tests were conducted on the products.

Table 6.46: Codes of the sintered fly ash samples

Fly Ash	Sintering Time (h)	Sintering Temperature (K)	Code of the Sintered Samples
Çayırhan Fly Ash	2	1298	CAYFA1298
		1323	CAYFA1323
		1348	CAYFA1348
		1373	CAYFA1373
Çan Fly Ash	2	1373	CFA1373
		1398	CFA1398
		1423	CFA1423
		1448	CFA1448
Çatalağzı Fly Ash	2	1373	CATFA1373
		1398	CATFA1398
		1423	CATFA1423
		1448	CATFA1448
Seyitömer Fly Ash	2	1373	SFA1373
		1398	SFA1398
		1423	SFA1423
		1448	SFA1448
Tunçbilek Fly Ash	2	1398	TFA1398
		1423	TFA1423
		1448	TFA1448
		1473	TFA1473
Orhaneli Fly Ash	2	1273	OFA1273
		1298	OFA1298
		1323	OFA1323
		1348	OFA1348
Afşin-Elbistan Fly Ash	2	1223	AEFA1223
		1248	AEFA1248
		1273	AEFA1273
		1298	AEFA1298

6.8.1 Experimental results of sintered CAYFA samples

6.8.1.1 Microstructural analysis of sintered CAYFA samples

Çayırhan fly ash samples were prepared according to the procedure in Section 5.7 and then fired at the temperatures of 1298, 1323, 1348 and 1373 K for 2h in an electric furnace with a heating rate of 10 K/min. Visual inspection of the sintered samples showed that the color of the samples changed from brown to dark brown and

the samples displayed smooth surfaces with glassy appearance with the increasing of firing temperature. The major oxides SiO_2, CaO and Al_2O_3 account for approximately 71 % of the fly ash mass. The amounts of SiO_2 and Al_2O_3 are the indication of the suitability of sintering process. XRD analysis of CAYFA1298, CAYFA1323, CAYFA1348 and CAYFA1373 samples revealed that the main crystalline phases were mullite ($Al_6Si_2O_{13}$), anorthite ($CaAl_2Si_2O_8$) and diopside ($Ca(Mg, Al)(Si, Al)_2O_6$) and the volume and the types of the crystalline phases changed with the firing temperatures. XRD patterns of CAYFA1298, CAYFA1323, CAYFA1348 and CAYFA1373 samples were given in Figure D.1 in Appendix D, respectively. Çayırhan fly ash comprised of quartz, mullite, anorthite, enstatite and hematite mineral phases as it was given in Section 5.3. As seen from Figure D.1, hematite and enstatite phases disappeared when the pressed samples were fired at 1298 K and further heating resulted to form a diopside phase in the CAYFA1323, CAYFA1348 and CAYFA1373 samples. The peak intensities and the locations changed when firing temperature was above 1298 K. The amount of mullite decreased gradually with the increasing of firing temperature. Diopside formed as the major crystalline phase at 1373 K together with a small amount of anorthite phase. The changes in the crystalline phases occurred in the CAYFA1298, CAYFA1323, CAYFA1348 and CAYFA1373 samples were given in Table 6.47. The structure of mullite in CAYFA1298 sample began to broken apart with the increasing of firing temperature. Then free Ca^{2+} and Mg^{2+} forced to rearrange mullite phase and unite with it since their amounts were high enough. Thus diopside and anorthite phases formed in the CAYFA1373 sample as the main crystalline phase. Diopside phase was more stable than the other phases in CAYFA 1348 and CAYFA 1373 samples.

SEM micrographs of both surfaces and interior crystalline structures of CAYFA1298, CAYFA1323, CAYFA1348 and CAYFA1373 samples are shown in Figures 6.83-6.86. As seen from Figures 6.83-6.86, the surface of the samples is getting smoother with the increasing of firing temperature. The volume of the pores decreased gradually and CAYFA1373 sample has a more dense structure with a much smoother surface. The surface of CAYFA1298 sample is rough and contains significant amount of pores, indicating a relatively poorly sintered material. The diameter of the pores is more than 2 μm (Figure 6.83(a)). With the increasing of firing temperature to 1323 K, the amount and the size of the pores decreased, as seen

from Figure 6.84(a). Small spherulitic crystallites occurred in the microstructure of the CAYFA1323 sample with the effect of high firing temperature. As seen from Figure 6.85(a), the surface of the CAYFA1348 sample is smoother than the CAYFA1323 sample. However, some spherical pores was still observed on the surface of the CAYFA1348 sample. It was thought that this was a result of the softening of the glassy phase present in the fly ash, together with simultaneous evaluation of gaseous species at this temperature. CAYFA1373 sample has a much smoother surface with a lower porosity than the other samples. More dense structure was obtained above 1348 K. Small crystallites can also be seen from Figure 86(a).

Inspection of crystalline structures of CAYFA1298, CAYFA1323, CAYFA1348 and CAYFA1373 samples revealed that the spherical diopside crystallites dispersed randomly in the microstructure of the samples. The crystalline size and the shape were changed with the increasing of firing temperature. In compliance with the XRD results, the amount of diopside crystallites also increased with the increasing of firing temperature. Figure 6.83(b) shows the SEM micrograph of CAYFA1298 sample. As can be seen from the figure, tiny spherulitic crystallites were dispersed randomly in the microstructure of the CAYFA1298 sample. It was also observed that there were relatively big crystallites with the irregular shapes in the microstructure of the CAYFA1298 sample. This difference in the crystalline size and the shape was expected since the three different crystalline phases were obtained from the XRD results. The remained glassy phase can also be seen from Figure 6.83(b). More spherulitic crystallites and less glassy phase were determined in CAYFA1323 sample as it was seen from Figure 6.84(b). There were still irregular shaped crystallites. It can be seen that the average crystalline size of CAYFA1348 sample is bigger than the CAYFA1323 sample if the Figures 6.84(b) and 6.85(b) were compared. The equiaxed crystallites were dispersed randomly in the microstructure of CAYFA1348 sample. The elongated and the irregular shaped crystallites were also detected in the CAYFA1348 sample. The volume of the glassy phase of CAYFA1348 sample was less than the CAYFA1323 sample. Figure 6.86(b) indicates that the only equiaxed crystallites occurred in the microstructure of CAYFA samples above 1348 K. The volume of the crystalline phase increased with the increase in firing temperatures. Crystal size and morphology appeared to play an important role in affecting physical

and mechanical properties of sintered materials, as will be discussed in the following section.

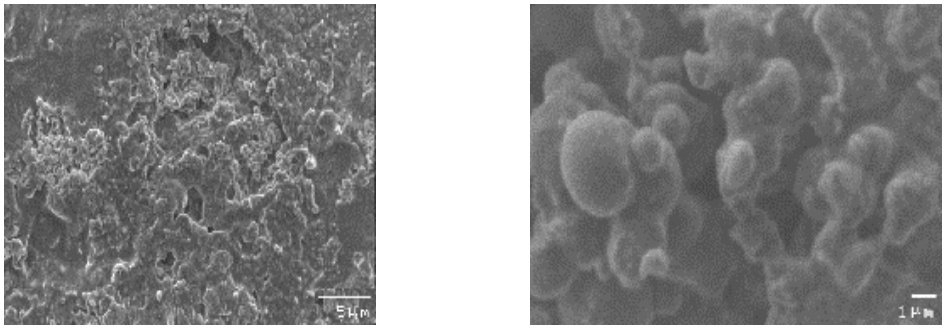

(a) (b)

Figure 6.83: SEM micrographs of CAYFA1298 sample at lower(a) and higher magnifications (b)

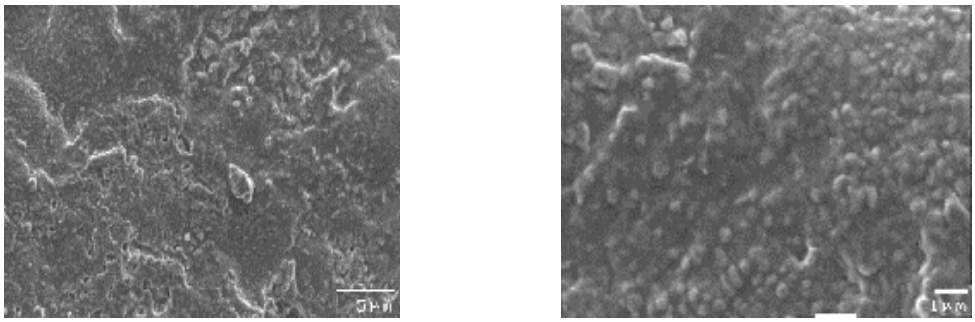

(a) (b)

Figure 6.84: SEM micrographs of CAYFA1323 sample at lower(a) and higher magnifications (b)

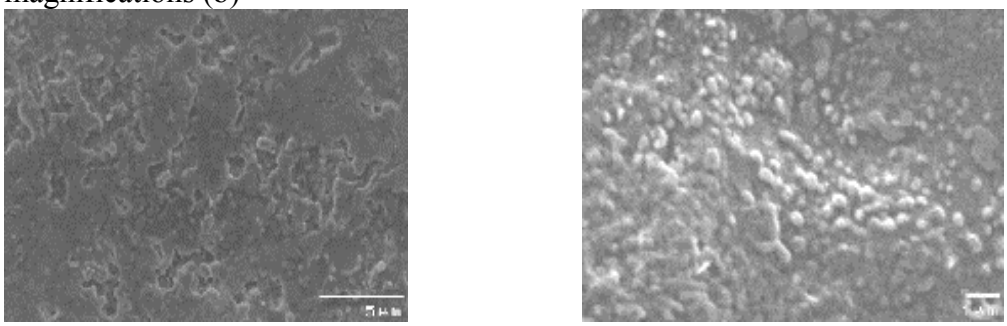

(a) (b)

Figure 6.85: SEM micrographs of CAYFA1348 sample at lower(a) and higher magnifications (b)

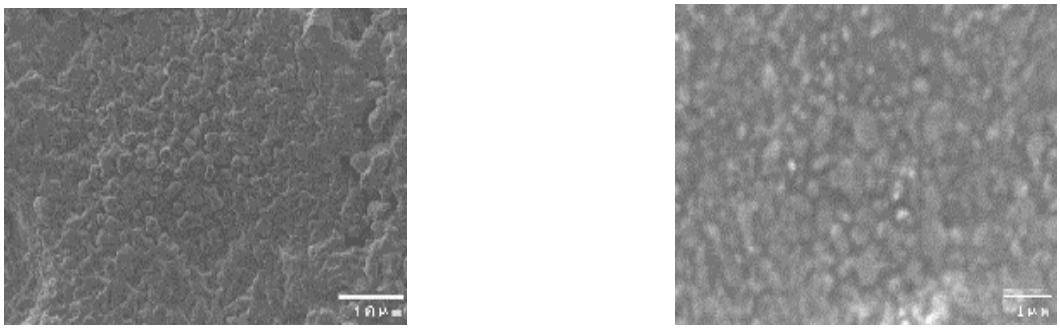

(a) (b)

Figure 6.86: SEM micrographs of CAYFA1373 sample at lower(a) and higher magnifications (b)

6.8.1.2 Physical and mechanical properties of sintered CAYFA samples

Physical and mechanical properties of CAYFA samples heat-treated at different temperatures were listed in Table 6.47. Densities of heat-treated samples were measured to be around 1.95-2.26 g/cm^3 that were higher than the pressed CAYFA samples. The density of the samples increased with the increase in firing temperature in consistent with the SEM observations as it was reported by the several researchers [15,238,239]. CAYFA1373 sample that has a more dense crystalline structure has the highest density value of all samples. The density values of CAYFA samples are found higher than the density values of bricks produced from fly ash by Lingling et al.[238]. The density value of CAYFA1348 and CAYFA1373 samples are very close to the commercial porcelainized stoneware [240]. The low density values of the CAYFA1298 and CAYFA 1323 samples indicate that these samples were not sintered effectively. At lower firing temperatures sintered samples exhibited a porous surface that was maintained up to 1373 K. Due to the existing open porosity, the water absorption was high for the CAYFA1298, CAYFA1323 and CAYFA1348 samples. The porosity decreased to the value of 5.6 % when the samples were heat treated at 1373 K. Therefore, water absorption reaches the lowest value of 3.1 % for the CAYFA1373 sample. Water absorption and porosity values are better than the values of the fly ash based-bricks reported by Lingling et al.[238], Jonker et al.[241], Artır et al.[242], Illic et al.[239] and Queralt et al.[15] who produced ceramic materials from coal fly ash obtained less water absorption values than the values reported in this study. Rockwell hardness values of sintered samples increased with the increasing of firing temperature, as it was expected. CAYFA1373 sample has the

highest value of 69 in the B scale since it has the highest crystalline phase in all samples. Microstructural, mechanical and physical properties of CAYFA1373 sample are better than the other samples. These results showed that the sintering can be achieved above 1348 K for Çayırhan fly ash.

Overall results showed that the fired samples have superior properties than the pressed samples. Conducting heat treatment process on the pressed samples resulted to improve the properties of the pressed samples.

Table 6.47: Properties of CAYFA samples

Sample Name	Crystalline Phases	Rockwell Hardness	Bulk Density (g/cm^3)	Porosity (%)	Water Absorption (wt. % loss)
Pressed Sample	Quartz, mullite, anorthite, enstatite and hematite	28	1.81	30.0	25.50
CAYFA1298	Mullite, anorthite and diopside	35	1.95	15.0	9.25
CAYFA1323	Mullite, anorthite and diopside	45	1.98	11.2	7.60
CAYFA1348	Anorthite and diopside	51	2.11	10.8	6.20
CAYFA1373	Anorthite and diopside	69	2.26	5.6	3.10

6.8.2 Experimental results of sintered CFA samples

6.8.2.1 Microstructural analysis of sintered CFA samples

Pressed Çan fly ash samples were heat treated at the temperatures of 1373, 1398, 1423 and 1448 K on the basis of preliminary experimental trials. The firing temperatures were selected higher than the temperatures applied for CAYFA samples. The reason of this is the higher SiO_2+Al_2O_3 and lower alkali oxide contents of CFA samples than the CAYFA samples. It is well known that, SiO_2+Al_2O_3 behave

as a glass former which increase the melting temperature while the alkali oxides decrease the melting temperature. Alkali oxide content affects the viscosity of the material and consequently the mass transport during the sintering process. The low melting temperature causes the occurrence of liquid phase which enhances the connecting of fly ash particles and reacting of components each other at lower temperatures. Therefore, high alkali oxide content lowers the sintering temperature. The color of the CFA samples changed from light to dark grey when the heat treatment process applied on the pressed samples. The surface of the samples is getting smoother and shiny dark color with the increasing firing temperature. In order to investigate the nature of phases resulting from thermal treatment, the XRD patterns of samples heat treated at different temperatures were compared. XRD patterns of CFA1373, CFA1398, CFA1423 and CFA1448 samples were given in Figure D.2 in Appendix D, respectively. As seen from Figure D.2, the peak intensities and the locations were slightly changed with the increasing of firing temperature. The intensities of the mullite peaks increased with the increasing firing temperatures. The changes in the crystallization phases can also be seen from Table 6.48. Enstatite and anorthite phases in the as-received fly ash sample disappeared in the sintered samples. Çan fly ash sample belongs to mainly SiO_2-Al_2O_3-Fe_2O_3 system. From phase diagrams for ceramics, the behavior of fly ash during firing can be predicted. The main composition of Çan fly ash is located in the primary phase field of mullite and therefore, this phase can be expected in the sintered CFA samples. The formation reaction of mullite in the SiO_2 and Al_2O_3 couple occurred by the following solid-state reactions [243]:

$$Al_2O_3.2SiO_2.2H_2O \xrightarrow{823\ K\text{-}843\ K} Al_2O_3.2SiO_2 + 2H_2O \qquad \textbf{(6.9)}$$

$$Al_2O_3.2SiO_2 \xrightarrow{1073\ K\text{-}1173\ K} Al_2O_3.SiO_2 + SiO_2 \qquad \textbf{(6.10)}$$

$$3(Al_2O_3.SiO_2) \xrightarrow{1273\ K} \underbrace{3Al_2O_3.2SiO_2}_{\text{3.2 Mullite}} + SiO_2 \qquad \textbf{(6.11)}$$

Since the Al_2O_3 and SiO_2 content of Çan fly ash is relatively high enough to form mullite phase, the main crystalline phase occurred in the sintered CFA samples is mullite ($Al_6Si_2O_{13}$) The mullitization reaction was practically completed at 1373 K

and mullite crystallinity increased with the further increase in firing temperature. The mullite phase occurred in the coal fly ash-based ceramics was also reported by Jung et al.[244] and Queralt et al.[15].

SEM observations of sintered samples indicated that the mullite crystallites formed in the microstructure of the sintered CFA samples. Figure 6.87-6.90 shows the surface and the crystalline structures of the CFA samples. CFA samples have more porous and rough surfaces at low sintering temperatures. Figure 6.87(a) shows the rough and porous surface of the CFA1373 sample. With the increasing of firing temperature from 1373 K to 1398 K, more smooth surface and less porosity was obtained (Figure 6.88(a)). As seen from Figure 6.88(a), a small amount of glassy phase and a crystalline site were also observed on the surface of the CFA1398 sample. CFA1423 sample has less porosity than the CFA1373 and CFA1398 samples (Figure 6.89(a)). Figure 6.89(a) indicates the elongated mullite crystallites on the surface of the CFA1423 sample even if at this low magnification. There was also a small glassy phase on the surface of the CFA1423 sample. Figure 6.90(a) showed that the CFA1448 sample has the more dense structure and smoother surface than the other CFA samples. There was a little glassy phase with the absence of porosity. It was also seen that interlocked crystallites homogeneously dispersed in the microstructure of the CFA1448 sample.

SEM micrographs taken at higher magnifications revealed the crystalline structure of the sintered samples. Figure 6.87(b) shows the interlocked elongated crystallites with small grains. A small amount of glassy phase can also be seen. Interlocked irregular shaped crystallites were dispersed in the microstructure of the CFA1398 sample as seen from Figure 6.88(b). There was also a small glassy phase between the crystalline particles. After a further increase in the firing temperature the volume fraction of elongated crystallites decreased while the equiaxed mullite crystallites increased (Figure 6.89(b)). In the later stage of sintering reaction, prismatic, equiaxed mulite crystallites embedded in a fine-grained matrix formed by solid state reactions (Figure 6.90(b)). The crystalline size varied in a wide range since the different crystalline shapes occurred in the microstructure. The crystallites strictly interlocked together to form a more dense structure. As seen from Figure 6.90(b), no glassy phase was detected in the microstructure of the CFA1448 sample. SEM observations

showed that the crystalline size decreased and more dense crystalline structure was observed when the firing temperature increased. Surface of the samples were getting smoother and no glassy phase or porosity could be observed in the sintered samples at higher temperatures. The microstructure of CFA1428 and CFA1448 samples are better than the microstructure of the sintered coal fly ash produced by Illic et al.[239].

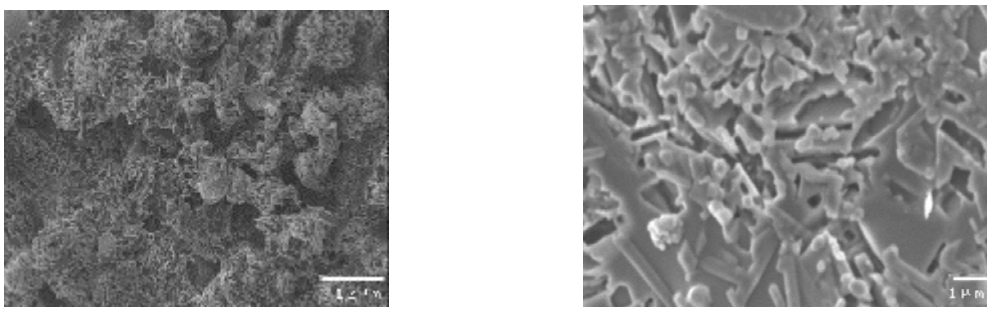

(a) (b)

Figure 6.87: SEM micrographs of CFA1373 sample at lower(a) and higher magnifications (b)

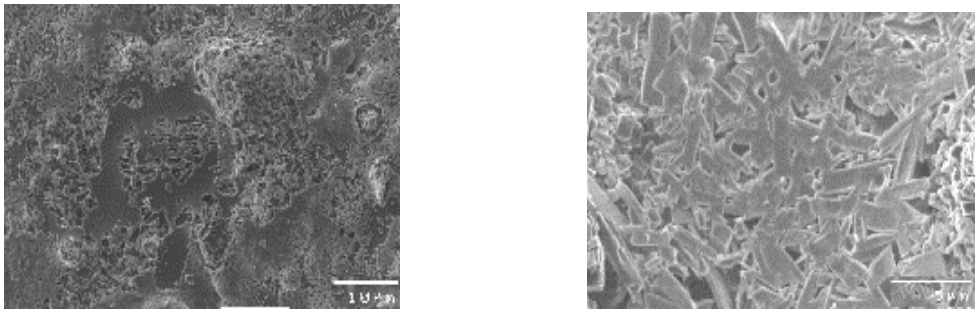

(a) (b)

Figure 6.88: SEM micrographs of CFA1398 sample at lower(a) and higher magnifications (b)

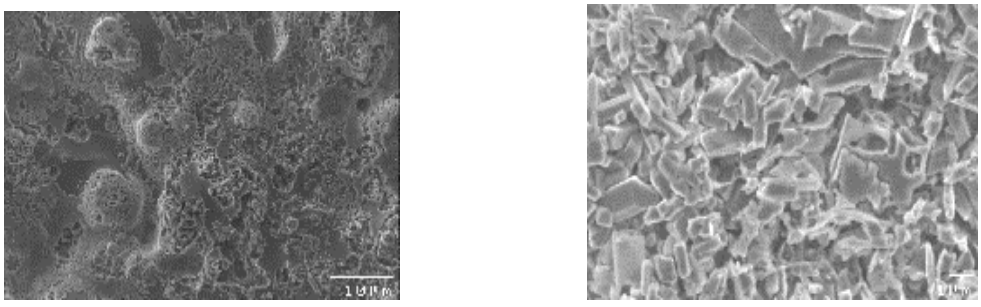

(a) (b)

Figure 6.89: SEM micrographs of CFA1423 sample at lower(a) and higher magnifications (b)

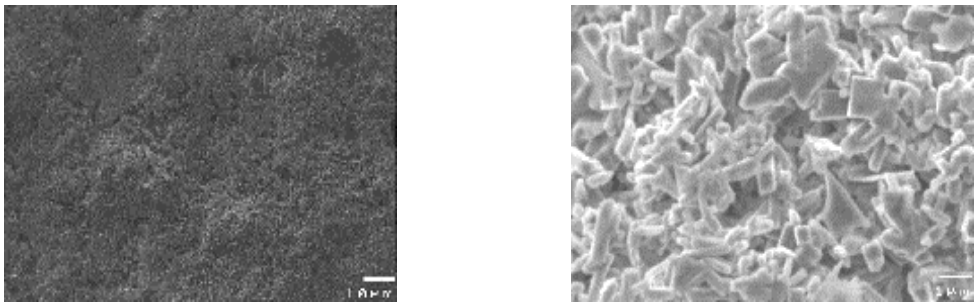

(a) (b)

Figure 6.90: SEM micrographs of CFA1448 sample at lower(a) and higher magnifications (b)

6.8.2.2 Physical and mechanical properties of sintered CFA samples

Table 6.48 shows the physical and mechanical properties of the sintered CFA samples. As seen from Table 6.48, density and Rockwell hardness values increased while the porosity and water absorption values decreased with the increasing of sintering temperature. The increasing of sintering temperature resulted in a densified structure as it was observed in SEM investigations. The density value reached the highest value of 2.55 g/cm^3 at 1448 K. This value is higher than the density values of sintered samples reported by the other researchers [239,244]. Densities obtained for sintered materials are comparable to those of commercially produced ceramics including clay-based sintered materials [245].

The water absorption values were ranged from 11.2% to 1.3 % depending on the sintering temperature. Similar results were also obtained by the studies on coal fly ash sintering at different temperatures. Illic et al.[239], Queralt et al.[15] and Pollettini et al.[246] found that the water absorption decreased with the increasing sintering temperatures. Kara et al.[247] and Jonker et al.[241] obtained higher water absorption values for sintered materials produced from different industrial wastes (such as fly ash, iron-rich waste and gypsum) than the water absorption value of CFA1448 sample.

CFA1448 sample has the lowest porosity value of 0.8 %. This result is in well agreement with the SEM observations; density and water absorption values. The low density and high water absorption values are the indicatives of a porous material.

Rockwell hardness values are also increased with the increase in sintering temperature as it was expected. More dense and tiny crystalline structure caused better mechanical properties. Large and irregular shaped crystallites, glassy phase and porosity decrease the mechanical properties of the materials. It was also known that the mullite properties (low thermal expansion, high hardness, low thermal conductivity) make it an ideal canditate for making ceramic bodies from fly ash [248]. Kim et al.[249] reported that the Rockwell hardness value of the traditional ceramics was in the range of 72.2-80.8 at the major load of 15 kg. The maximum hardness value of 82 for CFA148 sample was better than those values.

Table 6.48: Properties of CFA samples

Sample Name	Crystalline Phases	Rockwell Hardness	Bulk Density (g/cm^3)	Porosity (%)	Water Absorption (wt. % loss)
Pressed Sample	Quartz, mullite, anorthite and enstatite	38	1.98	25.0	11.20
CFA1373	Mullite and quartz	51	2.05	12.0	7.10
CFA1398	Mullite and quartz	63	2.27	7.0	4.30
CFA1423	Mullite and quartz	71	2.48	1.5	2.55
CFA1448	Mullite and quartz	82	2.55	0.8	1.30

6.8.3 Experimental results of sintered CATFA samples

6.8.3.1 Microstructural analysis of sintered CATFA samples

Çatalağzı fly ash samples sintered at 1373, 1398, 1423 and 1448 K after pressed at 40 MPa. It was observed that the pressed samples were in grey color, which tended to become pale brown after the heat treatment process. The surfaces of the sintered samples were became smoother with a glassy appearance when the firing temperature increased. XRD investigations revealed the crystalline phases occurred in the sintered samples. In Appendix D Figure D.3 shows the XRD patterns of CATFA1373, CATFA1398, CATFA1423 and CATFA1448 samples, respectively.

The crystalline phases occurred in each sample were given in Table 6.49. The sintered samples show the presence of quartz (SiO_2), mullite ($Al_6Si_2O_{13}$) and anorthite ($CaAl_2Si_2O_8$) phases while the untreated fly ash sample comprised of the quartz, mullite, anorthite and enstatite phases. Crystalline phases changed significantly with the increasing of firing temperature. Quartz and mullite phases were detected in the CATFA1373 sample (Figure D.3(a)). When the pressed samples were heated to 1398 K, anorthite phase occurred. As seen from Figure D.3(b), new peaks were observed at 22.5°, 24°, 27.2°, 28.3°, 30°, 30.5°, 36.5° and 37° 2θ corresponding to anorthite phase. The peak corresponding to quartz phase disappeared at 1398 K. Further heat treatment at higher temperature resulted to decrease in the intensity of the mullite phase. As seen from x-ray diffraction diagrams, the intensity of the anorthite peaks increased while the intensity of the mullite peaks decreased with the increase in firing temperature. The main crystalline phase occurred in CATFA 1448 sample was determined as anorthite ($CaAl_2Si_2O_8$). Figure D.3(d) shows only two peaks corresponding to the mullite peaks at 1448 K. The composition of Çatalağzı fly ash is in the SiO_2-Al_2O_3-CaO-Fe_2O_3 system. The compositions of Çan and Çatalağzı fly ash samples are similar to each other. However, CaO content of Çatalağzı fly ash is higher than Çan fly ash. The formation of the anorthite phase may be explained by the high CaO content of Çatalağzı fly ash. The presence of anorthite is generally associated with the substitution of Ca ion into the SiO_2-Al_2O_3 couple at high temperatures. Therefore, mulite phase transformed gradually into anorthite phase above 1373 K due to higher CaO content.

SEM examination results revealed the microstructural evolution of the sintered samples, as shown in Figures 6.91-6.94. Figures 6.91(a) and (b) are representative SEM micrographs of CATFA1373 sample both low and high magnifications, respectively. Glassy phase on the surface of the sample can be seen from the Figure 6.91(a). However, a small amount of crystalline sites which were randomly distributed on the surface of the sample was also observed. Surface of the CATFA1373 sample was highly porous. The high SiO_2-Al_2O_3 content and the low alkali oxides content resulted to the high melting temperature as it was discussed previously. The viscosity of the material is high at the relatively low temperatures. It is expected that the evolution of gasses from the material would start at lower temperatures than the sintering temperatures, when the particle coalescence is still

continuing. The combination of the evolution of gaseous species during thermal treatment and the high viscosity of the material, resulting in increasing the size and the number of pores. Particle coalescence is still continuing at 1373 K as seen from Figure 6.91(b). This result showed that the sintering stage could not be completed. Irregular shaped crystallites were detected in the CATFA1373 sample. There are also small pores on the microstructure of the sample. Figure 6.92(a) shows the surface of the CATFA1398 sample. The surface of the CATFA1398 sample is absolutely different from the CATFA1373 sample. No porosity was observed on the surface of the sample and needle-like mullite crystallites were also detected (Figure 6.92(a)). The volume of the glassy phase was less than the CATFA1373 sample. Needle-like crystallites can be clearly seen at higher magnification from Figure 6.92 (b). There was also a small amount of equiaxed crystallites on the surface of the CATFA1398 sample. Glassy phase can be still seen even if at higher magnifications. The microstructure of the sintered samples changed above the temperature of 1398 K. As seen from Figure 6.93 (a), the amount of the needle-like mullite crystallites decreased and small equiaxed crystallites occurred on the surface of the CATFA1428 sample. A small amount of glass phase was still observed on the surface of the sample. Figure 6.93 (b) shows the microstructure of the CATFA1428 sample at higher magnification. As seen from Figure 6.93 (b) irregular shaped crystallites dispersed homugeneously on the microstructure of the CATFA1428 sample. Both needle-like mullite crystallites and small equiaxed crystallites were embedded in the glassy matrix. Small crystallites were detected on the surface of the CATFA1448 sample (Figure 6.94 (a)). As seen from Figure 6.94 (a), a small amount of glassy phase remained in the CATFA1448 sample. The crystallites occurred in the CATFA1448 sample were small equiaxed crystals and some irregular shaped crystallites were also observed. It was clearly shown from the Figure 6.94 (b), small equiaxed crystallites interlocked together to form a more dense well-sintered microstructure with a uniform distribution of crystals. Any glassy phase could not be detected in the microstructure of the CATFA1448 sample. The shape and the size of the crystallites changed dramatically with the increasing of firing temperature. The equiaxed crystals formed in the microstructure of the sintered samples instead of the needle-like mullite crystallites with the thermal treatment of pressed samples above the temperature of 1398 K. The crystalline size also decreased with the increase in

firing temperature since the crystalline phase and the shape of the crystals are changed. These results are in well agreement with the XRD results.

(a) (b)

Figure 6.91: SEM micrographs of CATFA1373 sample at lower(a) and higher magnifications (b)

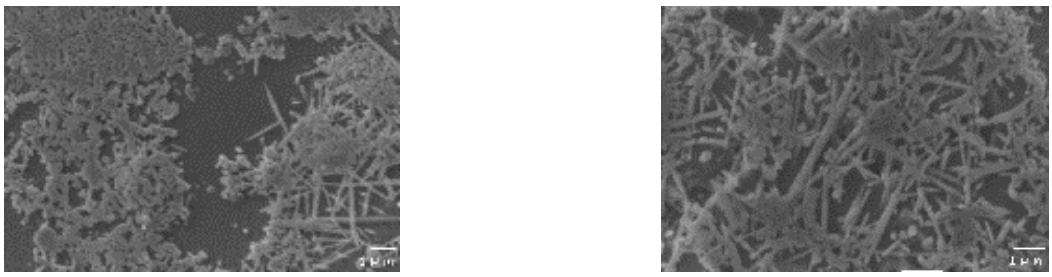

(a) (b)

Figure 6.92: SEM micrographs of CATFA1398 sample at lower(a) and higher magnifications (b)

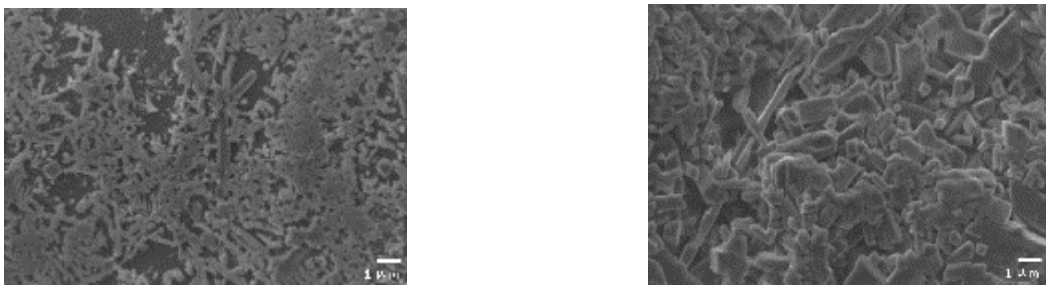

(a) (b)

Figure 6.93: SEM micrographs of CATFA1423 sample at lower(a) and higher magnifications (b)

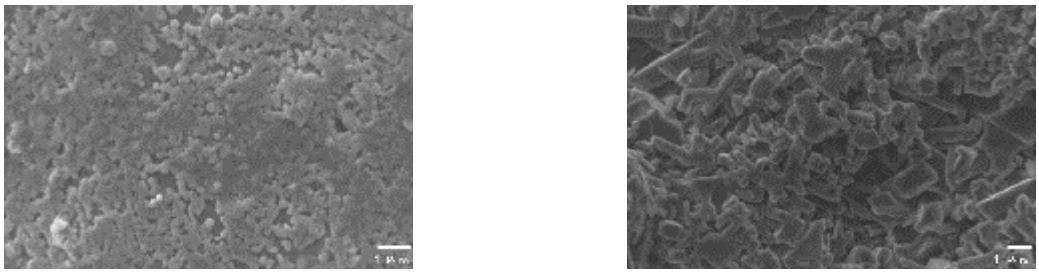

(a) (b)

Figure 6.94: SEM micrographs of CATFA1448 sample at lower(a) and higher magnifications (b)

6.8.3.2 Physical and mechanical properties of sintered CATFA samples

To determine the effects of firing temperatures on the properties of sintered materials physical and mechanical properties were determined and the results were given in Table 6.49. Densities of the sintered samples were in the range of 2.12-2.58 g/cm^3. The density of the pressed sample (1.97 g/cm^3) was improved by applying the heat treatment processes on this material. In consistent with SEM observations, CATFA1448 sample has the highest density value of 2.58 g/cm^3. A high degree of densification by sintering could be achieved at temperature above 1398 K. It was reported that the density values of sintered materials obtained from fly ashes (such as coal fly ash and incinerator fly ash) varied in a wide range between 0.8-2.48 g/cm^3 [15,238,239,246,250-252]. These reported values are lower than the density value of CATFA1448 sample. However, Hernandez et al.[240] produced a municipal solid waste fly ash based-sintered material with a density value of 2.73 g/cm^3 which is higher than the value of CATFA1448 sample.

As seen from Table 6.49, porosity and water absorption values of CATFA samples decreased with the increasing firing temperature as it was expected from the density values and SEM observations. Water absorption is an indication of the porosity of the material. Therefore, both porosity and water absorption values correlated well each other. Water absorption and porosity values of all sintered CATFA samples are lower than the values reported by Jonker et al.[241] and Artır et al.[242] even if CATFA1373 sample.

Rockwell hardness values of sintered samples were found in the range of 38-72. With the increasing of firing temperature, the crystallization degree increased and more dense crystalline structure occurred in the sintered samples. Therefore, CATFA1448 sample has the highest hardness value while the pressed sample has the lowest hardness value. Overall results showed that the heat treatment process yielded better characteristics for physical and mechanical properties of CATFA samples.

Table 6.49: Properties of CATFA samples

Sample Name	Crystalline Phases	Rockwell Hardness	Bulk Density (g/cm^3)	Porosity (%)	Water Absorption (wt. % loss)
Pressed Sample	Quartz, mullite, anorthite and enstatite	30	1.97	21.0	15.7
CATFA1373	Mullite and quartz	38	2.12	15.2	9.8
CATFA1398	Mullite, anorthite and quartz	48	2.29	8.5	8.3
CATFA1423	Mullite and anorthite	53	2.42	5.7	6.1
CATFA1448	Anorthite	72	2.58	3.2	3.2

6.8.4 Experimental results of sintered SFA samples

6.8.4.1 Microstructural analysis of sintered SFA samples

1373, 1398, 1423 and 1448 K were selected as the sintering temperatures for Seyitömer fly ash according to the preliminary experimental trials. Color and the texture of the pressed Seyitömer fly ash samples changed with the heat treatment process. Pressed brown samples with rough surfaces transformed to dark brown sintered samples with a smooth shiny surfaces. Mineralogical composition of the samples also changed with the increasing of firing temperature. Transformation of phases can be seen from Figure D.4 in Appendix D. The crystalline phases found in the sintered samples and as-received fly ash were listed in Table 6.50. As seen from Table 6.50 and Figure D.4, only hematite phase disappeared when the heat treatment

process was applied on the pressed samples at 1373 K comparing with the as-received fly ash mineralogical composition. The increase in firing temperature only changed the intensity of the mullite ($Al_6Si_2O_{13}$) and anorthite ($CaAl_2Si_2O_8$) peaks. The intensity of the mullite and anorthite peaks (at 33.2^o and 36^o 2θ, respectively) decreased at SFA1398 sample as seen from Figure D.4(b9. Quartz peak which shows the glassy phase formed in the microstructure has the highest intensity in all peaks detected in the XRD patterns of SFA1398 sample. As seen from Figure D.4(c), quartz intensity deceased while the mullite and anorthite peak intensities increased sharply in the XRD pattern of SFA 1423 sample. A new anorthite peak occurred at 22^o 2θ and the intensity of the anorthite peaks at 24^o, 36^o, 49.5^o 2θ increased in SFA1423 sample. The intensity of mullite peak at 33.2^o 2θ increased sharply while the intensity of quartz peak at 26.9^o 2θ decreased. Anorthite peak at 28^o 2θ has the highest intensity in the XRD patterns of SFA1448 sample as seen from Figure D.4(d). Further increase in the sintering temperature caused to decrease in the amount of quartz phase while the amount of anorthite and mullite phases increased in the SFA1448 sample. Transformation to anorthite phase at higher temperatures is higher than the mullite phase since the relatively high CaO content of Seyitömer fly ash compare to the Çan fly ash. Chemical compositions of Çatalağzı and Seyitömer fly ashes are similar to each other and therefore, mullite and anorthite phases were detected in both sintered CATFA and SFA samples. However, Fe_2O_3 and MgO content of Seyitömer fly ash is higher than the Çatalağzı fly ash. So, enstatite phase remained in the sintered SFA samples because of the high Fe_2O_3 and MgO content of Seyitömer fly ash.

SEM observations revealed that the surface of the sintered SFA samples was smooth and any porosity could not be detected on the surface of the samples as seen from Figures 6.95 (a)-6.98(a). Figure 6.95(a) is a representative SEM micrograph of SFA1373 sample. It was clearly seen from this figure that the large crystalline sites formed on the surface of the sample with glassy phase regions. Figure 6.96 (a) indicates that the surface of the sample could not changed when the temperature was raised to 1398 K. The amount of the crystalline sites and the glassy phase are similar in SFA1373 and SFA1398 samples. Further increase in the firing temperature resulted to decrease in the amount of glassy phase in the SFA1423 sample as it was

observed in the XRD investigations. Large irregular shaped crystallites were detected on the surface of the SFA1423 sample even if at low magnification (Figure 6.97 (a)). As seen from Figure 6.98 (a), the amount of glassy phase in the SFA1448 sample was less than the glassy phase remained in the SFA1423 sample. However, the similar crystalline sites were observed in both SFA1448 and SFA1423 samples.

The detailed SEM investigations on the crystalline size and the shapes of the sintered SFA samples were performed at higher magnifications. As seen from Figure 6.95 (b), the needle-like mullite crystallites varied in the range of 1-2 μm. The small equiaxed crystallites were also observed with glassy phase regions. The amount of the needle-like mullite crystallites decreased when the temperature was raised to 1398 K. As seen from Figure 6.96 (b), there was still glassy region and size of the equiaxed crystallites decerased. With the effect of higher firing temperature, the more dense microcrystalline structure was obtained in the SFA1423 sample (Figure 6.97 (b)). The needle-like mullite crystallites were still observed in the microstructure. Some big crystallites with irregular shapes were detected in the SFA1423 sample. Small equiaxed crystallites were interlocked together. Small glassy regions still remained between the needle-like and equiaxed crystallites. As seen from Figure 6.98 (b), more dense structure with interlocked equiaxed crystallites was obtained in the SFA1448 sample. Small glassy regions can also be seen in this figure. Some irregular shaped crystallites were detected in the SFA1448 sample. The amount of the needle-like crystals observed in the SFA1448 sample is less than the SFA1423 sample. Consequently, overall results indicated that SEM observations confirm XRD results.

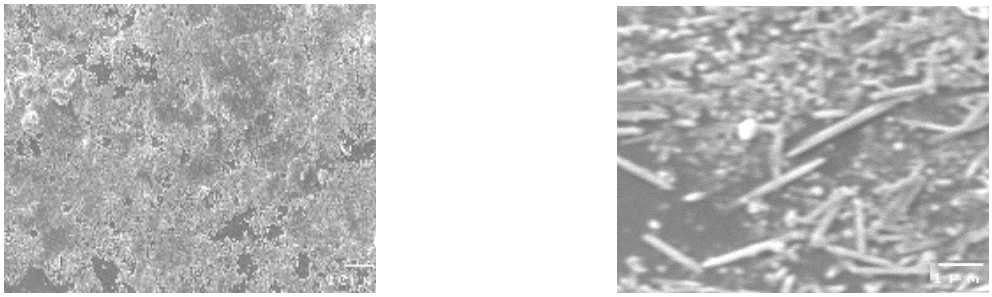

(a) (b)

Figure 6.95: SEM micrographs of SFA1373 sample at lower(a) and higher magnifications (b)

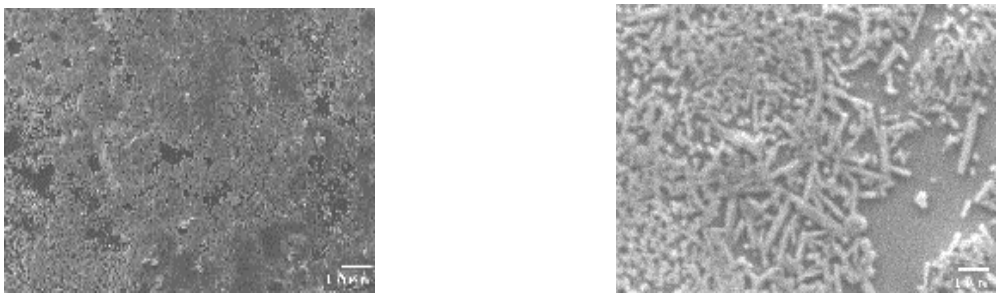

(a) (b)

Figure 6.96: SEM micrographs of SFA1398 sample at lower(a) and higher magnifications (b)

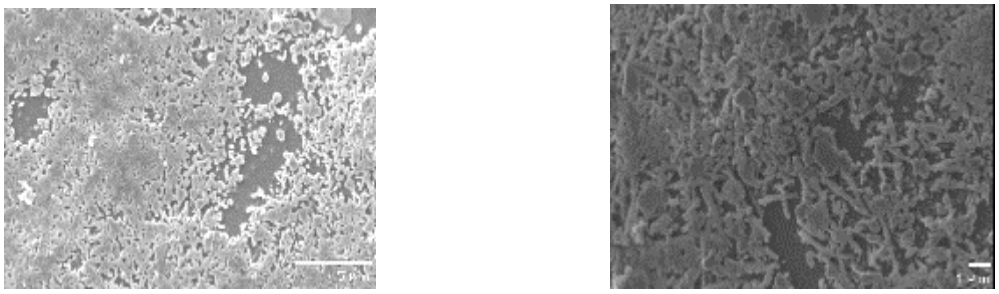

(a) (b)

Figure 6.97: SEM micrographs of SFA1428 sample at lower(a) and higher magnifications (b)

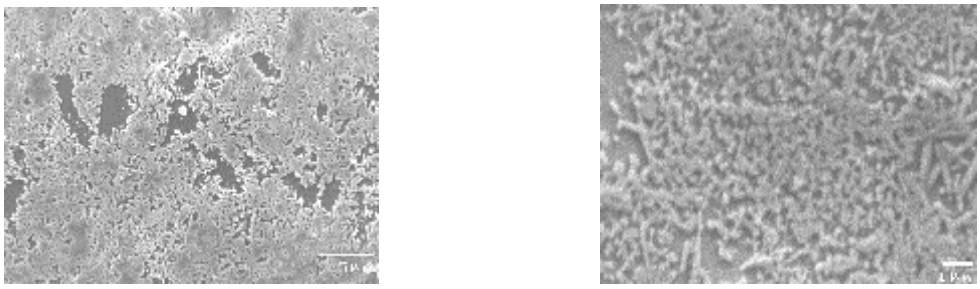

(a) (b)

Figure 6.98: SEM micrographs of SFA1448 sample at lower(a) and higher magnifications (b)

6.8.4.2 Physical and mechanical properties of sintered SFA samples

Physical and mechanical properties of SFA samples were listed in Table 6.50. It was seen from Table 6.50 that sintering process has a strong effect on the densification behavior. The density of the pressed samples increased significantly from the value of 1.78 g/cm^3 to the highest value of 2.14 g/cm^3 when it was sintered at 1448 K. For sintering process the increase in the sintering temperature promotes densification.

The density values of the sintered fly ash samples obtained by Bernavidez et al.[251], Lingling et al.[238] and Artır et al.[242] were lower than the density values of sintered SFA samples. The densities obtained for the sintered SFA samples are close to the porcelains and glasses [239].

Water absorption data demonstrates the reduction in open, water accessible porosity with increased firing temperature. In compliance with the water absorption values, porosity values decreased with increasing sintering temperature. The lowest water absorption value of 3 % is an indicative of the lowest porosity value of 2.1 % for the SFA1448 sample. The water absorption and porosity values of sintered SFA samples were lower than the values reported by Lingling et al.[238] and Artır et al.[242]. However, Illic et al.[239] obtained the lower water absorption value of 0.1 % and the higher density value of 2.48 g/cm^3 for the sintered coal fly ash samples at 1443 K. Those properties are better than the properties of the sintered SFA samples. It was also important to note that the particle size of the coal fly ash (7.3 μm) used by Illic et al.[239] was significantly lower than the particle size of Seyitömer fly ash (261 μm). It was stated by Illic et al.[239] that the particle size play an important role on the properties of the sintered fly ash samples. According to the studies carried out by Illic et al.[239], microstructural and physical properties of the sintered fly ah samples improved with the decrease in particle size. Rockwell hardness values of the SFA samples were found in the range of 35-53. The hardness values were getting better with the increase in firing temperature as it was expected. The more dense crystalline structure and therefore, less glass phase resulted to higher hardness values.

6.8.5 Experimental results of sintered TFA samples

6.8.5.1 Microstructural analysis of sintered TFA samples

Pressed Tunçbilek fly ashes were sintered at 1398, 1423, 1448 and 1473 K. These temperatures are the highest firing temperatures applied to all sintered samples. Tunçbilek fly ash has the highest Al_2O_3 - SiO_2 content and the lowest alkali oxides content so that the melting point would be higher as it was discussed previously. Therefore, firing temperatures were selected higher than the all other samples according to the preliminary experimental trials.

Table 6.50: Properties of SFA samples

Sample Name	Crystalline Phases	Rockwell Hardness	Bulk Density (g/cm^3)	Porosity (%)	Water Absorption (wt. % loss)
Pressed Sample	Quartz, mullite, anorthite, hematite and enstatite	35	1.78	19.6	12.61
SFA1373	Mullite, anorthite, enstatite and quartz	42	1.92	10.1	11.20
SFA1398	Mullite, anorthite, enstatite and quartz	48	2.02	7.1	10.10
SFA1423	Mullite, anorthite, enstatite and quartz	53	2.14	5.6	8.20
SFA1448	Mullite, anorthite and enstatite	57	2.43	2.1	3.00

Visual inspection of the color and texture of the TFA samples showed that the dark red color of the pressed samples became brown after the thermal treatment. The rough surface of the pressed sample was getting smoother and further heat treatment caused to shiny glassy texture on the surface of the sintered samples. The crystalline phases occurred in the sintered TFA samples changed with the increase in the firing temperature. As seen from Figure D.5 in Appendix D, the intensity and the location of the peaks changed. The crystalline phases detected in TFA samples were given in Table 6.51. Both anorthite and hematite phases disappeared when the pressed TFA samples heat treated at 1398 K. Quartz, (SiO_2) mullite ($Al_6Si_2O_{13}$) and enstatite ($(Mg, Fe)SiO_3$) phases can be seen from the Table 6.47 and Figure D.5(a). It can be inferred from the XRD pattern of TFA1398 sample that the amounts of enstatite and mullite phases were higher than the quartz phase. The intensities of quartz and enstatite peaks (at 27^o and 35.6^o 2θ, respectively) decreased when the TFA sample sintered at 1423 K. When the sintering temperature increased to 1448 K the quartz peak at 27^o 2θ disappeared in the XRD pattern of TFA1448 sample. The intensity of the mullite and enstatite peaks increased sharply at 1448 K. This result indicates that

the amount of glassy phase decreased while the amount of crystalline phase increased. At 1473 K, enstatite and mullite phases are the two main phases in the microcrystalline structure of the TFA1473 sample. High Al_2O_3 - SiO_2 content of Tunçbilek fly ash caused the mullite phase while the enstatite phase was an indicative of high Fe_2O_3 content of it.

To investigate the microstructural evolution, SEM was conducted on the sintered TFA samples. Figures 6.99-6.102 are the representative SEM micrographs of the TFA1398, TFA1423, TFA1448 and TFA1473 samples, respectively. As seen from Figure 6.99(a), the surface of the TFA1398 sample was rough and some small pores can be seen. Figure 6.99(b) shows the SEM micrograph of the TFA1398 sample at higher magnification. It was clearly seen from this micrograph that small amount of crystallites occurred in the glassy matrix. The elongated crystallites gathered to form a bigger crystalline size. These gathered crystallites were surrounded by the glassy phase. The surface of the TFA1423 sample can be seen from Figure 6.100(a). The surface of the TFA1423 was still rough but smoother than the TFA1398 sample. The gathered crystallites can be seen from the surface micrograph of TFA1423 sample. Figure 6.100(b) shows these gathered crystallites at higher magnification. Crystalline size and the shape can clearly be seen at the higher magnification. The microstructures of these two samples are very similar to each other. The amount of the crystallites occurred on the microstructure of both samples were low. Microstructure of the sintered TFA samples changed when the sintering temperature was raised. As seen from Figure 6.101(a), the amount of the crystallites increased in the microstructure of the TFA1448 sample. The gathered crystallites dispersed in the microstructure randomly. The surface of the TFA1448 sample was smoother than the TFA1423 sample. Figure 6.101(b) is a SEM micrograph of the TFA1448 sample at higher magnification. As seen from this figure, more elongated crystallites dispersed in the microstructure of the sample. The amount of the crystallites increased with the increase in sintering temperature. Small pores can be seen on the surface of the sample. The pore diameter also decreased with the increase in firing temperature. It was clearly seen from the Figure 6.102(a) that the surface of the TFA1473 sample was smoother than the other sintered TFA samples. The elongated crystallites were observed on the microstructure of the sample. Figure 6.102(b) shows these crystals closer at the higher magnification. The crystalline size and the shape were similar

with the crystallites formed in the TFA1448 sample. However, the microcrystalline structure was denser than the microstructure of TFA1448 sample. The amount of the crystallites increased in the TFA1473 sample. The elongated crystallites interlocked together to form a more dense crystalline structure. Small amount of glassy phase still remained in the microstructure of the TFA1473 sample. SEM observations revealed that the crystalline size decreased with the increase in sintering temperature and more dense crystalline structure occurred.

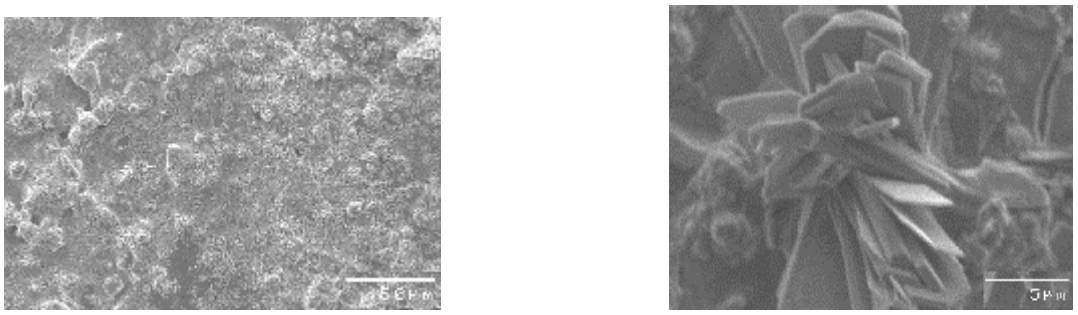

(a) (b)

Figure 6.99: SEM micrographs of TFA1398 sample at lower(a) and higher magnifications (b)

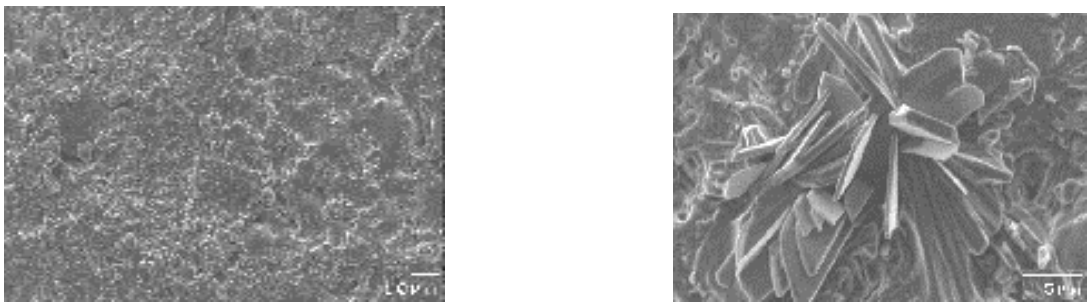

(a) (b)

Figure 6.100: SEM micrographs of TFA1423 sample at lower(a) and higher magnifications (b)

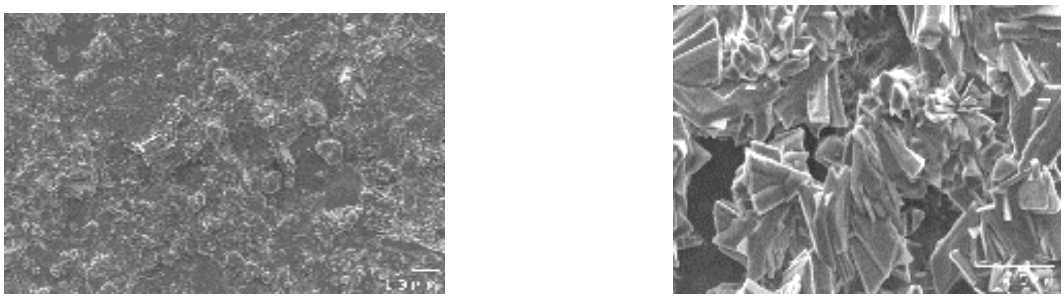

(a) (b)

Figure 6.101: SEM micrographs of TFA1448 sample at lower(a) and higher magnifications (b)

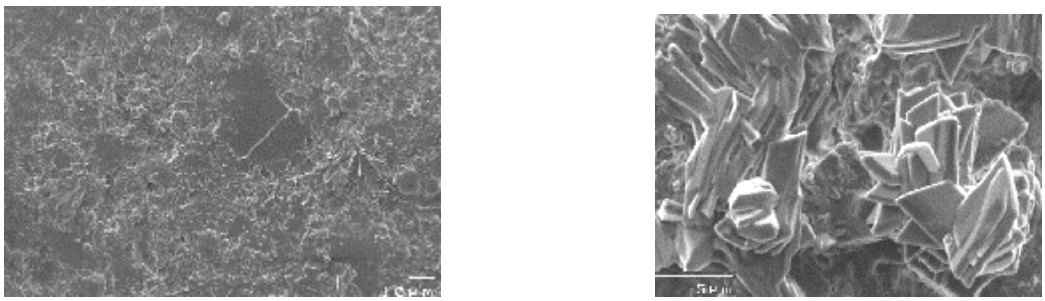

(a) (b)

Figure 6.102: SEM micrographs of TFA1473 sample at lower(a) and higher magnifications (b)

6.8.5.2 Physical and mechanical properties of the sintered TFA samples

To determine the effect of sintering temperatures on the properties of sintered TFA samples, some physical and mechanical properties of the samples were measured and the results were given in Table 6.51. By increasing the sintering temperature the TFA samples displayed smooth surfaces with glassy appearance. The structural changes observed at macroscopic level were mirrored by their physical and mechanical properties. Density is a parameter that can be used as an indicator of the degree of sintering. Density values increased from 1.81 g/cm^3 to 2.37 g/cm^3 during the thermal treatment of the samples. Increasing of density values is a result of more dense crystalline structure with a less glassy phase and porosity. Therefore, with the increase in density values the water absorption values are also decreased. The density values of sintered TFA samples are higher than the density values of sintered fly ash samples produced by Artır et al.[242], Polettini et al.[246] and Lingling et al.[238].

The water absorption and the porosity values were also better than the values reported by Lingling et al.[238] and Artır et al.[242].

The Rockwell hardness values increased with the increase in sintering temperatures as it was observed in the density values. From SEM observations, we can clearly see that the average crystal sizes of both TFA1448 and TFA1473 samples were smaller than the other samples and the hardness values were better. It was reported in the literature that the fine-grained ceramic materials possess better hardness property together with finer crystal size [253]. Overall results showed that the TFA1473 sample had more dense microcrystalline structure with better physical and mechanical properties than those of the other sintered TFA samples.

Table 6.51: Properties of TFA samples

Sample Name	Crystalline Phases	Rockwell Hardness	Bulk Density (g/cm^3)	Porosity (%)	Water Absorption (wt. % loss)
Pressed Sample	Quartz, mullite, anorthite, hematite and enstatite	32	1.81	18.0	15.60
TFA1398	Mullite, enstatite and quartz	40	1.93	15.3	13.20
TFA1423	Mullite, enstatite and quartz	43	2.03	12.1	9.70
TFA1448	Mullite and enstatite	53	2.17	8.6	6.78
TFA1473	Mullite and enstatite	58	2.37	6.3	5.12

6.8.6 Experimental results of sintered OFA samples

6.8.6.1 Microstructural analysis of sintered OFA samples

The sintering temperatures were selected as 1273, 1298, 1323 and 1348 K for the Orhaneli fly ash. These temperatures are lower than those of the sintering

temperatures for CAYFA, CFA, CATFA, SFA and TFA samples. Low Al_2O_3 - SiO_2 and high alkali oxides contents caused to decrease the sintering temperatures of OFA samples. The structural changes occurred in the sintered OFA samples observed at macroscopic level are: The color of the pressed OFA samples changed from light green to dark green when the heat treatment processes were conducted on the samples; the rough surface of the pressed OFA samples was getting smoother with the increase in sintering temperatures.

To determine the mineralogical changes, XRD analyses were performed on the sintered OFA samples. XRD patterns of OFA1273, OFA1298, OFA1323 and OFA1348 samples can be seen from Figure D.6, respectively in Appendix D. The crystalline phases obtained in the sintered samples and Orhaneli fly ash were given in Table 6.52. Table 6.52 and Figure D.6(a) revealed that the quartz (SiO_2), mullite ($Al_6Si_2O_{13}$), anorthite ($CaAl_2Si_2O_8$) and enstatite ($(Mg, Fe)SiO_3$) phases detected in Orhaneli fly ash sample disappeared and wollastonite ($CaSiO_3$) and gehlenite ($Ca_2Al_2SiO_7$) phases occurred in the OFA1273 sample. The amount of the wollastonite phase is more than the gehlenite phase. Only one peak at 31.5^o 2θ corresponded to gehlenite peak. Orhaneli fly ash belongs mainly to the CAS system because of the chemical composition of it. The crystallization behavior can be explained by the theory of stable energy of glassy structure unit [235]. According to this theory, the structure units of CAS system are (SiO_4) and ((AlO_4)Ca(AlO_4)). When CAS system material is heated, the structure unit ((AlO_4)Ca(AlO_4)) begin to broken apart and the free Ca^{2+} join to (SiO_4) tetrahedrals and therefore wollastonite formed first. After wollastonite deposits, (AlO_4) tetrahedrals remain in the structure. It becomes harder for free Ca^{2+} to meet (SiO_4) because of the presence of (AlO_4) tetrahedrals. Though ((AlO_4)Ca(AlO_4)) is very large and inconvenient to regroup as a whole, it is forced to rearrange and unite with (SiO_4) tetrahedrals [235]. Therefore, gehlenite deposits from the glass structure after wollastonite deposits. When the temperature was raised to 1298 K, the peak intensity of the gehlenite phase at 31.5^o 2θ increased while the peak intensities of wollastonite phase decreased. The location and the intensity of the wollastonite peak changed with the increase in firing temperature as seen from Figure D.6(b). The wollastonite peaks at 25.5^{o}and 60^o 2θ disappeared and new wollastonite peaks at 29^o, 30^o, 35^o and 36^o 2θ formed in the

microstructure of the OFA1298 sample. A new gehlenite peak was also detected at 24.2^{o} 2θ. The peak positions and the shapes did not change above 1298 K as seen from Figures D.6(c) and D.6(d). The main crystalline phases were determined as gehlenite and wollastonite in the microstructure of the sintered OFA samples.

Both surface and the microcrystalline SEM investigations were conducted on the sintered OFA samples. Figure 6.103 (a) shows the surface of the OFA1273 sample. The surface of the OFA1273 sample was rough and some porosity was also detected. With the increase in sintering temperature, the surface of the sintered samples was getting smoother as seen from Figure 6.104(a). The surface of the OFA1298 sample was still rough but it was smoother than the OFA1273 sample. The porosity was less than of the OFA1273 sample. The surface of the OFA1323 sample was smoother than those of the OFA1273 and 1298 samples. (Figure 6.105(a)). Some porosity still existed on the surface of the OFA1323 sample. Figure 6.106(a) shows the smooth surface of OFA1348 sample with less porosity. The pore size decreased with the increase in sintering temperature.

Microstructural SEM investigations were performed also at higher magnifications. Figure 6.103(b) shows the dentritic crystallites occurred in the OFA1273 sample. The shape of the crystallites resembles to flower. There was also some glassy phase determined in the OFA1273 sample. The same structure was also observed in the OFA1298 sample as seen from Figure 6.104 (b). Same crystallites and some glassy regions were observed in the OFA1298 sample. Further increase in sintering temperatures resulted to change the shape and the size of the crystallites (Figure 6.105(b)). The more dense crystalline structure was obtained with dentritic crystallites. The shape of the crystallites was like a leaf-shaped as it was observed in the microstructure of the ORSGC samples. The same crystalline shape was also observed in the microstructure of the OFA1348 sample (Figure 6.106(b)). It was also observed that the small amount of glassy phase remained in the microstructure of the OFA1348 sample.

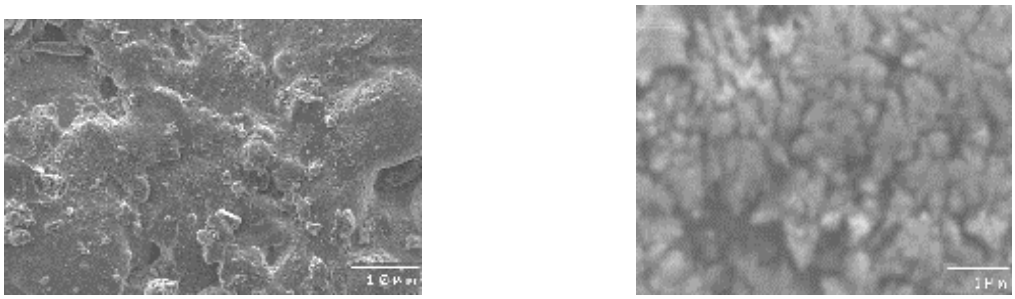

(a) (b)

Figure 6.103: SEM micrographs of OFA1273 sample at lower(a) and higher magnifications (b)

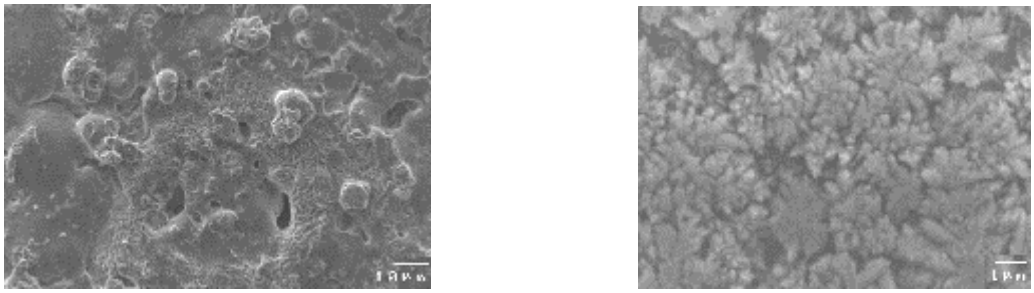

(a) (b)

Figure 6.104: SEM micrographs of OFA1298 sample at lower(a) and higher magnifications (b)

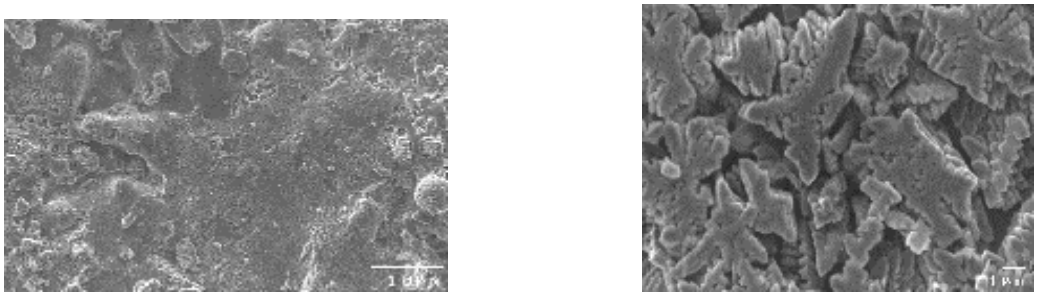

(a) (b)

Figure 6.105: SEM micrographs of OFA1323 sample at lower(a) and higher magnifications (b)

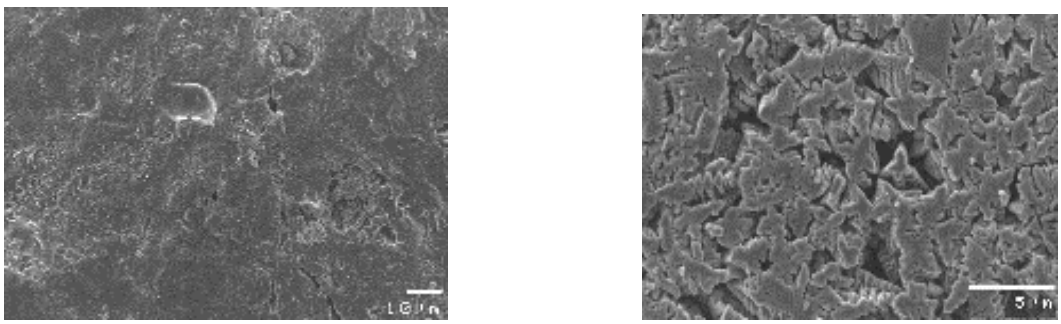

(a) (b)

Figure 6.106: SEM micrographs of OFA1348 sample at lower(a) and higher magnifications (b)

6.8.6.2 Physical and mechanical properties of the sintered OFA samples

Table 6.52 shows the variations in density, water absorption, porosity and the Rockwell hardness values with sintering temperatures. The density values of the pressed and the sintered OFA samples were ranging from 2.5 g/cm^3 to 2.7 g/cm^3. The sintered density slightly increased as increasing firing temperature. The densification degree was low at the lower sintering temperatures because of the high porosity of those sintered samples. The higher density of 2.7 g/cm^3 was achieved at 1348 K. The density values of the sintered samples are better than those of the sintered materials produced in different studies from coal fly ash [239,242,252,254]. The water absorption values increased with the decrease in the sintering temperature. The water absorption rate has been used as an indication of porosity for the sintered materials. The accuracy of this statement was seen from the Table 6.52. Both porosity and water absorption values well correlated each other. The high water absorption and porosity values of pressed Orhaneli fly ash samples decreased from 18.12 % and 24.12 % to 4.12 % and 4.1 %, respectively. The lowest porosity and water absorption values of the OFA1348 sample are indicatives of dense well-sintered microstructure with a minimum volume of porosity. This result is in well agreement with the SEM observations of OFA1348 sample.

Similar to density values, as the sintered materials became more crystalline, the hardness of the sintered OFA samples increases. It is known that the remaining glassy phase resulted to the lower hardness values. Therefore, OFA1273 sample has the lowest hardness value while the OFA1348 sample has the highest hardness value.

6.8.7 Experimental results of the sintered AEFA samples

6.8.7.1 Microstructural changes of the sintered AEFA samples

Afşin-Elbistan fly ash sample was sintered at 1223, 1248, 1273 and 1298 K on the basis of the preliminary experimental trials. The sintering temperatures of AEFA samples were the lowest temperatures among all sintered fly ash samples. This result was expected since the Afşin-Elbistan fly ash sample has the lowest SiO_2+Al_2O_3 content.

The color and the texture of the sintered samples changed when the temperature was raised. The AEFA1223 sample was weak and chalky. The surface of the AEFA1223 sample was also rough compare to the other sintered samples. Sintering in between 1248-1298 K resulted to produce well-sintered materials. Sintering above 1298 K caused to agglomeration and sticking problems in AEFA samples. The grey color of the pressed AEFA sample changed to dark grey by sintering process.

Table 6.52: Properties of OFA samples

Sample Name	Crystalline Phases	Rockwell Hardness	Bulk Density (g/cm^3)	Porosity (%)	Water Absorption (wt. % loss)
Pressed Sample	Quartz, mullite, anorthite and enstatite	32	2.50	24.12	18.12
OFA1273	Gehlenite and wollastonite	39	2.60	18.60	15.78
OFA1298	Gehlenite and wollastonite	47	2.63	14.70	13.98
OFA1323	Gehlenite and wollastonite	68	2.68	10.20	8.16
OFA1348	Gehlenite and wollastonite	72	2.70	4.10	4.12

XRD analysis revealed that the gehlenite ($Ca_2Al_2SiO_7$) and wolastonite ($CaSiO_3$) phases occurred in the pressed AEFA samples after heat treatment. XRD patterns of AEFA1223, AEFA1248, AEFA1273 and AEFA1298 samples can be seen from Figure D.7, respectively in Appendix D. The crystalline phases occurred during the sintering process were also given in Table 6.53. As seen from Table 6.53 quartz, mullite and anorthite phases disappeared when the pressed samples were sintered at different temperatures. Only gehlenite phase remained in the sintered samples. The main crystalline peaks obtained in the AEFA1223 sample corresponded to the gehlenite at 31.5^o 2θ and wollastonite at 25.5^o 2θ. (Figure D.7(a)). As seen from Figure D.7(b), the wollastonite peak at 25.5^o 2θ disappeared when the sintering

temperature was raised to 1248 K. A small wollastonite peak was detected at 29.2^{o} 2θ in the XRD pattern of AEFA1248 sample. The main crystalline phase is gehlenite in the AEFA1248 sample. Figure D.7(c) and D.7(d) show the XRD patterns of AEFA1273 and 1298 samples, respectively. The XRD patterns of these samples are similar to each other and to AEFA1248 sample. The same crystalline phases (gehlenite+wollastonite) were obtained in both OFA and AEFA samples since they had the similar chemical compositions with low SiO_2+Al_2O_3 and high CaO contents. However, gehlenite was the main crystalline phase in AEFA1248, AEFA1273 and AEFA1298 samples comparing to the sintered OFA samples. High CaO content of Afşin-Elbistan fly ash can cause to this result. Chemical composition of Afşin-Elbistan fly ash is close to the CAS system. It can be inferred from the phase diagrams for the ceramics that chemical composition of Afşin-Elbistan fly ash was placed in the phase field of gehlenite. The phase diagrams of ceramics were also supported the XRD results of sintered AEFA samples.

SEM micrographs of the sintered AEFA samples heat treated at 1223-1298 K are shown in Figures 6.107-6.110. The changes occurred as a result of thermal treatment are clear. Figure 6.107(a) shows the surface of the AEFA1223 sample. As seen from Figure 6.107 (a), AEFA1223 sample contained some spherical pores. These pores are believed to form when the glass viscosity falls to a level which gas forming decomposition reactions take place. The gas release can produce the voids observed [255,256]. AEFA1223 sample has a rough surface. As seen from Figure 6.107 (b), sintering at 1223 K resulted in the microstructure of the AEFA1223 sample significant amount of glassy phase. Tiny crystallites were dispersed randomly in the microstructure of AEFA1223 sample. AEFA1248 sample has still a rough surface. However, the amount and the size of the pores decreased when the sintering temperature was raised to 1248 K as it was observed in Figure 6.108(a). The amount of the crystallization increased with the increase in sintering temperature in contrast to the glassy phase content. More dense, interlocked crystalline structure was detected in AEFA1248 sample as seen from Figure 6.108 (b). AEFA1248 and AEFA1273 samples had similar microstructures. The surfaces of both AEFA1248 and AEFA1273 samples are rough and had some porosity. Crystallization degree increased above the sintering temperature of AEFA1248 sample. The amount of glassy phase was also decreased in the AEFA1273 sample as it was observed from

Figure 6.109(b). Further increase in sintering temperature caused to occur a different microcrystalline structure. The surface of the AEFA1298 sample was smoother than those of the sintered AEFA samples. More compact structure with a less porosity occurred on the surface of the sample as a result of sintering temperature (Figure 6.110(a)). The more dense crystalline structure was obtained in AEFA1298 sample. Small crystallites dispersed randomly in the microstructure of the AEFA1298 sample. Some porosity can be seen from Figure 6.110(b).

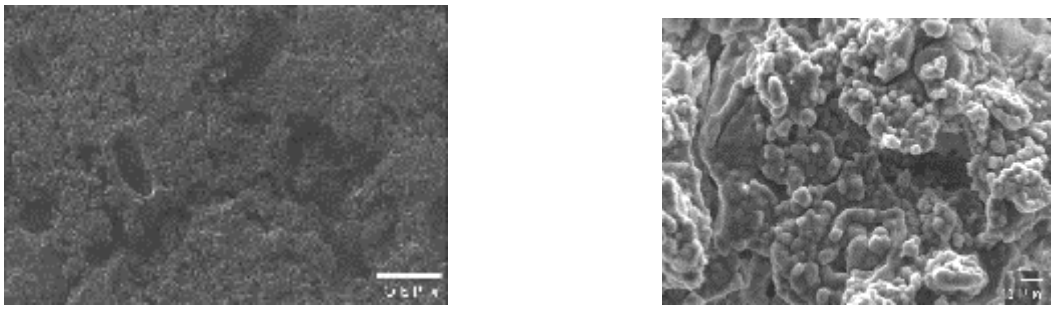

(a) (b)

Figure 6.107: SEM micrographs of AEFA1223 sample at lower(a) and higher magnifications (b)

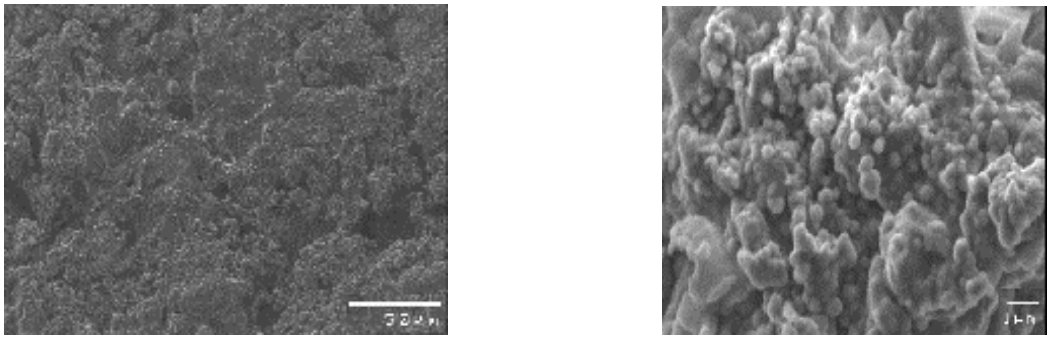

(a) (b)

Figure 6.108: SEM micrographs of AEFA1248 sample at lower(a) and higher magnifications (b)

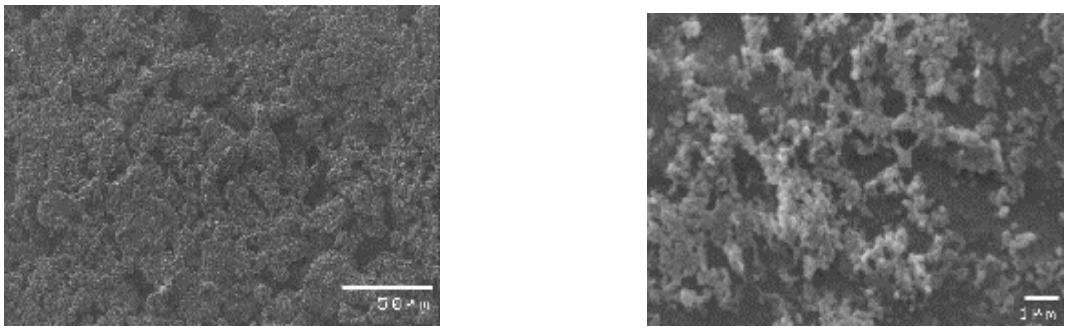

(a) (b)

Figure 6.109: SEM micrographs of AEFA1273 sample at lower(a) and higher magnifications (b)

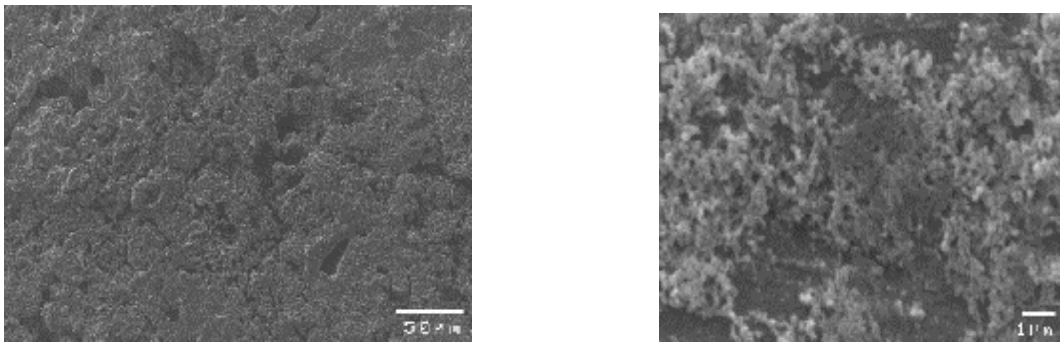

(a) (b)

Figure 6.110: SEM micrographs of AEFA1298 sample at lower(a) and higher magnifications (b)

6.8.7.2 Physical and mechanical properties of the sintered AEFA samples

The effect of firing temperature on the properties of sintered AEFA samples is shown in Table 6.53. The improvement of physical and mechanical properties of sintered materials with the increase in sintering temperature is a common behavior of all samples. The density reached a maximum value of 2.58 g/cm^3 for the sample heat treated at 1298 K. This value is higher than the density values of most of the sintered materials produced in different studies from coal fly, incinerator fly ash and sewage sludge ash [255,257-259]. Vilches et al.[260] obtained fireproof products from coal fly ash with an average density of 0.74 g/cm^3 and high porosity. The density values of the all sintered materials produced in this study even if the pressed samples are much higher than the value reported that by Vilches et al.[260]. The water absorption of the sintered AEFA samples reduced with increasing firing temperature, indicating

a reduction in open, water accessible porosity. This result is in well agreement with the porosimetry studies of sintered AEFA samples. The decrease in porosity and water absorption may be due to formation of low silica glass, which has lower viscosity and flows easily to fill up open pores. As seen from Table 6.53 Rockwell hardness values of sintered AEFA samples are much lower than those of the sintered samples from other fly ashes. This result can be explained with the microstructural formation of the sintered AEFA samples. The crystallization degree and the number of the crystallites occurred on the microstructure of the sintered AEFA samples are so low and the volume of the glassy phase is high compare to the other sintered fly ash samples on the basis of SEM investigations. The volume of the crystallites and the glassy phase are important factors for the hardness of the samples. It was reported that the remaining glassy phase wrecked continuity of the crystal phase and decreased the hardness of the ceramic materials [235]. Therefore, hardness values of sintered AEFA samples were lower than those of the other sintered fly ash samples.

Table 6.53: Properties of AEFA samples

Sample Name	Crystalline Phases	Rockwell Hardness	Bulk Density (g/cm^3)	Porosity (%)	Water Absorption (wt. % loss)
Pressed Sample	Quartz, mullite, anorthite and enstatite	20	2.013	25.20	31.7
AEFA1223	Gehlenite and wollastonite	30	2.180	19.30	26.3
AEFA1248	Gehlenite and wollastonite	38	2.370	18.71	18.3
AEFA1273	Gehlenite and wollastonite	45	2.460	12.16	10.4
AEFA1298	Gehlenite and wollastonite	48	2.580	9.13	7.6

6.8.8 Overall results of the sintered fly ash samples

The experiments carried out have shown that the sintered CFA samples have the best physical, mechanical and microstructural properties among all sintered fly ash samples. The properties of the produced materials are dependent on the sintering conditions. The important variables in the sintering process are determined as: The sintering temperature and time, the particle size and distribution of the powder, the composition of the system and packing pressure. Although the sintering time and packing pressure are the same for all fly ash samples during the sintering process, sintering temperature, particle size and chemical composition of the fly ash samples are different from each other. Sintering temperature of the produced materials is dependent on the chemical composition of the fly ash samples as it was determined previously in this study. Properties of the sintered materials improved with the increase in the sintering temperature. The chemical composition and the particle size of the fly ashes are the other important factors which effect the properties of the resultant materials. The average particle size of Çan fly ash sample is lower than the other fly ash samples except Çatalağzı fly ash sample. The decrease in particle size caused to increase in surface area. Increasing the surface area promotes the sintering process. It was also reported that the decreasing the particle size of fly ash samples resulted to the improvement of the properties of the sintered fly ash samples [245]. Therefore, sintered Çan and Çatalağzı fly ash samples had better properties with the lowest particle size. High Al_2O_3 + SiO_2 contents caused the mullite formation in the sintered CFA samples. It is known that high Al_2O_3 content and mullite formation improve the properties of the ceramic materials [248]. So, sintered material, with the highest hardness value is the CFA1448 sample that had the highest crystallization degree with the lowest glassy phase. The low Al_2O_3 + SiO_2 content of Afşin-Elbistan fly ash resulted to the worst microcrystalline structure in the sintered AEFA samples compare to the other sintered fly ash samples in this study. Overall results showed that using a simple, cost effective powder technology method and relatively low sintering temperatures sufficiently dense materials produced from coal fly ashes.

7. CONCLUSIONS AND RECOMMENDATIONS

7.1 Conclusions

In this study, the possibility of using waste coal fly ashes, silica fume and red mud in glass, glass-ceramic and ceramic production as a raw material source was investigated. It was aimed at the optimizing the experimental condition for the development of glass, glass-ceramic and ceramic materials from these industrial wastes. On the basis of the results reported in this study, the following conclusions can be drawn:

1- Seyitömer, Tunçbilek, Çayırhan, Orhaneli, Afşin-Elbistan fly ash ashes were successfully vitrified without any additives. Glass samples can not be produced from Çan and Çatalağzı fly ashes because of the high viscosity of their melts at 1773 K.
2- DTA graphs of the AEG, TG, CG, OG and SG samples showed endothermic peaks corresponding to T_g in the temperature range of 938-1023 K. However, any exothermic peak could not be detected in the DTA graphs of these samples except TG sample.
3- XRD patterns of the glass samples indicated the amorphous state of all glass samples. No significant crystalline phase could be determined.
4- SEM investigations of the produced glasses showed that all samples had featureless surfaces and were bubble free and homogeneous without any crystalline structure. However, a significant volume of spherical pores in the glass matrix of AEG sample was detected.
5- Physical and mechanical properties of the produced glasses strictly depended on the amount of SiO_2 and Al_2O_3 content of the flay ash samples. Density and microhardness values of the glass samples increased with higher SiO_2 + Al_2O_3 content. Both water adsorption and porosity correlated well with each other and decreased with the increase of the density values of the produced glasses.

6- TCLP results indicated that the heavy metals successfully solidified into the glass matrix of all samples. Since the produced glass samples showed high leaching resistance they can be taken as non-hazaourdous materials.

7- The chemical durability of glasses was good enough. However, they have relatively high weight losses for HNO_3 durability. The produced glasses show high resistance to alkali solutions rather than acidic solutions.

8- AEG sample had the worst properties of all glass samples because of the lowest SiO_2-Al_2O_3, which are main glass network formers, content of Afşin-Elbistan fly ash.

9- When the heat-treatment process was applied to the glass samples, the amorphous phase had practically disappeared and diopside, augite, gehlenite and wollastonite phases occurred in the samples.

10- It was observed that high Al_2O_3 and Fe_2O_3 contents of fly ash samples had great influence on the microcrystalline structure of the heat-treated glass samples. TG1000 samples had the best microcrystalline structure in all heat-treated samples because of the high Al_2O_3 and Fe_2O_3 content of Tunçbilek fly ash.

11- Physical, mechanical and chemical properties of the heat-treated glass samples are better than those of the produced glass samples. It is clearly seen that heat treatment process improved the properties of the glass samples.

12- Glasses which are suitable for glass-ceramic production were obtained from Çayırhan, Orhaneli fly ashes with the addition of red mud and silica fume. The studies on the re-production of glasses from Seyitömer and Afşin-Elbistan fly ashes with the addition of red mud and silica fume showed that those glasses were not suitable for glass-ceramic production since they had no crystallization tendency.

13- DTA results of the produced glass samples showed that crystallization peak temperatures increased with the increase in particle size, while the crystallization peak height decreased.

14- Using the Ozawa equation, the Avrami constants, n, were calculated as 3.42, 3.68 and 4.84 for coarse CRG, ORSG and TG samples, respectively, indicating that bulk crystallization occurs in all glasses by three dimensional growth. n values of fine samples showed that the crystallization mechanism is one-dimensional surface crystallization.

15- The activation energies of crystal growth which were determined by using non-isothermal methods for the coarse CRG, ORSG and TG glasses are in the range of 233-370 kJ/mol, 305-446 kJ/mol and 444-578 kJ/mol, respectively while the activation energies of fine CRG, ORSG and TG glasses are changed in the range of 369-372 kJ/mol, 444-469 kJ/mol and 645-662 kJ/mol, respectively.

16- The activation energy values for crystallization increased with the decrease in particle size of the waste glasses.

17- The crystallization activation energies determined from Matusita-Sakka and isothermal Kissinger methods are close to each other in each glasses of both coarse and fine particles.

18- On the basis of isothermal analysis, crystallization activation energy values were obtained as 435 kJ/mol, 548 kJ/mol and 297 kJ/mol for coarse ORSG, TG and CG-97 glasses, respectively while the n values of those glasses were 3.37, 4.1 and 2.5, respectively.

19- The crystallization activation energies and n values of fine glasses are in the range of 348-610 kJ/mol and 1.08-1.71, respectively.

20- For coarse glasses, crystallization activation energy values determined by using isothermal method are lower than those of fine glasses as it was observed in the non-isothermal methods.

21- The Avrami constants and crystallization activation energy values of all coarse and fine glasses for the non-isothermal and isothermal methods are roughly close. However, activation energy values obtained from non-isothermal methods were higher than that obtained from isothermal method.

22- On the basis of DTA results, maximum nucleation temperatures, maximum nucleation times and crystallization temperatures of the produced glass samples were determined as 963 K, 4 h and 1135 K for CG glass; 988 K, 2 h and 1188 K for ORSG glass; 948 K, 2 h and 1140 K for TG glass; 958 K, 4 h and 1142 K for CG-97 glass, respectively.

23- The studies on glass-ceramic production showed that CRGC-B60, ORSGC-P60, TGC-B60 and CGC-P60 samples have the best microstructural, mechanical, physical and chemical properties among all glass-ceramic samples produced from Çayırhan, Orhaneli, Tunçbilek fly ashes with or

without the addition of red mud and silica fume at different heat treatment conditions.

24- XRD studies revealed that the crystalline phase of TGC samples is different from the other glass-ceramic sample's crystalline phases since the chemical composition of TG sample is different from the other glass compositions.

25- SEM observations showed that the crystalline size and the shapes of the ORSGC samples are different from those of the other produced glass-ceramic samples.

26- It was also observed that the volume of the crystalline phase increased with the increase in holding time at the crystallization temperature in all glass-ceramic samples and this result caused to improve the physical, mechanical and chemical properties of the glass-ceramic samples.

27- The properties of the bulk glass-ceramic samples were influenced by the glass composition, glass production conditions and the heat treatment process while the properties of the sintered glass-ceramic samples are depending on the glass composition, particle size, the addition of the binder, heating rate, sintering pressure and the firing temperature.

28- TCLP results indicated that the produced glass-ceramic samples can be taken as non-hazardous materials.

29- The results of the sintered CRGC, ORSGC and CGC samples indicated that it is possible to produce sintered glass-ceramic materials by applying the nucleation and crystallization heat treatment processes on the basis of DTA results, instead of using the classical sintering technique of one firing cycle.

30- It was observed that, in all glass-ceramic samples, except TGC-P samples, addition of PVA improved the properties of the produced samples.

31- Owing to their physical, microstructural and mechanical properties, CGC-P60 and TGC-B60 sample have the best properties in all sintered and bulk glass-ceramic samples, respectively.

32- The properties of the bulk glass-ceramic samples are better than those of the produced glass samples.

33- Bulk and sintered glass-ceramic possessing desirable properties to fulfill many applications were produced from Tunçbilek and Çayırhan (obtained in 1997) fly ashes, respectively without any additives by applying suitable heat treatments.

34- It was also noted that Çayırhan (obtained in 2000) and Orhaneli fly ashes can be used as raw materials to produce glass-ceramic materials with or without the addition of red mud and silica fume and those produced materials have several desirable properties that would make them attractive to industrial use in construction, tiling and cladding applications.
35- The sintering process results showed that the properties of the produced materials are depending the sintering temperature and time, the particle size and distribution of the powder, the composition of the system and packing pressure.
36- The properties of the sintered materials improved with the increase in the sintering temperature since the crystallization degree also increased with the increase in sintering temperature.
37- Sintering temperature of the produced materials is strongly dependent on the chemical composition of the fly ash samples.
38- Decreasing the particle size of fly ash samples resulted to the improvement of the properties of the sintered fly ash samples.
39- Higher Al_2O_3 + SiO_2 contents caused to better properties in all sintered materials.
40- The sintered CFA samples have the best physical, mechanical and microstructural properties among all sintered fly ash samples.
41- It can be said that using a simple, cost effective powder technology method and relatively low sintering temperatures resulted to sufficiently dense materials obtained from coal fly ashes.

Overall results showed that it is possible to produce glass, glass-ceramic and sintered materials from coal fly ashes without or with the addition of binder and additives such as PVA, red mud and silica fume. It was observed that microstructures of the produced glass, glass-ceramic and sintered materials were completely different from each other since the production methods and the chemical compositions of those materials were different. The produced bulk glass-ceramic samples had superior properties than the obtained glass and sintered materials. It was also concluded that the produced glass, glass-ceramic and sintered materials can be good candidates for industrial use in the construction sector.

7.2 Recommendations for Future Work

Based on the experimental data collected so far, the following future works are suggested:

1- Seyitömer, Tunçbilek, Çayırhan, Orhaneli, Afşin-Elbistan fly ash ashes were transformed into glass materials. However, glasses can not be produced from Çan and Çatalağzı fly ashes. One goal would be to add different amount of fluxes such as K_2O instead of Na_2O and CaO to be able to produce glass materials.

2- The properties of the glasses produced from Seyitömer, Tunçbilek, Çayırhan, and Orhaneli, fly ashes were better than those of glass obtained from Afşin-Elbistan fly ash. The oxides such as SiO_2 and Al_2O_3 could be added to Afşin-Elbistan fly ash to improve the properties of the glass produced from Afşin-Elbistan fly ash.

3- Glass samples obtained from Seyitömer and Afşin-Elbistan fly ashes can not be transformed into glass-ceramic materials. Different nucleating agents such as TiO_2 and P_2O_5 should be added to those fly ashes to improve the crystallization tendency of the glasses. A more detailed study of the crystallization tendency of glasses produced from Çayırhan, Orhaneli and Tunçbilek fly ashes with various additions of TiO_2 and P_2O_5 should also be undertaken to better understand the behavior of glassy and crystalline forms of those materials.

4- The average glass particle sizes should be widen instead of using only coarse (800-1000 μm) and fine glasses (~ 180 μm) to investigate the effect of particle size on the crystallization mechanism.

5- Glass-ceramic materials with good properties were produced by applying sintering method to the glass powders except TGC-S and TGC-P samples. To improve the properties of TGC-S and TGC-P samples; particle size, the binder, sintering pressure, heating rate and the heat treatment schedule should be changed.

6- Sintered glass-ceramic materials were produced by applying two-step heat treatment schedules which are nucleation and crystallization processes. One firing heat treatment cycle at different temperatures should be applied to the

glass powders to compare one firing cycle method with the two-step heat treatment method.

7- Further investigations on mechanical properties such as bending strength, electrical properties such as dielectric constant will provide valuable information to be able to determine the suitable application areas for the produced glass-ceramic materials.

8- Thermal expansion coefficient of the produced glass-ceramics should be determined to better understanding of the thermal behavior of those samples.

9- Seven different fly ashes were sintered to form ceramic materials. Particle size of the fly ashes, sintering pressure could be changed and different binders could also be added to the fly ashes to get better properties for the produced materials.

10- The properties of the AEFA samples are not good enough comparing with those of other sintered materials. Silica fume should be added to the Afşin-Elbistan fly ash to produce ceramic material with good properties.

11- Seven different coal fly ashes, red mud from aluminum production and silica fume were used as raw material sources in the production of glass, glass-ceramic and sintered materials. Glass, glass-ceramic and sintered materials can be produced from different industrial wastes such as municipal incinerator fly ash, slags obtained from different metallurgical industries and steel fly ash.

8. REFERENCES

[1] Al-Almouidi, A., Maslehuddin, M., 1996, Performance and correlation of the properties of fly ash, cement and concrete, *Cement Concrete Res.*, **18**, 253-260.

[2] McCarthy, M.J., Dhir, P.K., 1999, Towards maximizing the use of fly ash as a binder in concrete, *Cement Concrete Res.*, **78**, 121-132.

[3] Takada, T., Hashimoto, I., Tsutsumi, K., Shibata, Y., Yammer, S., Kamada, T., Inoue, K., Tsuzura, K., Yoshida, K., 1995, Utilization of coal ash from fluidized bed incineration boilers as a road base material, *Resour. Concer. Recycl.*, **14**, 69-77.

[4] Akram, M.H., Gabr, M.A., Head, W.J., 1994, Low cement content stabilization of fly ash/scrubber sludge grouts, Hazardous and Industrial wastes, *Proc. 26th Mid-Atlantic Industrial WasteConference*, Ed. Huang, C.P., Technomart Publishing, 567-575.

[5] Temimi, M., Camps, J.P., Lacquerbe, M., 1995, Valorisation of fly ash in the cold stabilization of clay materials, *Resour. Concer. Recycl.,* **15**, 219-234.

[6] Türker, P., Erdoğan, B., Katras, F., Yeğinobalı, A., 2004, Türkiye'deki uçucu küllerin sınıflandırılması ve özellikleri, Türkiye Çimento Müstahsilleri Birliği, Ar-Ge Enstitüsü, Ankara.

[7] Iyer, R.S., Scott, J.A., 2001, Power station fly ash- a review of value added utilization outside of the construction industry, *Resour. Conser. Recycl.*, **31**, 217-228.

[8] Bocaccini, A.R., Kopf, M., Stunpfe, W., 1995, Glass-ceramics from filter dusts from waste incinerator, *Ceramic International*, **21**, 231-235.

[9] Suzuki, S., Tanaka, M., Koneko, T., 1997, Glass-ceramic from sewage sludge ash, *J. Materials Sci.*, **32**, 1775-1779.

[10] Boccacini, A.R., Petitmermet, M., Wintermantel, E., 1997, Glass-ceramics from municipal incinerator fly ash, *Am. Ceram. Soc. Bull.*, **Nov. 97**, 75-78.

[11] Barbieri, L., Manfredini, T., Queralt, I., Rincon, J. M. and Romero,M., 1997, Vitrification of fly ash from thermal power stations, *Glass Technology*, **38**, 165-170.

[12] Sivasundaram, M., 2000, Glass-ceramics from pulp and paper waste ash, *MSc. Thesis*, Department of Mining and Metallurgical Engineering, McGill University, Canada.

[13] James, P.F, 1995, Glass-ceramics: New composition and uses, *J. Non-crystalline Solids*, **181**, 1-15.

[14] Partridge, G., 1994, An overview of glass-ceramics Part I: Development and principal bulk applications, *Glass Tech.*, **35**, 116-127.

[15] Queralt, I., Querol, X., Lopez-Soler, A. and Plana, F., 1997, Use of coal fly ash for ceramics : a case study for a large Spanish power station, *Fuel*, **76**, 787-791.

[16] Carty, V.M., Senapati, U., 1998, Porcelain-Raw materials, processing, phase evaluation and mechanical behaviour, *J. Am. Ceram. Soc.*, **81**, 3-20.

[17] Palmonari, C., Nassetti, G., 1994, Evaluation and future trends of traditional ceramics, *Am. Ceram. Soc. Bull.*, **73**, 42-46.

[18] McMillan, P.W.,1979, Glass Ceramics, Second Edition, Academic Press, London.

[19] McColm, I.J., 1983, Ceramic Science for Materials Technologist, Chapman and Hall, New York.

[20] Yamane, M., Aso, S., Sakaino, T., 1978, Preparation of gel from metal alkoxide as a precursor of oxide glass, *J. Mater. Sci.*, **13**, 865.

[21] Chiang, Y.M., Birnie, D., Kingery, W.D., 1997, Physical Ceramics, John&Wiley Sons., Inc., New York.

[22] Paul, A., 1990, Chemistry of glasses, Chapman and Hall, 2nd edition, London.

[23] Shelby, J.E., 1997, Introduction to glass science and technology, The Royal Society of Chemistry, Cambridge, UK.,

[24] Varshanaya, A.K., 1994, Fundamentals of inorganic glasses, Academic Press, Inc., San Diego, CA.

[25] Vitrification Technologies for treatment of Hazardous and Radioactive Waste, 1992, EPA Handbook, EPA/625/R-92/002, 1-40

[26] Hemmings, R.T., Berry, E.E., 1988, On the glass in coal fly ashes: Recent advances, *Materials Research Society Symposium Proceedings*, **13**, 3-38.

[27] Vitrification of fly ash, 1997, Technical Documentation, Europlasma, France, 1-26.

[28] Jantzan, C.M., Brown, K.G., 1993, Statistical process control of glass manufactured for nuclear waste disposal, *American Ceramic Society Bulletin*, **72**, 55-59.

[29] McMillan, P.W., 1970, The constitution, microstructure and properties of glass-ceramics, *Phys. Chem. Glasses*, **11**, 224.

[30] Haller, W.K., 1989, Phase separated and reconstructured glasses, In advances in ceramics, Commercial glasses, **18**, Eds. Boyd, D.C. and MacDowell, J.F., *American Ceramic Society*, Westerville, Ohio, 133-139.

[31] Philips, S.V., Crozier, D.S., McMillan, P.W., Taylor, J. McC, 1974, Sea water desalination using glass hollow fire membranes, *Desalination*, **14**, 209-216.

[32] Ford, N., Todhunter, R., 1989, Applications of microporous glass, In glasses and ceramics, Ed. Lewis, M.H., Chapman&Hall, London, 203-225.

[33] Stookey, S.D., 1959, Catalyzed crystallization of glass in theory and practise, *Fifth int. congr. on glass*, Glastech. Ber., 32K, Paper V/1.

[34] James, P.F., 1989, Volume nucleation in silicate glasses, In glasses and ceramics, Ed. Lewis, M.H., Chapman&Hall, London, 59-105.

[35] Partridge, G., 1982, Nucleation and crystallization phenomena in low expansion Li_2O-Al_2O_3-SiO_2 glass-ceramics, *Glass Tech.*, **23**, 133-138.

[36] Strand, Z., 1986, Glass-ceramic materials, Glass science and technology, Elsevier, Amsterdam.

[37] Pye, L.D., Stevens, H.J., LaCourse, W.C., 1972, Introduction of glass science, Plenum Press, New York.

[38] Matusita, K., Sakka, S., Matsui, Y., 1975, Determining of the activation energy of crystal growth by DTA, *J. of Materials Sci.*, **10**, 961-966.

[39] Matusita, K., Tashiro, M., 1973, *Phys. Chem. Glasses*, **14**, 77. (Taken from reference 38)

[40] Stookey, S.D., 1962, Ceramics made by nucleation glass comparison of microstructure and properties with sintered ceramics, In symposium nucleation and crystallization in glasses and melts, Eds. Reser, M.K., Smith, G., Insley, H., The American Ceramic Society, Colombus, Ohio.

[41] Thakur, R.L., 1971, Determining the stability of nucleating agents for glass-ceramics, In advanced in nucleation and crystallization in glasses, Eds. Hench, L.L., Freiman, S.W., The American Ceramic Society, Colombus, Ohio.

[42] Borchardt, H.J., Daniels, F., 1957, *J. Amer. Ceram. Soc.*, **79**, 41. (Taken from reference 38)

[43] Clinton, D., Mercer, R.A., Miller, R.P., 1970, *J. Mater. Sci.*, **5**, 171. (Taken from reference 38)

[44] Matusita, K., Tashiro, M., 1973, *Phys. Chem. Glasses*, **11**, 471. (Taken from reference 38)

[45] Tomazawa, M., 1972, *Phys. Chem. Glasses*, **13**, 161. (Taken from reference 38)

[46] Ito, M., Sakaino, T.,Moriya, T., 1968, *Bull. Tokyo Inst. Tech.*, **88**, 127. (Taken from reference 38)

[47] Nakagawa, K., Izumitani, T., 1969, *Phys. Chem. Glasses*, **10**, 179. (Taken from reference 38)

[48] Idem, Yogyo-Kyokai-Shi, 1973, *J. Ceram Soc. Japan*, **81**, 500. (Taken from reference 38)

[49] Matusita, K., Maki, T., Tashiro, M., 1975, *Phys. Chem. Glasses*, **7**, 77. (Taken from reference 38)

[50] Fine, M.E., 1964, Introduction to phase transformation in condensed systems, MacMillan, New York.

[51] Matusita, K., Komatsu, T., Yokota, R., 1984, Kinetic of non-isothermal crystallization process and activation energy for crystal growth in amorphous materials, *J. Mat. Sci.*, **19**, 291-296.

[52] Znidarsic, V., Kolar, D., 1991, The crystallization of diabese glass, *J. Mater. Sci.*, **26**, 2490-2494.

[53] Park, H.C., Lee, S.H., Ryu, B.K., Son, M.M., Yasui, I., 1996, Nucleation and crystallization kinetics of $CaO\text{-}Al_2O_3\text{-}2SiO_2$ in powdered anorthite glass, *J. Mater. Sci.*, **31**, 4249-4253.

[54] Matusita, K., Sakka, S., 1980, Kinetic study on crystallization of glass by DTA-criterion on application of Kissinger plot, *J. Non-crystalline Sol.*, **38-39**, 741-746.

[55] Abel-Rahim, M.A., Ibrahim, M.M., Dongol, M., Gaber, A., 1992, *J. Mat. Sci.*, **27** 4685.

[56] Yınnon, H., Uhlmann, D.R., 1983, Application of thermoanalytical techniques to the study of crystallization kinetics in glass forming liquids, Part I :Theory, *J. Non-Cryst. Solids*, **54**, 253.

[57] Donald I.W., 1995, The crystallization kinetics of a glass based on the cordierite composition studied by DTA and DSC, *J. Mater. Sci.*, **30**, 904-915.

[58] Cheng, K., 1999, Determining crystallization kinetic parameters of $Li_2O\text{-}Al_2O_3\text{-}SiO_2$ glass from derivative DTA curves, *Mater. Sci. and Eng.*, **60**, 194-199.

[59] Johnson, W.A., Mehl, R.F., 1939, *Trans. Am. Inst. Min. Metall. Pet. Eng.*, **135**, 416. (Taken from reference 58)

[60] Avrami, M., 1939, *J. Cem. Phys.*, **7**, 1103. (Taken from reference 58)

[61] Avrami, M., 1940, *J. Cem. Phys.*, **8**, 212. (Taken from reference 58)

[62] Avrami, M., 1941, *J. Cem. Phys.*, **9**, 177. (Taken from reference 58)

[63] Kissinger, H.E., 1957, Reaction kinetics in DTA, *Analytical Chemistry*, **29**, 1702-1706.

[64] Basal, N.P., Doremus, R.H., 1984, *J. Therm. Anal.*, **29**, 115. (Taken from reference 58)

[65] Augis, J.A., Bennett, J.E., 1978, *J. Therm. Anal.*, **13**, 283. (Taken from reference 58)

[66] Marotta, A., Saiello, S., Baranda, Buri, A., 1982, *J. Mater. Sci.*, **17**, 105. (Taken from reference 58)

[67] Marseglia, E.M., 1980, *J. Non-Cryst. Solids*, **41**, 31. (Taken from reference 58)

[68] Ozawa, T., 1965, *Bull. Chem. Soc. Japan*, **38**, 1881. (Taken from reference 58)

[69] Takhor, R.T., 1972, Advances in nucleation and crystallization of glasses, *Am. Ceram. Soc.*, Columbus, 166. (Taken from reference 58)

[70] Kissinger, H.E., 1956, *J. Res. Nat. Bur. Standards*, **57**, 217. (Taken from reference 57)

[71] Matusita, K., Sakka, S., 1979, Kinetic study of crystallization of glasses by DSC, *Phy. Chem. Glasses*, **20**, 81-84.

[72] Xu, X.J., Ray. C. S., Day, D.E., 1991, Nucleation and crystallization of Na_2O-2CaO-3SiO_2 glass by DTA, *J. Am. Ceram. Soc.*, **74**, 909-914.

[73] Ozawa, T., 1971, Kinetics of non-isothermal crystallization, *Polymer*, **12**, 150-158.

[74] Jera, A.K., Chaturvedi, M.C., 1992, Phase transformations in materials, Prentice Hall, New Jersey.

[75] Wright, A.F., Fitch, A.N., Hayter, .B., Fender, B.E., 1985, Nucleation and crystallization of cordierite-TiO_2 glass-ceramic, Part I-small angle neutron scattering measurements and simulations, *Phys. Chem. Glasses*, **26**, 113-118.

[76] Lillic, H.R., 1960, Ceramic materials produced from glass, *Glass Tech.*, **1**, 115-120.

[77] Lewis, M.H., 1989, Glasses and glass-ceramics, Chapman and Hall, London.

[78] Partridge, G., 1970, Phases and transformations in lithium-zinc-silicate glass-ceramics, *Glass Tech.*, **20**, 246-251.

[79] De Vikey, R.C., Majunbar, A.J., 1973, The effect of fabrication variables on the preparation of cordierite based glass-ceramics, Part 1-The effect of variations in heat treatments, *Glass Tech.*, **14**, 125-134.
[80] USP 3 407 866, 1968.
[81] Wallece, F.J., Alexander, W.D., Reiter, H., Wilson, M., 1990, The application of glass-ceramics to diesel engine piston crowns, *Br. Ceram. Soc.*, **46**, Ed. Morrel, R., Institute of ceramics, Stoke on trent, 141-148.
[82] Holand, W., Vogel, W., Mortier, W.J., Duvigneaud, P.H., Naessens, G., Plumat, E.,1983, A new type of phlogopite crystal in machinable glass-ceramics, *Glass Tech.*, **24**, 318-322.
[83] Corning glass works, 1978, Macor machinable glass-ceramic, Leaflet issued by the materials business, Corning glass works, New York.
[84] Leng-Ward, G., Lewis, M.H., 1989, Oxynitride glasses and their glass-ceramic dervatives, *Glasses and glass-ceramics*, 106-155.
[85] Brow, R.K., Pantano, C.G., 1984, Nitrogen coordination in oxynitride glasses, *Comm. Am. Ceram. Soc.*, **67**, 72-75.
[86] Partridge, G., 1992, Glass-ceramics with unusual electric properties, *Adv. Mater.*, **4**, 668-673.
[87] BP 905 253, 1962.
[88] BP 1 003 898, 1965.
[89] Hayward, P.J., 1988, The use of glass-ceramics for immobilising high level wastes from nuclear fuel recycling, *Glass Tech.*, **29**, 122-136.
[90] Hayward, P.J., Vance E.R., Cann, C.D., Doern, D.C.,1989, Crystallization of titonisilicate glasses for nuclear waste immobilization, *J. Am. Ceram. Soc.*, **72**, 579-586.
[91] Beal, G.H., Duke, D.A., 1969, Transparent glass-ceramics, *J. Mater. Sci.*, **4**, 340-352.
[92] Partridge, G., Philips, S.V.A., 1991, A review of transparency in glass-ceramics, *Glass Tech.*, **32**, 82-90.
[93] Partridge, G., 1991, Electromagnetic windows, Electronic ceramics, Ed. Steele, B.C.H., Elsevier Science Publishers, London, 121-145.
[94] Hiller, S., 1983, Gas laser tubes, a challenge for glasses and glass-ceramics, *Glass Tech.*, **24**, 302-308.

[95] Partridge, G., 1991, Glass-ceramics wide ranging engineering materials, Glass Production Technology International, Ed. Rawson, H., Sterling Publications International Ltd., London, 203-210.

[96] Hyde, A.R., Partridge, G., 1990, Composite coating on metals, *Br. Ceram. Proc.*, **46**, Advanced Eng. with Ceram., Ed. Morrel, R., Institute of ceramics, Stoke on trent, 345-350. (Taken from reference 14)

[97] Lewis, C.F., 1991, Cool applications of high superconductors, *Mater. Edge*, 17-20. (Taken from reference 14)

[98] Onishi, M., Kyoto, M., Watanabe, M., 1991, Properties of Ba-Pb-Sr-Ca-Cu-O glass-ceramic fibres formed by glass drawing method, *Jpn. J. Appl. Phys.*, **30**, 988-990.

[99] Zheng, H. Hu, Y., Mackenzie, J.D., 1991, Continuous drawing of Ba-Pb-Sr-Ca-Cu-O glass fibres from a preform, *Appl. Phys. Lett.*, **58**, 1679-1681.

[100] Mack, J., 1987, Advanced ceramics, casting the new part, *Mater. Edge*, 38-48. (Taken from reference 14)

[101] Lin, F.H., Hon, M.H., 1989, A high strength bioglass-ceramic containing $Ca_2P_2O_7$, *J. Aust. Ceram. Soc.*, **1**, 41-49.

[102] Niederamer, G.G., McGee, T.D., Kudej, R.K., 1991, Evaluation of bioactive ceramic composite as a dental implant, *Ceram. Bull.*, **70**, 1010-1015.

[103] Partridge, G., 1992, Glass-ceramics in biomedical applications, *Adv. Mater.*, **4**, 364-367.

[104] www.ics.trieste.it/documents/hightech/newmaterials

[105] Veasey, T. J., 1973, Recent developments in the production of glass-ceramics, *Miner. Sci. Eng.*, **5**, 92-107.

[106] Kim, J.M., Kim, H.S., 2004, Processing and properties of a glass-ceramic from coal fly ash from a thermal power plant through an economic process, *J. Eur. Ceram. Soc.*, **24**, 2825-2833.

[107] Rabinovich, E.M., 1982, Glass in nucleation and crystallization of glasses-Advanced in ceramics, *Am. Ceram. Soc.*, 334.

[108] Cumpston, B., Shadman, F., Risbud, S., 1992, Utilization of coal ash minerals for technological ceramics, *J. Mater. Sci.*, **27**, 1781-1784.

[109] Barbieri, L., I. Lancelotti, T. Manfredini, I. Queralt, J.M., Rincan, M. Romero, 1999, Design, obtainment and properties of glasses and glass-ceramics from coal fly ash, *Fuel*, **78**, 271-276.

[110] Barbieri, L., Lancelotti, I., Manfredini, T., Pellaconi, G.C., Rincon, J.M., Romero, M., 2001, Nucleation and crystallization of new glasses from fly ash originating from thermal power plants, *J. Am. Ceram. Soc.*, **84**, 1851-1858.

[111] Alvarez-Mendez, A., Torres-Gonzalez, L.C., Alvarez, N., Torres-Martinez, L.M., 2003, Kinetic thermal analysis of glass-ceramics from industrial wastes, *J. Non-crystalline Solids*, **329**, 73-76.

[112] Barbieri, L., Ferrari, A.M., Lancelotti, I., Leonelli, C., Rincon, J.M., Romero, M., 2000, Crystallization of (Na_2O-MgO)-CaO-Al_2O_3-SiO_2 glassy systems formulated from waste products, *J. Am. Ceram. Soc.*, **83**, 2515-2520.

[113] Francis, A.A., Rawlings, R.D., Sweeney, R., Boccaccini, A.R., 2002, Processing of coal ash into glass-ceramic products by powder technology and sintering, *Glass Technology*, **43**, 58-62.

[114] Francis, A.A., Rawlings, R.D., Boccaccini, A.R., 2002, Glass-ceramic from mixtures of coal ash and soda lime glass by petrurgic method, *J. Mater. Sci. Lett.*, **21**, 975-980.

[115] Sheng, J., Huang, B.X., Zhang, J., Zhang, H., Sheng, J., Yu, S., Zhang, M., 2003, Production of glass from coal fly ash, *Fuel*, **82**, 181-185.

[116] Peng, F., Liong, K., Hu, A., Shao, H., 2004, Nono-crystal glass-ceramics obtained by crystallization of vitrified coal fly ash, *Fuel*, **83**, 1973-1977.

[117] Leroy, C., Ferro, M.C., Monteiro, R.C.C., Fernandes, M.H.V., 2001, Production of glass-ceramics from coal ashes, *J. European Ceram. Soc.*, **21**, 195-202.

[118] Erol, M., Genç, A., Öveçoğlu, M.L., Küçükbayrak, S., Taptık, Y., Yücelen, E., 2000, Characterization of a glass-ceramic produced from thermal power plant fly ashes, *J. European Ceram. Soc.*, **20**, 2209-2214.

[119] Erol, M., Demirler, U., Küçükbayrak, S., Ersoy-Meriçboyu, A., Öveçoğlu, M.L., 2003, Characterization investigations of a glass-ceramics developed from Seyitömer thermal power plant fly ash, *J. European Ceram. Soc.*, **23**, 757-763.

[120] Erol, M., Küçükbayrak, S., Ersoy-Meriçboyu, A., Öveçoğlu, L., 2004, Characterization of fly ash based glass-ceramic samples quenched in air followed by crystallization stage, *Key Engineering Materials*, **264-268**, 1931-1936.

[121] Van der Sloot, H.A., Hoede, D., 1997, Leaching behavior of amorphous, mixed and crystalline vitrified MSW fly ash, *The Netherlands Energy Research Foundation ECN*, ECN-C-97-003, Petten, The Netherlands.

[122] Park, Y.J., Heo, J., 2002, Vitrification of fly ash from municipal solid waste incinerator, *J. Hazard. Mater.*, **91**, 83-93.

[123] Karamanov, A., Pelino, M., Hreglich, A., 2003, Sintered glass-ceramics from municipal solid waste incinerator fly ashes-part I :The influence of the heating rate on the sinter crystallization, *J. Euro. Ceram. Soc.*, **23**, 827-832.

[124] Karamanov, A., Pelino, M., Salvo M., Metekovits, I., 2003, Sintered glass-ceramics from incinerator fly ashes-part II :The influence of particle size and heat treatment on the properties, *J. Euro. Ceram. Soc.*, **23**, 1609-1615.

[125] Cheng, T.W., 2003, Combined glassification of EAF dust and incinerator fly ash, *Chemosphere*, **50**, 47-51.

[126] Barbieri, L., Corradi, A., Lancelotti, I., 2002, Thermal and chemical behavior of different glasses containing steel fly ash and their transformation into glass-ceramics, *J. Euro. Ceram. Soc.*, **22**, 1759-1765.

[127] Barbieri, L., Corradi, A., Lancelotti, I., 2000, Alkaline and alkaline-earth silicate glasses and glass-ceramics from municipal and industrial wastes, *J. Eur. Ceram. Soc.*, **20**, 2477-2483.

[128] Öveçoğlu, M.L., 1998, Microstructural characterization and physical properties of a slag-based glass-ceramic crystallized at 950 and 1100^{o}C, *J. European Ceram. Soc.*, **18**, 161-168.

[129] Ferreira, E.B., Zanorrto, E.D., Scudeller, L.A.M., 2002, Glass and glass-ceramic from basic oxygen furnace (BOF) slag, *Glass Sci. Technol.*, **75**, 75-86.

[130] Gomes, V. De Borba, C.D.G., Riella, H.G., 2002, Production and characterization of glass-ceramics from steelwork slag, *J. Mater. Sci.*, **37**, 2581-2585.

[131] Romero, M., Rawlings, R.D., Rincon, J.M., 1999, Development of a new glass-ceramic by means of controlled vitrification and crystallization of inorganic wastes from urban incineration, *J. Eur. Ceram. Soc.*, **19**, 2049-2058.

[132] Boccaccini, A.R., Rawlings, R., 2002, Producing of glass-ceramic from waste materials, *Mater. World*, **May**,16-18.

[133]Park, Y.J., Heo, J., 2002, Nucleation and crystallization kinetics of glass derived from incinerator fly ash waste, *Ceramics Int.*, **28**, 669-673.

[134] Cioffi, R., Pernice, P., Aronne, A., Quattroni, G., 1993, Nucleation and Crystal Growth in Fly Ash Derived Glass, *Journal of Materials Science*, **28**, 6591-6594.

[135] Erol, M., Küçükbayrak, S.,Ersoy-Meriçboyu, A., Öveçoğlu, M. L., 2001, Crystallization behavior of glasses produced from fly ash, *Journal of European Ceramic Society*, **21**, 2835-2841.

[136] Erol, M., Küçükbayrak, S., Ersoy-Meriçboyu, A., Öveçoğlu, L., 2004, Crystallization kinetics of fly ash based glasses, *Key Engineering Materials*, **264-268**, 1931-1936.

[137] Francis, A.A., Rawlings, R.D., Sweeney, R., Boccacini, A.R., 2004, Crystallization kinetics of glass particles prepared from a mixture of coal ash and soda lime cullet glass*, J. Non-crystalline Solids*, **333**, 187-193.

[138] Kitalgorodskli, I.I., Bondarov, K.T., 1963, Glass-ceramics-A new universal material, *Soviet Daily Newspaper*, March 22, Pravda.

[139] Davies, M.W., Kerrison, B., Gross, W.E., Robson, M.J., Wichall, D.W., 1970, *J. Iron Steel Inst.*, **208**, 348. (Taken from reference 104)

[140] Riha, K., Mokry, B., 1971, *Hutnik*, **21**, 447. (Taken from reference 104)

[141] Rogers, P., Robertson, J., 1989, *Interceram*, **38**, 37. (Taken from reference 104)

[142] Bickford, D.F., 1993, Proc. 3rd Int. Conf. On advances in fusion and processing of glass, *Ceram. Trans.*, **29**, 473. (Taken from reference 104)

[143] Gorokhovsky, A., Escalante-Garcia, J.I., Gorokhovsky, V., Mescheryakov, D., 2001, Oil-shale ash raw material to produce glass and glass-ceramics, *Am. Ceram. Soc. Bull.*, **80**, 49-52.

[144] Rakhmanbekov, N., Sidykova, T.D., 1992, *Uzb. Khim. Zh.*, **2**, 22. (Taken from reference 104)

[145] Rabinovich, E.M., 1980, The 5th Conf. on mineral eng.: The mineral industry in Israel- The 4th decade of the state, Qiryal Anavim, Israel, 108. (Taken from reference 104)

[146] Pelino, M., Cantalini, C., 1995, Italian patent, RM 93A 000067.

[147] Pelino, M., 2000, Recyling of zinc hydrometallurgy wastes in glass and glass-ceramic materials, *Waste Management*, **20**, 561-568.

[148] Yang, S.Z., Song, H.T., Li, W.G., 1993, *Wuhan gongye daxue xuebao*, **15**, 39. (Taken from reference 104)

[149] Chen, H.J., Ding, D.K., Chen, Y.F., Lin, J., 1988, *Baoli Yu Tangci*, **16**, 1. (Taken from reference 104)

[150] Abdrakhimov, V.Z., 1991, *Izv. Vyssh. Uchebn. Zaved. Stroit. Arkhit.*, **4**, 62. (Taken from reference 104)

[151] Pestryakov, B.V., Pavlov, V., Gavrilin, K.V., 1986, *Khim. Tverd. Topl.*, **5**, 136. (Taken from reference 104)

[152] Li, J.P., Qian, W.J., Li, X.T., 1992, *Wuji, Cailiao Xuebao*, **7**, 251. (Taken from reference 104)

[153] Barbieri, L., Corradi, A., Lancelotti, I., De Oliveira, A.P.N., Alarcon, O.E., 2002, Nucleation and crystal growth of a MgO-CaO-Al_2O_3-SiO_2 glass with added steel fly ash*, J. Am. Ceram. Soc.*, **85**, 670-674.

[154] Boccaccini, A.R., Kopf, M., Stumpfe, W., 1995, Glass-ceramics from filter dusts from waste incinerators, *Ceram. Int.*, **21**, 231-235.

[155] Cheng, T.W., 2004, Effect of additional materials on the properties of glass-ceramic produced from incinerator fly ashes, *Chemosphere*, **56**, 127-131.

[156] Colombo, P., Brusatin, G., Bernardo, E., Scarinci, G., 2003, Inertization and reuse of waste materials by vitrification and fabrication of glass-based products, *Current Opinion Solid State Materials Science*, **7**, 225-239.

[157] Karamanov, A., Gutzow, I., Chamokov, I., Christov, J., Kostov, L., 1994, Synthesis of wall-covering glass-ceramics from waste raw materials, *Glastech. Ber. Glass Sci. Technol*., **67**, 227-230.

[158] Gutzow, I., Pascova, R., Karamanov, A., Schelmelzer, J., 1998, The kinetics of surface induced sinter crystallization and the formation of glass-ceramic materials, *J. Mater. Sci.,* **33**, 5265-5273.

[159] Clark, T.J., Reed, J.S., 1986, Kinetic process involved in the sintering and crystallization of glass powders, *J. Am. Ceram. Soc.*, **69**, 837-846.

[160] Müller, R., Zanotto, E.D., Folkin, V.M., 2000, Surface crystallization of silicate glasses: nucleation sites and kinetics, *J. Non-crystalline Solids*, **274**, 208-231.

[161] Prado, M.O., Zanotto, E.D., 2002, Glass sintering with concurrent crystallization, *C.R. Chimie*, **5**, 773-786.

[162] Karamanov, A., Taglieri, G., Pelino, M., 1998, Iron rich sintered glass-ceramics from industrial wastes, *J. Am. Ceram. Soc.*, **82**, 3006-3012.

[163] Cheng, T.W., Ueng, T.H., Chen, Y.S., Chiu, J.P., 2002, Production of glass-ceramic from incinerator fly ash, *Ceramics Int.*, **28**, 779-783.

[164] Brusatin, G., Bernstein, A.G., Bonsembiante, E., Calzolari, G., Colombo, P., Dall'lgna, R., 2002, Vitrification of hazardous wastes, *Glass Mach. Plants Acc*, **4**, 77-81.

[165] Boccaccini, A.R., Schawohl, J., Kern, H., Schunk, B., Rincon, J.M., Romero, M., 2000, Sintered glass-ceramics from municipal incinerator fly ash, *Glass Tech.*, **41**, 99-105.

[166] Barbieri, L., Corradi, A., Lancelotti, I., 2000, Bulk and sintered glass-ceramics by recycling municipal incinerator bottom ash, *J. Euro. Ceram. Soc.*, **20**, 1637-1643.

[167] Cheng, T.W., Chen, Y.S., 2004, Characterization of glass-ceramics made from incinerator fly ash, *Ceram., Int.*, **30**, 343-349.

[168] German, R.M., 1996, Sintering theory and practice, John&Wiley Sons, New York.

[169] German, R.M., 1994, Powder Metallurgy Science, The Pensilvania State University, 2nd Edition.

[170] Kingery, W.D., 1992, Sintering from prehistoric times to the present, Sintering 91, Eds. Chaklader, A.C.D. and Lund, J.A., Trans. Tech., Brookfield, 1-10.

[171] Smith, D.W., 1983, Elements of powder metallurgy, Ed. E. Klar, Powder Metallurgy, Carnes Publication Service, 7-38.

[172] R. Sadlen, 1983, Designing for powder metals, Ed. Klar, E., Powder Metallurgy, Carnes Publication Service, 43-51.

[173] Thummler, F., Thomma, W., 1967, The sintering process, *Met. Rev.*, **12**, 69-108.

[174] Exner, H.E., 1979, Principles of single phase sintering, *Rev. Powder Met. Phys. Ceram.*, **1**, 7-251.

[175] Waldron, M.B., Daniel, B.L., 1978, Sintering, Heyden, London.

[176] Yon, M.F., 1982, Sintering of ceramics and metals, Advances in powder technology, Ed. Chin, G.Y., *Am. Soc. For Metals*, Metals Park, 99-133.

[177] Handworker, C.A., Blendell, J.E., Coble, R.L., 1988, Sintering of ceramics, Science of ceramics, Eds. Uskokovic, D.P., Palmour, H., Spriggs, R.M., Plenum Press, New York, 3-37.

[178] Shaw, N.J., 1989, Densification and coarsening during solid state sintering of ceramics: A review of models I Densification, *Powder Metallurgy Intern.*, **21**, 16-21.

[179] Shaw, N.J., 1989, Densification and coarsening during solid state sintering of ceramics: A review of models II Grain Growth, *Powder Metallurgy Intern.*, **21**, 31-33.

[180] Shaw, N.J., 1989, Densification and coarsening during solid state sintering of ceramics: A review of models III Coarsening, *Powder Metallurgy Intern.*, **21**, 25-29.

[181] ASTM, 1983, ASTM C618-80-Standard specification for fly ash and raw or calcined natural pozzolan for use as a mineral admixture in Portland cement concrete, in ASTM standards in building codes, Vol. II, Maltimore M.D., USA, 329-332.

[182] MacManis, Kenneth L., 1987, Laboratory evaluation of fly ash treated embankment and base materials, TRB record No.1031.

[183] Luke, W.I., 1961, Nature and distribution of various size in fly ash, Technical report No:6-583, US army engineer waterways experiment station, Vicksburg, 21.

[184] Kost, P.J. (ed.), 1991, Use of fly ash in concrete, ACI manual of concrete practice-Part I-Materials and general properties of concrete, 226.3R.1-226.3R.29,ACI.

[185] www.mrs.org/publications/bulletin2001/June

[186] Allaire, C., 1993, Use of red mud for the production of aluminum reduction cell potlining refractories, *Am. Ceram. Soc. Bull*., **72**,59-64.

[187] Neville, A., Brooks, J.J., 1990, Concrete technology, revised reprint, Longman scientific and technical, Essex.

[188] www.silicafume.org

[189] Malhotra, V. M., Ramachandran, V. S., Feldman, R. F., and Aitcin, Pierre-Claude.
Condensed Silica Fume in Concrete. Florida: CRC Press, Inc.

[190] Annual Book of ASTM Standards,1977, Part 13, Method C-25-72.

[191] Merck Reagents,1982, Complexometric Assay Methods with Titriplex, 30-47, 72-73.

[192] Annual Book of ASTM Standarts,1977, Part 26, D2795-63, Analysis of Coal and Coke Ash.

[193] Karatepe, N.,1996, Değişik Sorbentler Yardımıyla Baca Gazlarından Kükürt Dioksit'in Giderilmesi, *PhD. Thesis*, ITU Institute of Science and Technology.

[194] Ulubaş, T., 2000, Uçucu Küllerin Ağır Metal (Cu^{2+}, Pb^{2+}) Gideriminde Kullanımı, *MSc. Thesis,* ITU Institute of Science and Technology.

[195] Yılmaz,Ş., Özkan,O.T., Günay,V., 1996, Crystallization kinetics of basalt glass, *Ceramics International*, **22**, 477-481.

[196] http://www.calce.umd.edu/general/Facilities/Hardness_ad_.

[197] Annual Book of ASTM Standarts, 2005, D-18, Standard Test Methods for Rockwell Hardness and Rockwell Superficial Hardness for Metallic Materials.

[198] US EPA, 1992, US Environmental Protection Agency Method 1311(Reviewed), Washington DC.

[199] Annual Book of ASTM Standards, 2000, C-20, Standard Test Methods for Appearent Porosity, Water Absorption, Appearent Specific Gravity and Bulk Density of Burned Refractory Brick and Shapes by Boiling Water.

[200] Ellison, AJG, Mazer, J.J., Ebert, W.L., 1994, Effect of glass composition on waste from durability:a critical review, Argonne National Laboratuvary, ANL-92/28.

[201] Sheng, J., 2001, Vitrification of borate waste from nuclear power plant using coal fly ash: (I) Glass formulation development, *Fuel*, **80**, 1365-1369.

[202] Vogel, W., 1992, Glass Chemistry, 2nd edition, Springer, New York, 32-34.

[203] Bansal, N.P., Doremus, R.H., 1985, Handbook of Glass Properties, Academic Press, New York, 223-377.

[204] Shao, H., Liang, K., Zhaou, F., Wang, G., Peng, F., 2004, Characterization of cordierite-based glass-ceramics produced from fly ash, *J. Non-crystalline Solids*, **337**, 157-160.

[205] Park, Y.J., Heo, J., 2002, Vitrification of fly ash from municipal solid waste incinerator, *J. Hazard. Mater*., **B91**, 83-93.

[206] Kavouras, P., Komniou, Ph., Crissafis, K., Kaimakamis, G., Kokkou, S., Paraskevopoulos, K., Karakostas, Th., 2003, Microstructural changes of processed vitrified solid waste products, *J. European Ceram. Soc*., **23**, 1305-1311.

[207] Barbieri, L., Lancelotti, I., Manfredini, T., Pellaconi, G.C., Rincon, J.M., Romero, M., 2001, Nucleation and crystallization of new glasses from fly ash originating from thermal power plants, *J. Am. Ceram. Soc.,* **84**, 1851-1858.

[208] Rogers, P.S., Williamson, J., 1969, The nucleation of crystalline phases in silicate glasses containing iron oxides, *Glass Tech*., **10**, 2049-2058.

[209] Romero, M., Rawlings, R.D., Rincon, J.M., 2000, Crystal nucleation and growth in glasses from inorganic wastes from urban incineration, *J. Non-crystalline solids*, **271**, 106-118.

[210] Kavouras, P., Kaimakamis, G., Ioannidis, Th.A., Kehagias, Th., Komniou, Ph., Kokkou, Pavlidou, E., Antonopoulos, I., Sofoniou, M., Zouboulis, A., Hadjiantoniou, C.P., Nouet, G., Prakouras, A., Karakostas, Th., 2003, Vitrification of lead-rich solid ashes from incineration of hazardous industrial wastes, *Waste Management*, **23**, 361-371.

[211] Boccaccini, A. R., Ondracek, G., Janczak, J. and Kern, H., 1993, Development of composite materials under ecological aspects as recycling concept for coal mining wastes. In *Proceedings of 4th International Symposium on the Reclamation, Treatments and Utilization of Coal Mining Wastes*, Ed. by K. M. Skarzynska, Krakow, Poland, 719-726.

[212] Verduch, A.G., 1980, Materiales obtenidos a partir da rocas y escorias fundidas, *Jornadas Cientificas Sobre Ceramica y Vidrio*, 120-151. (Taken from reference 110)

[213] Raschin G.A., Tschetveritkov, S.D., 1964, Metodo petrocufmico para evaluar materias primas petrurgicas, *Izv. Rev. Inv. Geol. Prospec.,* **9**, 71-79. (Taken from reference 110)

[214] Kanazirsky, M., Yotzo, Y., 1972, Etude preliminiare sur les posibilites geologiques d'ne production au maroc de basaltes fondus, *Mines. Geol.,* **36**, 49-56. (Taken from reference 110)

[215] Mose, A., 1980, *Basalt Phase Diagrams,* Springer-Verlag, New York.

[216] Voldan, J., 1979, Crystallisation controloe des roches fondues, *Verres Refract.,* **19**, 230-233. (Taken from reference 110)

[217] Li, W., Mitchell, B.S., 1999, Nucleation and crystallization in calcium aluminate glasses, *J. Non-Crystalline Solids,* **255**, 199-207.

[218] Ray, C.S., Day, D.E., 1990, Determining the nucleation rate curve for lithium disilicate glass by DTA, *J. American Ceram. Soc.,* **73**, 439-442.

[219] Sung, Y.M., Sung, J.H., 1998, Crystallization behavior of calcium aluminate glass fibres-Part I DTA study, *J. Materials Science*, **33**, 4733-4737.

[220] Ray, C.S., Huang, W., Day, D.E., 1991, Crystallization kinetics of a Lithia-silica glass: Effect of sample characteristics and thermal analysis measurement techniques, *J. American Ceram. Soc.,* **74**, 60-66.

[221] Kim, S.J., Kim, J.E., Rim, Y.H., Yang, Y.S., 2004, Kinetics of non-isothermal crystallization process in various sized $Li_2B_4O_7$ glasses, *Solid State Communications,* **131**, 129-133.

[222] Ray, C.S., Day, D.E., 1996, Identifying internal and surface crystallization by DTA for the glass-to-crystal transformations, *Thermochimica Acta,* **280-281**, 163-174.

[223] Costa, B.J., Poulain, M., Messaddeq, Y., Ribeiro, S.J.L., 2000, Non-isothermal study of the devitrification kinetics of fluoroindate glasses, *J. Non-crystalline Solids,* **273**, 76-80.

[224] Jean, J.H., Fang, Y.C., Dai, S.X., Wilcox, D.L., 2001, Devitrification kinetics and mechanisms of K_2O-CaO-SrO-BaO-B_2O_3-SiO_2 glass-ceramic, *J. American Ceram. Soc.,* **84**, 1354-1360.

[225] Gotor, F.J., Criado, J.M., Malek, J., 2001, Limitations of the Augis and Bennett method for kinetic analysis of he crystallization of glasses and conditions for correct use, *J. American Ceram. Soc.,* **84**, 1797-1802.

[226] Hyatt, M.J., Bansal, N.P., 1996, Crystal growth kinetics in $BaOAl_2O_32SiO_2$ and $SrOAl_2O_32SiO_2$ glasses, *J. Materials Science*, **31**, 172-184.

[227] Husband, J., Aguirre, F., Ferguson, P., Metz, R.B., 1999, Vibrationally, resolved photofragment spectroscopy of FeO^+, *Journal of Chemical Physics,* **3**, 1433-1437.

[228] Barbieri, L., Leonelli, C., Manfredini, T., Siligardi, C., 1993, Non-isothermal kinetic equations applied to crystallization of glasses, *Thermochimica Acta,* **227**, 125-133.

[229] Johnson, B.R., 2001, Kinetics and pathways, for crystallization of amorphous mullite and YAG, *PhD. Thesis*, University of Illinois at Urban Campaign.

[230] Öveçoğlu, M. L., Kuban, B. and Özer, H., 1997, Characterization and crystallization kinetics of a diopside-based glass-ceramic developed from glass industry raw materials*, Journal of the European Ceramic Society*, **17**, 957-962.

[231] Powder Diffraction File, Card no. 21-1276, 1992 Database Edition,JointCommittee on Powder Diffraction Standards (JCPDS), Swathmore, PA, USA.

[232] Hong, K.J., Kim, J.M., Kim, H.S., 2003, Microstructure and properties of CaO-ZrO_2-SiO_2 glass-ceramics prepared by sintering, *Journal of the European Ceramic Society*, **23**, 2193-2202.

[233] Pelino, M., Cantalini, C., Rincon, J.M., 1997, Preparation and properties of glass-ceramic materials obtained by recycling geothite industrial waste, *J. Materials Science*, **32**, 4655-4660.

[234] Haun Labs, 2000, Densification, crystallization and sticking behavior of crushed waste glass sintered in refractory molds with release agents, *Haun Labs Technical Report*, Report No: **GL-00-2**, California, USA.

[235] Peng, F., Liang, K., Hu, A., 2005, Nano-crystal glass-ceramics obtained from high alumina coal fly ash, *Fuel,* **84**, 341-346.

[236] Chick, L.A., Lokken, R.O., Thomas, L.E., 1983, *Ceram. Bull.,* **62**, 505. (Taken from reference 237)

[237] Romero, M., Rincon, J.M., Rawlings, R.D., Boccaccini, A.R., 2001, Use of vitrified urban incinerator waste as a raw material for production of sintered glass-ceramics, *Materials Research Bulletin*, **36**, 383-395.

[238] Lingling, X., Wei, G., Tao, W., Nanru, Y., 2005, Study on fired bricks with replacing clay by fly ash in high volume ratio, *Construction and Building Materials,* **19**, 243-247.

[239] Ilic, M., Cheeseman, C., Sollars, C., Knight, J., 2003, Mineralogy and microstructure of sintered lignite coal fly ash, *Fuel,* **82**, 331-336.

[240] Hernandez-Crespo, M.S., Rincon, J.M., 2001, New porcelainized stoneware materials obtained by recycling of MSW incinerator fly ashes and granite sawing residues, *Ceramics International,* **27**, 713-720.

[241] Jonker, A., Potgieter, J.H., 2005, An evaluation of selected waste resources for utilization in ceramic materials applications, *Journal of the European Ceramic Society*, **25**, 3145-3149.

[242] Artır, R., Yılmaz, Ş., Bindal, C., 2004, Some properties and sintering behavior of B_2O_3 added fly ah, *Key Engineering Materials,* **264-268**, 2477-2480.

[243] Özgen., S., 1991, Advanced Ceramic Materials and Manufacturing Techniques, ITU Institute of Science and Technology Materials Engineering Program Coarse Notes, İstanbul.

[244] Jung, J.S., Park, H.C., Stevens, R., 2001, Mullite ceramics derived from coal fly ash, *J. Materials Science*, **20**, 1089-1091.

[245] Morrel, L., 1989, Handbook of properties of technical and engineering ceramics, Part I-An Introduction for the engineer and designer, HMSO Publications, London.

[246] Pollettini, A., Pomi, R., Trinci, L., Muntoni, A., Mastro, S.L., 2004, Engineering and environmental properties of thermally treated mixtures containing MSWI fly ash and low-cost additives, *Chemosphere,* **56**, 901-910.

[247] Kara, A., Kurama, H., Kara, Y., Kurama, S., 2004, Utilization of coal combustion fly ash in terracotta bodies, *Key Engineering Materials,* **264-268**, 2513-2516.

[248] Schneider H., Okada, K., Pask, J.A., 1994, Mullite and Mullite Ceramics, Wiley Publications, New York.

[249] Kim, H., Kim, T., 2002, Measurement of hardness on traditional ceramics, *Journal of the European Ceramic Society*, **22**, 1437-1445.

[250] Olgun, A., Erdoğan, Y., Ayhan, Y., Zeybek, B., 2005, Development of ceramic tiles from coal fly ash and tincal ore waste, *Ceramics International,* **31**, 153-158.

[251] Benavidez, E., Graselli, C., Quaranta, N., 2003, Densification of ashes from a thermal power plant, *Ceramics International,* **29**, 61-68.

[252] Chandra, N., Agnihotri, N., Bhasin, S., Khan, A.F., 2005, Effect of addition of talc on the sintering characteristics of fly ash based ceramic tiles, *Journal of the European Ceramic Society*, **25**, 81-88.

[253] Ferro, M.C., Leroy, C., Monteito, R.C.C., Fernandes, M.H.V., 2002, Fine-grained glass-ceramics obtained by crystallization of vitrified coal ashes, *Key Engineering Materials,* **230-232**, 408-411.

[254] Fang, Y., Chen, Y., Sisbee, M.R., Roy, D.M., 1996, Microwave sintering of fly ash, *Materials Letters,* **27**, 155-159.

[255] Cheeseman, C.R., Sollars, C.J., McEntee, S., 2003, Properties, microstructure and leaching of sintered sewage sludge ash, *Resource Conservation&Recycling,* **40**, 13-25.

[256] Ducman, V., Mladenovic, A., Suput, J.S., 2002, Lightweight aggregate based on waste glass and its alkali-silica reactivity, *Cement and Concrete Research,* **32**, 223-226.

[257] Dana, K., Das, S., Das, S.K., 2004, Effect of substitution of fly ash for quartz in triaxial kaolin-quartz-feldspar system, *Journal of the European Ceramic Society*, **24**, 3169-3175.

[258] Cheeseman, C.R., Makinde, A., Bethanis, S., 2005, Properties of lightweight aggegate produced by rapid sintering of incinerator bottom ash, *Resource Conservation&Recycling,* **43**, 147-162.

[259] Appendino, P., Ferraris, M., Matekovits, M., Salvo, M., 2004, Production of glass-ceramic bodies from the bottom ashes of municipal solid waste incinerators, *Journal of the European Ceramic Society*, **24**, 803-810.

[260] Vilches, L.F., Fernandez-Pereira, C., Olivars del Valle, J., Vale, J., 2003, Recycling potential of coal fly ash and titanium waste as a new fireproof products, *Chemical Engineering Journal,* **95**, 155-161.

APPENDIX A

X-RAY DIFFRACTION PATTERNS OF THE PRODUCED GLASSES

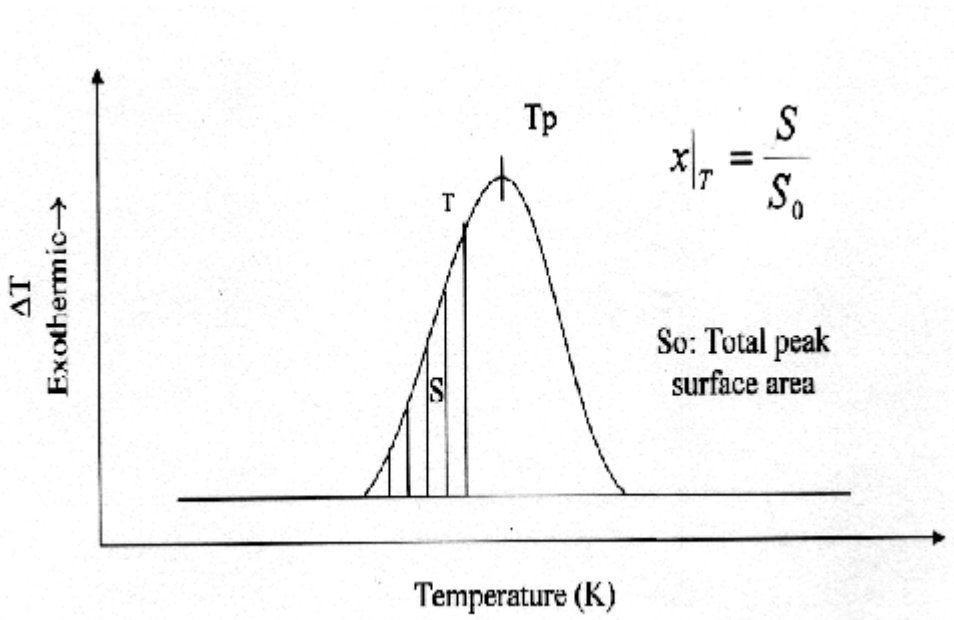

Figure A.1. Method of calculating volume fraction crystallized, $x|_T$, at T

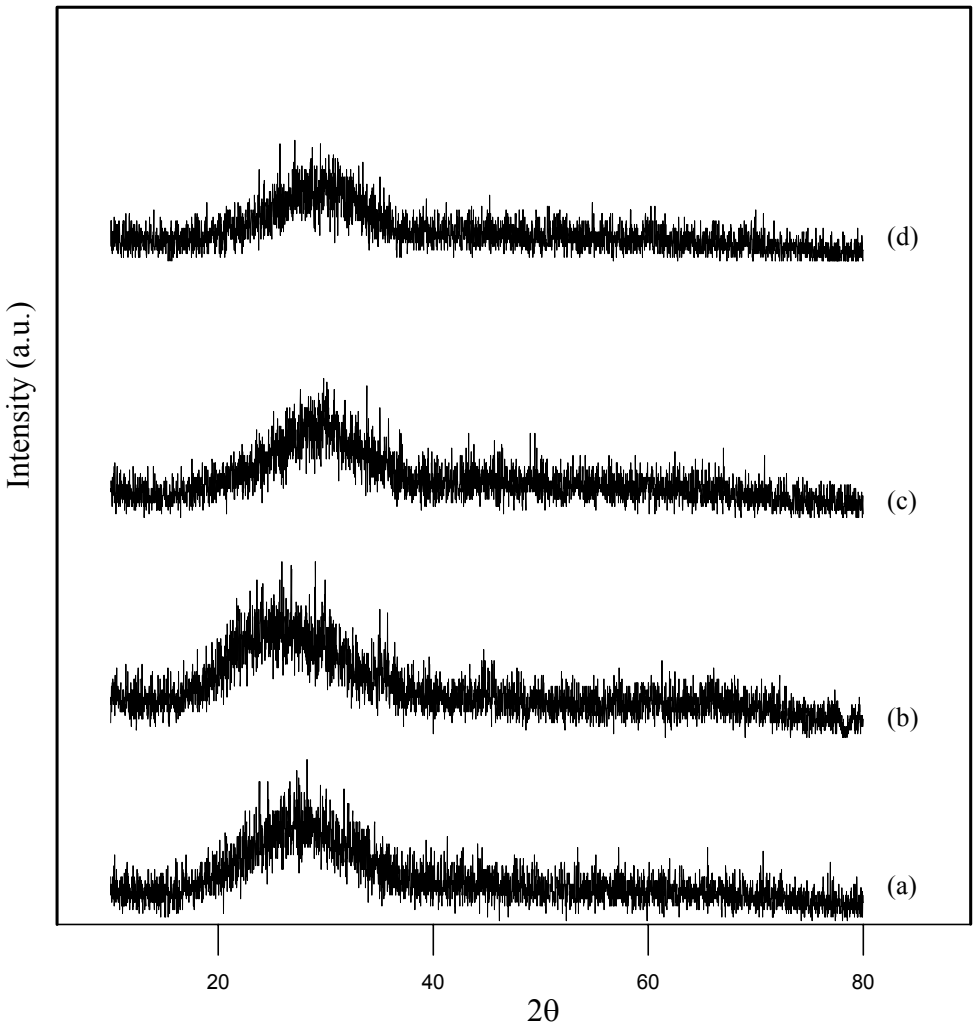

Figure A.2. XRD patterns of CG (a), SG (b), AEG (c) and OG (d)

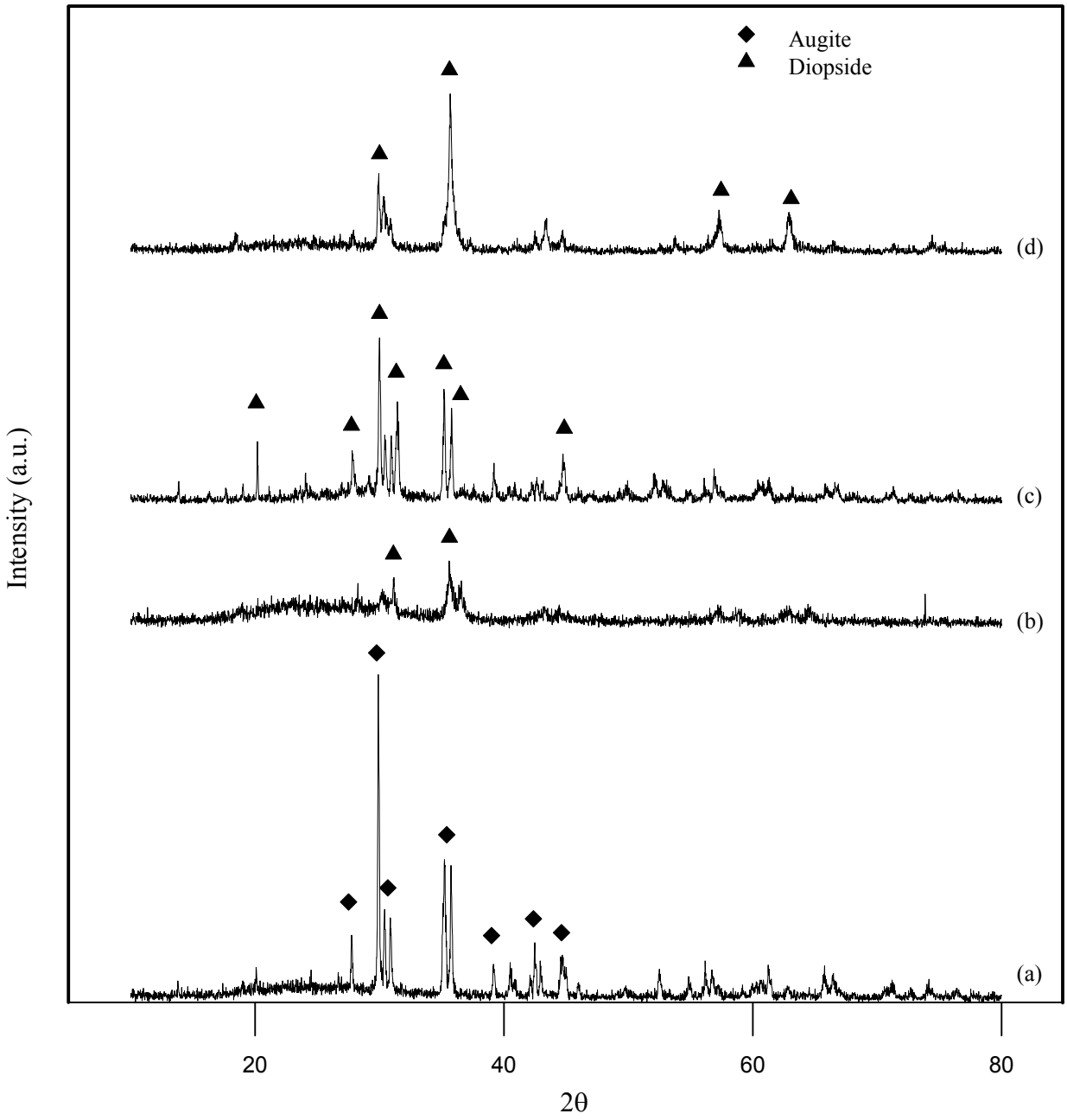

Figure A.3. XRD patterns of TG (a), AEG (b), CG (c) and SG (d)

APPENDIX B

DTA GRAPHS OF THE PRODUCED GLASSES

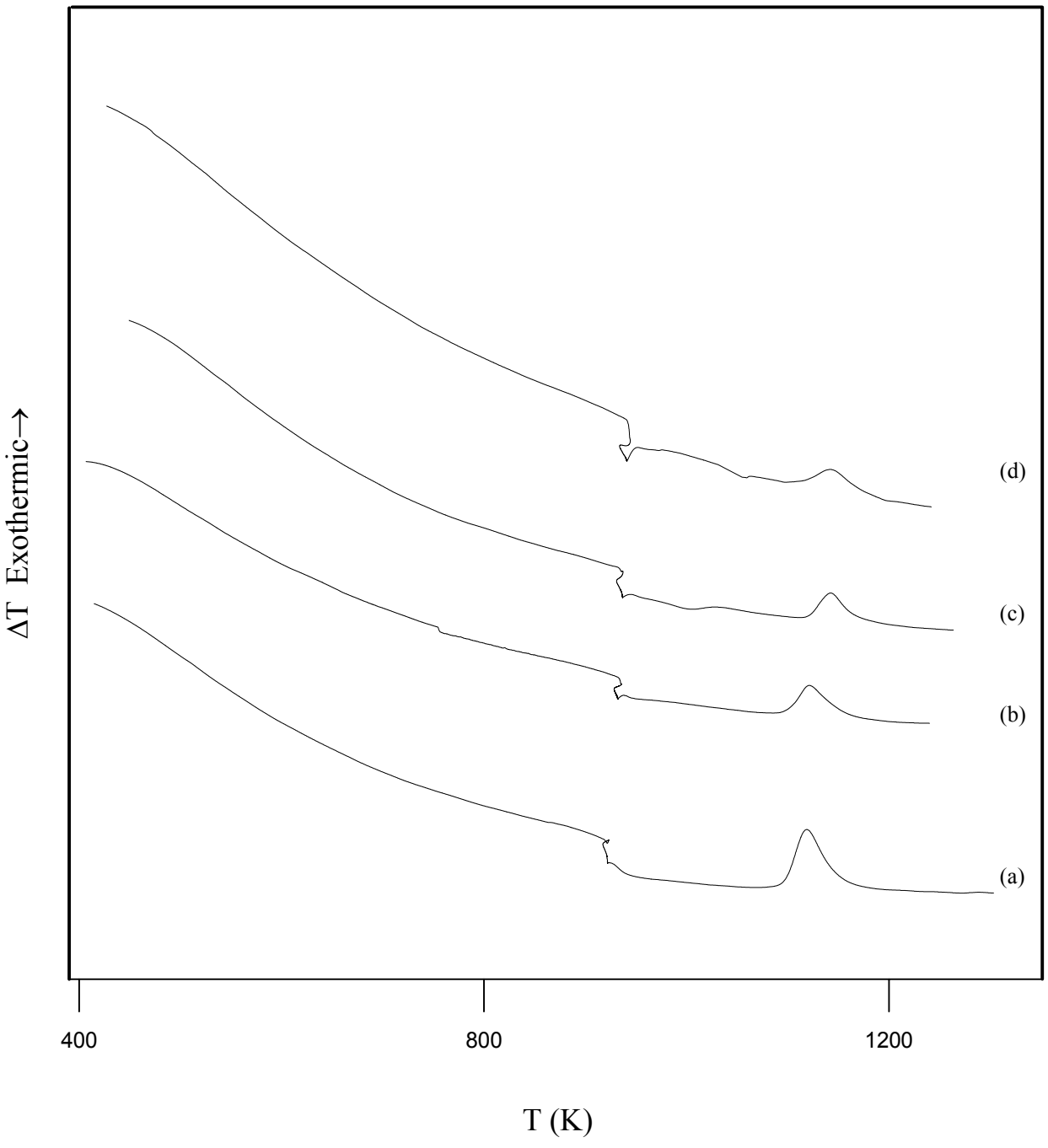

Figure B.1. DTA plots of the CG glasses nucleated at the temperatures of: a) 958 K, b) 963 K, c) 968 K and d) 973 K.

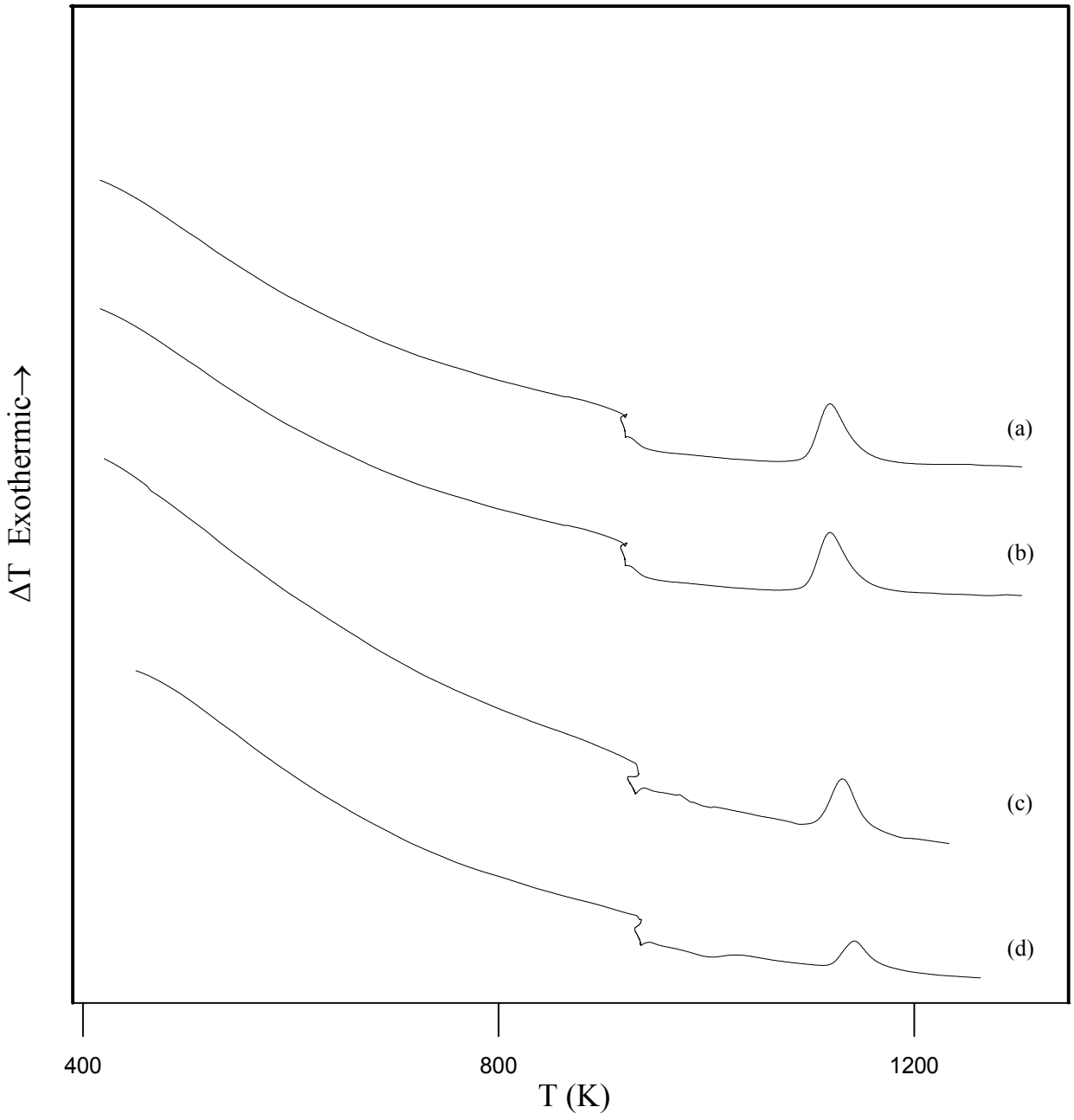

Figure B.2. DTA plots of the CG glasses nucleated at 963 K for the holding times of: a) 1 h, b) 2 h, c) 3 h and d) 4 h.

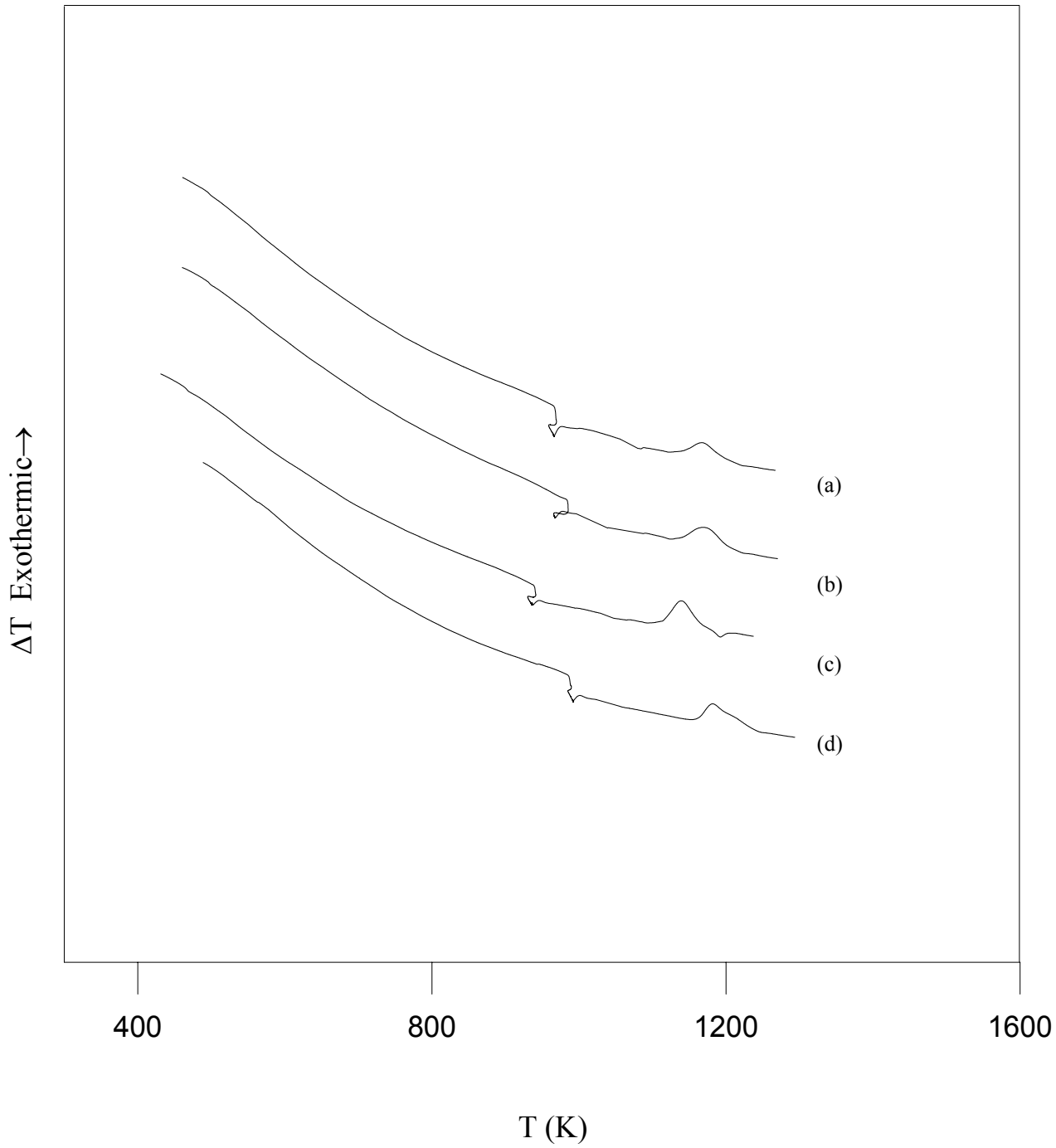

Figure B.3. DTA plots of the ORSG glasses nucleated at the temperatures of: a) 978 K, b) 983 K, c) 988 K and d) 993 K.

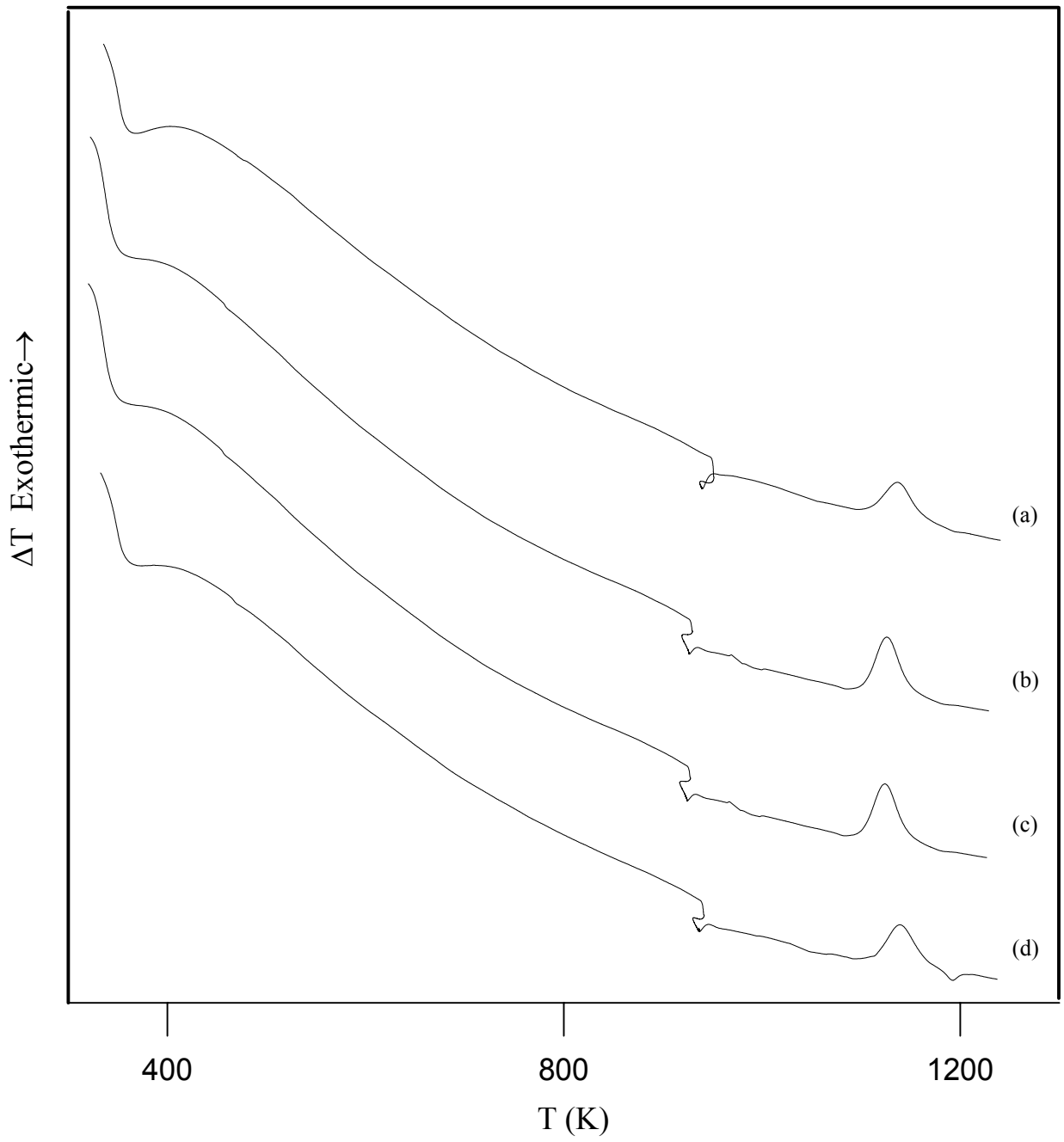

Figure B.4. DTA plots of the ORSG glasses nucleated at 988 K for the holding times of: a) 1 h, b) 2 h, c) 3 h and d) 4 h.

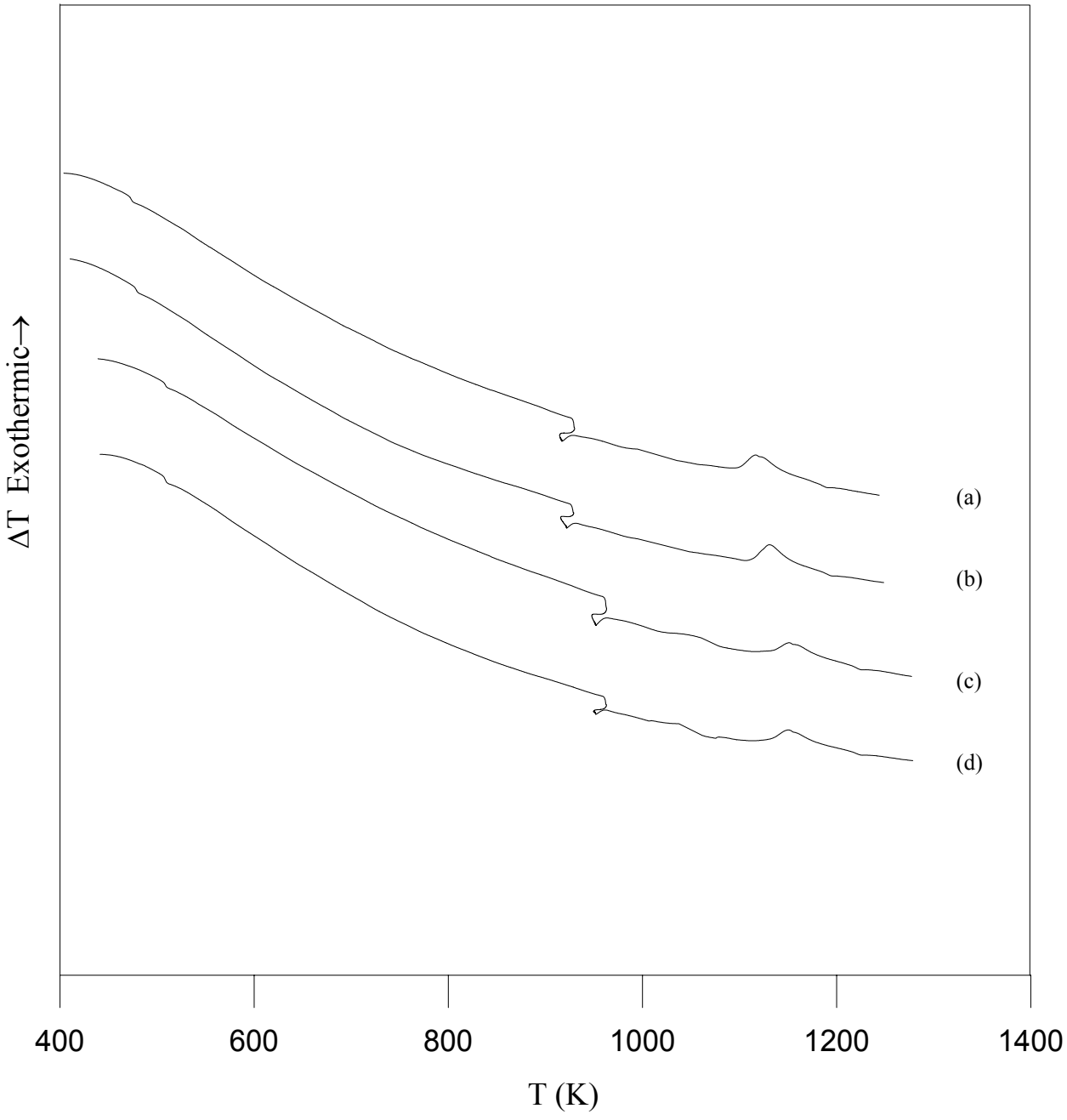

Figure B.5. DTA plots of the TG glasses nucleated at the temperatures of: a) 943 K, b) 948 K, c) 953 K and d) 958 K.

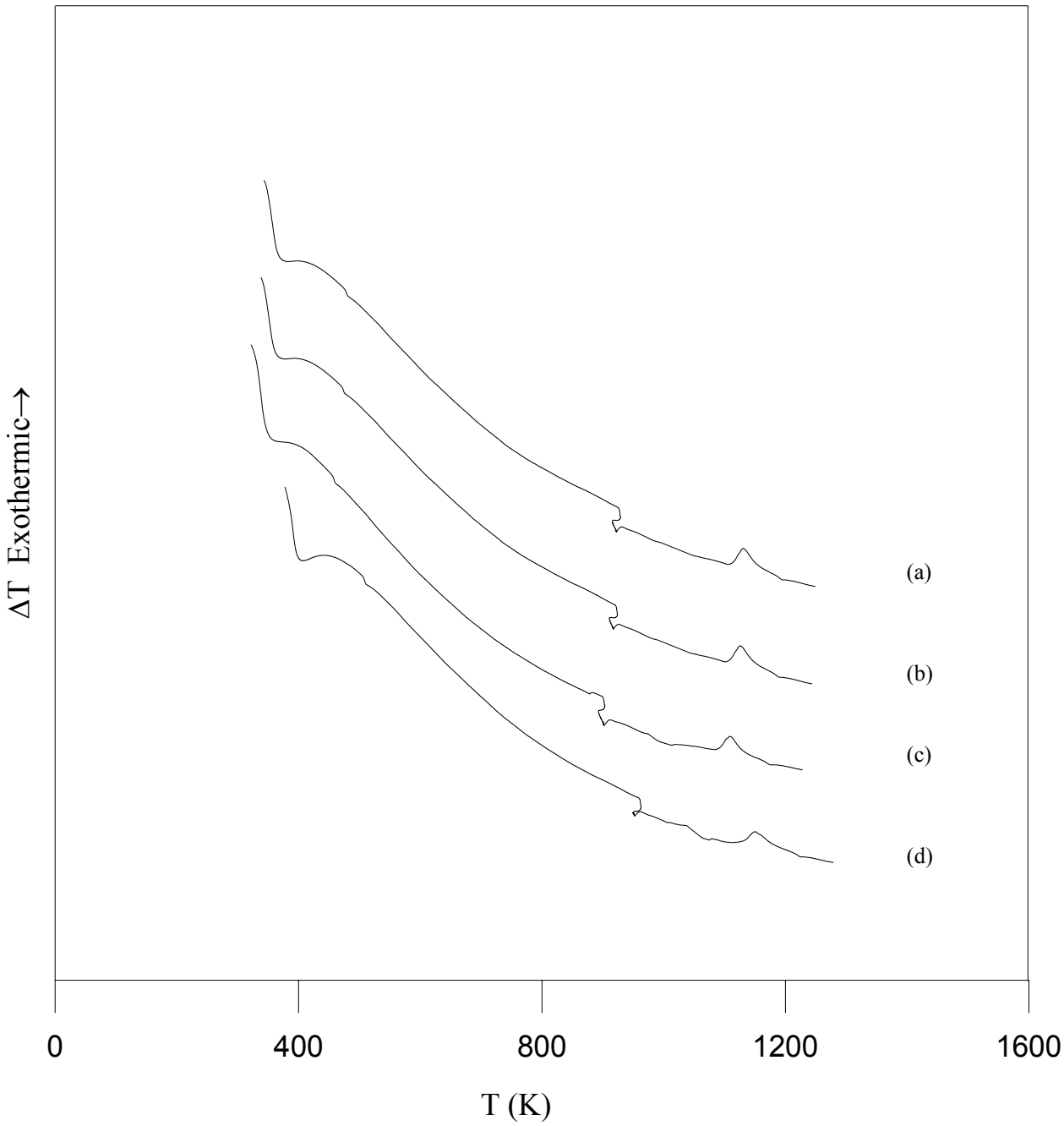

Figure B.6. DTA plots of the TG glasses nucleated at 948 K for the holding times of: a) 1 h, b) 2 h, c) 3 h and d) 4 h.

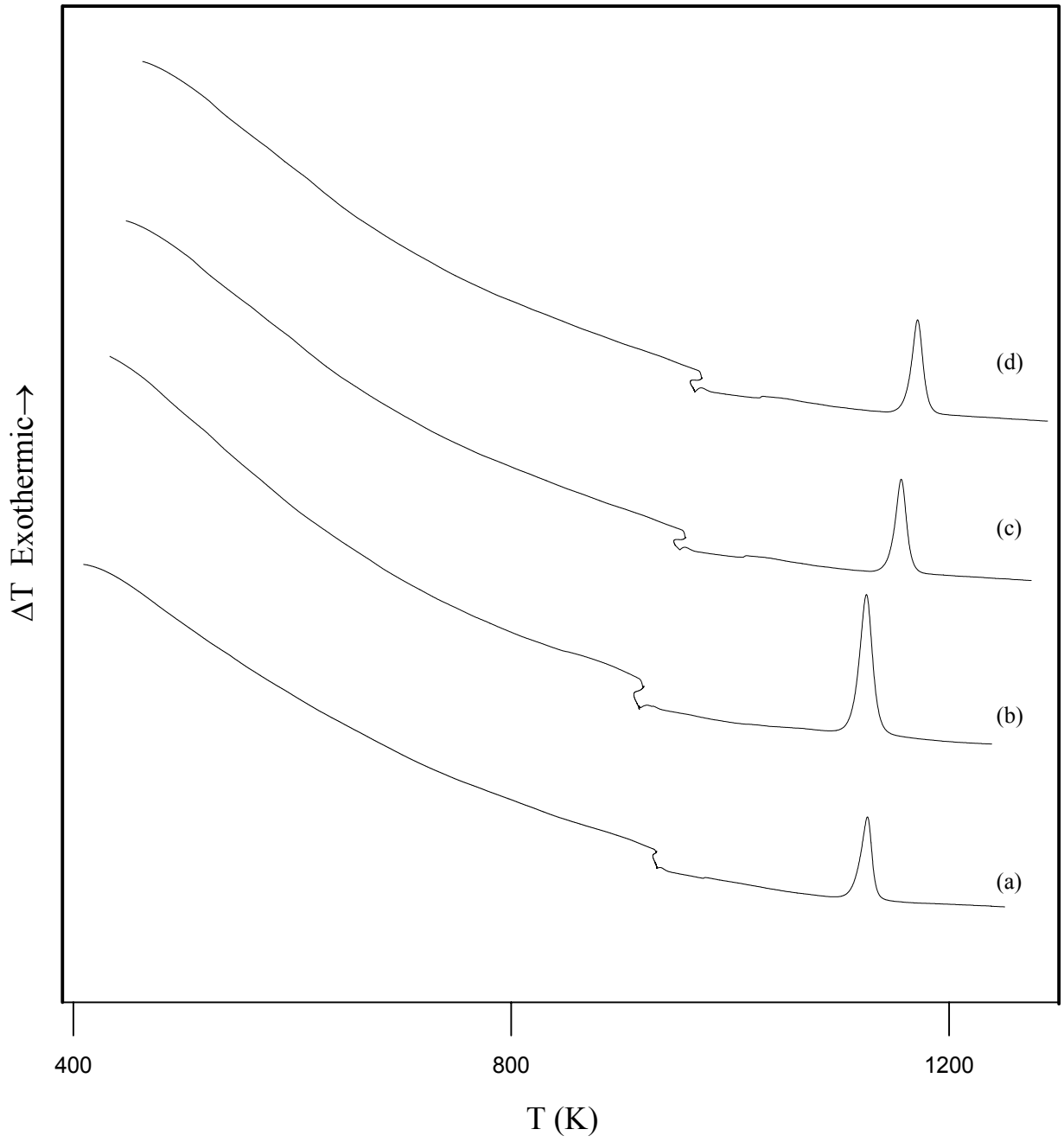

Figure B.7. DTA plots of the CRG glasses nucleated at the temperatures of: a) 953 K, b) 963 K, c) 968 K and d) 973 K.

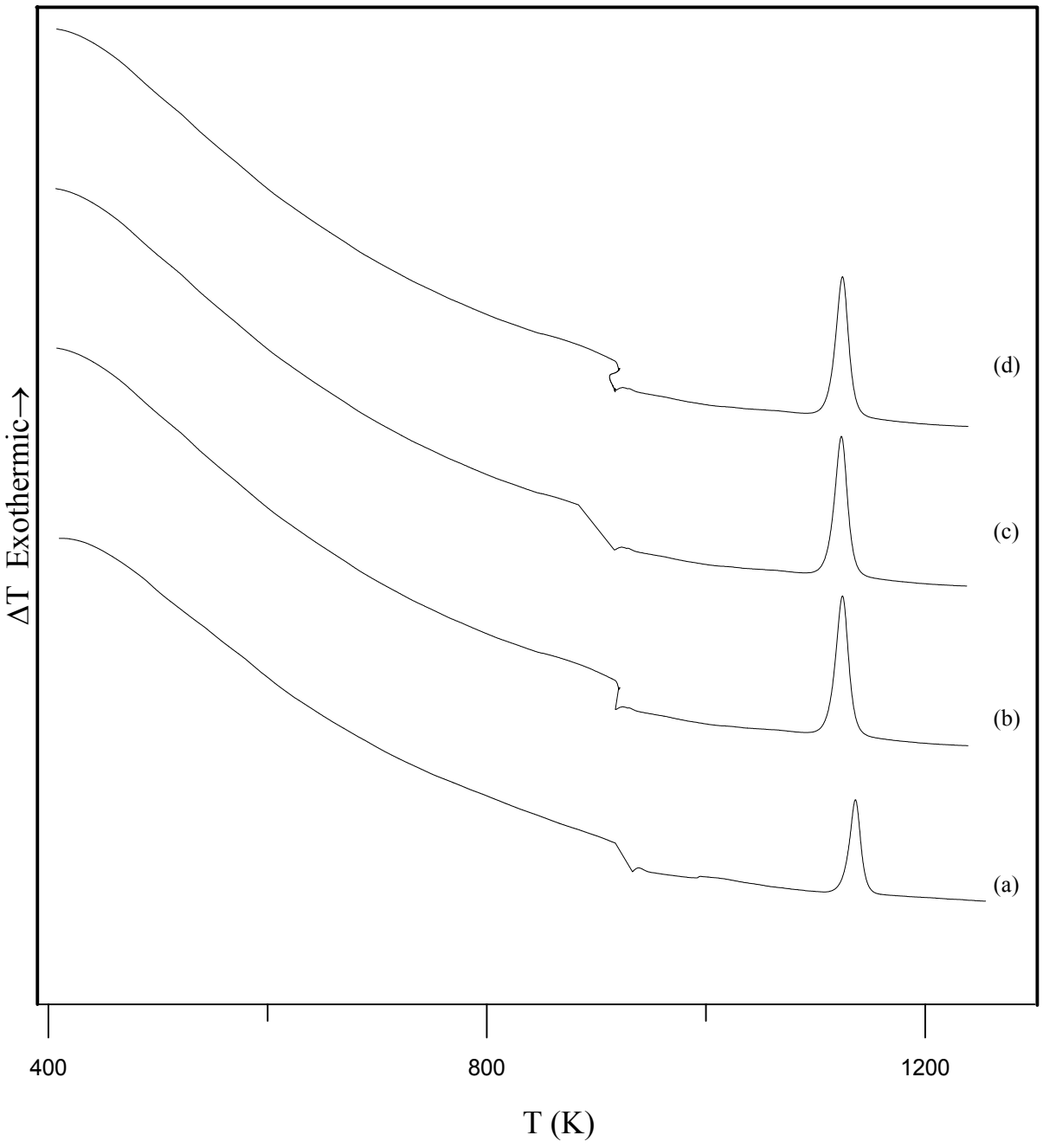

Figure B.8. DTA plots of the CRG glasses nucleated at 988 K for the holding times of: a) 1 h, b) 2 h, c) 3 h and d) 4 h.

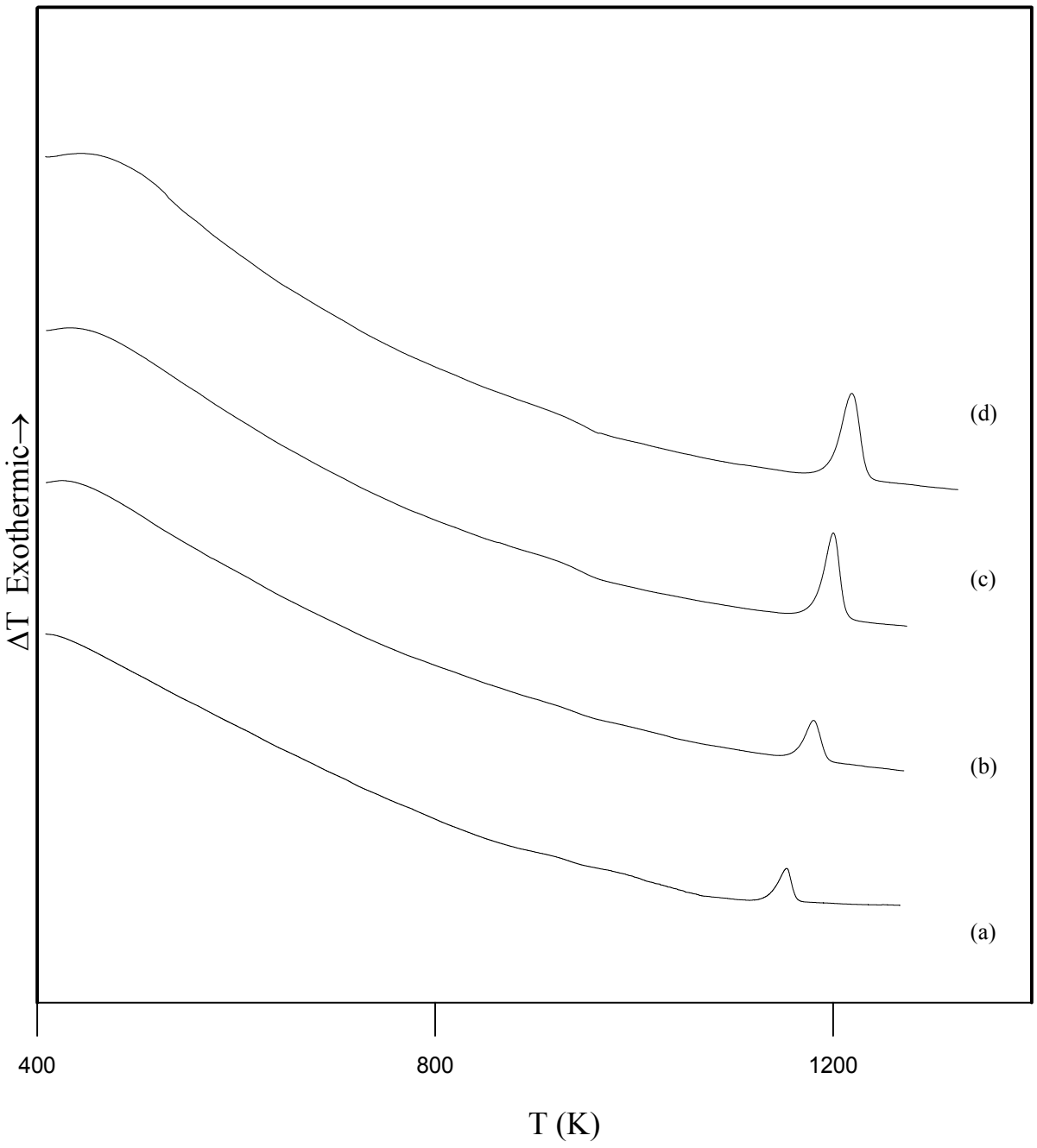

Figure B.9. DTA plots of the coarse CRG glasses scanned at the heating rates of: a) 5 K/min, b) 10 K/min, c) 15 K/min and d) 20 K/min.

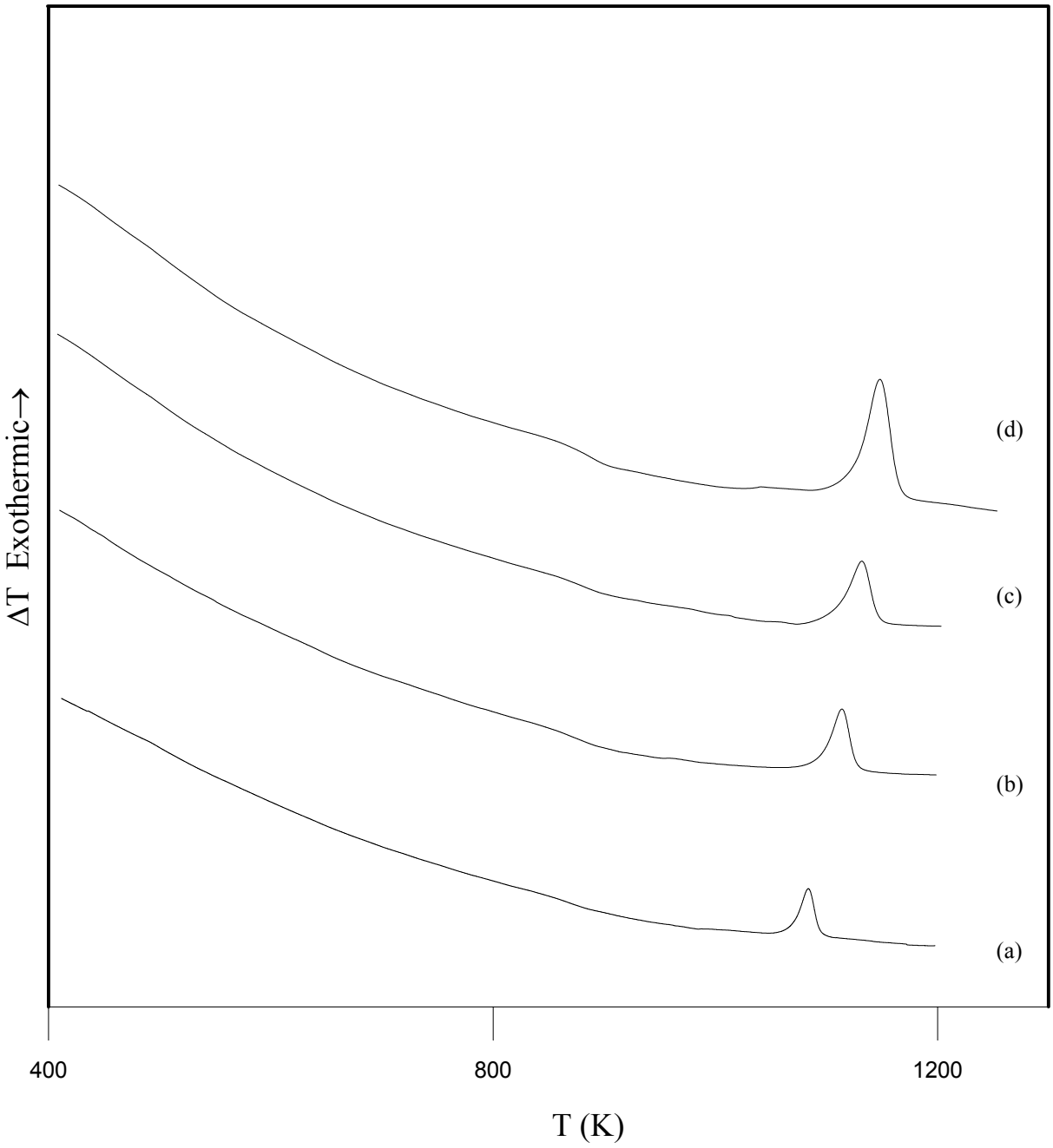

Figure B.10. DTA plots of the fine CRG glasses scanned at the heating rates of: a) 5 K/min, b) 10 K/min, c) 15 K/min and d) 20 K/min.

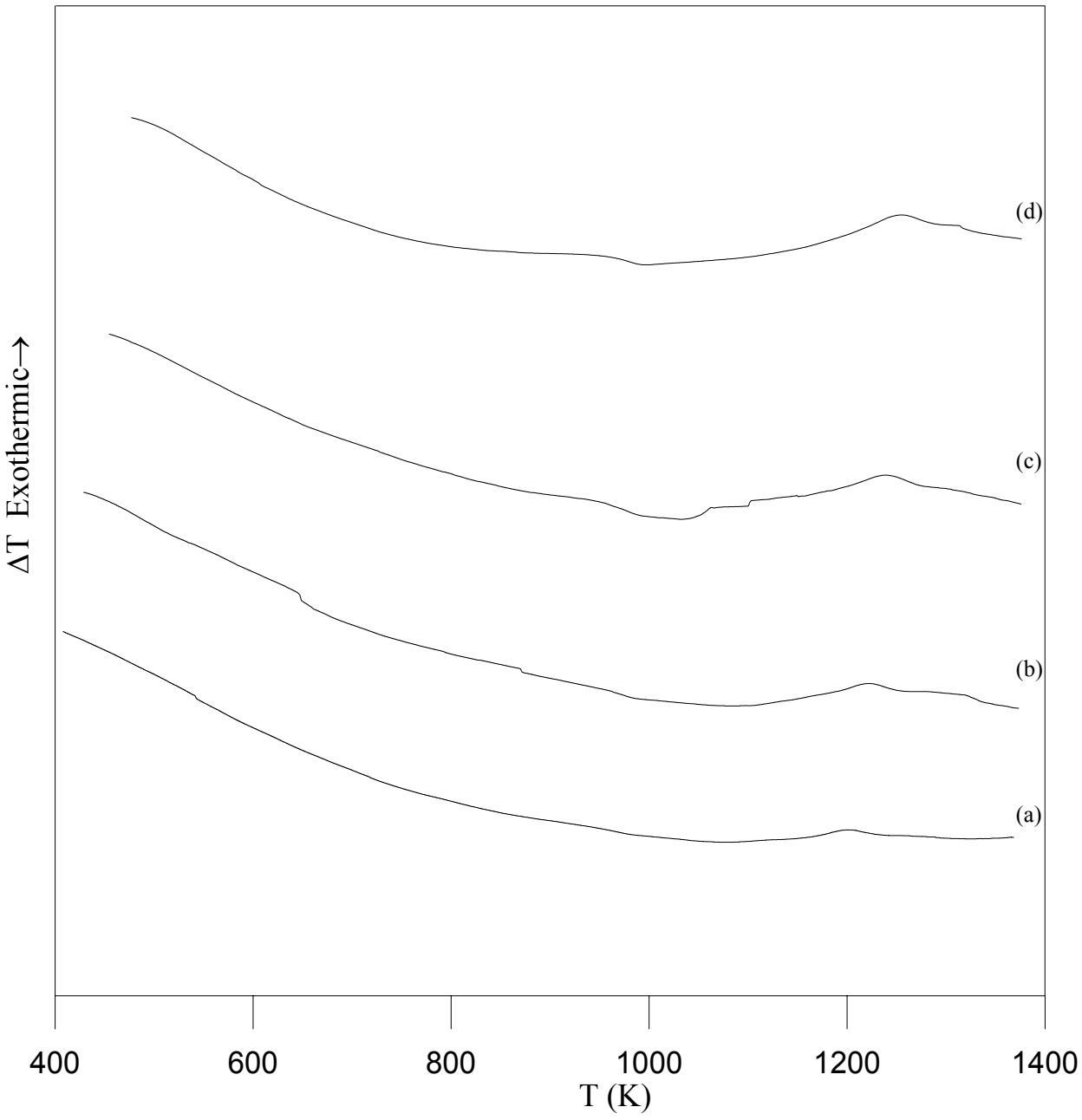

Figure B.11. DTA plots of the coarse ORSG glasses scanned at the heating rates of: a) 5 K/min, b) 10 K/min, c) 15 K/min and d) 20 K/min.

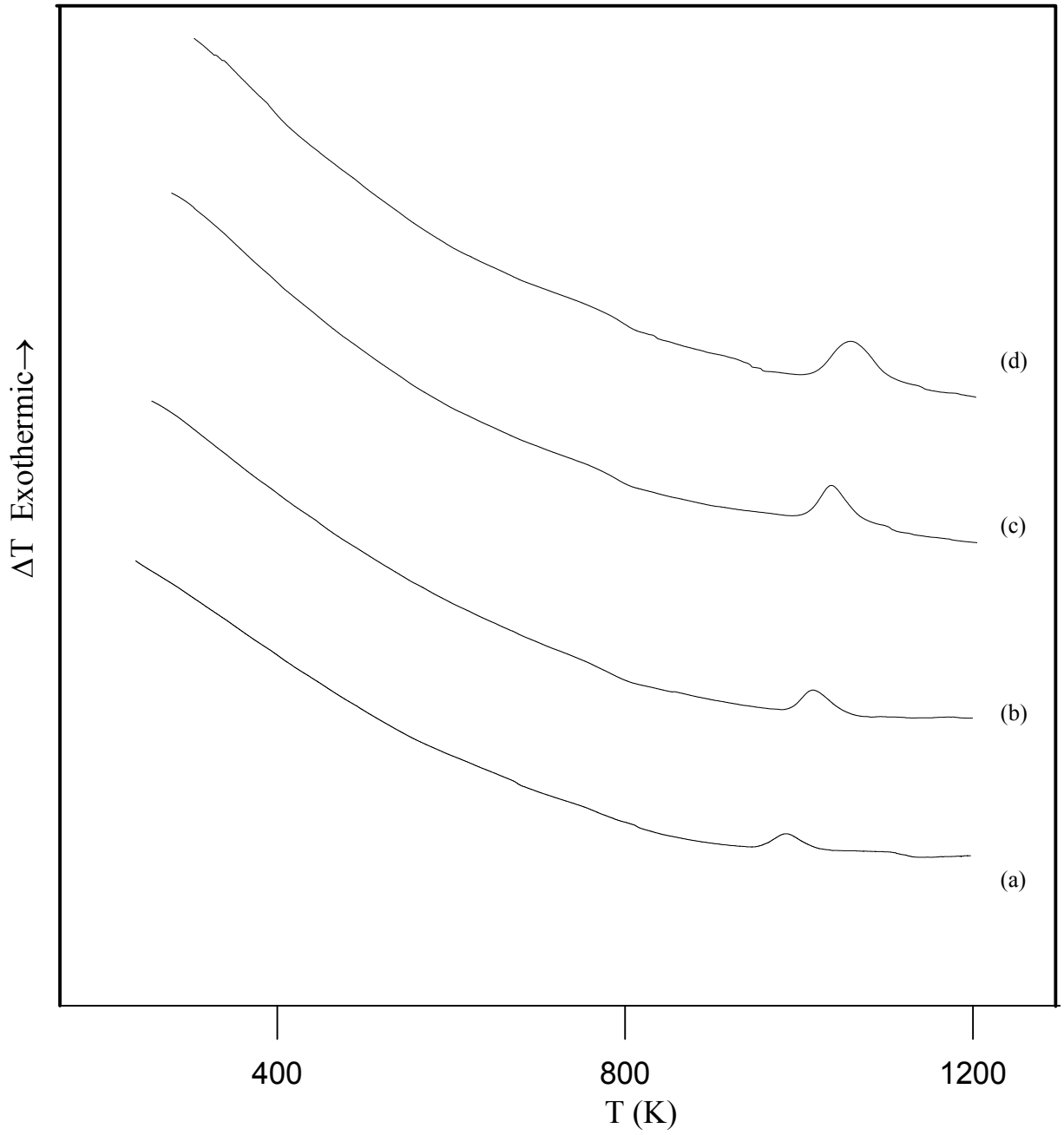

Figure B.12. DTA plots of the fine ORGS glasses scanned at the heating rates of: a) 5 K/min, b) 10 K/min, c) 15 K/min and d) 20 K/min.

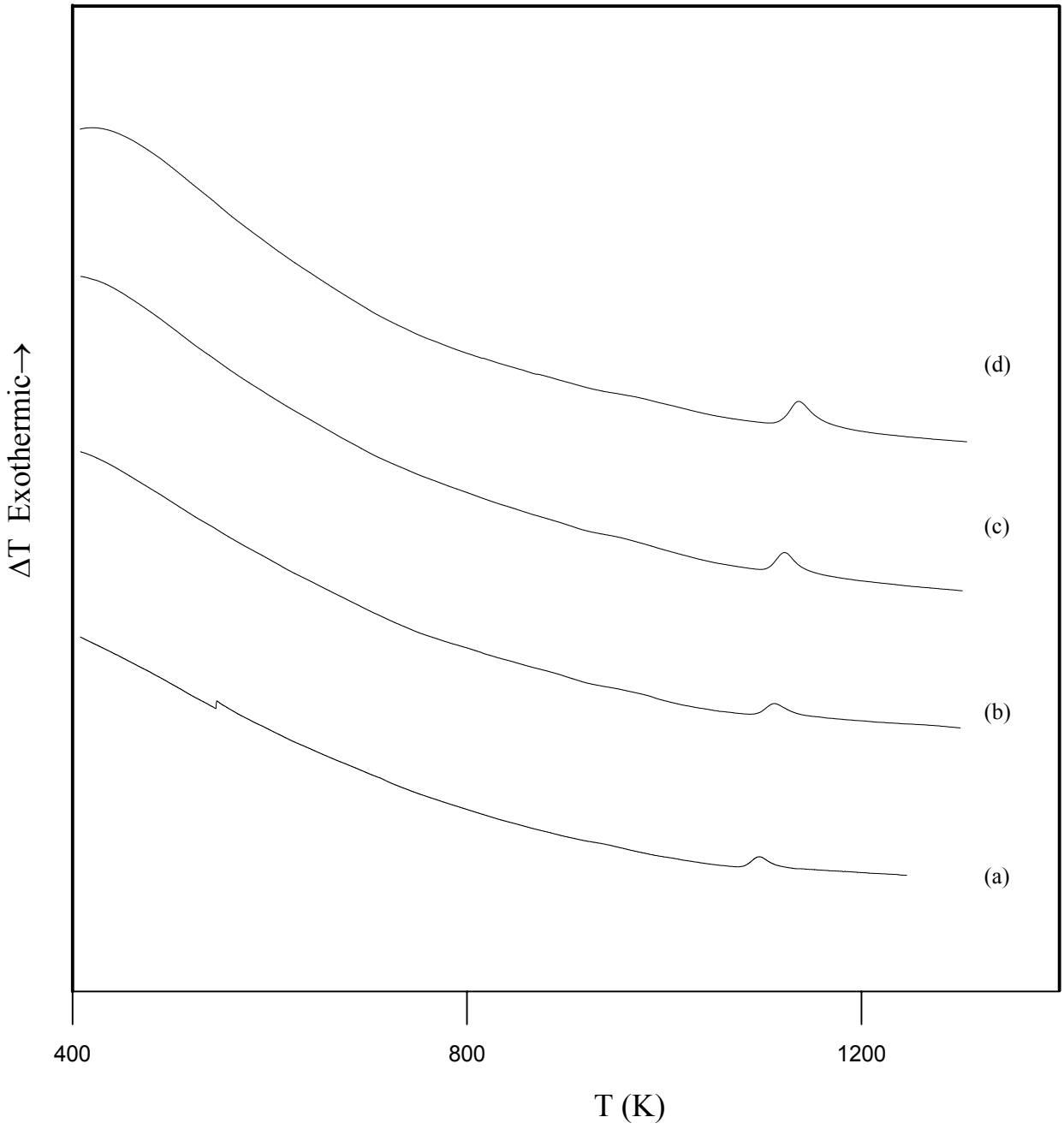

Figure B.13. DTA plots of the coarse TG glasses scanned at the heating rates of: a) 5 K/min, b) 10 K/min, c) 15 K/min and d) 20 K/min.

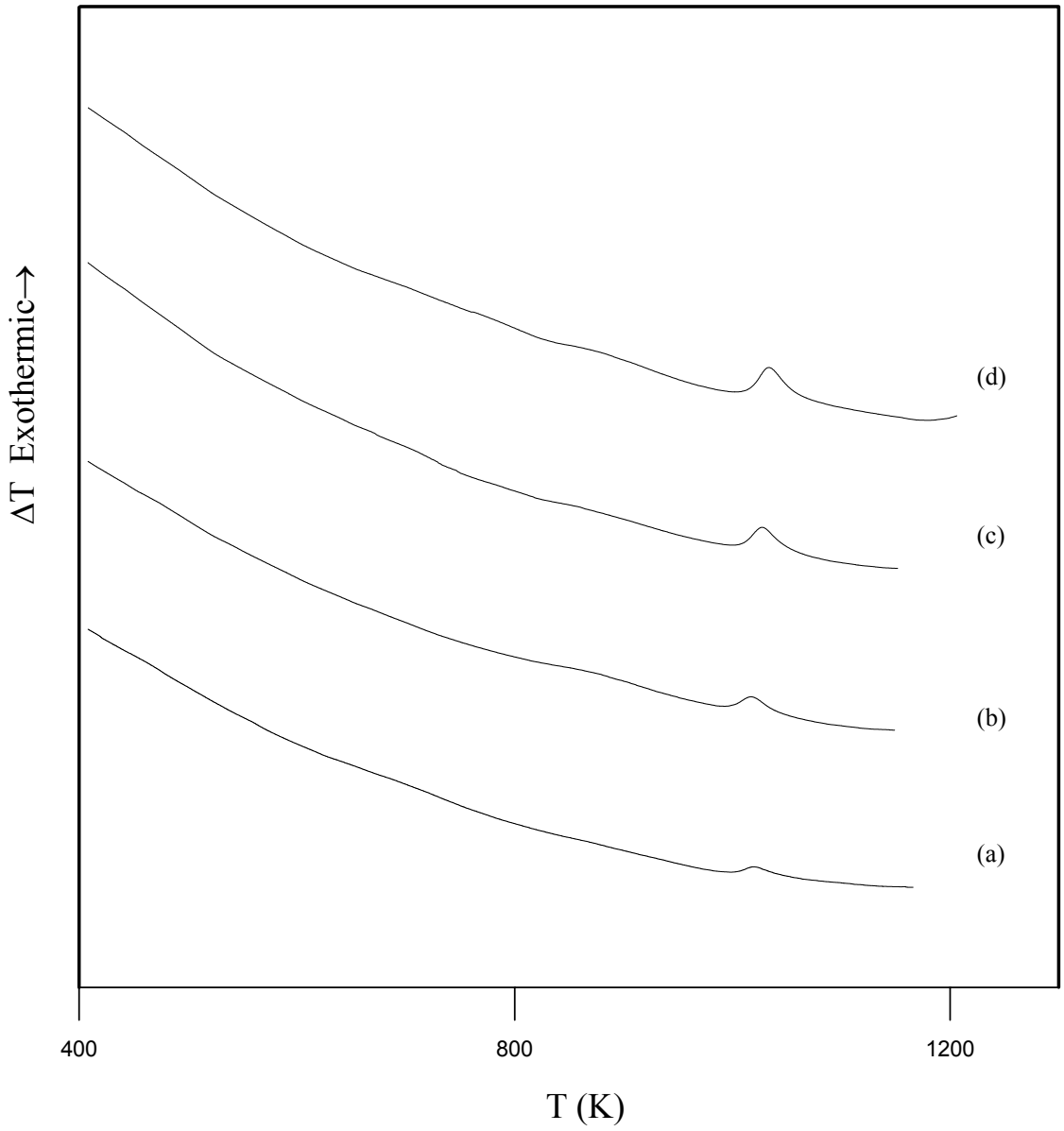

Figure B.14. DTA plots of the fine TG glasses scanned at the heating rates of: a) 5 K/min, b) 10 K/min, c) 15 K/min and d) 20 K/min.

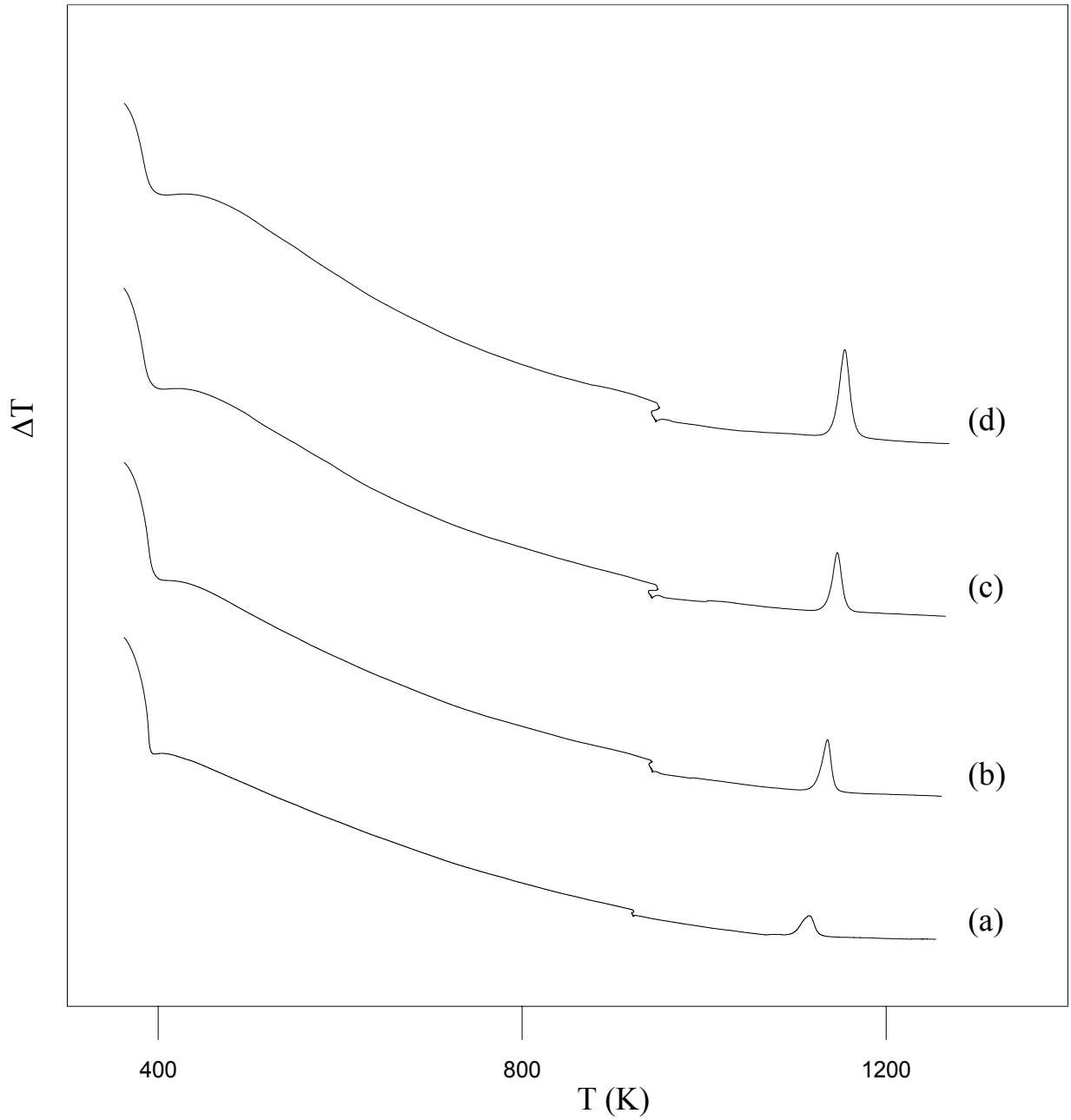

Figure B.15. DTA plots of the nucleated coarse CRG glasses scanned at the heating rates of: a) 5 K/min, b) 10 K/min, c) 15 K/min and d) 20 K/min.

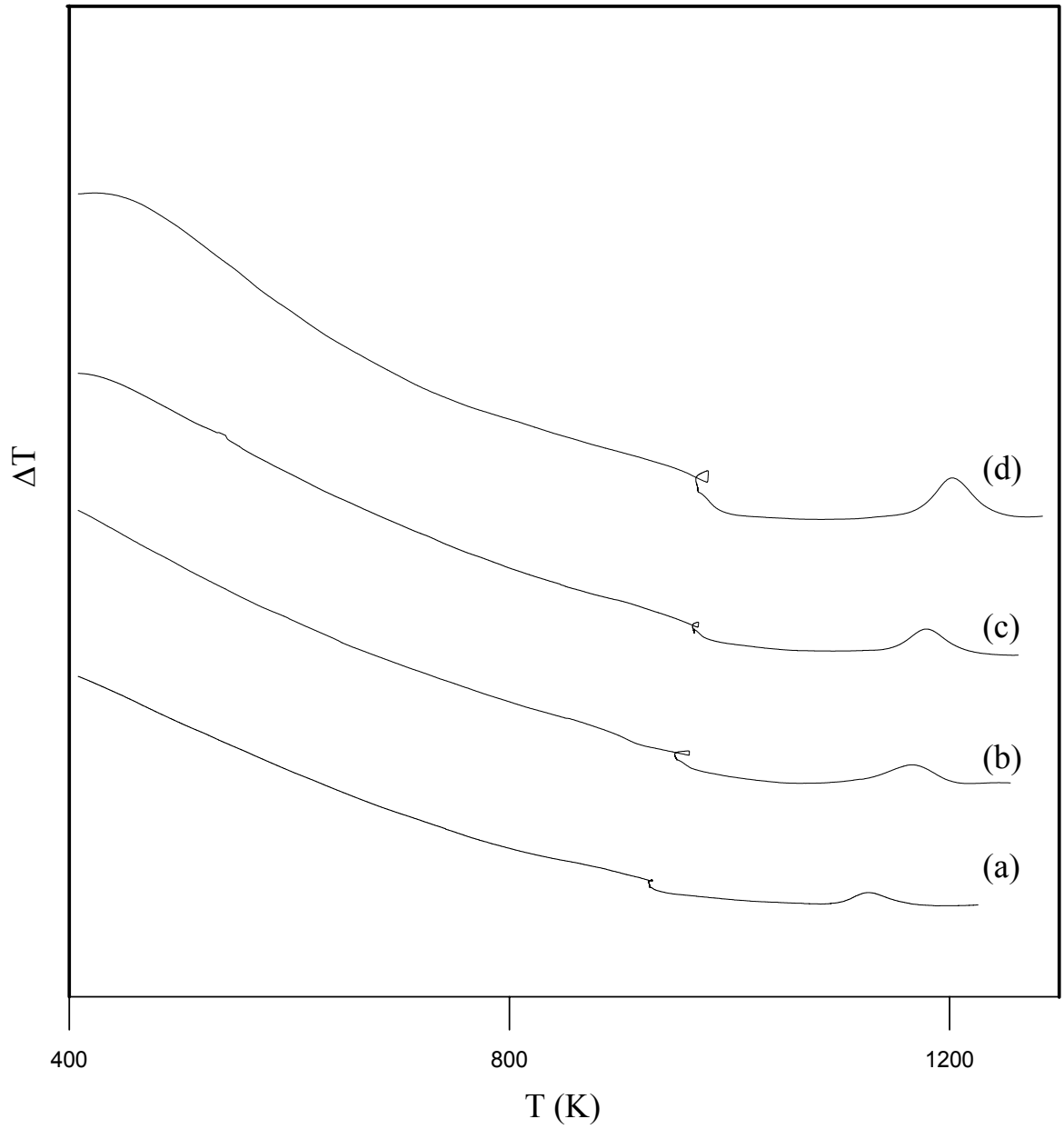

Figure B.16. DTA plots of the nucleated coarse ORSG glasses scanned at the heating rates of: a) 5 K/min, b) 10 K/min, c) 15 K/min and d) 20 K/min.

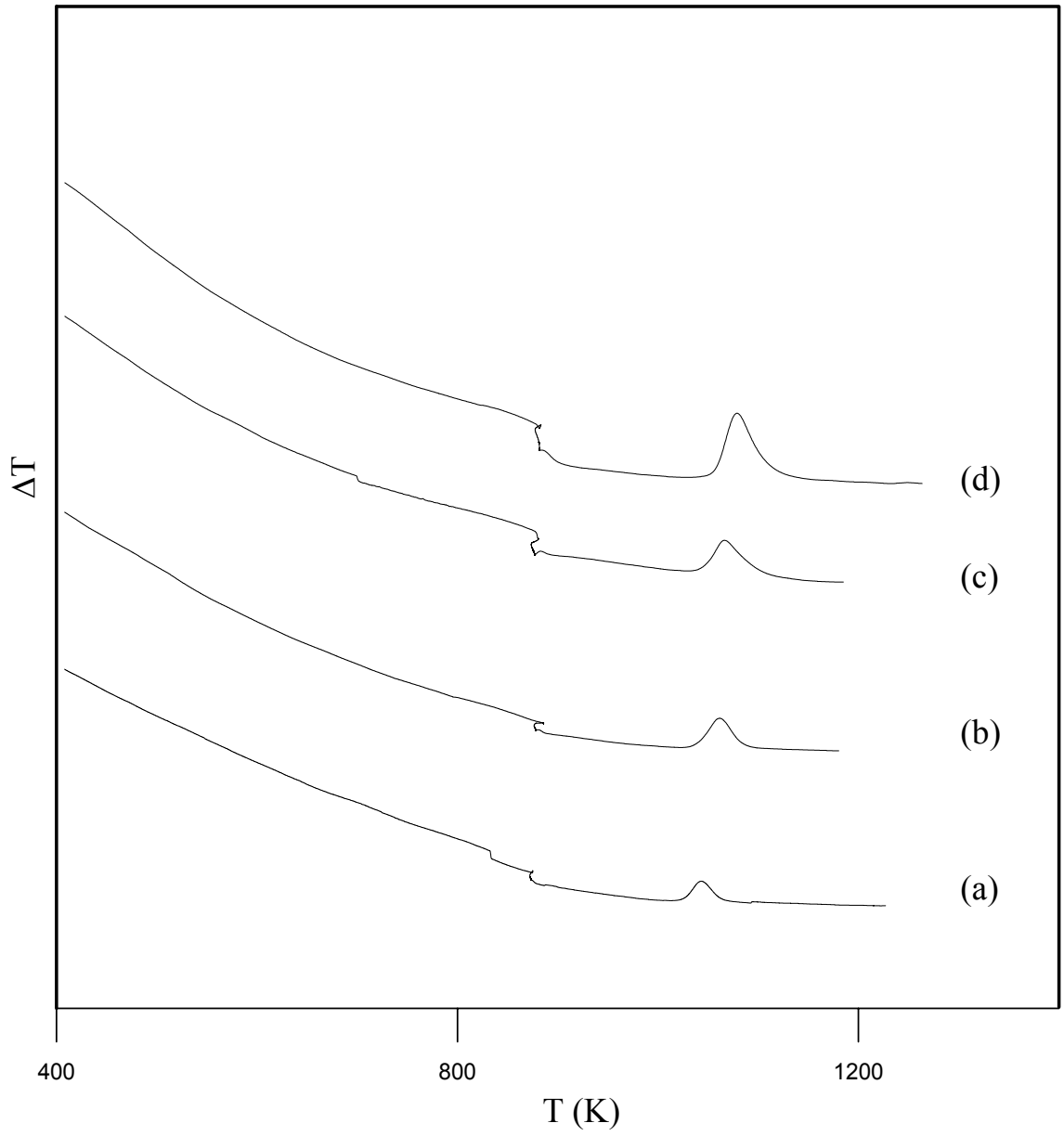

Figure B.17. DTA plots of the nucleated fine ORSG glasses scanned at the heating rates of: a) 5 K/min, b) 10 K/min, c) 15 K/min and d) 20 K/min.

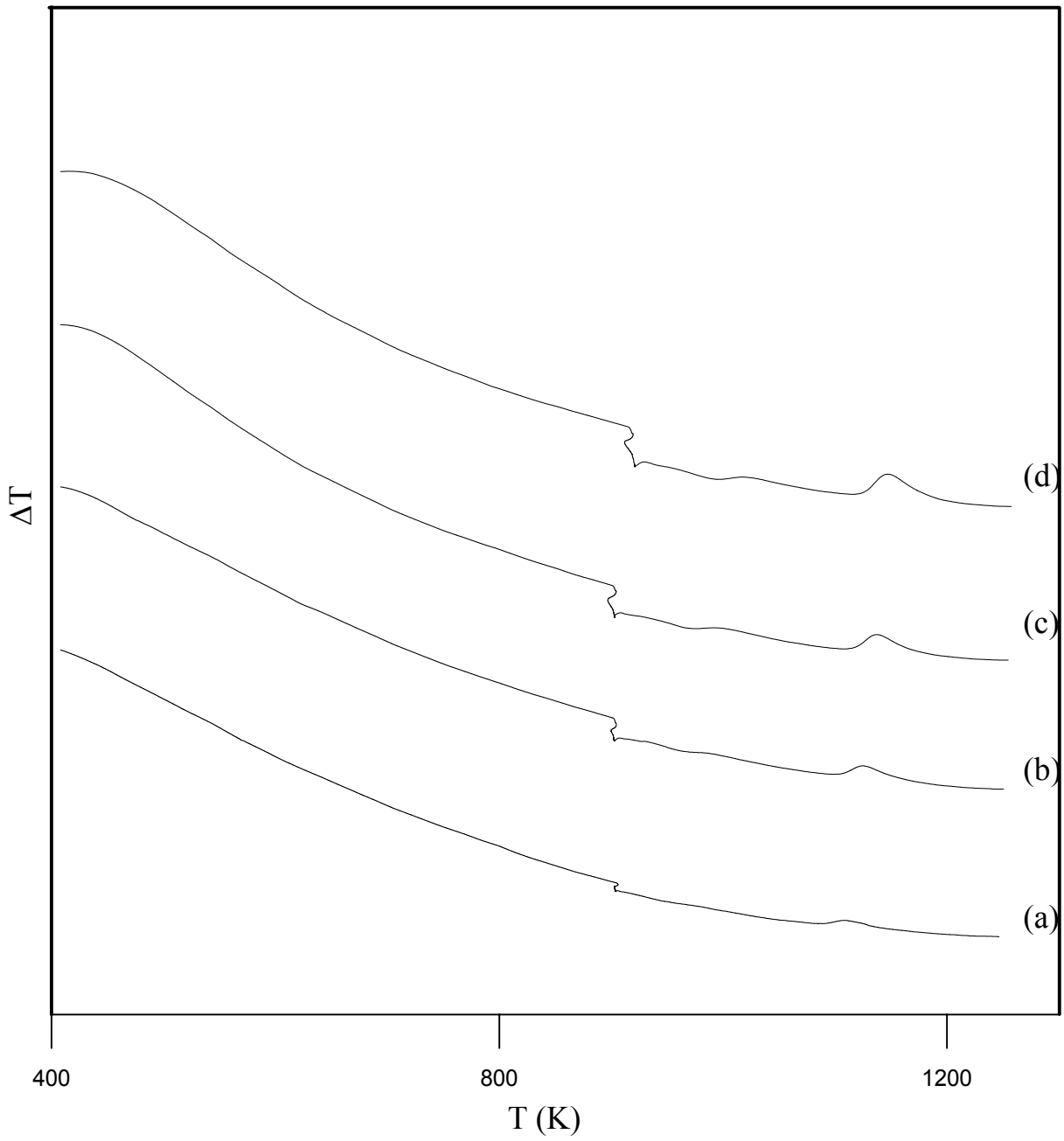

Figure B.18. DTA plots of the nucleated coarse TG glasses scanned at the heating rates of: a) 5 K/min, b) 10 K/min, c) 15 K/min and d) 20 K/min.

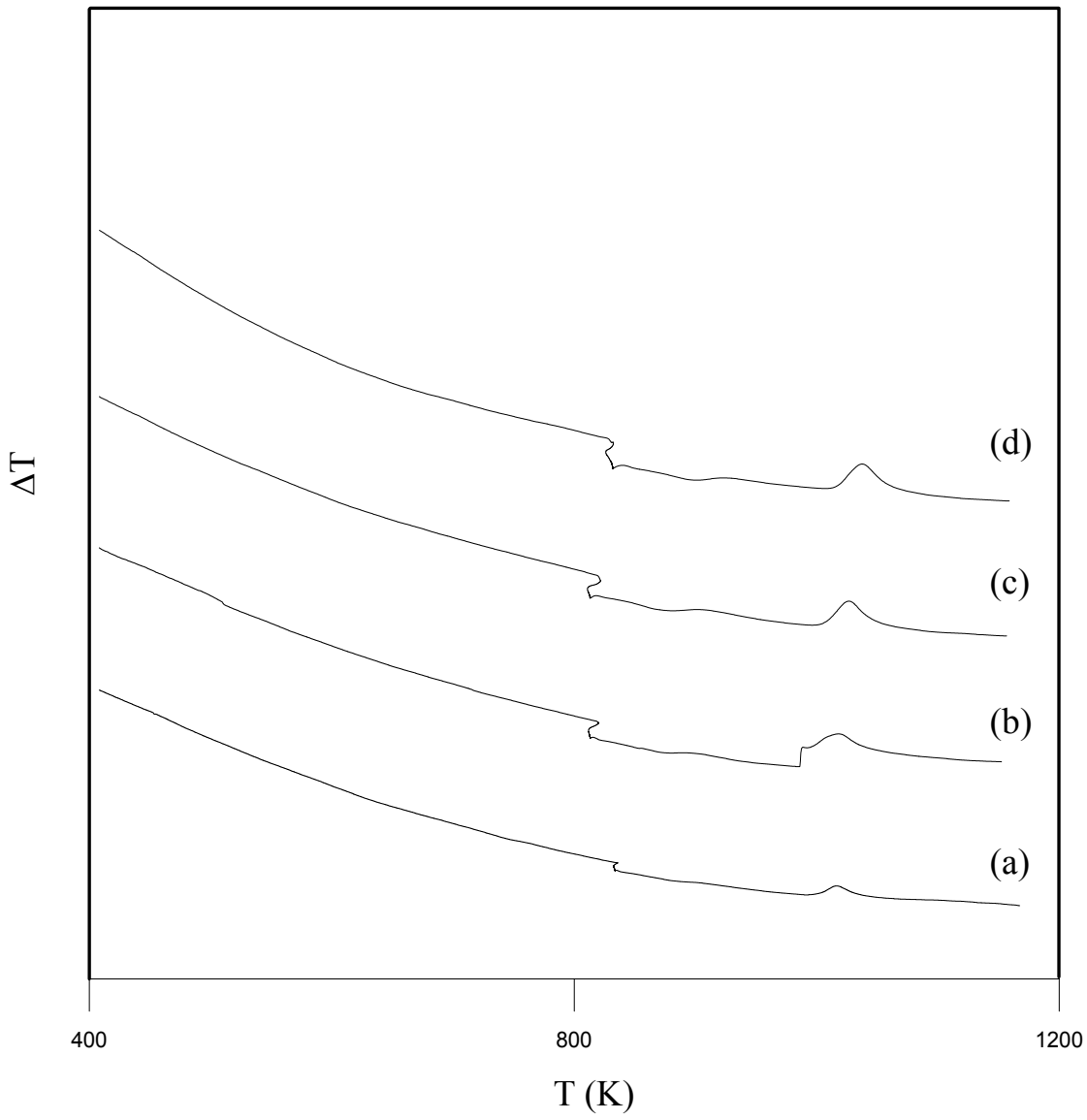

Figure B.19. DTA plots of the nucleated fine TG glasses scanned at the heating rates of: a) 5 K/min, b) 10 K/min, c) 15 K/min and d) 20 K/min.

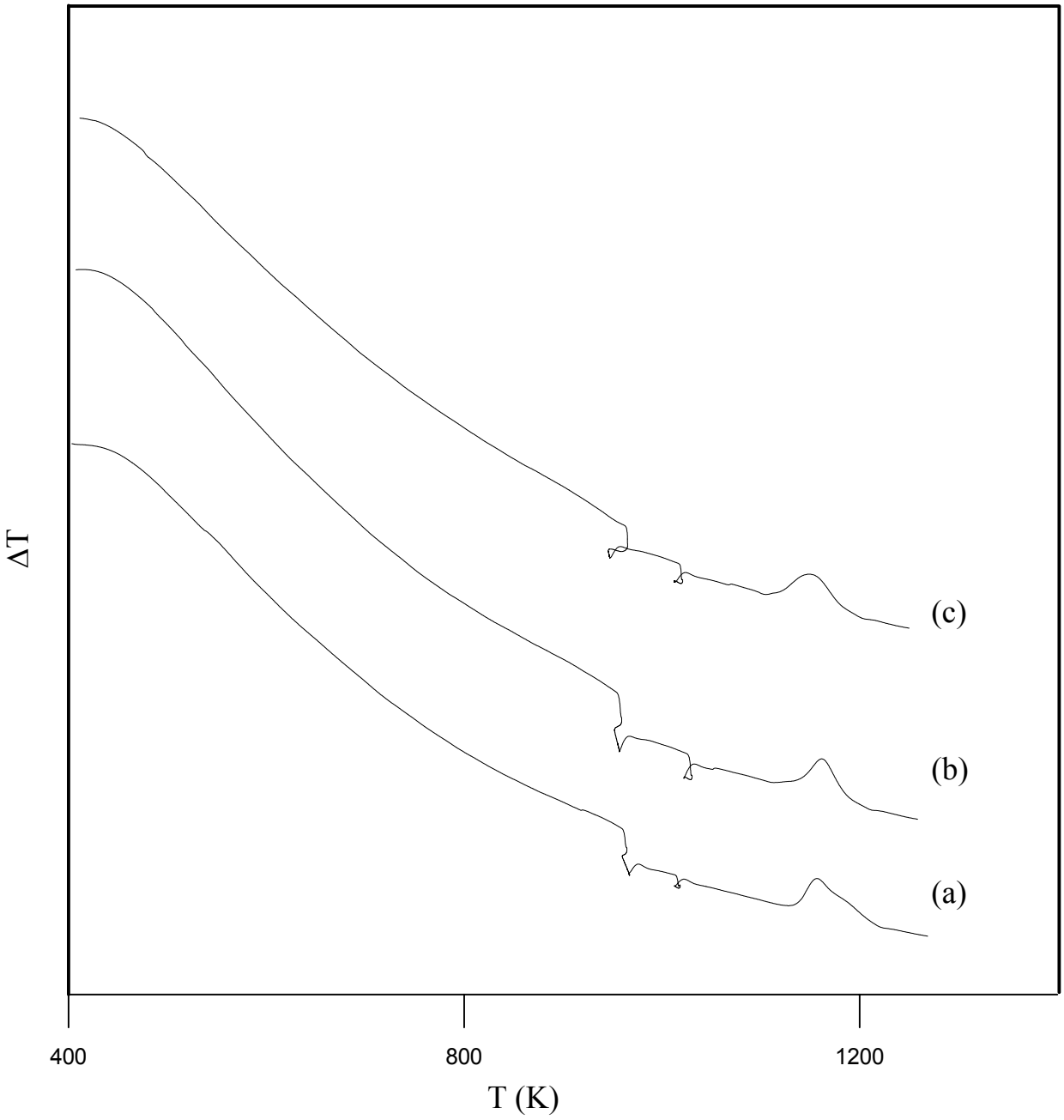

Figure B.20. DTA plots of the coarse CRG glasses heat-treated at 1038 K for the holding times of: a) 15 min, b) 30 min and c) 60 min.

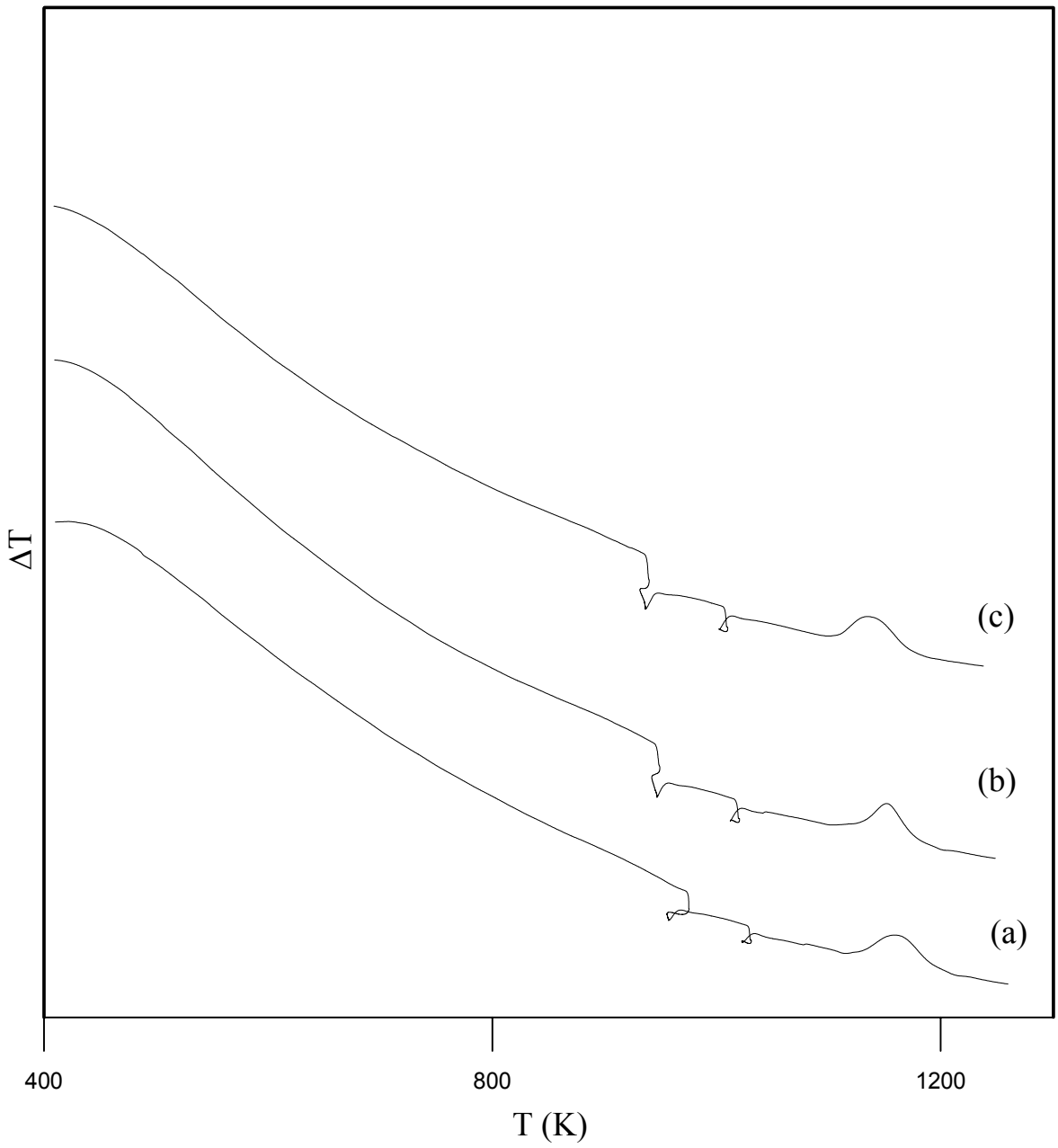

Figure B.21. DTA plots of the coarse CRG glasses heat-treated at 1048 K for the holding times of: a) 15 min, b) 30 min and c) 60 min.

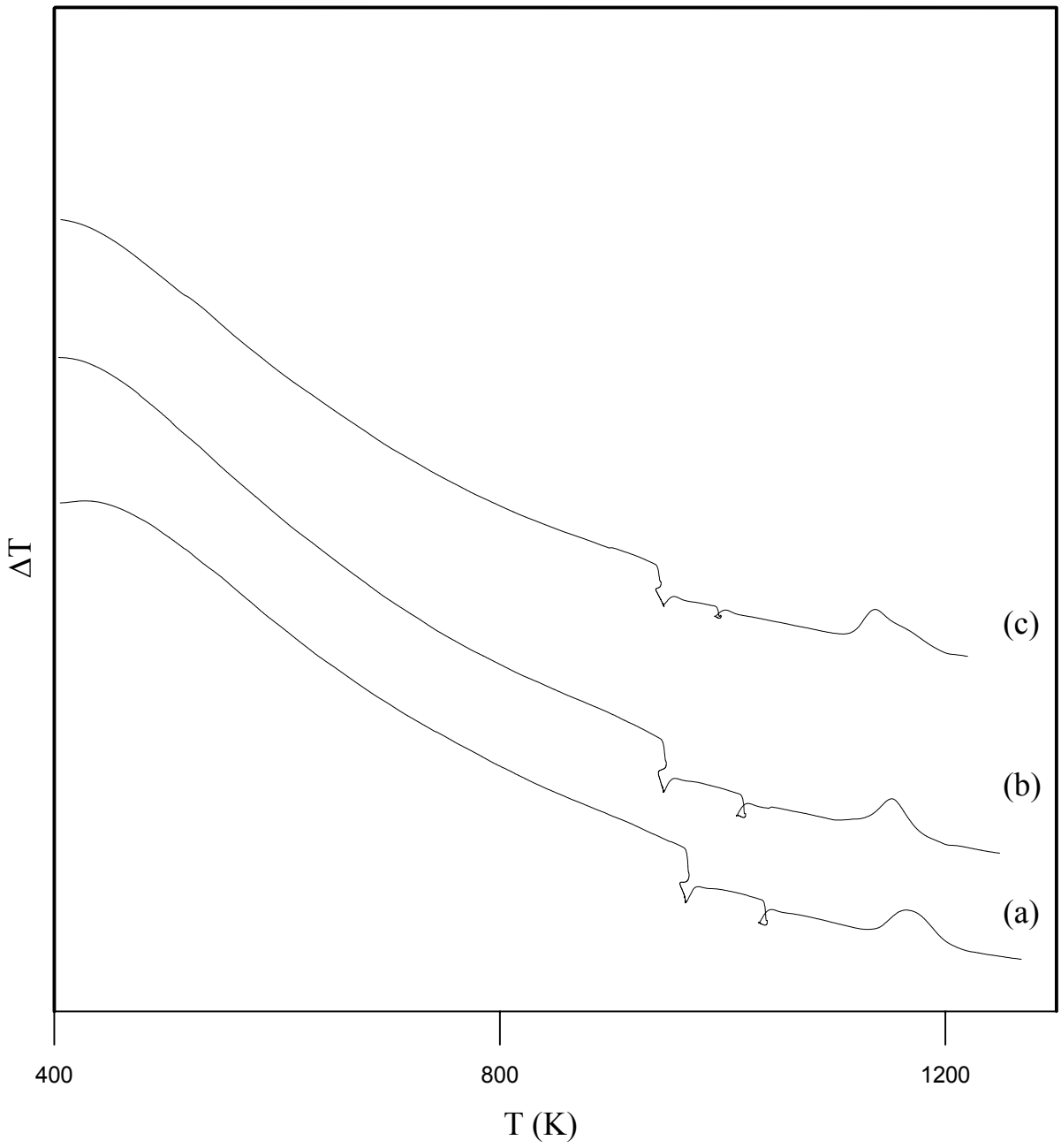

Figure B.22. DTA plots of the coarse CRG glasses heat-treated at 1058 K for the holding times of: a) 15 min, b) 30 min and c) 60 min.

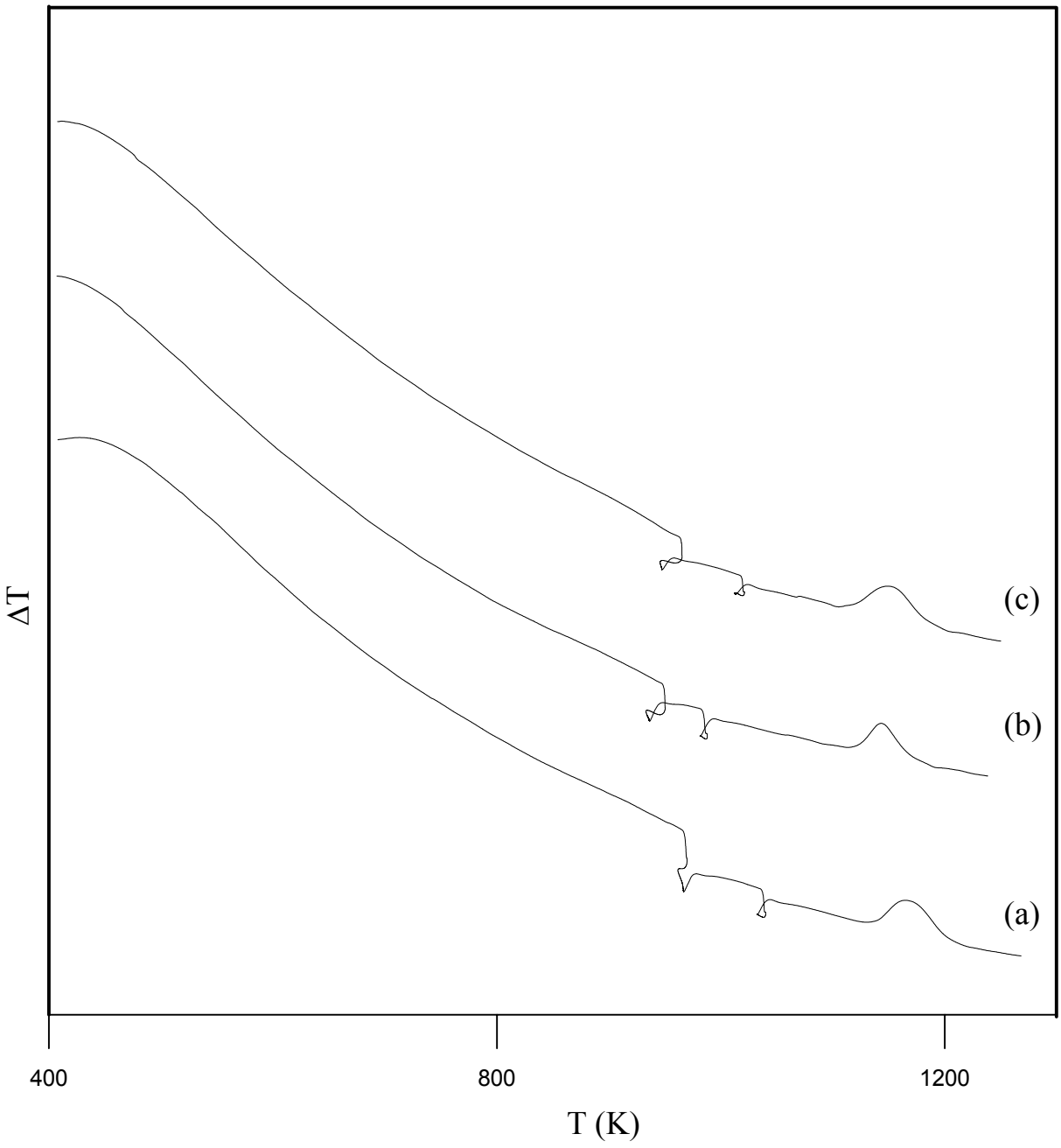

Figure B.23. DTA plots of the fine CRG glasses heat-treated at 1023 K for the holding times of: a) 15 min, b) 30 min and c) 60 min.

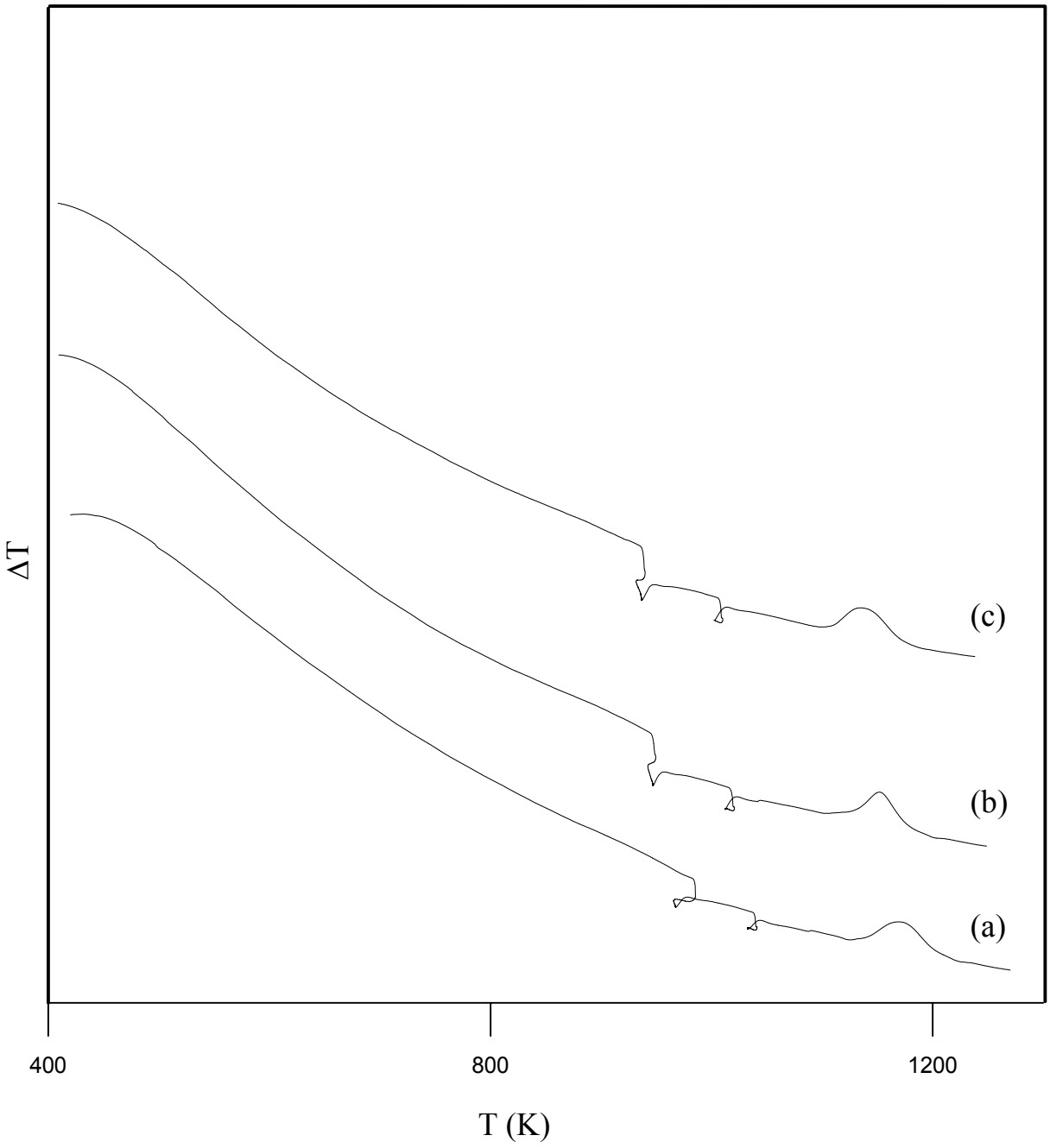

Figure B.24. DTA plots of the fine CRG glasses heat-treated at 1033 K for the holding times of: a) 15 min, b) 30 min and c) 60 min.

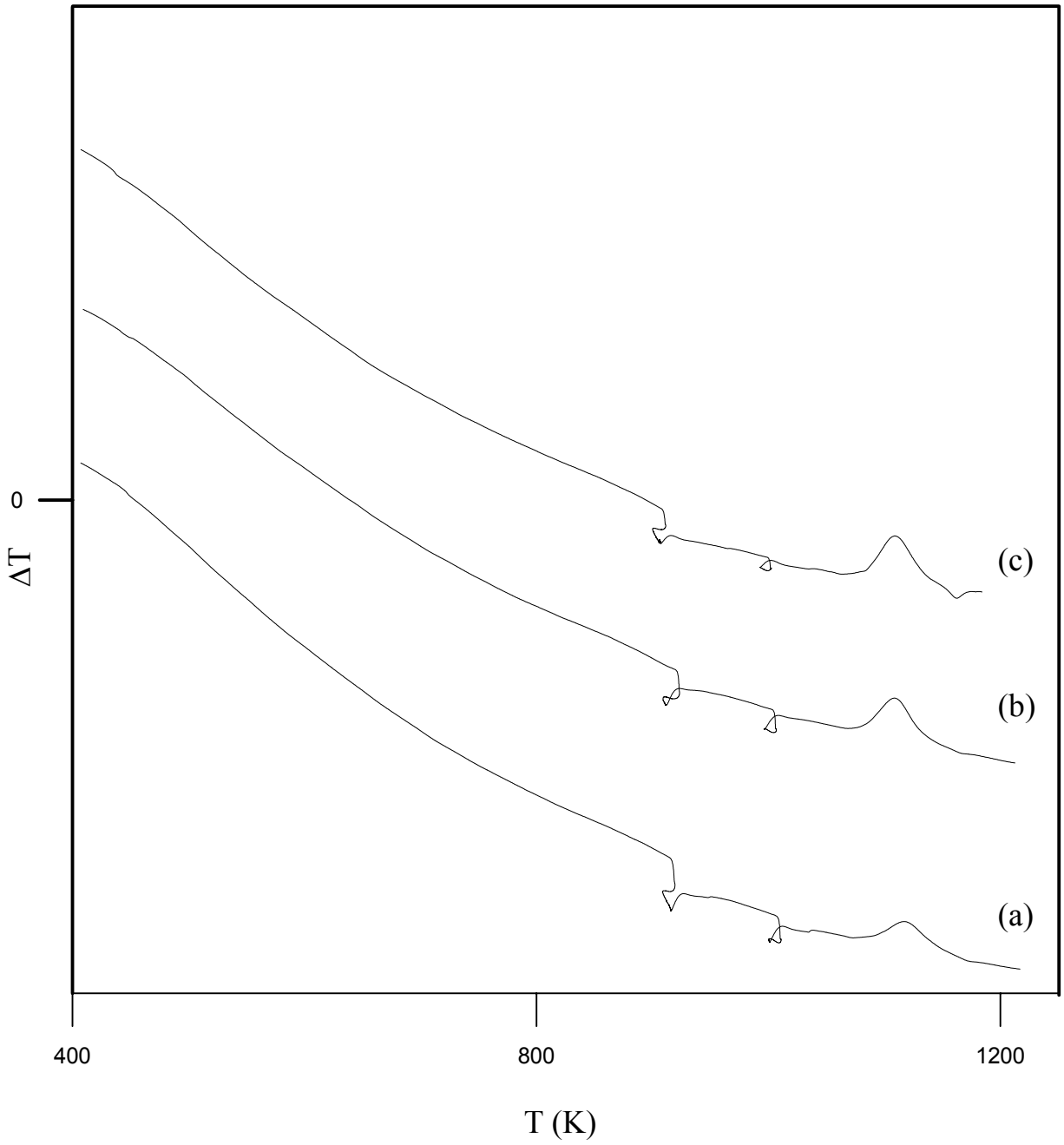

Figure B.25. DTA plots of the fine CRG glasses heat-treated at 1043 K for the holding times of: a) 15 min, b) 30 min and c) 60 min.

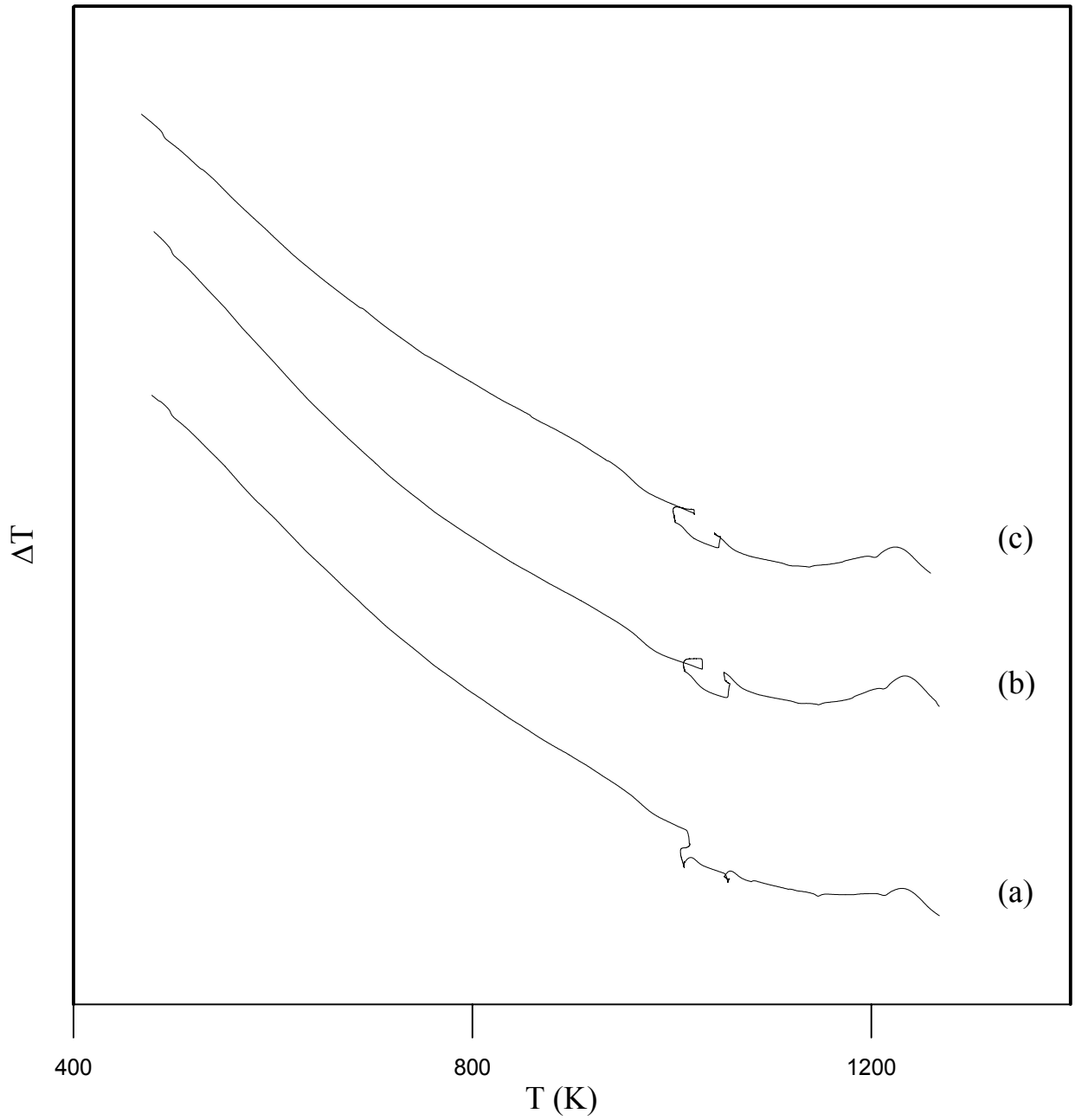

Figure B.26. DTA plots of the coarse ORSG glasses heat-treated at 1073 K for the holding times of: a) 15 min, b) 30 min and c) 60 min.

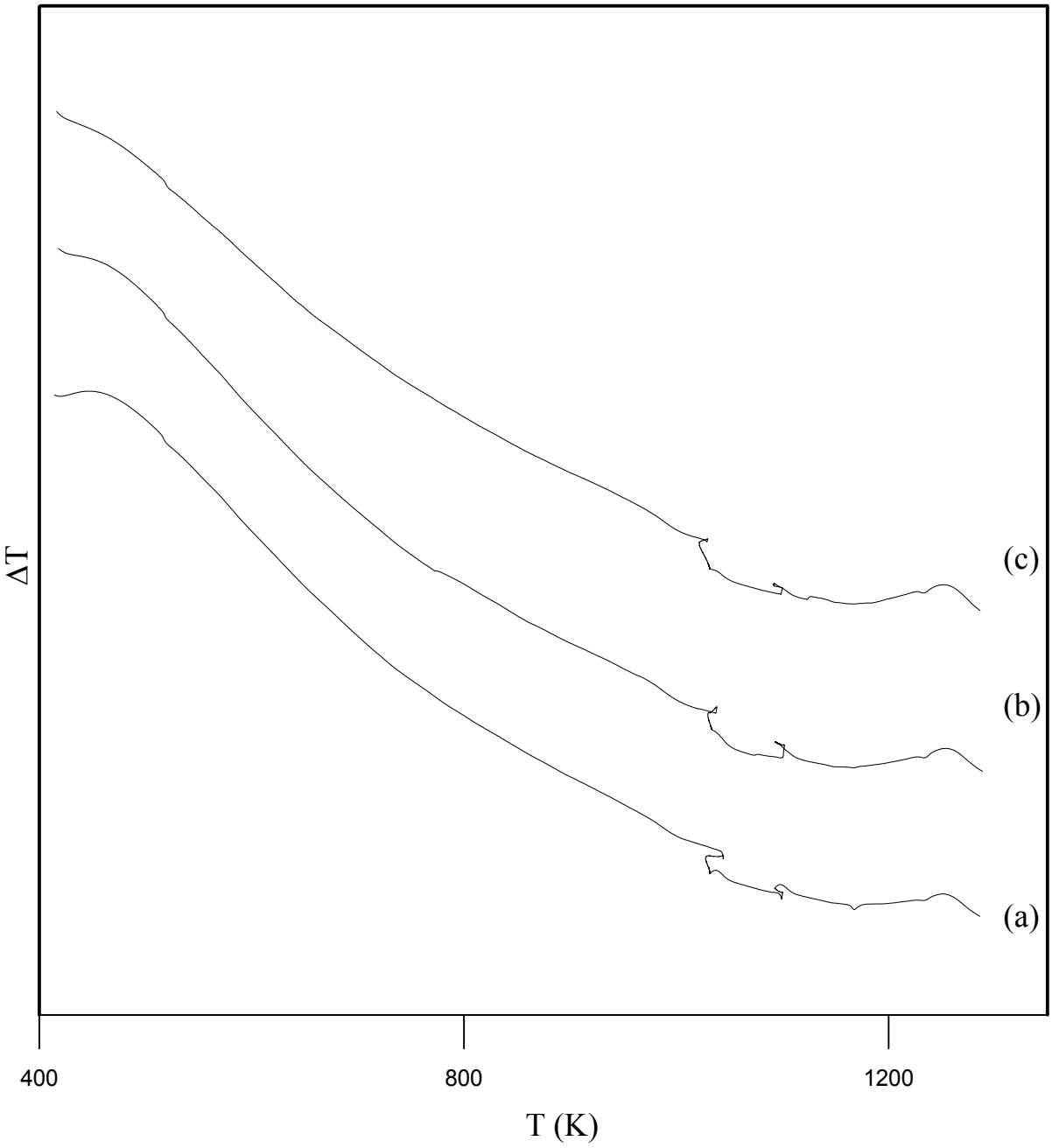

Figure B.27. DTA plots of the coarse ORSG glasses heat-treated at 1093 K for the holding times of: a) 15 min, b) 30 min and c) 60 min.

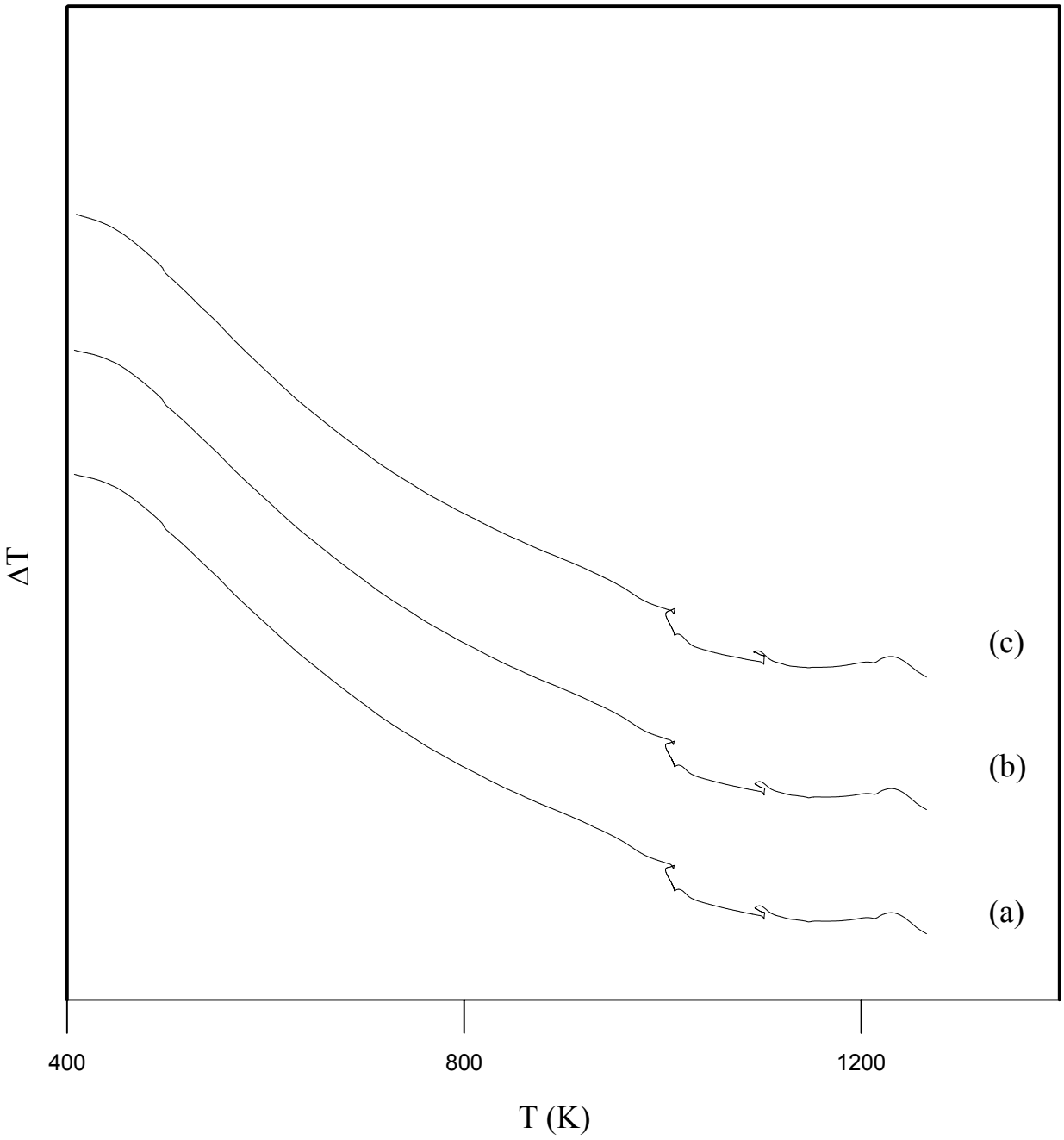

Figure B.28. DTA plots of the coarse ORSG glasses heat-treated at 1113 K for the holding times of: a) 15 min, b) 30 min and c) 60 min.

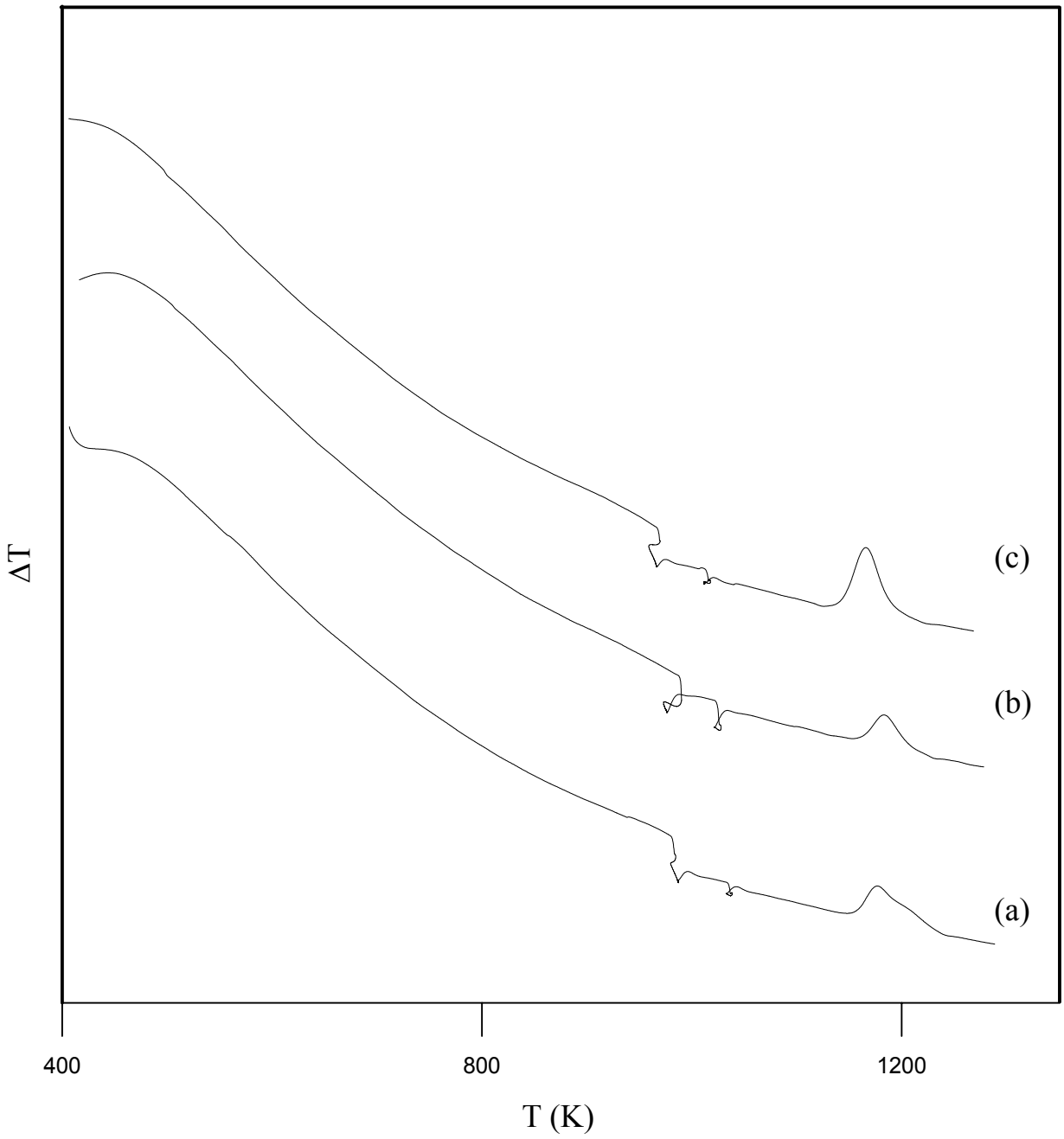

Figure B.29. DTA plots of the fine ORSG glasses heat-treated at 1033 K for the holding times of: a) 15 min, b) 30 min and c) 60 min.

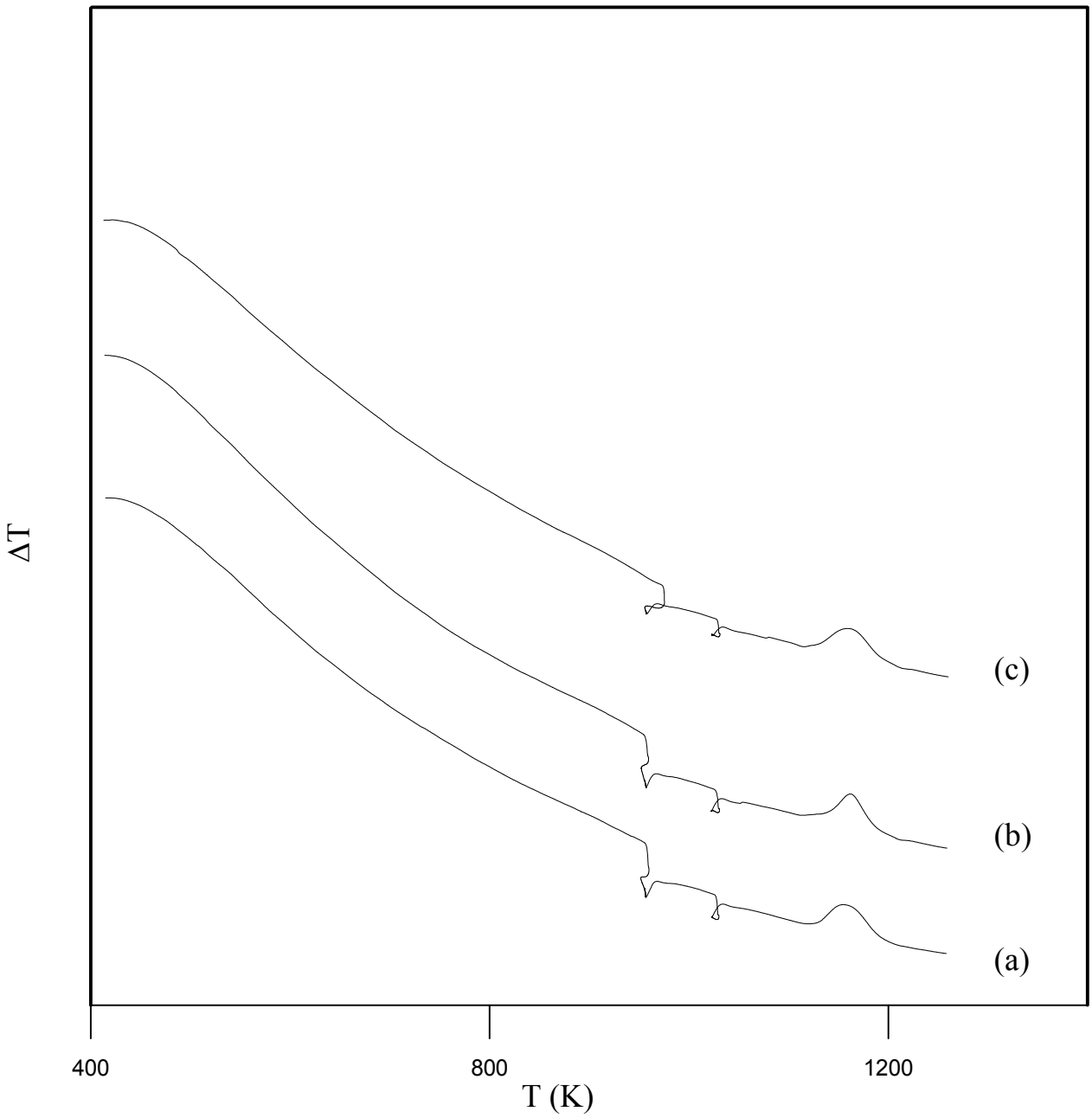

Figure B.30. DTA plots of the fine ORSG glasses heat-treated at 1053 K for the holding times of: a) 15 min, b) 30 min and c) 60 min.

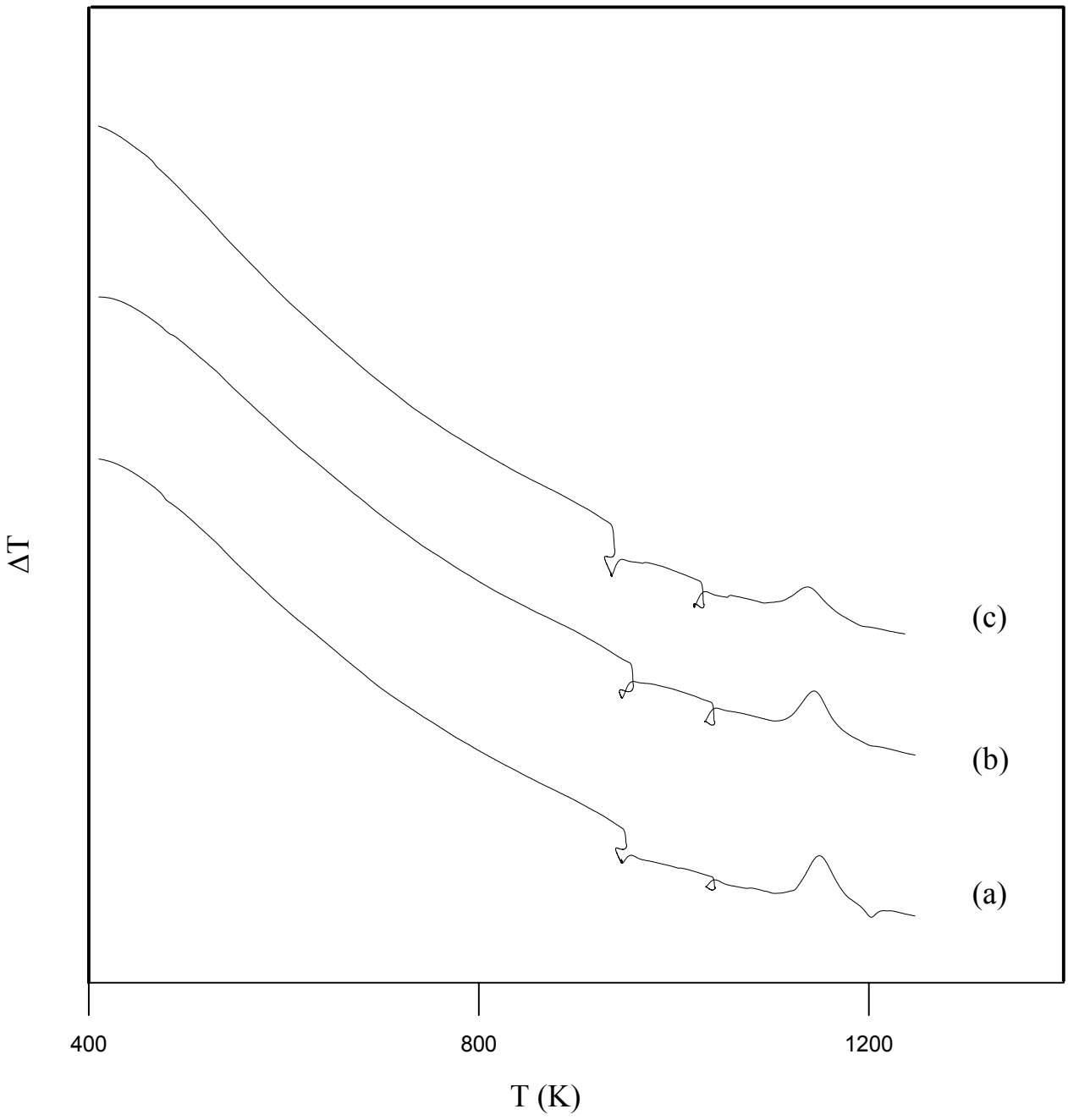

Figure B.31. DTA plots of the fine ORSG glasses heat-treated at 1073 K for the holding times of: a) 15 min, b) 30 min and c) 60 min.

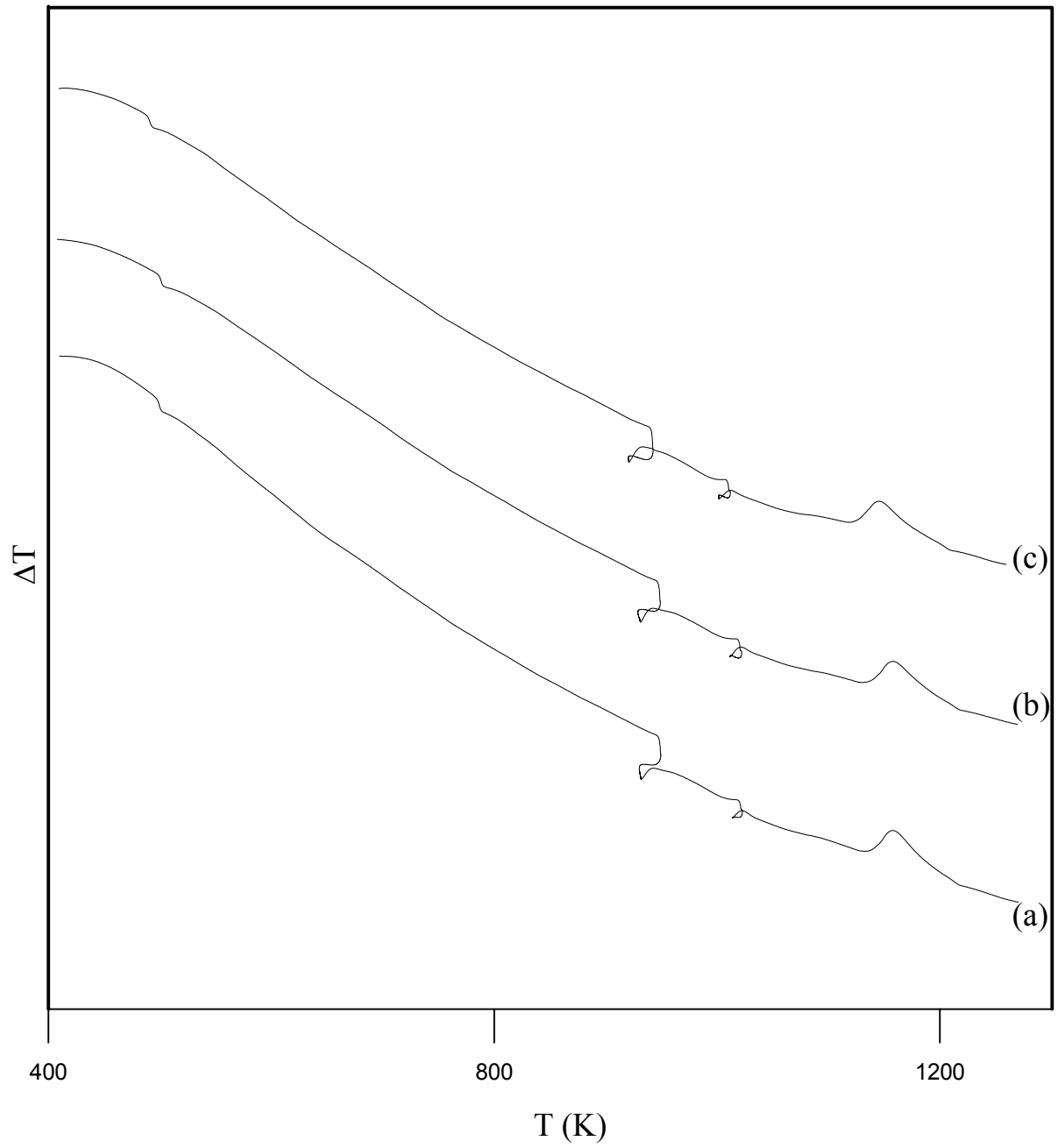

Figure B.32. DTA plots of the coarse TG glasses heat-treated at 1033 K for the holding times of: a) 15 min, b) 30 min and c) 60 min.

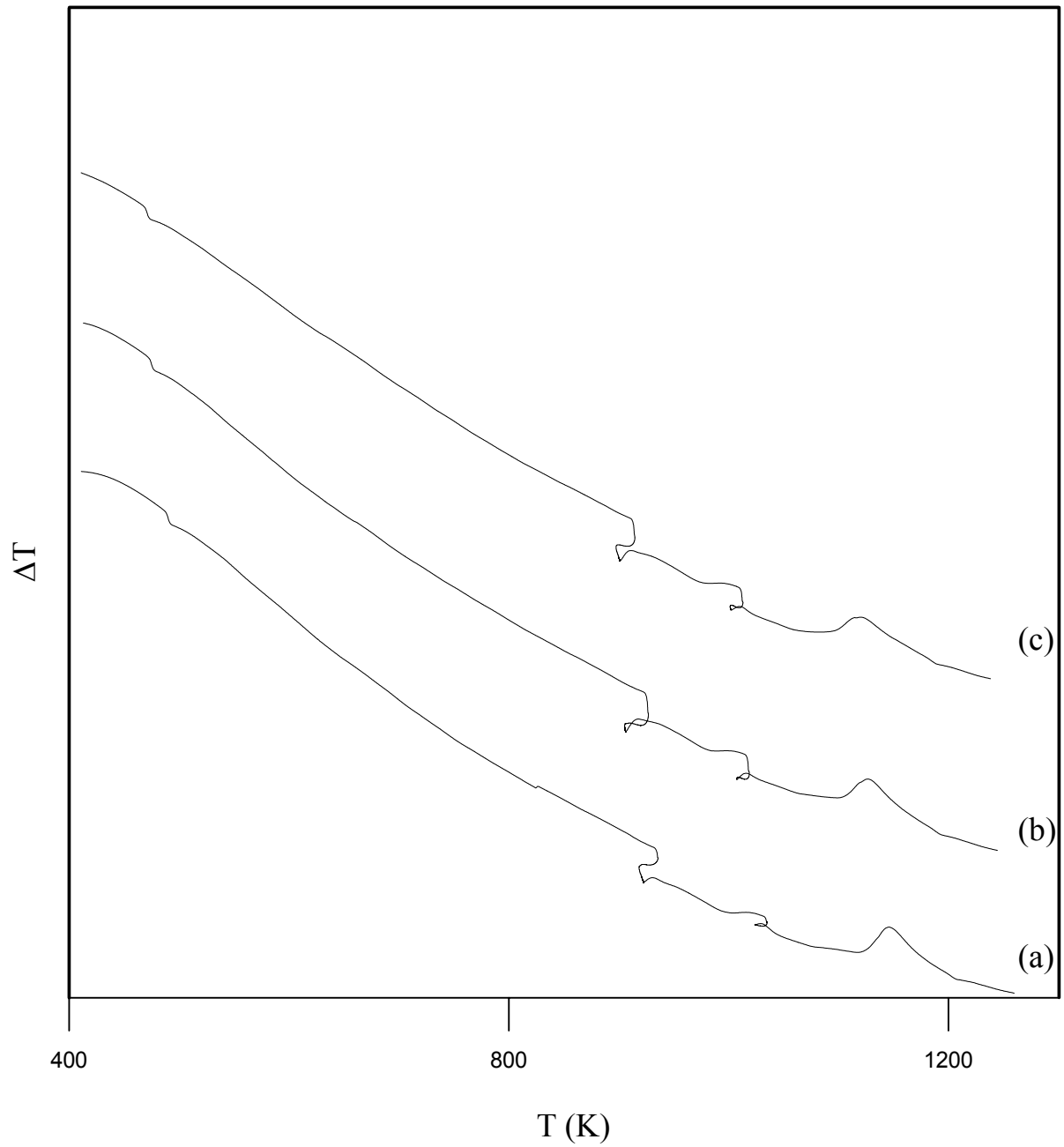

Figure B.33. DTA plots of the coarse TG glasses heat-treated at 1053 K for the holding times of: a) 15 min, b) 30 min and c) 60 min

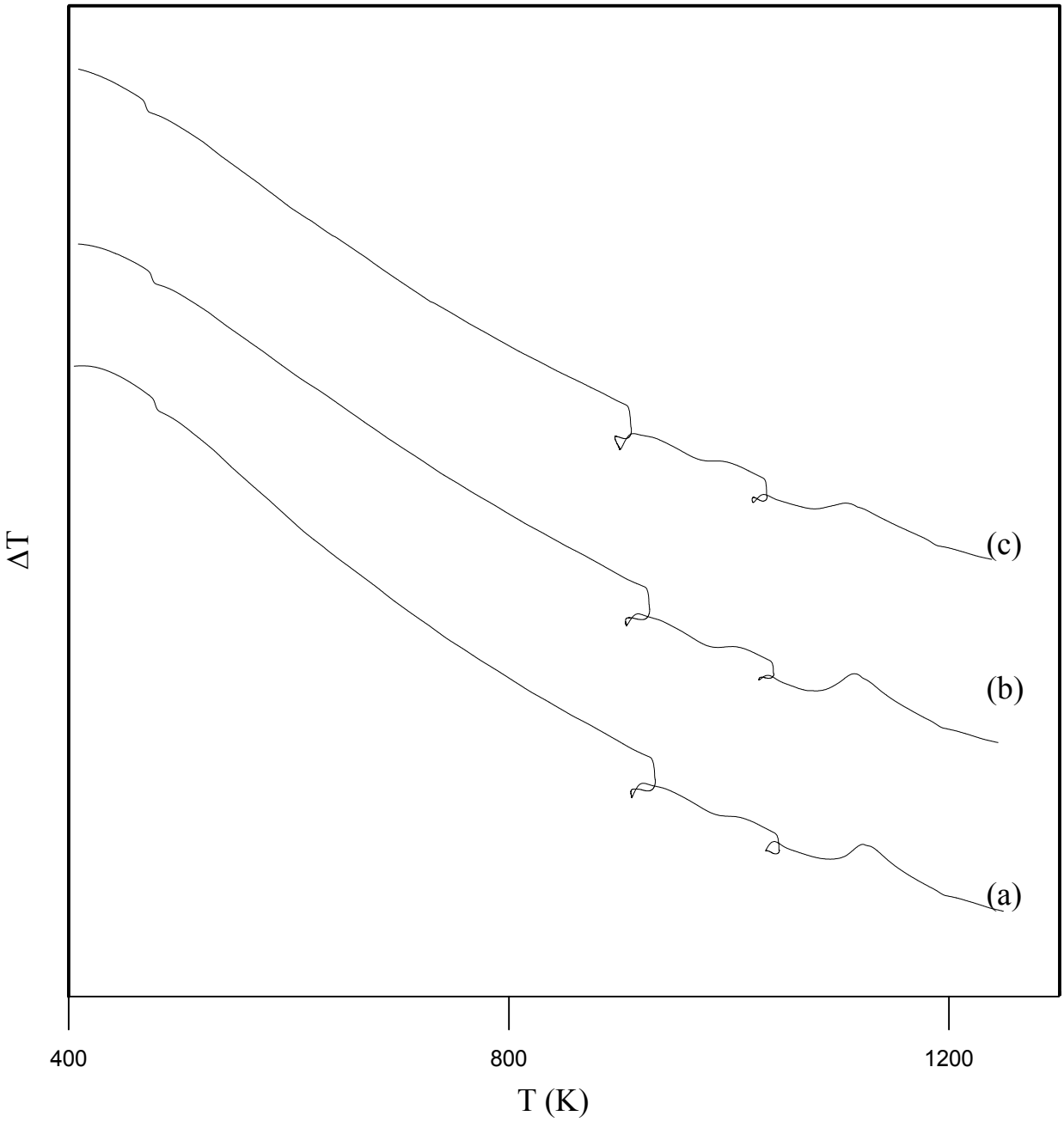

Figure B.34. DTA plots of the coarse TG glasses heat-treated at 1073 K for the holding times of: a) 15 min, b) 30 min and c) 60 min

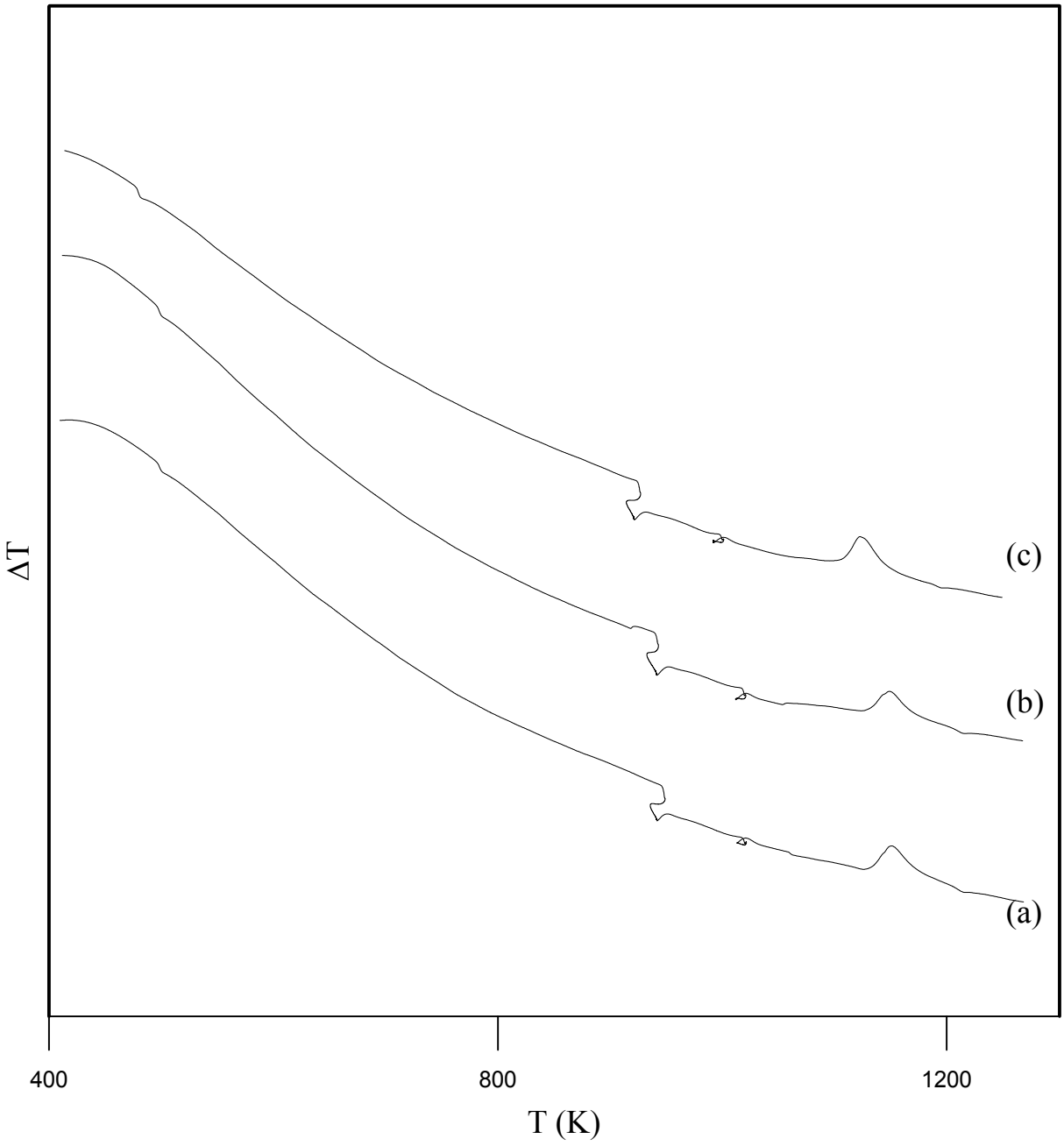

Figure B.35. DTA plots of the fine TG glasses heat-treated at 1033 K for the holding times of: a) 15 min, b) 30 min and c) 60 min

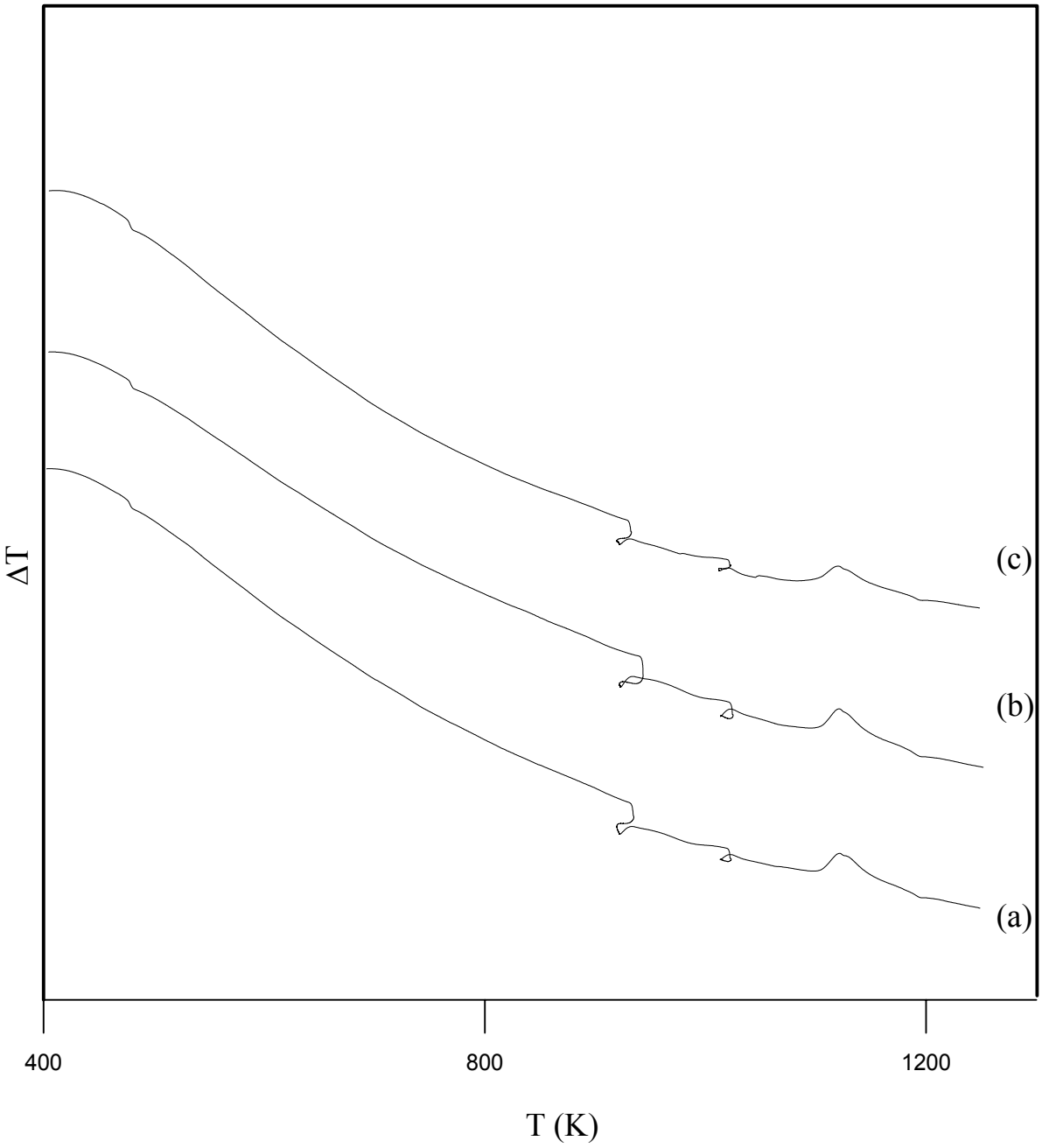

Figure B.36. DTA plots of the fine TG glasses heat-treated at 1053 K for the holding times of: a) 15 min, b) 30 min and c) 60 min

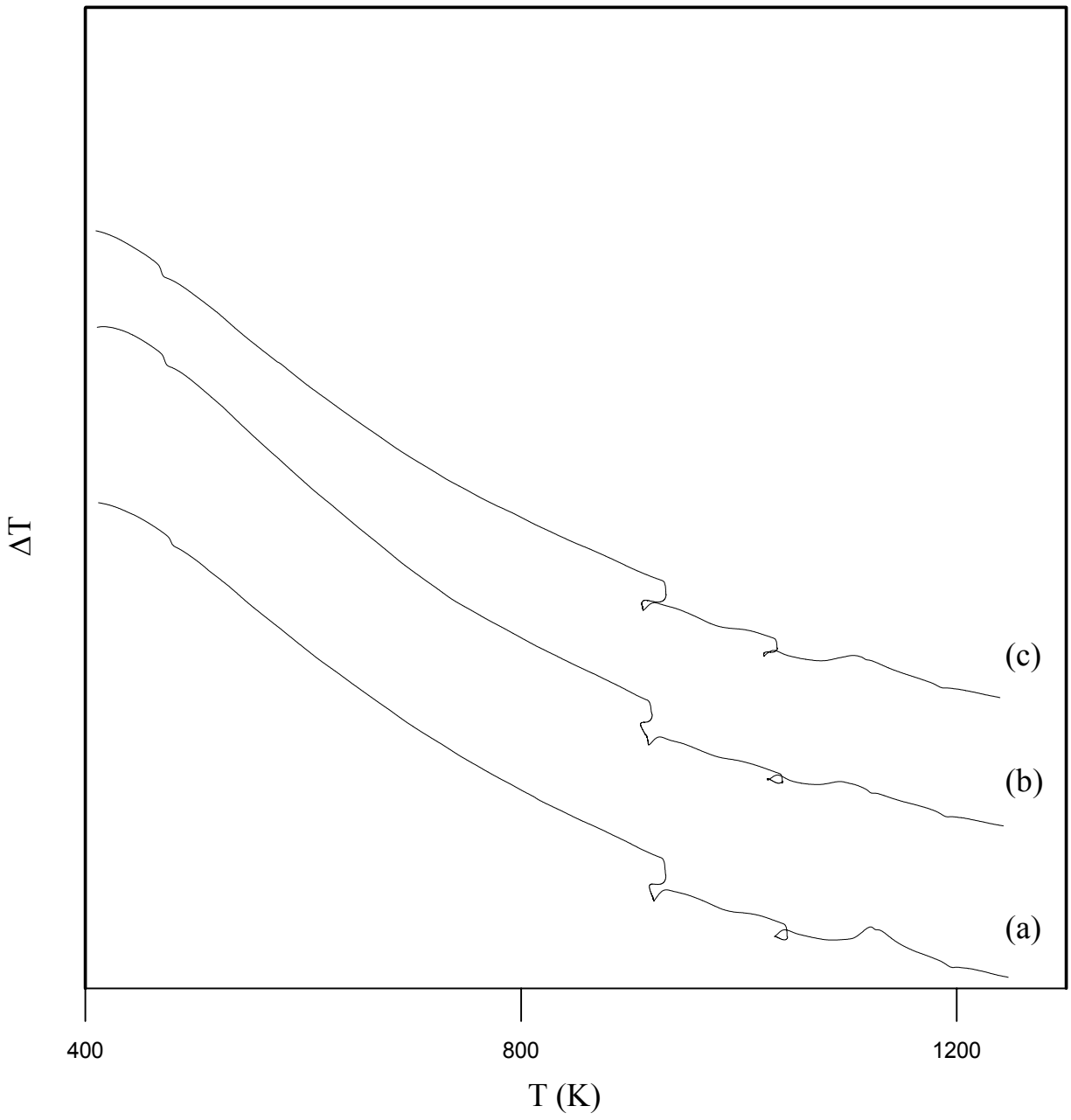

Figure B.37. DTA plots of the fine TG glasses heat-treated at 1073 K for the holding times of: a) 15 min, b) 30 min and c) 60 min

APPENDIX C

X-RAY DIFFRACTION PATTERNS OF THE PRODUCED GLASS-CERAMICS

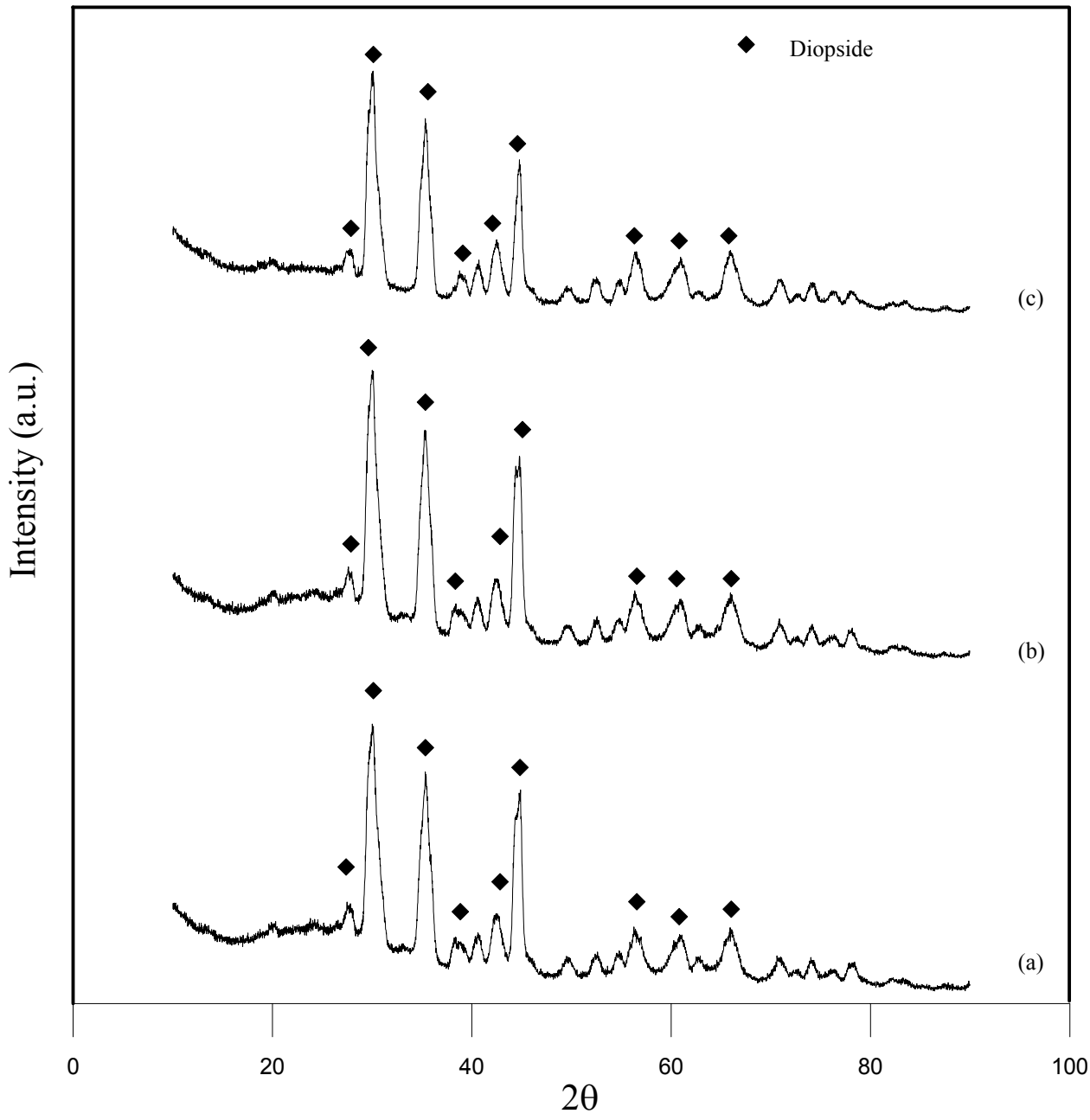

Figure C.1. XRD patterns of CRGC-B samples crystallized at 1135 K for : (a) 15 min, (b) 30 min and (c) 60 min

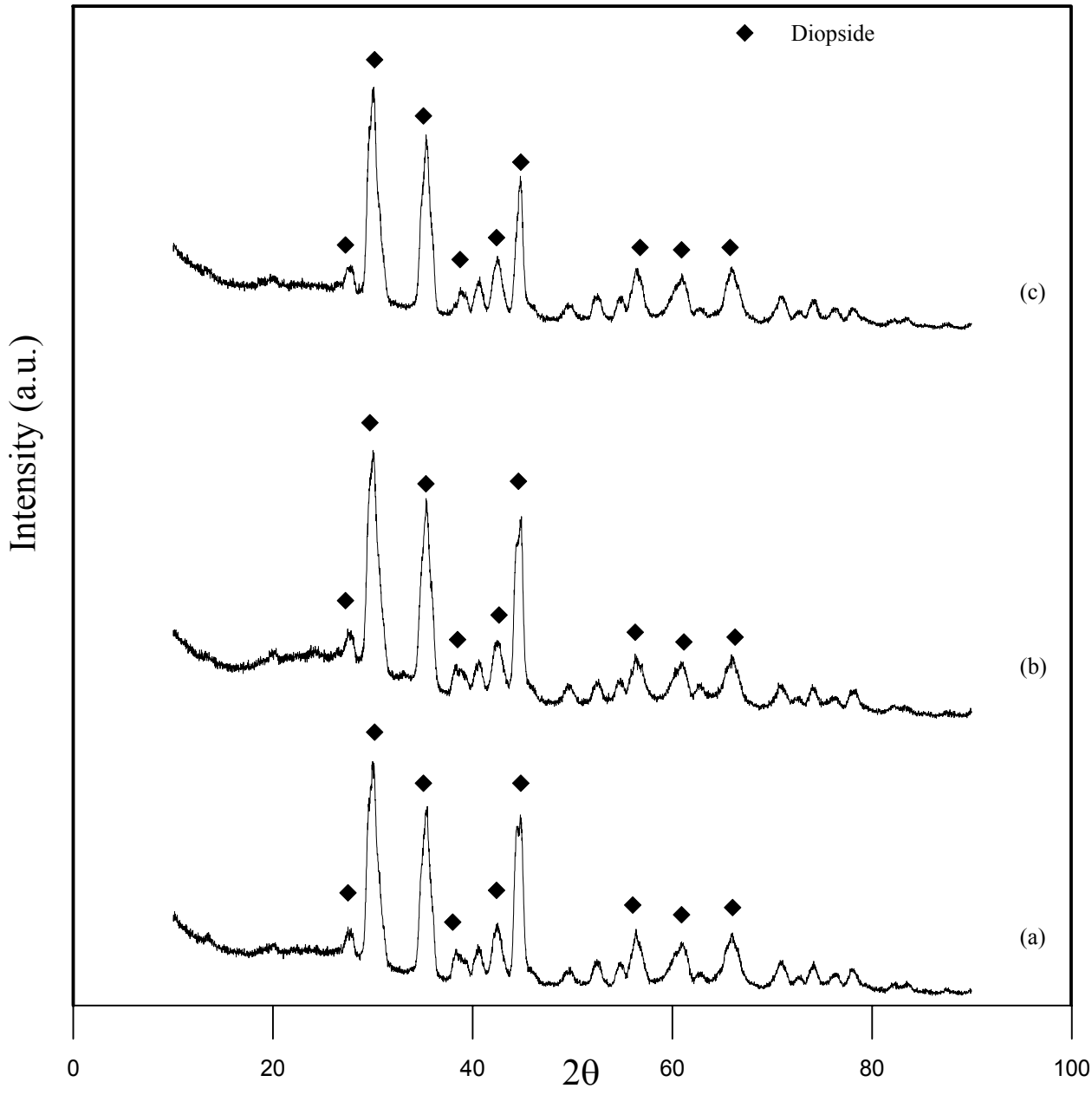

Figure C.2. XRD patterns of CRGC-S samples crystallized at 1135 K for : (a) 15 min, (b) 30 min and (c) 60 min

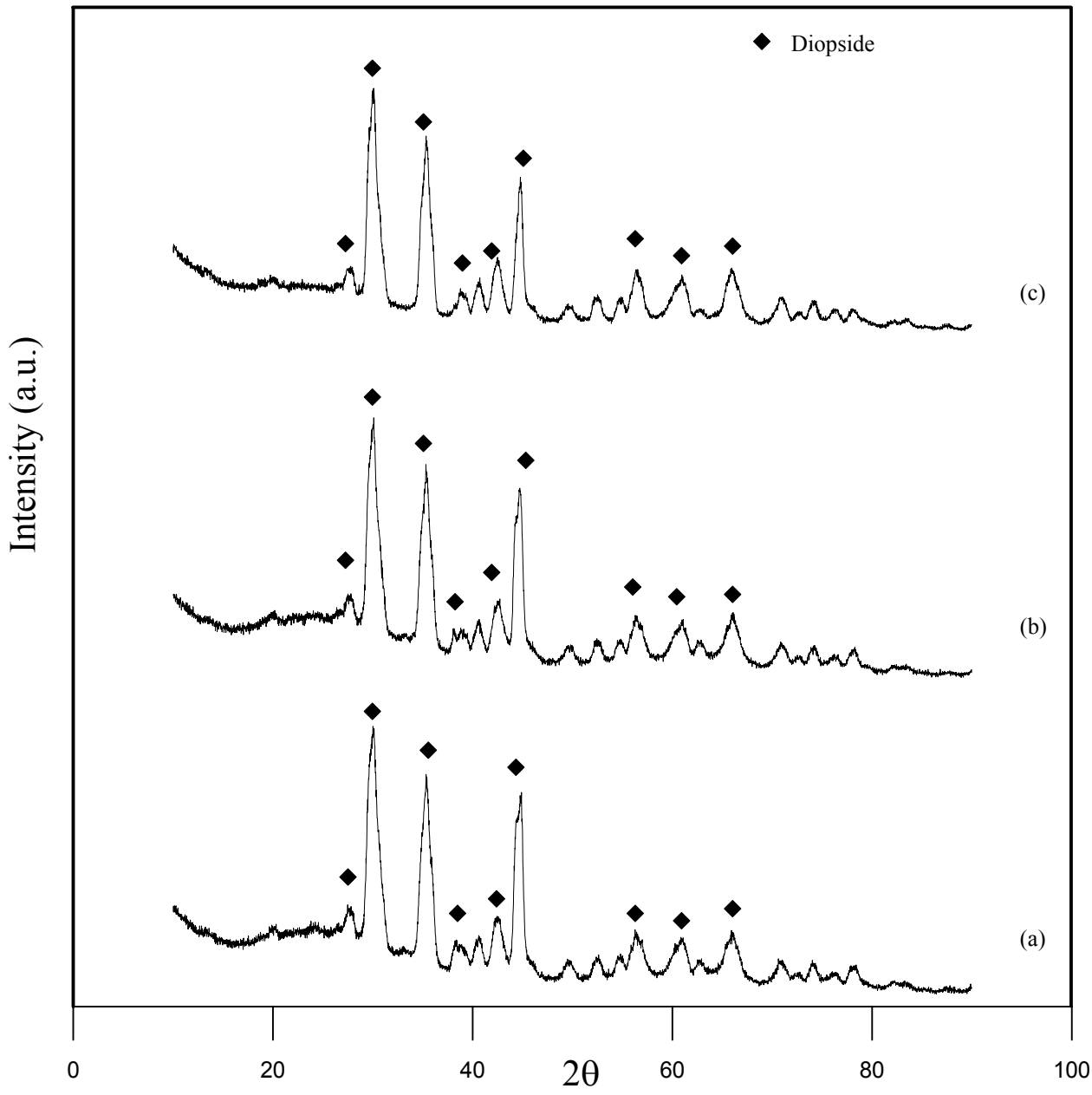

Figure C.3. XRD patterns of CRGC-P samples crystallized at 1135 K for : (a) 15 min, (b) 30 min and (c) 60 min

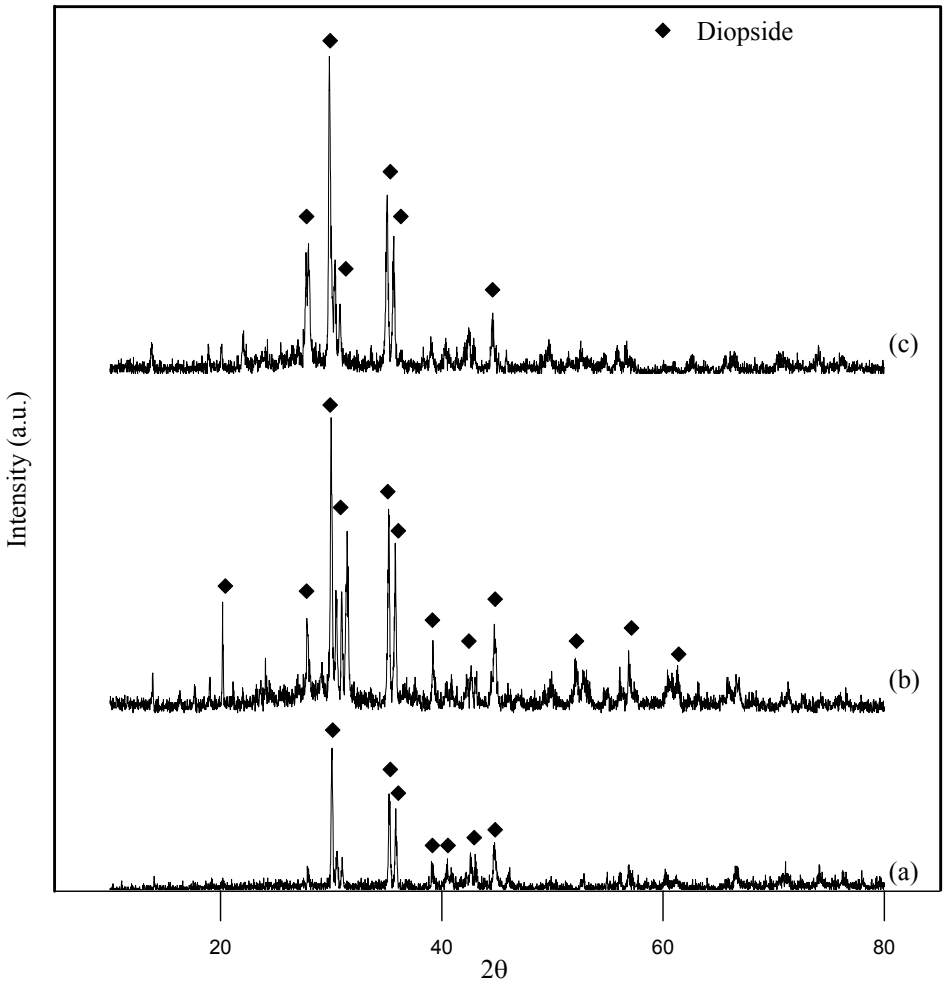

Figure C.4. XRD patterns of ORSGC-B samples crystallized at 1188 K for : (a) 15 min, (b) 30 min and (c) 60 min

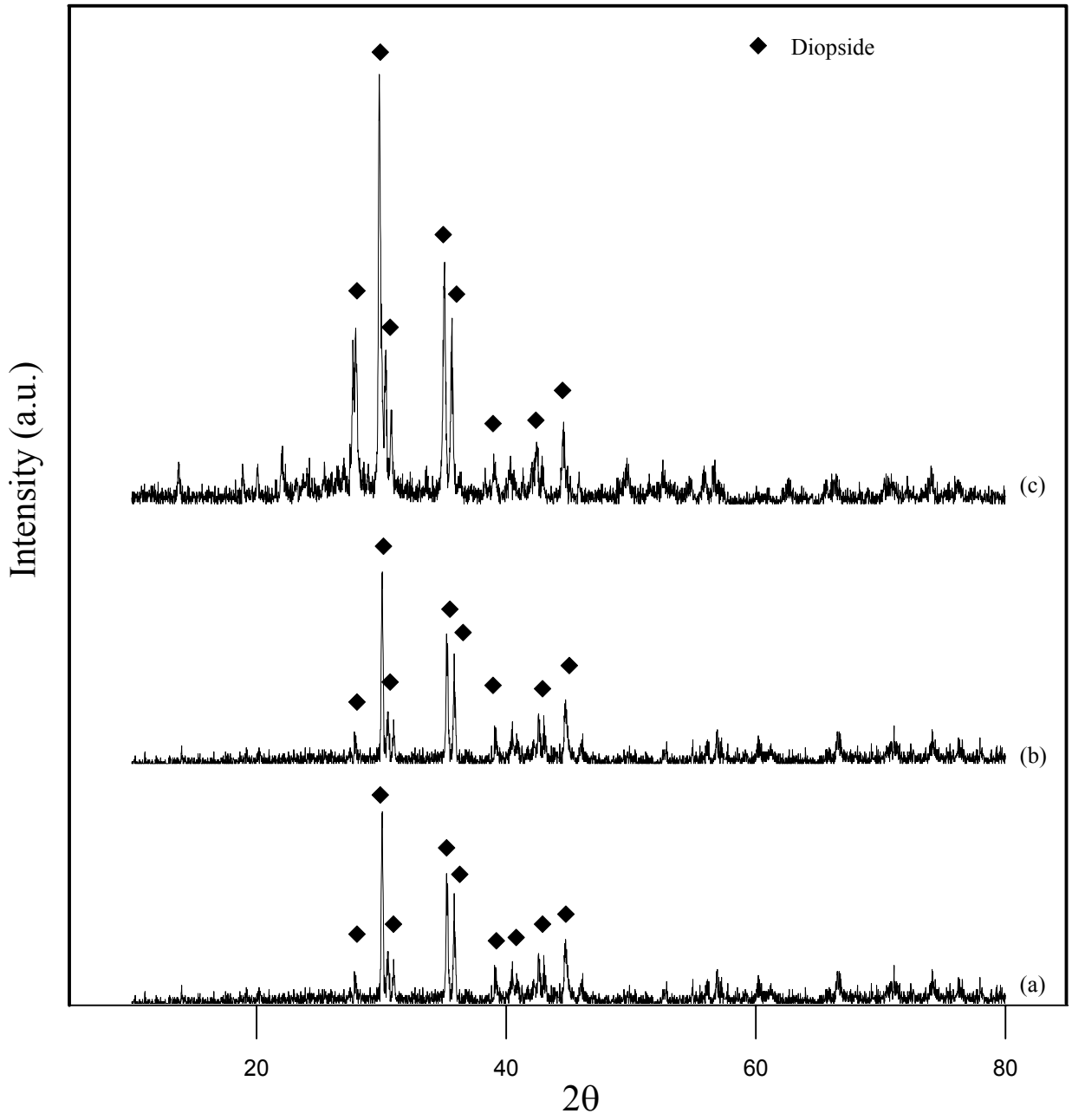

Figure C.5. XRD patterns of ORSGC-S samples crystallized at 1188 K for : (a) 15 min, (b) 30 min and (c) 60 min

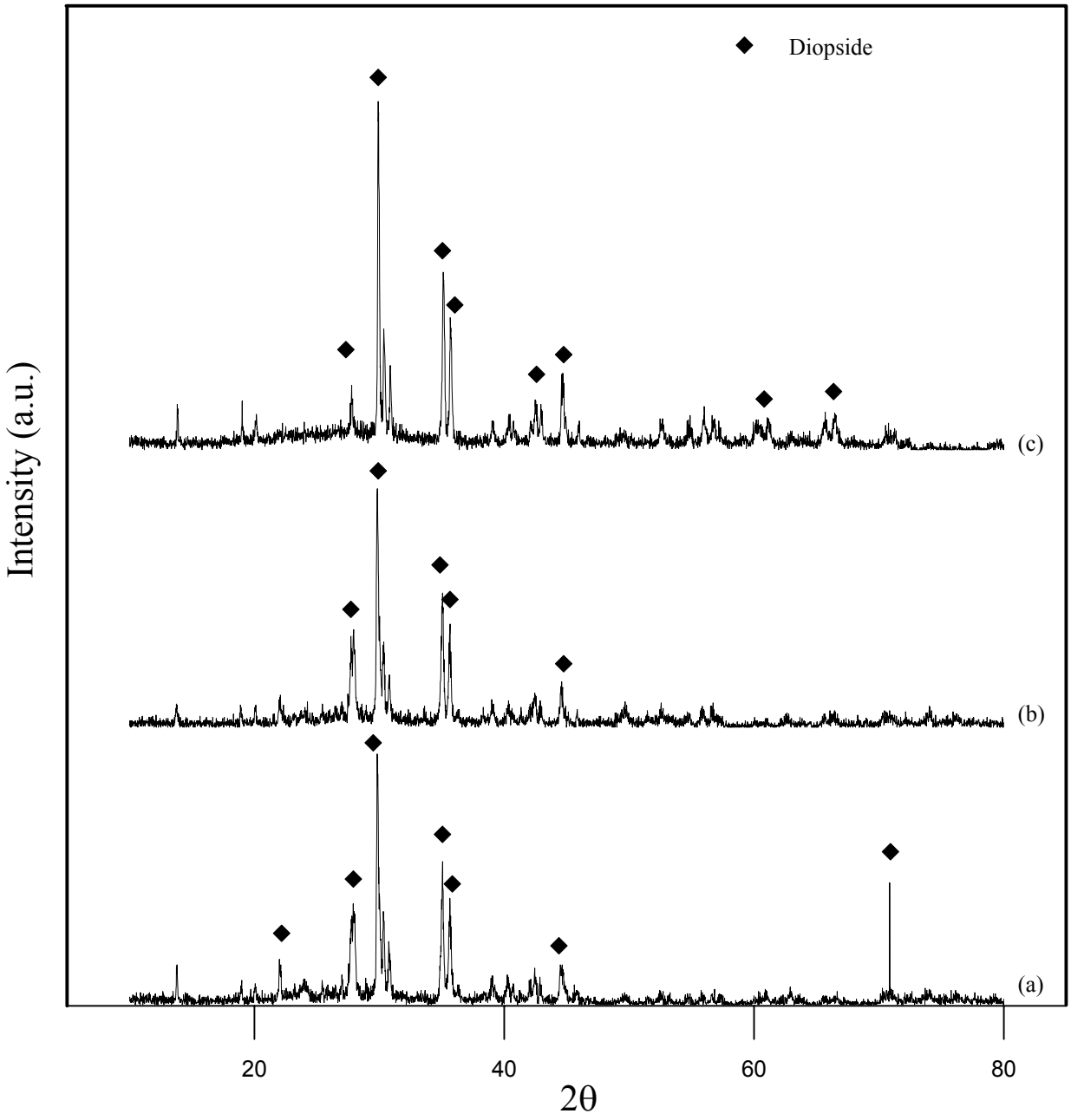

Figure C.6. XRD patterns of ORSGC-P samples crystallized at 1188 K for : (a) 15 min, (b) 30 min and (c) 60 min

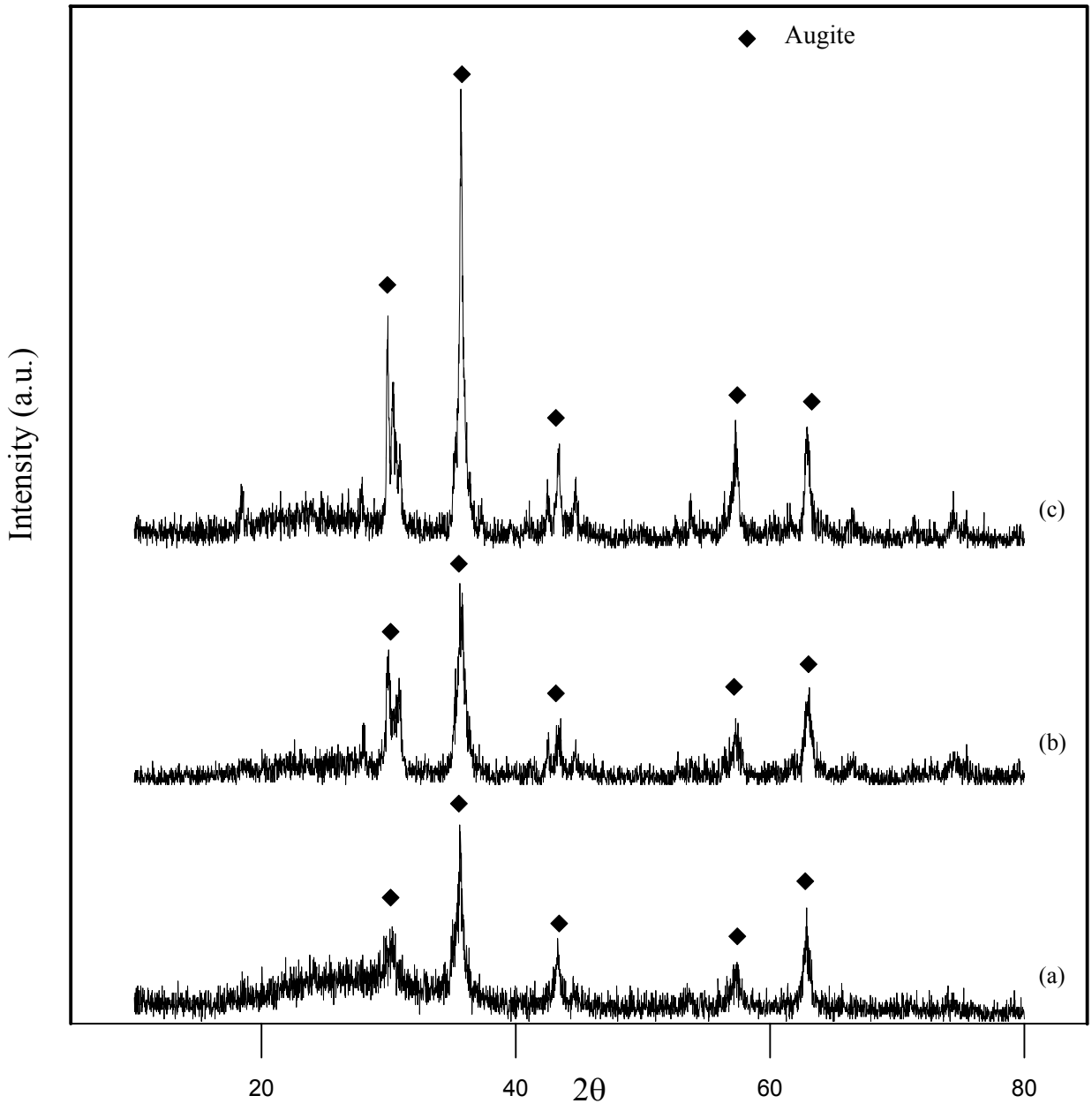

Figure C.7. XRD patterns of TGC-B samples crystallized at 1140 K for : (a) 15 min, (b) 30 min and (c) 60 min

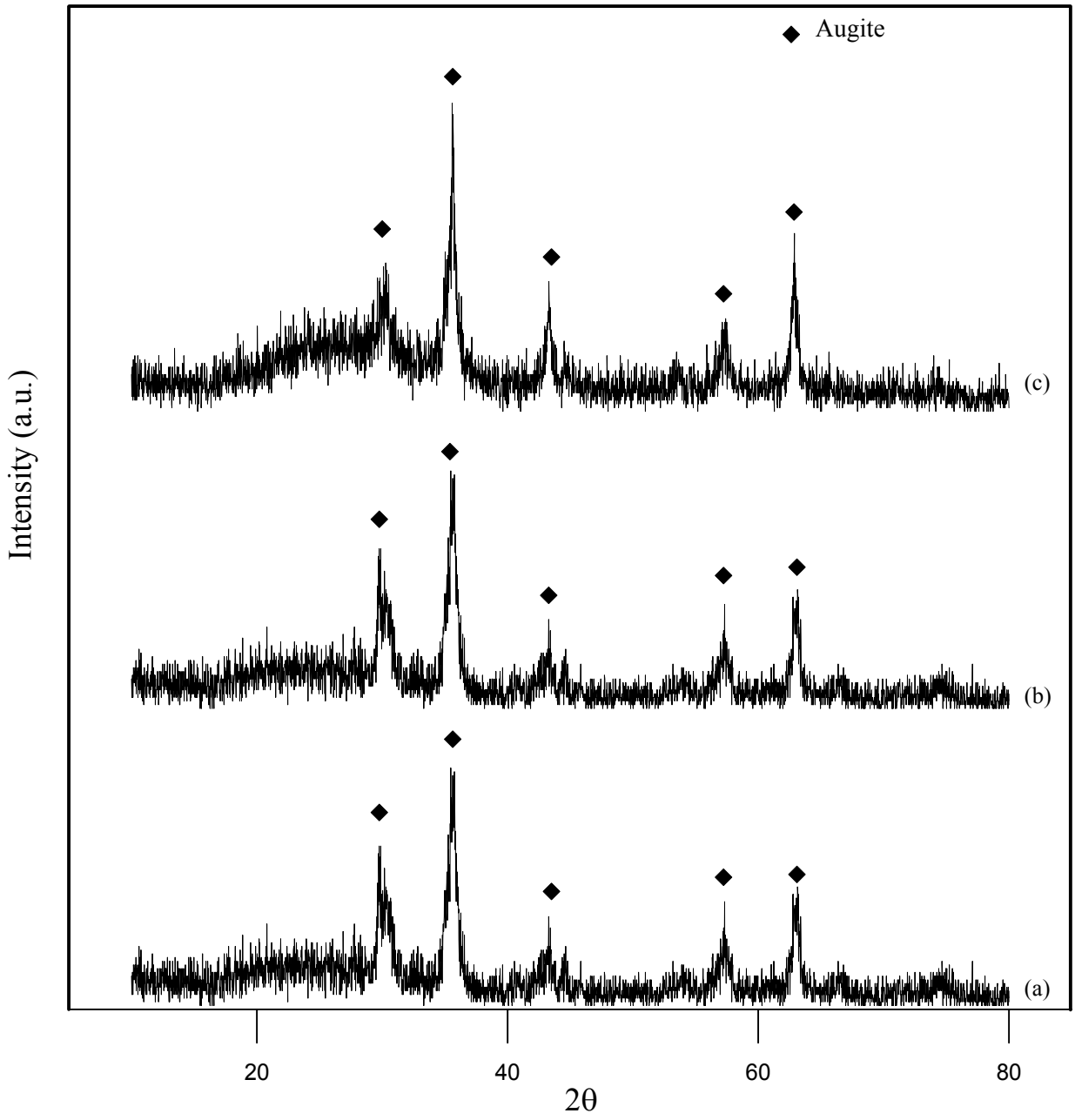

Figure C.8. XRD patterns of TGC-S samples crystallized at 1140 K for : (a) 15 min, (b) 30 min and (c) 60

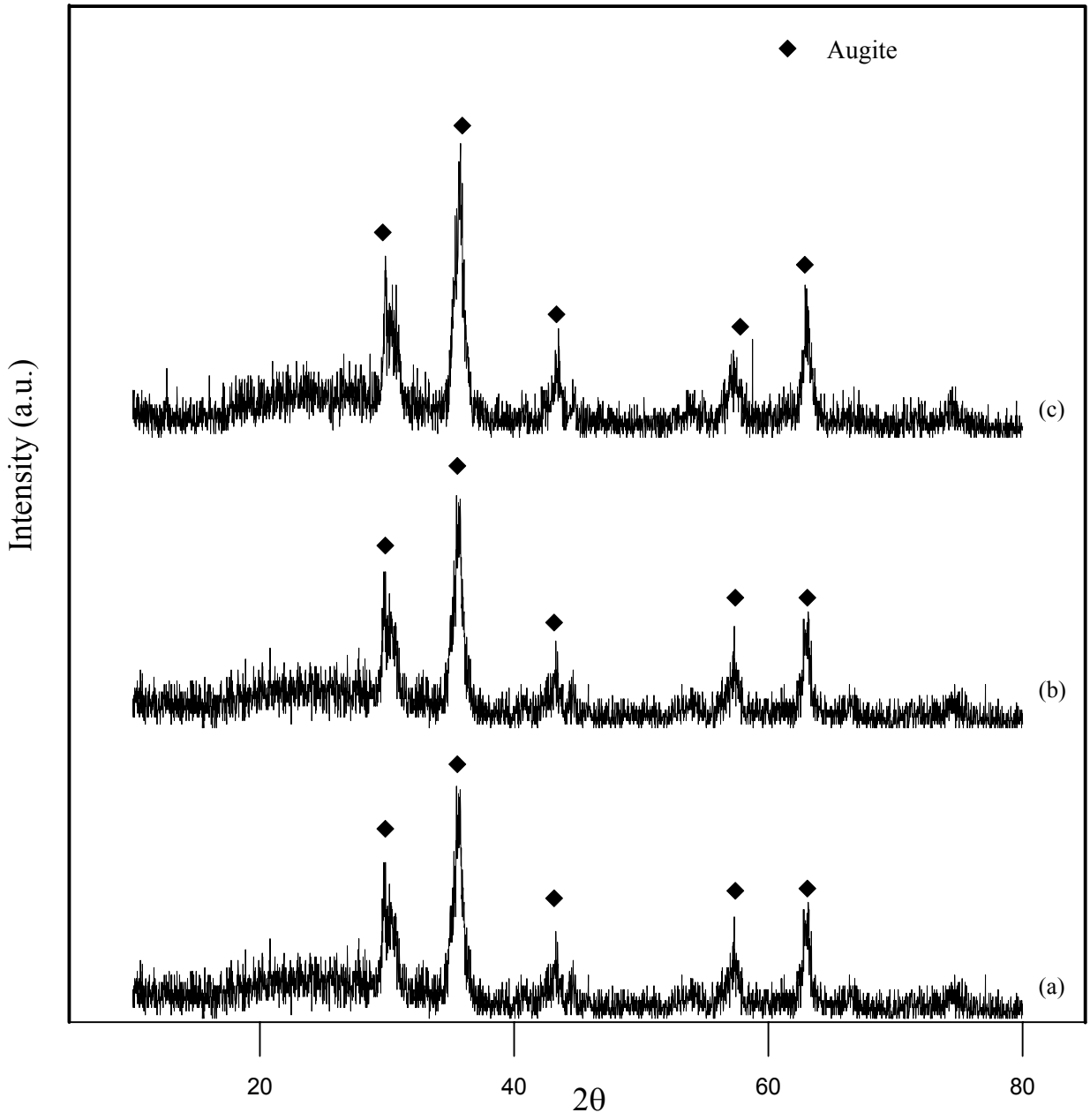

Figure C.9. XRD patterns of TGC-P samples crystallized at 1140 K for : (a) 15 min, (b) 30 min and (c) 60

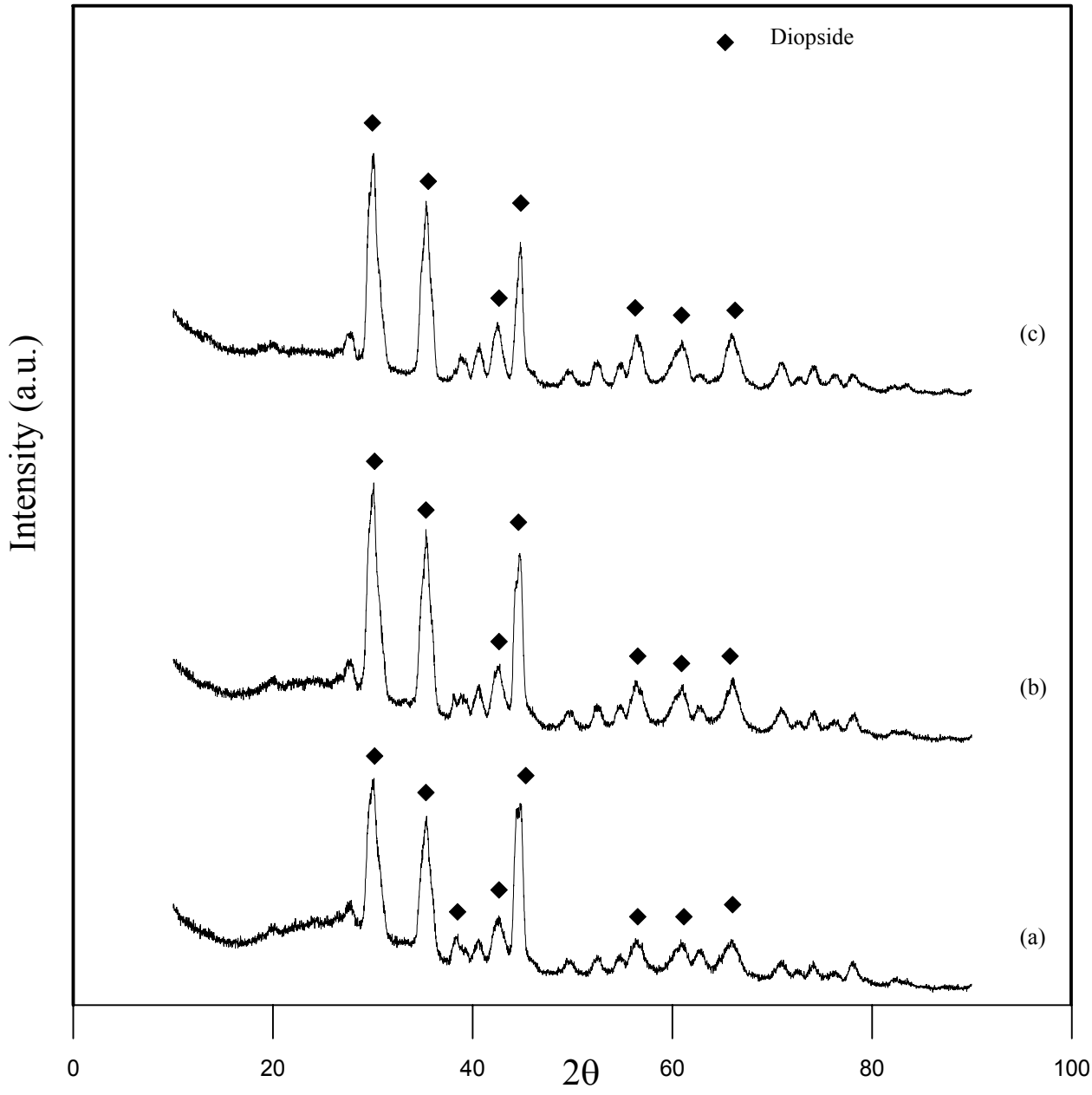

Figure C.10. XRD patterns of CGC-S samples crystallized at 1142 K for : (a) 15 min, (b) 30 min and (c) 60 min

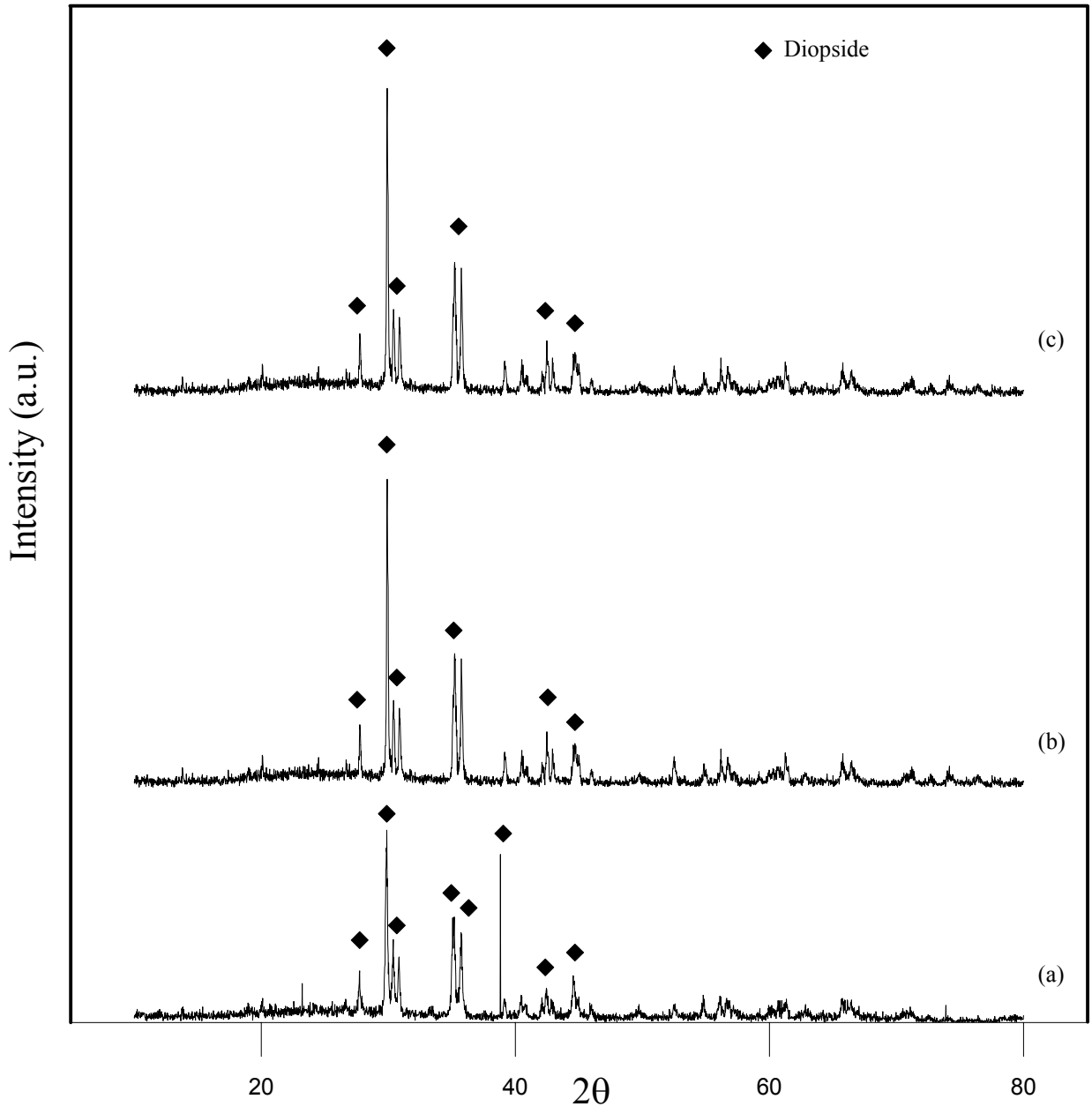

Figure C.11. XRD patterns of CGC-P samples crystallized at 1142 K for : (a) 15 min, (b) 30 min and (c) 60 min

APPENDIX D

X-RAY DIFFRACTION PATTERNS OF THE PRODUCED SINTERED SAMPLES

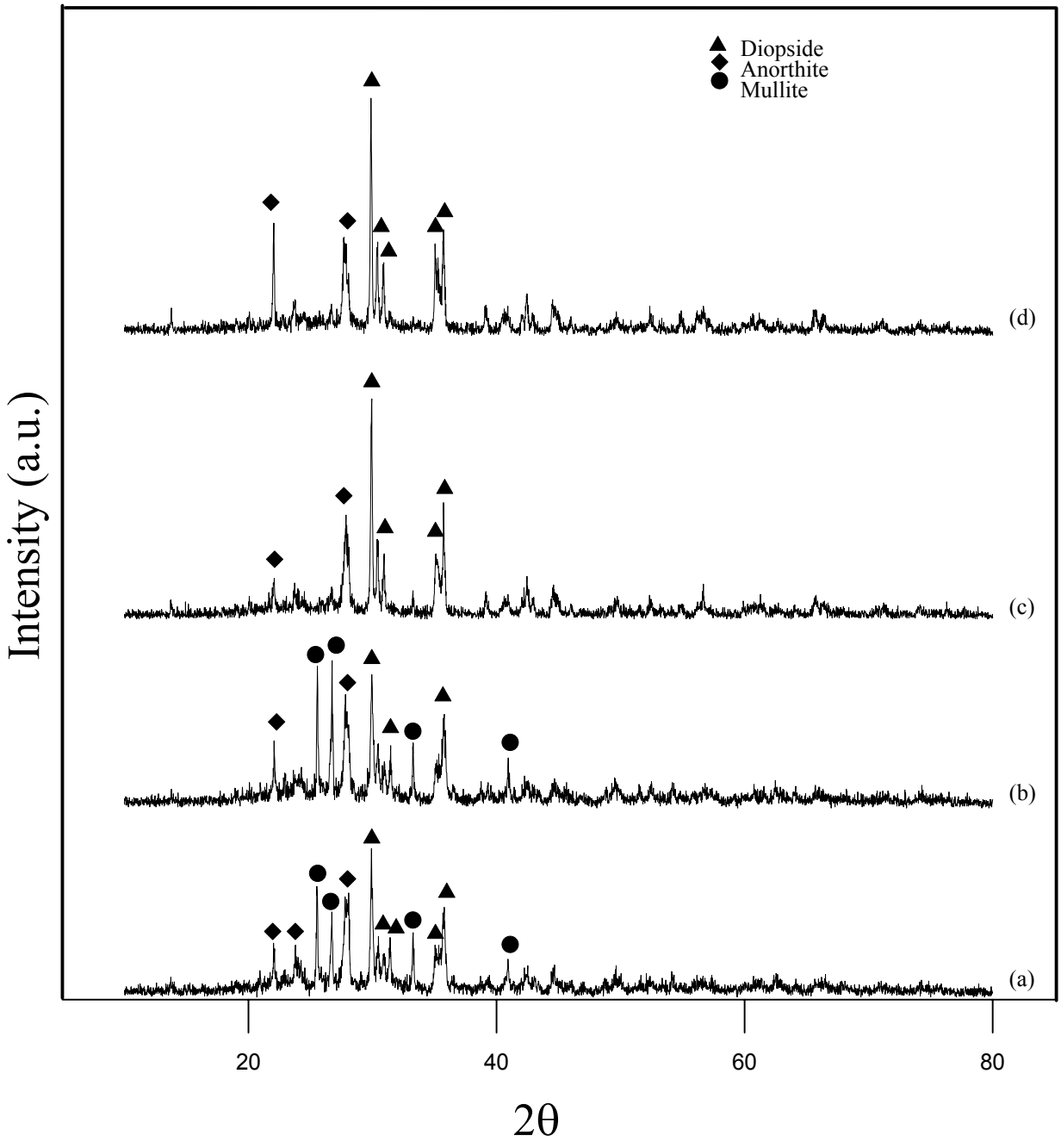

Figure D.1. XRD pattern of CAYFA samples sintered at the temperatures of : (a) 1298 K, (b) 1323 K, (c) 1348 K and (d) 1373 K

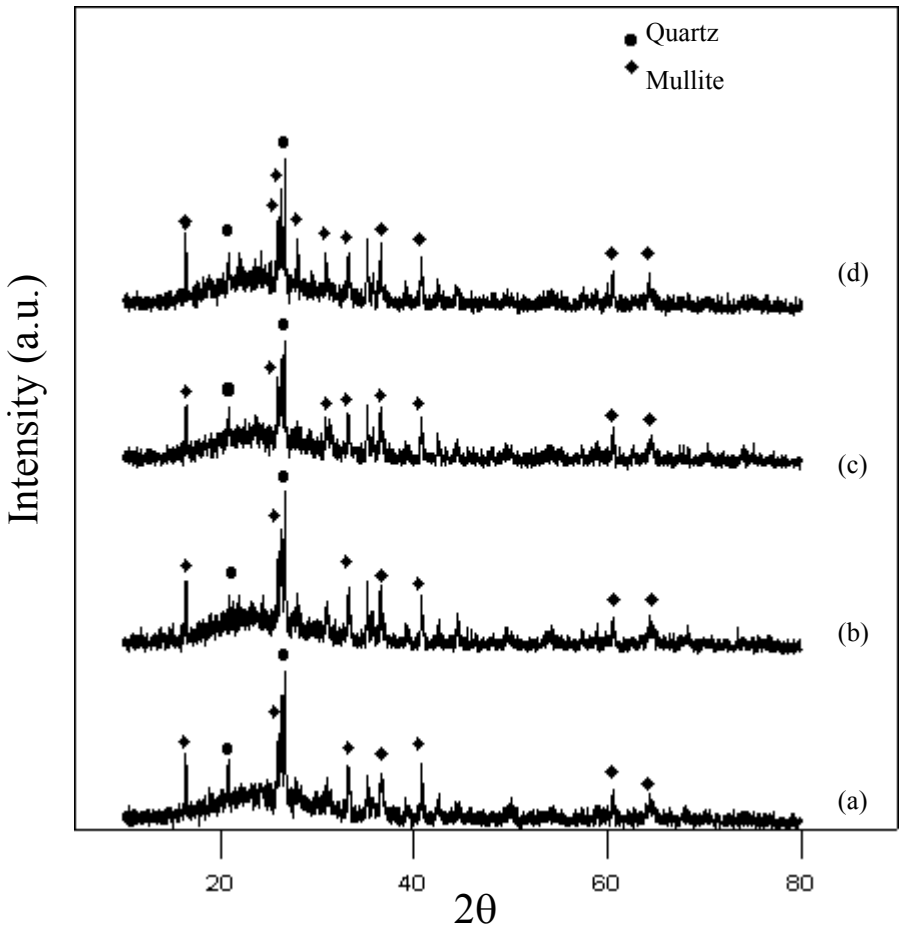

Figure D.2. XRD pattern of CFA samples sintered at the temperatures of : (a) 1373 K, (b) 1398 K, (c) 1423 K and (d) 1488 K

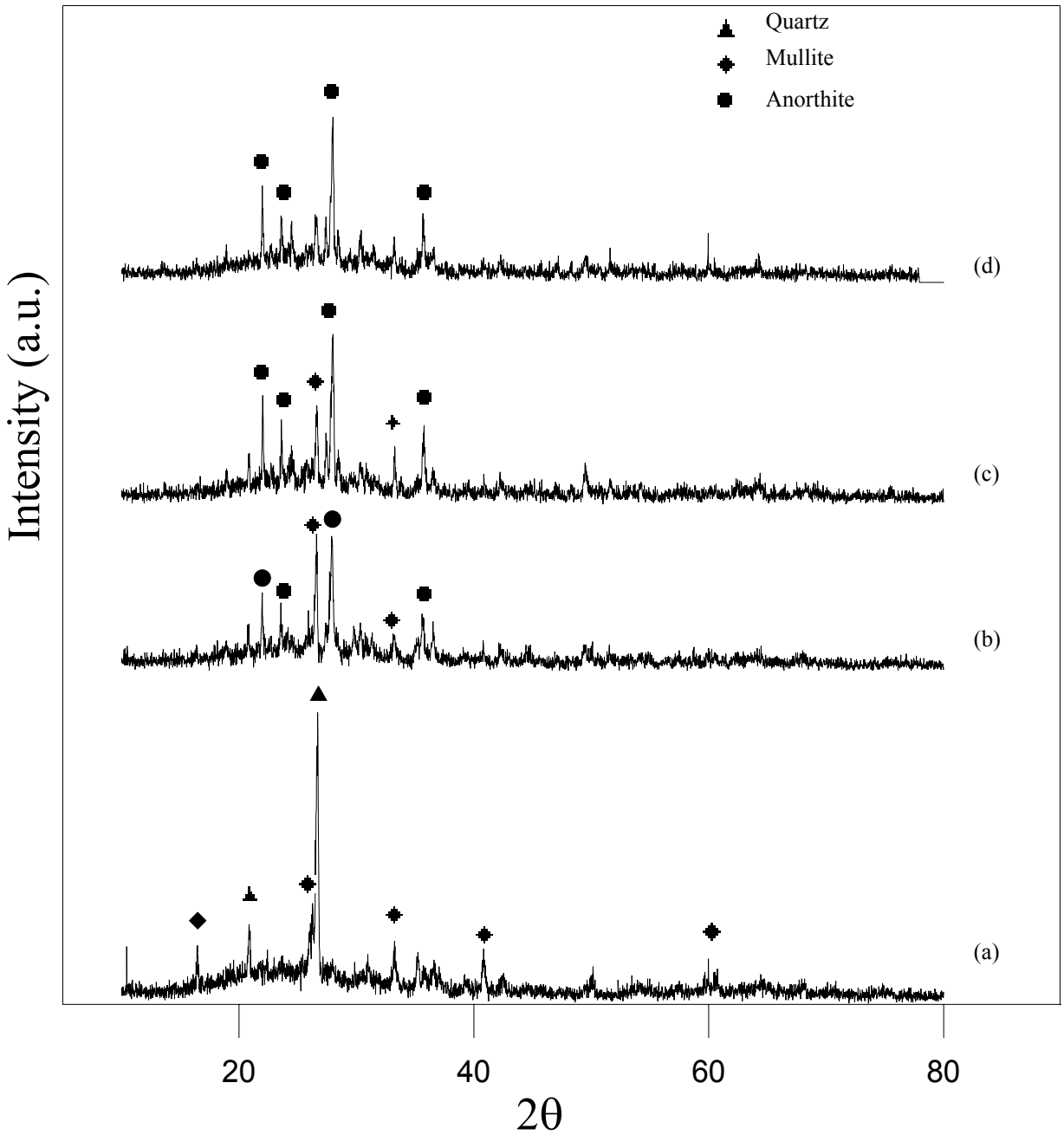

Figure D.3. XRD pattern of CATFA samples sintered at the temperatures of : (a) 1373 K, (b) 1398 K, (c) 1423 K and (d) 1488 K

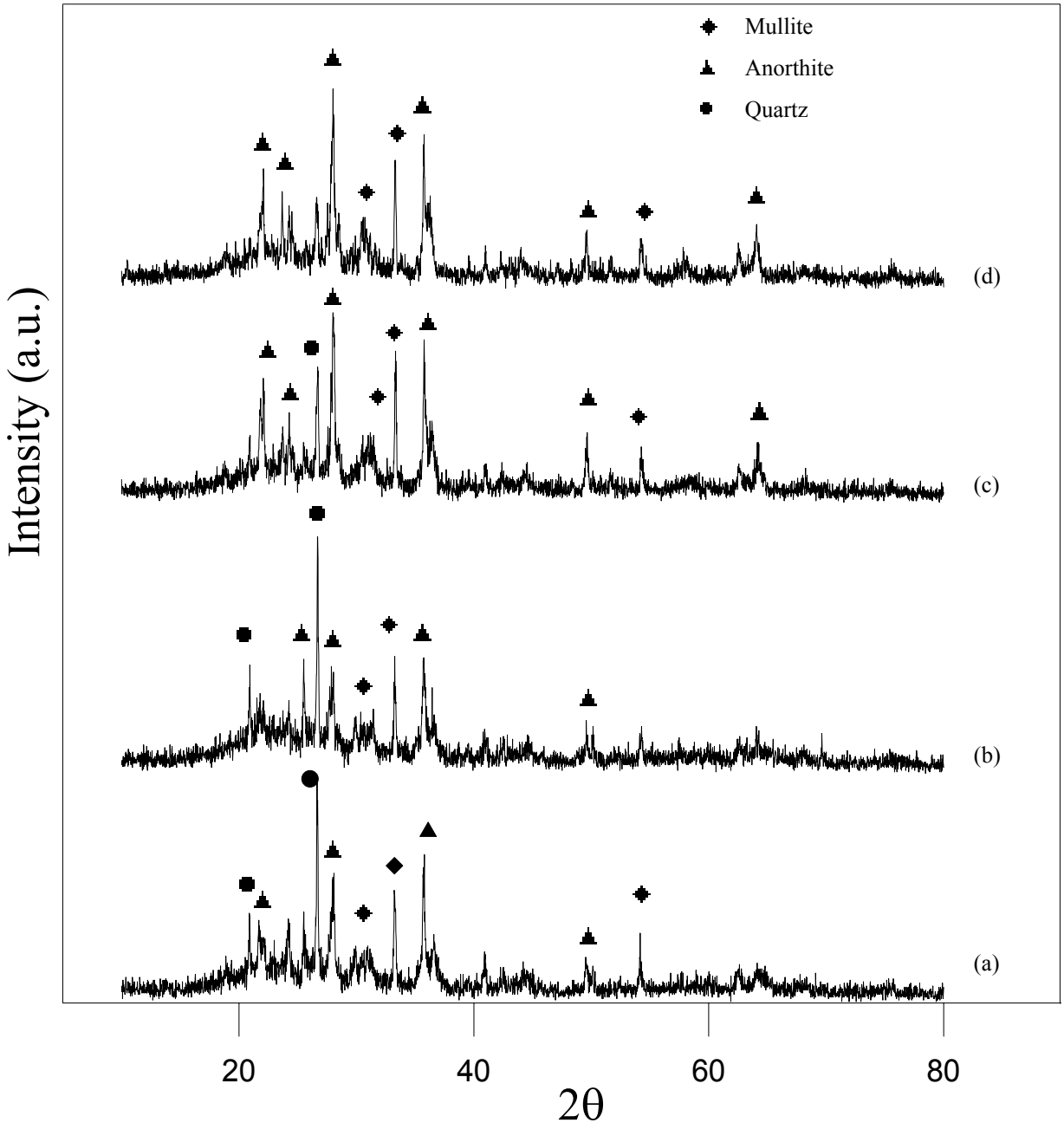

Figure D.4 XRD pattern of SFA samples sintered at the temperatures of : (a) 1373 K, (b) 1398 K, (c) 1423 K and (d) 1488 K

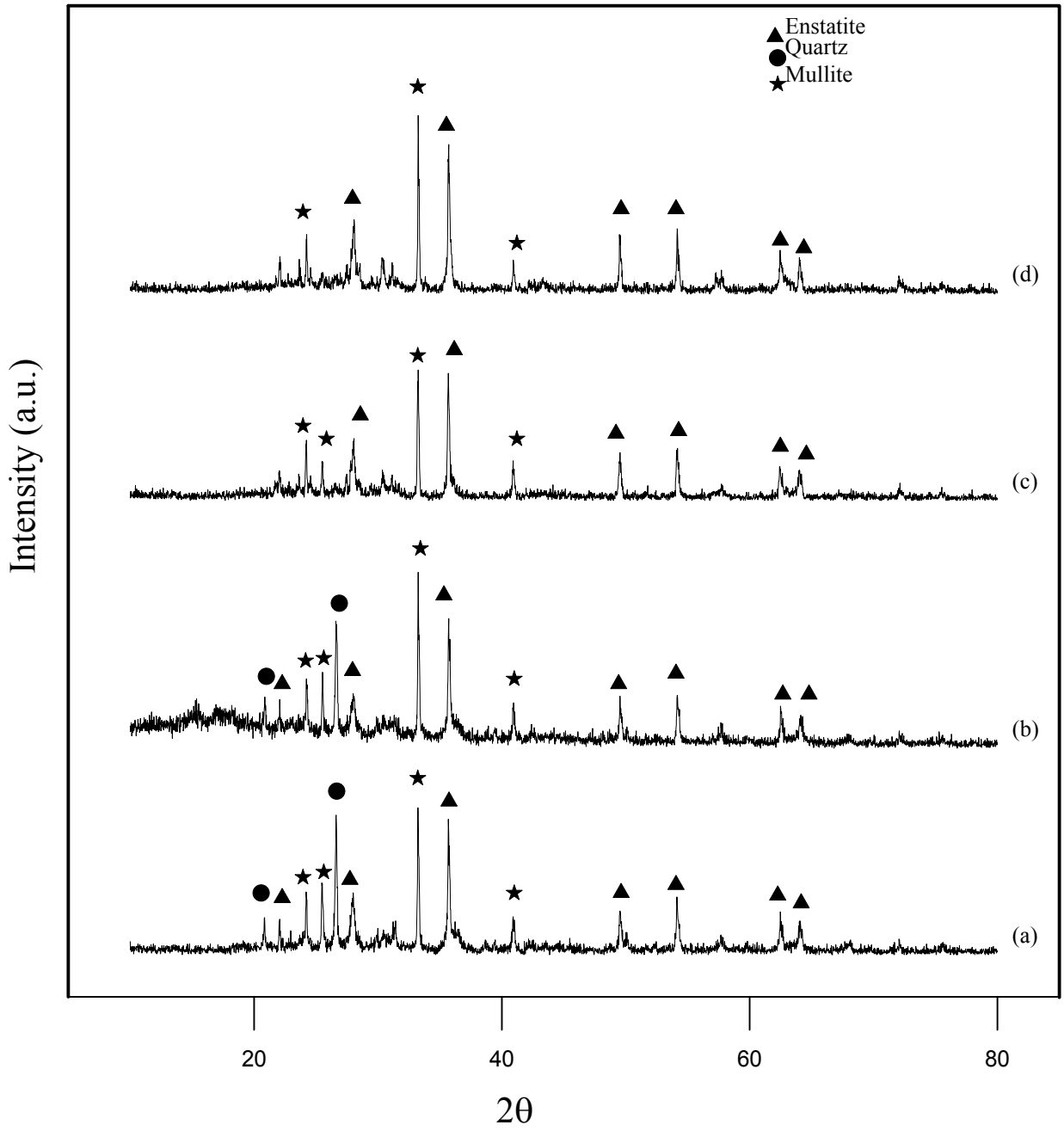

Figure D.5. XRD pattern of TFA samples sintered at the temperatures of : (a) 1398 K, (b) 1423 K, (c) 1448 K and (d) 1473 K

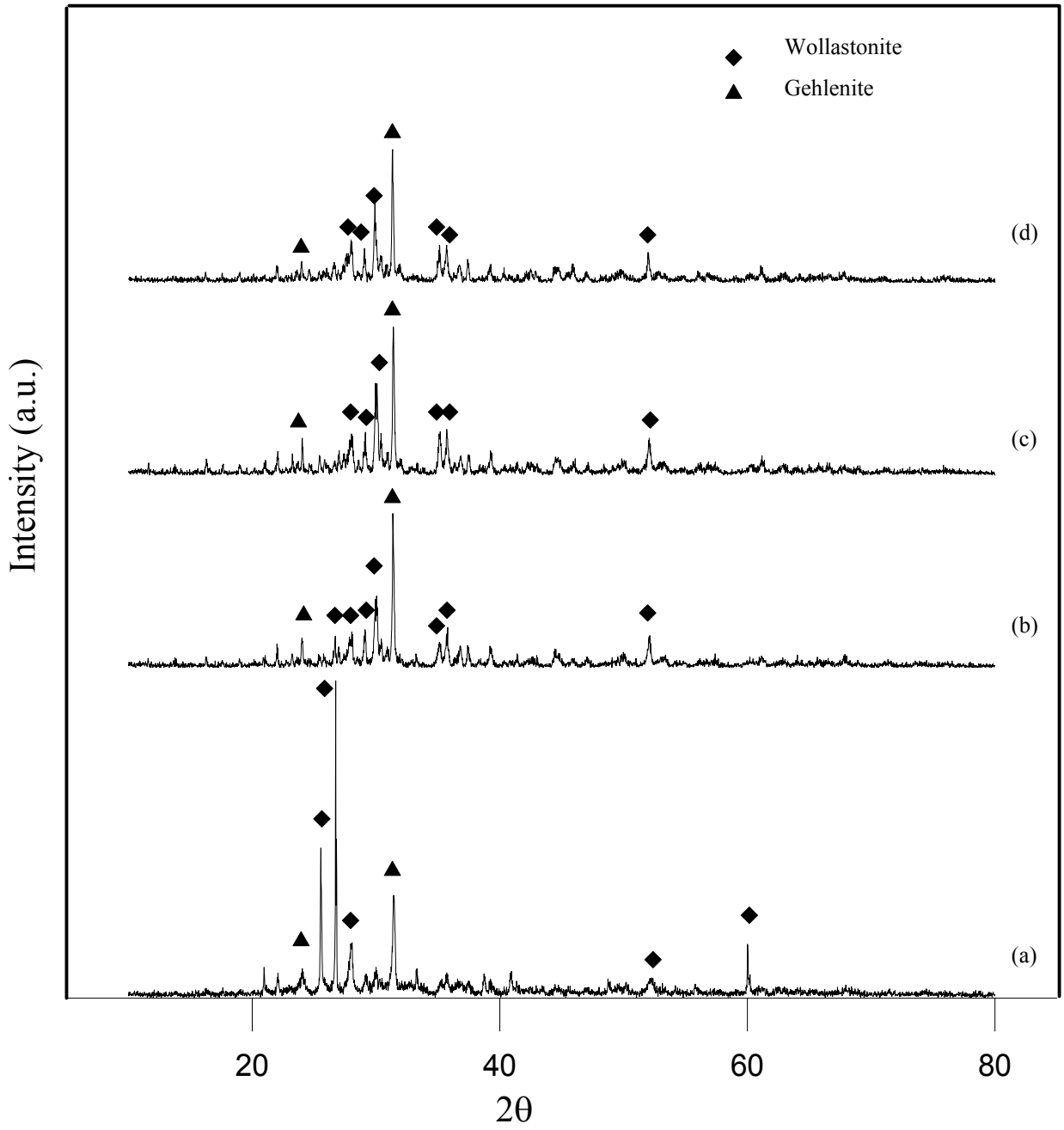

Figure D.6. XRD pattern of OFA samples sintered at the temperatures of : (a) 1273 K, (b) 1298 K, (c) 1323 K and (d) 1348 K

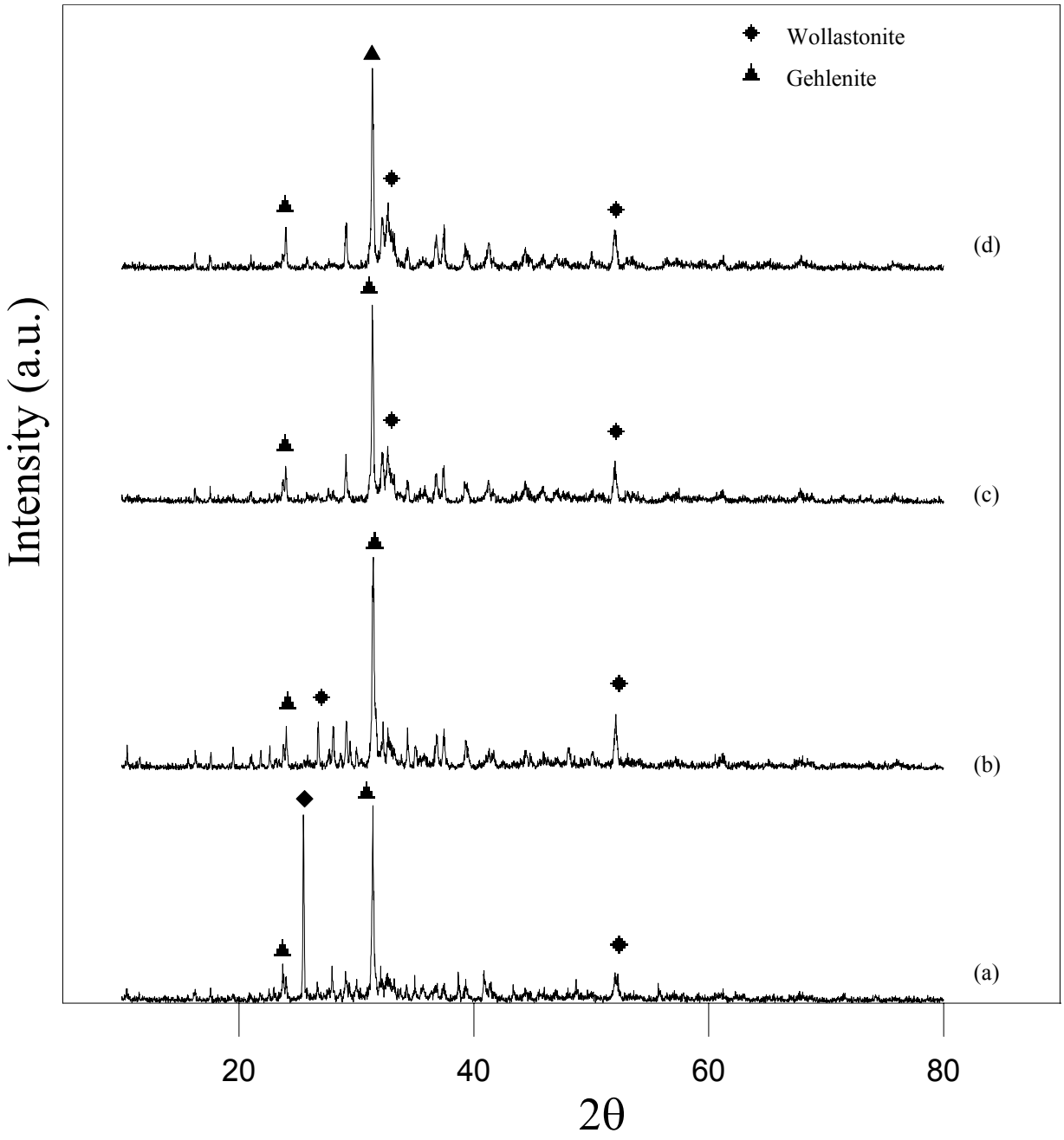

Figure D.7. XRD pattern of AEFA samples sintered at the temperatures of : (a) 1223 K, (b) 1248 K, (c) 1273 K and (d) 1298 K

CIRRICULUM VITAE

M. Melek EROL was born on May 18, 1975 in İstanbul. She had Bachelor's and Master's degrees from the Department of Chemical Engineering of ITU, in June 1996 and June 1999, respectively. She began to work in Chemical Engineering Department of ITU in 1998 as a research&teaching assistant. She has been enrolled Ph.D. Program of Chemical Engineering Department of ITU since 1999. She is still working as a research&teaching assistant in this department.